THE SYNTHESIS AND ANION COORDINATION CHEMISTRY OF NOVEL MONO- AND MULTI-FUNCTIONAL BORYLMETALLOCENES

Joanna Day BSc. (Hons.)

A thesis submitted to Cardiff University in accordance with the requirements for the degree of Doctor of Philosophy in the Faculty of Science, School of Chemistry, Cardiff University.

April 2008

Abstract

The synthesis, characterisation and anion binding properties of a series of mono-, tris- and tetrakis-functional boronic esters of ferrocene are reported. Mono-borylated systems: ($\eta^5C_5H_5$)Fe($\eta^5C_5H_4BO_2R$) [where O_2R = ethane-1,2-diolato (**1a**) and pinanediolato (**1b**)], tris-functional borylated systems: [(η^5-$C_5H_3EtBO_2R$)Fe(η^5-$C_5H_3(BO_2R)_2$] [where O_2R = ethane-1,2-diolato (**3a**), stilbenediolato (**3b**) and pinanediolato (**3c**)] and tetrakis-functional borylated systems: [(η^5-$C_5H_3(BO_2R)_2$)]$_2$Fe [where O_2R = ethane-1,2-diolato (**4a**), stilbenediolato (**4b**), pinanediolato (**4c**) and napthalenediolato (**4d**)] have been synthesised and characterised by NMR, UV/Vis and IR spectroscopy, mass spectrometry and in most cases by X-ray diffraction. Electrochemical analyses of most of the above-mentioned boronic esters of ferrocene have demonstrated the influence of the number of boronic ester groups on the redox potential of the ferrocene backbone, and have allowed a comparison of the different substituents.

The anion-binding properties of the above-mentioned boronic esters have been monitored by spectroscopic (including NMR and UV/Vis) and electrochemical methods. Bis-functionalised boronic esters of ferrocene have previously shown a colorimetric response to fluoride, and have been shown to bind two equivalents of fluoride per receptor. An analogous colorimetric response to fluoride is observed with the tris- and tetrakis-functionalised boronic esters, which also display a particular affinity for fluoride. The kinetics of the colorimetric response have been probed using time-resolved UV/Vis experiments, with the tris- and tetrakis-functionalised compounds shown to effect a more rapid response to fluoride. Kinetic experiments have revealed that the response to fluoride is greatly enhanced with tris- and tetrakis-functionalised receptors, and also revealed a binding stoichiometry of 2:1 (anion: receptor) in all cases; thus the binding of more than two equivalents of fluoride by the additional boryl groups is not responsible for enhanced kinetics.

The synthesis and characterisation of a range of dimeric, macrocyclic and polymeric ferroceneboronic esters has been undertaken. Dimeric ferrocene boronic esters; (η^5-C_5H_5)Fe(η^5-C_5H_4)R(η^5-C_5H_4)Fe(η^5-C_5H_5) [where R = $BO_2C_8H_{12}O_2B$ (**7a**), $B(OCH_2)_2C(CH_2O)_2B$ (**8a**) and $BO_2(C_6H_2)O_2B$ (**9a**)], macrocyclic ferrocene boronic esters: [(η^5-C_5H_4)Fe(η^5-C_5H_4)BRB]$_2$ [where R = $BO_2C_8H_{12}O_2B$ (**7b**) and $B(OCH_2)_2C(CH_2O)_2B$ (**8b**)], and the polymeric ferrocene boronic ester [(η^5-C_5H_4)$BO_2C_8H_{12}O_2B$(η^5-C_5H_4)Fe]$_n$ polymer (**7c**) have been synthesised and characterised by NMR and UV/Vis spectroscopy, mass spectrometry and in some cases by X-ray diffraction. Electrochemical analyses of some of the above-mentioned boronic esters of ferrocene have demonstrated the lack of electronic communication between iron centres with the saturated pentaerythritol and cyclooctanetetraol linker groups. Investigation into the factors controlling assembly of boronic ester units into poly-, oligomeric or macrocyclic products has been possible. The two different linker groups have revealed very different product distributions under analogous reaction conditions with ferrocene-bis-boronic acid. The pentaerythritol linker favours macrocycle formation, whilst the cyclooctanetetraol linker favours polymer formation. Thus reactions can be driven with high selectivity towards either macrocyclic or polymeric products depending on choice of linker group.

Acknowledgements

Firstly I would like to say a huge thank you to my supervisors Dr. Simon Aldridge and Dr. Ian A. Fallis for all of their guidance, support, supervision and above all their creative minds.

Big thanks also to Dr. Debbie Kays for all her guidance on air-sensitive techniques in the early days, general help throughout and for answering many questions chemical and otherwise.

Many thanks to Dr. Christopher Bresner for his guidance throughout and his expertise on all things of a colorimetric fluoride sensing nature.

Acknowledgements must also be made to following people:

Drs. Li-Ling Ooi, Andrew Cowley and S. J. Coles and Profs. Cameron Jones and M. B. Hursthouse for crystallography.

Thanks to the EPSRC National Crystallography and Mass Spectrometry Service Centres in Southampton and Swansea correspondingly.

Many thanks to the good friends of Labs 1.124, 1.125 and S12 past and present, in particular: Mini, Gles, Alex, Tom and Matt.

I would also like to thank Rob Jenkins and Robin for all those time when NMR machines gave up! Alan, Ricky, Mal and John Bowley, and the stores team: Gaz, Dave and Steve.

Massive thanks to the Blanchminster Trust in recognition of a generous grant awarded during writing-up.

Special thanks to Dan, Mum, Dad, Nan and Granddad, Polly, Rosie, Marc and Lilli for all their love and encouragement.

Notes

The following abbreviations have been used in the text:

amu = atomic mass units

Ar = aryl

bipy = 2,2'-bipyridine

br = broad

^{n}Bu = $-CH_2CH_2CH_2CH_3$

^{t}Bu = $-C(CH_3)_3$

18-C-6 = 18-crown-6

calc. = calculated

COD = cyclooctadiene

Cp = cyclopentadienyl, η^5-C_5H_5

CV = cyclic voltammetry

Da = Dalton

Dba = dibenzylidene acetone

DCM = dichloromethane

δ = NMR chemical shift

DFT = density functional theory

DME = dimethoxyethane

DMF = dimethylformamide

DMSO = dimethylsulphoxide

DNA = deoxyribosenucleic acid

d = doublet

E = oxidation potential

EI = electron ionisation

^{i}Pr = $-CH(CH_3)_2$

ES = electrospray

Et = $-CH_2CH_3$

Fc = ferrocenyl, $(\eta^5\text{-}C_5H_5)Fe(\eta^5\text{-}C_5H_4)$

fc = ferrocenediyl, $(\eta^5\text{-}C_5H_4)Fe(\eta^5\text{-}C_5H_4)$

fc' = ferrocenetetryl, $(\eta^5\text{-}C_5H_3)Fe(\eta^5\text{-}C_5H_3)$

FcH = ferrocene, $(\eta^5\text{-}C_5H_5)_2Fe$

FcH^+ = ferrocenium, $[(\eta^5\text{-}C_5H_5)_2Fe]^+$

FT = Fourier Transform

GPC = gel permeation chromatography

h = hours

i = current

IR = infrared

J = coupling constant

λ = wavelength

LUMO = lowest unoccupied molecular orbital

m = multiplet

MALDI = matrix-assisted laser desorption/ionisation

max = maximum

md = medium

Me = $-CH_3$

Mes = mesityl

min. = minutes

MS = mass spectrometry

ν = stretching frequency

M_W = molecular weight

NHC = N-heterocyclic carbene

NOESY = Nuclear Overhauser effect spectroscopy

NMR = nuclear magnetic resonance

obs. = observed

Ph = -C_6H_5

ppm = parts per million

q = quartet

Ref. = reference

RT = room temperature

s = singlet

st = strong

t = triplet

TBAF = tetrabutylammonium fluoride

TGA = thermogravimetric analysis

THF = tetrahydrofuran

Tol = toluene, tolyl

tmeda = tetramethylethylenediamine

UV/Vis = ultraviolet/visible

VT-NMR = variable temperature nuclear magnetic resonance

w = weak

1 Torr = 1 mmHg = 133.3 Pa

Contents

Page

Appendix One

Appendix Two

Appendix Three

Appendix Four

Chapter One

Introduction

1.1 Introduction

Supramolecular chemistry involves the design of functional molecular arrays, in which the most important feature is not necessarily the covalently bonded molecules from which these arrays are built, but the non-covalent intermolecular forces by which they are held together. The multidisciplinary field of supramolecular chemistry has grown to become an area of intense research interest over recent decades, often combining biological, chemical, physical and technical aspects; from biological inspiration through to chemical design, followed by investigation into the physical properties and finally incorporation of the product into a functioning technical device. Supramolecular chemistry is based upon the critical concept of complementarity, in which nature is the expert, providing insight with numerous examples. The most significant example of complementarity in nature must be the base pairing displayed in the DNA double helix; each DNA strand consists of purine and pyrimidine bases linked to a framework of phosphorylated sugars. The two strands of the double helix are held together by complementary hydrogen bonds between base pairs. However it is chemical design and synthesis towards complementarity in supramolecular binding chemistry of functional molecules that is particularly relevant to the work presented in this thesis. Contributing significant input to the broader field of supramolecular chemistry, the studies of cation and anion recognition have grown to become areas of intense research interest over recent decades. Early examples of cation receptors are the well-known crown ethers, reported in 1967 by C. J. Pederson;[1] crown ethers are still used extensively for the encapsulation of metal cations today, and "proton sponge" reported by Alder *et al.* in 1968.[2] This and other early discoveries have led to extensive research interest in the field of cation binding, which has until now largely over-shadowed the field of anion recognition. Although the first report of an inorganic anion receptor was made back in 1968,[3] the complexation of anions has received somewhat less attention over the years.

There are several reasons why the field of anion recognition has received less research attention. Anions possess a negative charge and are more diffuse in comparison to their cationic analogues; hence receptors for anions must be able to accommodate their larger ionic radii to achieve effective binding. In the case of the fluoride anion, a relatively small ionic radius means that the fluoride anion possesses a higher charge density, a feature that makes it easier to accommodate when designing a receptor, compared to other larger anions with relatively disperse charge. The solvent can play a significant role in the binding process, if the solvent strongly solvates either the host or the guest species, this can dramatically alter the host-guest equilibrium and make recognition non-specific. Anions in general display a high free energy of solvation; a good acceptor solvent solvates anions very effectively, hence careful choice of solvent and design of the receptor molecule are required for binding processes that are to take place in solution. Anionic species can also be very sensitive to pH, for example phosphate anions become protonated at low pH values, reducing their negative charge. A further complication is that different anions can adopt a vast range of different geometries, for example halide anions are spherical and azide anions are linear, whereas phosphate and sulphate anions are tetrahedral. All of these factors add to the challenge of designing an anion specific receptor. This chapter aims to summarise the literature reports that are relevant to the chemistry presented in this thesis; this will include a summary of the various anion-binding reports, particularly fluoride binding by Lewis acid systems. A summary of sensors designed to give a colorimetric or spectroscopic response to anion binding will be included, together with a final overview of organometallic polymer chemistry and the applications of organometallic polymers in the field of anion sensing.

1.2 Host-Guest Interactions

By definition a supramolecular structure is built via non-covalent interactions between specific molecules. There are a number of alternative interactions accessible to form a host-guest complex, the most important being electrostatic, hydrogen bonding and Lewis acid/base interactions. Electrostatic binding is very strong and has been widely employed in the design of anion receptors. The basis for electrostatic interactions is the Coulombic attraction between opposite charges. These can incorporate ion-ion, ion-dipole and dipole-dipole interactions (Figure 1.1).

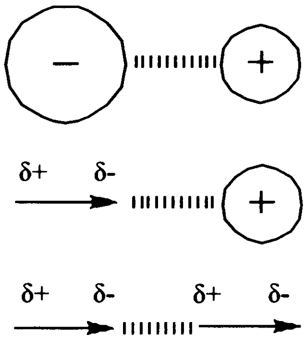

Figure 1.1 Electrostatic interactions

It is common for hydrogen bond donor molecules to be incorporated in the design of a electrostatic host molecules, to support and strengthen the electrostatic interaction, and there are few examples of receptor systems utilizing purely electrostatic binding interactions. Hydrogen bonding provides another alternative non-covalent interaction, capable of strong binding where a host has been designed with the directional nature of the hydrogen bond in mind, i.e. one hydrogen bond will not provide a strong guest-host interaction, but precise design to incorporate an array of potential hydrogen bonding sites presents the means of achieving a strong guest-host interaction. The coordination of anionic guest species via arrays of hydrogen bonds is demonstrated in many biological systems, for example the formerly cited DNA double helix (Figure 1.2).

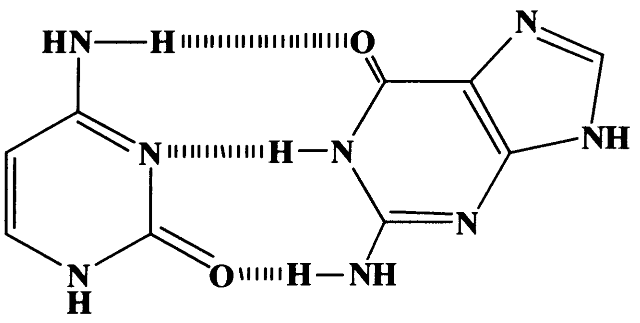

Figure 1.2 Base pairing (C-G) by hydrogen bonding in DNA.

In nature, where anion specificity can be essential, anion complexation is often made selective for a particular anion by the use of appropriately positioned hydrogen bonding sites. There are also numerous examples of anion receptors chemically designed to promote hydrogen-bonding interactions. In addition to electrostatic and hydrogen-bonding interactions, anion binding via Lewis acidic interactions has also been widely researched. Anions donate an electron pair in forming a hydrogen bond with a hydrogen bond donor, and in the same way a Lewis acid is capable of accepting a pair of electrons. Trigonal three coordinate boron acts as a strong Lewis acid, possessing only six electrons in its outer shell and a formally vacant p_z-orbital into which an electron pair can be donated from an anion/Lewis base thereby completing its octet. These guest-host interactions will be discussed in greater detail with examples from the literature in the following sections.

1.2.1 Anion recognition via electrostatic and hydrogen bonding interactions

As discussed, electrostatic and hydrogen bonding interactions have been widely used in the development of anion receptors, many examples of systems using purely hydrogen bonding interactions are known.[4] In contrast, relatively few systems are known to achieve anion complexation through electrostatic interactions alone. Using a positive charge to bind a negative charge is an obvious method of anion complexation, although it does cause a design setback, in that positive charges will repel each other, hence to incorporate an array of positive charges into a receptor they need to be constrained within a rigid framework. Early synthesis of a purely electrostatic receptor featured a quaternized analogue of the well-known ammonium-based electrostatic/hydrogen-bonding macrocyclic receptors, achieved by Schmidtchen in an attempt to minimise the influence of pH on ammonium-based receptors and to investigate the effect of hydrogen bonding on the affinity of the host for the guest.[5] Hossain and Ichikawa reported a similar species,[6] featuring a quarternized ammonium based binding cavity (Figure 1.3).

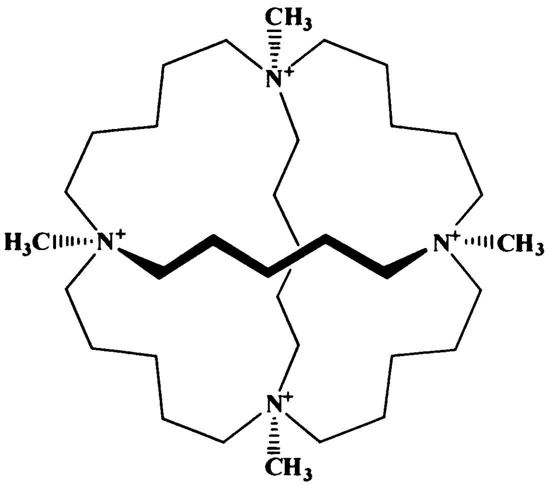

Figure 1.3 A macrotricyclic receptor for electrostatic fluoride binding.

The fluoride anion is encapsulated within the binding cavity created by constraining four positively charged ammonium groups within a macrocyclic framework. Fluoride is strongly bound by the electrostatic interaction with the oppositely charged ammonium groups. In this case, selectivity is governed by the size of the cavity, which can be easily tuned, by alteration of the cavity size, to be selective for a number of different anions. Previous reports of halide inclusion by larger analogous receptors featuring quaternary ammonium ions,[7] led the authors to the conclusion that fluoride selectivity could be achieved by decreasing the size of the binding cavity. The binding chemistry between the tetra-ammonium host and fluoride in aqueous solution was assayed by ^{19}F NMR using $[^{n}Bu_4N]^+F^-$ as the source of fluoride. ^{19}F NMR spectra indicated a fluoride-encapsulated species (δ_F = -28 ppm), evident as an upfield shift from free solvated F^- (δ_F = 0 ppm); the stability constant of the resulting complex was determined from the ^{19}F NMR data ($K \sim 1.5 \times 10^4$ M^{-1}).

Although hydrogen-bonding receptors can have some disadvantages, for example pH dependence in some cases, an array of hydrogen bonds can offer a complementary interaction to electrostatics, and there have been many literature reports that have capitalised on including both types of interaction in the design of anion receptors. One of the earliest examples of this kind of cooperative binding was reported by Graf and Lehn in 1976, featuring a protonated cryptate (Figure 1.4) that was observed to bind F^-, Cl^- and Br^- anions.[8]

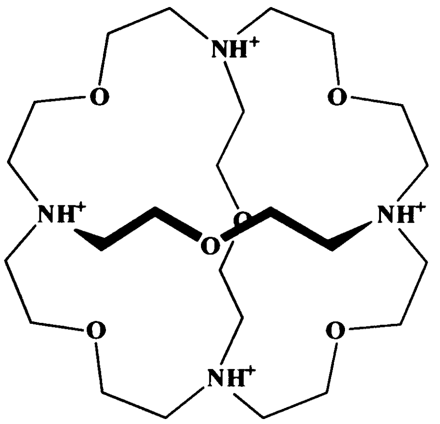

Figure 1.4 Protonated cryptate capable of halide encapsulation.

The protonated cryptate was found to achieve effective anion encapsulation, making use of both hydrogen bonding and electrostatic interactions. During initial studies it was found that this receptor binds chloride anions, resulting in the formation of the guest-host complex as evidenced by significant changes in the ^{13}C NMR spectrum. Analogous binding was observed upon treatment of this receptor with fluoride and bromide anions. A subsequent study by Metz *et al.*[9] solved the X-ray structure of the chloride cryptate; close inspection of the structure revealed that the anion is bound via a tetrahedral array of N-H•••X hydrogen bonds. These studies were followed up to include alternative cryptand systems, incorporating an array of $^+NH_2$ groups within a macrocycle (Figure 1.5), thereby providing a receptor capable of increased hydrogen bond donation.[10]

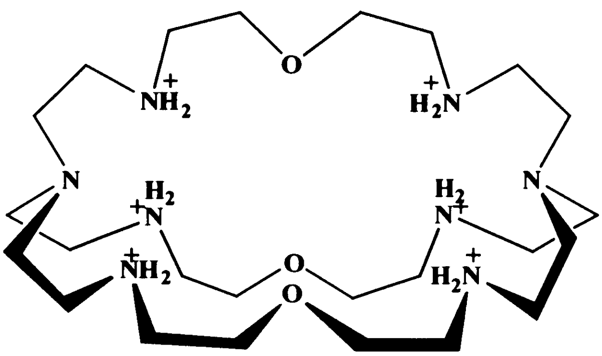

Figure 1.5 Protonated cryptate systems for the binding of F^-, Cl^-, Br^- and N_3^- anions.

Crystal structures of the fluoride, chloride, bromide and azide guest-host complexes were obtained, however the X-ray diffraction data revealed that the different anions are bound in different modes; the smaller fluoride anion is bound within just one half of the binding cavity, coordinated to four ammonium centres in a tetrahedral fashion. This observation indicates that the fluoride anion is too small to bind to each of the six protons within the cavity. By contrast, the larger chloride and bromide anions were found to bind via an octahedral array of hydrogen bonds to the six ammonium centres, almost precisely located on the N-N axis. The linear azide anion is found to bind on the N-N axis, with each terminal nitrogen forming three hydrogen bonds with three ammonium centres. The increased number of hydrogen bond donors has allowed the additional binding of halide ions outside the binding cavity. The authors went on to pursue the development of a fluoride specific polyammonium receptor, via alteration of the size of the binding cavity. The resulting octaaza-cryptand system displayed high fluoride selectivity; X-ray diffraction studies revealed that the fluoride anion is bound to six ammonium centres within the cavity.[11]

Since the early reports of the coordination chemistry of polyammonium macrocycles by Lehn *et al.* research interest in this field has been fast evolving and today includes a huge variety of different receptors, from acyclic to mono-, bi- and polycyclic species. As discussed, protonated amines make use of both hydrogen bonding and electrostatic interactions simultaneously, however the development of receptors that function only through hydrogen bonding is an equally vast area of research interest. It is important when designing an anion receptor based on hydrogen bonding interactions, to appreciate the geometry of the anion and to design the receptor accordingly. It is crucial that hydrogen bonding sites are suitably orientated, with the hydrogen atoms in a convergent manner, and the first example of a purely hydrogen bonding based receptor illustrates this principle perfectly. Reported by Spergel *et al.* this receptor features three convergent amide protons directed into the cavity (Figure 1.6).[12]

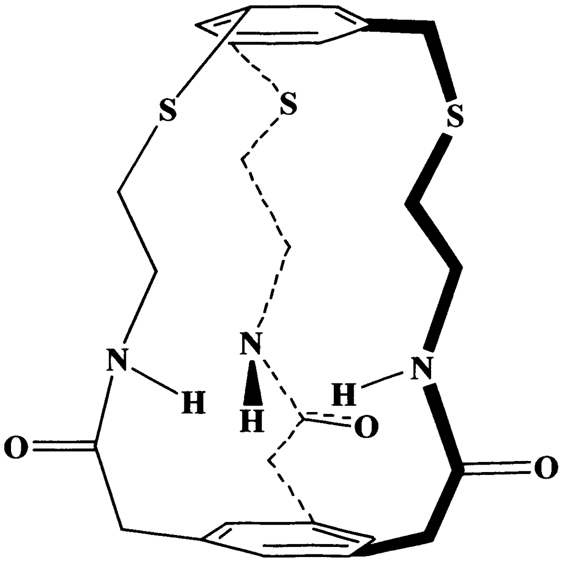

Figure 1.6 Amide-based hydrogen bonding receptor for fluoride.

When the receptor was treated with a source of fluoride, ^1H and ^{19}F NMR provided evidence that the receptor binds fluoride anions, although the studies did not indicate whether the three amide hydrogen bond donors hold the fluoride anion within the cavity. Although this receptor was treated with fluoride, the trigonal arrangement of hydrogen bond donors is particularly complementary to trigonal planar and tetrahedral anions, for example phosphate anions, the binding of which is of biological relevance. Since this initial report, the development of neutral amide-based receptors for anion encapsulation has rapidly expanded and many examples of these types of receptors are now known.[13]

Another approach to anion binding via hydrogen bonding has been established, using not amide protons but the pyrollic protons of a pyrrole-based receptor. Early work by Sessler *et al.* in developing pyrrole-based anion receptors with built-in chromophores led to the use of these compounds as colorimetric anion sensors,[14] making use of both UV/Vis and fluorescence spectroscopies to assay anion binding. The application of fluorescence and UV/Vis spectroscopies in monitoring anion binding is discussed in detail in Section 1.3. Subsequent research by Camiolo and Gale was aimed at modification of the pyrrole framework to incorporate longer and bulkier functional groups, to create "super-extended cavities" (Figure 1.7).[15]

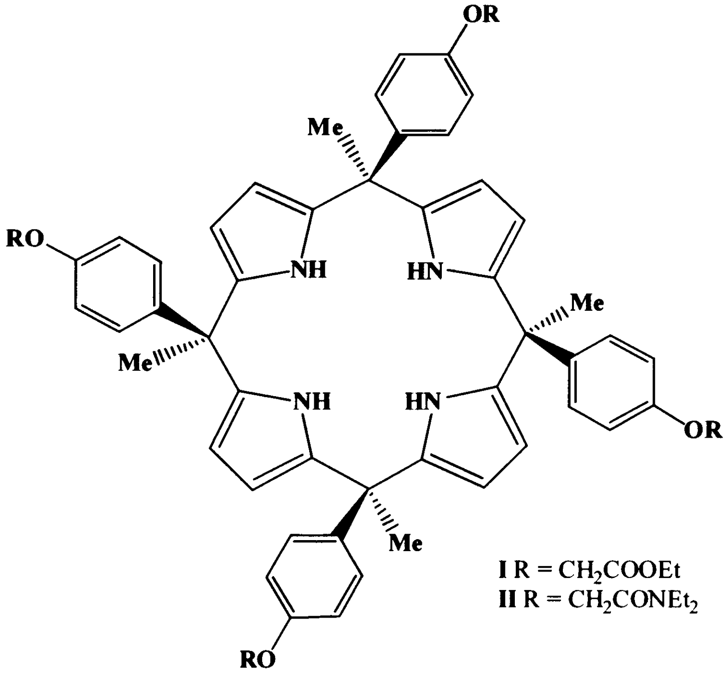

Figure 1.7 Fluoride specific calix[4]pyrrole-based receptors **I** and **II**.

These macrocycles have displayed remarkable selectivity for fluoride over other anions in solution. Solution binding properties were investigated by ^{1}H NMR titration experiments in d$_6$-DMSO; it was found that addition of excess Cl^-, Br^-, I^-, $H_2PO_4^-$ and HSO_4^- anions caused no changes in the ^{1}H NMR spectra. On addition of fluoride anions however, new resonances were observed in the ^{1}H NMR spectra, giving evidence of interaction with fluoride. Furthermore, coupling between the NH protons of calix[4]pyrrole and the bound fluoride is observed in room temperature ^{19}F NMR spectra, with coupling constants of 47 Hz determined for both compounds **I** and **II**. The bulky functional groups pendant to the calix[4]pyrrole ring resemble the array of phenol groups present in the lower-rim of an un-functionalised calixarene in the cone conformation. Calix[4]arenes consist of cyclic arrays of phenol groups linked via methylene groups, which can adopt four different geometries depending on whether one or more or none of the phenol groups is directed downwards. For example *p*-tert-butylcalix[4]arene typically adopts the cone geometry, in which all four phenol OH groups are convergent forming a lower-rim capable of anion binding via hydrogen bonding interactions. Both the lower and upper rims may be easily substituted to incorporate alternative functional groups. The aromatic cavities of these species can function as effective cation receptors, however it is the anion-binding properties of these compounds that is particularly relevant to this work.

A system featuring two adjoined calix[4]arene fragments linked via covalent amide bonds was reported by Beer *et al* (Figure 1.8).[16]

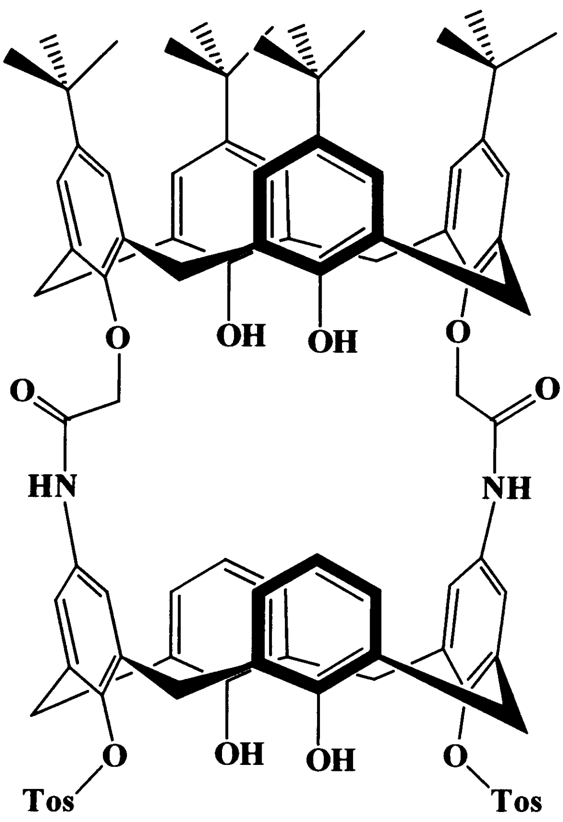

Figure 1.8 Bis-calix[4]arene receptor for chloride and fluoride inclusion.

Anions are bound via hydrogen bonding interactions with the phenol OH and amide protons, the two amide groups encourage binding within the cavity due to their positioning, between the two calix[4]arene rings. Anion binding studies revealed that the chloride and fluoride anions are bound by the receptor, but that the cavity is too small to bind hydrogen sulphate and di-hydrogen phosphate anions. ^{1}H NMR titration experiments were performed revealing that the host-guest complex forms in a 1:1stoichiometry. Stability constants for each host-guest complex were determined from this data, the receptor having nearly an order of magnitude greater selectivity for fluoride (1330 M^{-1}) over chloride (172 M^{-1}) anions. By comparison the interaction of the receptor with hydrogen sulphate and di-hydrogen phosphate is very much weaker. The difference in stability constants is probably attributable to anion size; fluoride has an ionic radius of 1.33 Å, where chloride has an ionic radius of 1.81 Å, hydrogen sulphate, for example, has a larger ionic radius of 2.35 Å and di-hydrogen phosphate larger still. A complete review of electrostatic and hydrogen bonding receptors is beyond the scope of this chapter, representative examples of such receptors have been discussed. For further information on electrostatic and hydrogen bonding receptors see, for example, reviews published by Beer and Gale.[17]

1.2.2 Anion recognition and binding via Lewis acid/base interactions

A well-established alternative route to anion recognition and binding uses Lewis acid/base interactions. Although less exploited in research effort, there has been growing interest in this approach. Incorporation of a Lewis acidic moiety into a potential anion sensor may allow direct recognition by a neutral host. As discussed, trigonal three-coordinate boron acts as a widely tunable Lewis acid possessing only six electrons in its outer shell and a formally vacant p_z-orbital into which an electron pair can be donated from an anion/Lewis base. Although boron has found application in an extensive range of receptors to date, other Lewis acid systems have been reported, making use of alternative Lewis acids such as mercury, silicon, aluminium, gallium and tin. Chelation of anions has been a particular focus in research, due to the potential for added stability of the resulting host-guest complex. This section aims to summarise some of the most significant publications regarding both simple binding and chelation of anions via Lewis acid/base interactions.

One of the earliest reports of anion chelation by a Lewis acid-based receptor was published by Shriver *et al.* in 1967.[18] This early report sparked much research interest in the chelation of anions via Lewis acids and the role the chelate effect could play in bringing increased stability to the host-guest complex. The authors found that 1,2-*bis*(difluoroboryl)ethane was capable of chelating a methoxide anion (Figure 1.9).

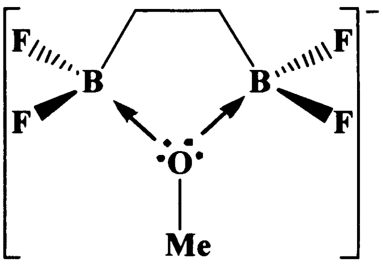

Figure 1.9 A methoxide adduct of 1,2-*bis*(difluoroboryl) ethane

In order to encourage chelation it was thought that the Lewis base (anion) must possess two lone pairs of electrons on a single atom to be capable of simultaneous interaction with two boron centres, and have sufficient basicity so as to interact with both boron centres but not be a strong enough base to effect boron – halogen bond cleavage. Hence the choice of oxygen containing bases such as ethers, ketones and the methoxide ion; the investigation spanned interaction of this species with each of these bases. Ethers and ketones were found not have sufficient basicity to coordinate to both boron centres. However the methoxide anion provided the perfect balance and was found to interact strongly in a chelating fashion with 1,2-bis(difluoroboryl)ethane (Figure 1.9).

The significant research effort of Katz *et al.* offered in many publications, has provided some considerable insight into the field on anion recognition by Lewis acid/base interactions. One early report in 1985 details the development of 1,8-*bis*-(dimethylboryl)napthalene framework for the chelation of hydride. By analogy with the 1,8-di(amino)napthalene system, this Lewis acid system is known as the hydride sponge (Figure 1.10).[19]

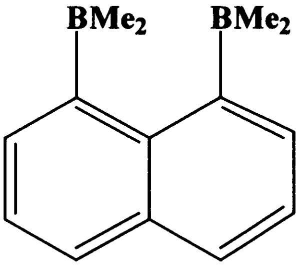

Figure 1.10 "Hydride sponge"

Binding was investigated by titration with KEt_3BH and monitored by ^{11}B NMR. Binding of a hydride anion is evident from the observed upfield shift, from the hydride-free compound at $\delta_B = 79$ ppm, to the host-guest complex at $\delta_B = 5$ ppm. The hydride-bound species was also characterised by X-ray diffraction, which revealed the hydride anion to be un-symmetrically situated between the two boron centres. Host-guest complexes of this rigid bidentate Lewis acid with fluoride and hydroxide anions have also been characterised by NMR spectroscopy. The chelate effect plays a significant role in the stability of these compounds, and this was tested by placing 1,8-*bis*-(dimethylboryl)napthalene in competition for a halide anion already bound to another non-chelating Lewis acid receptor, dimethyl-1-napthylborane. 1,8-*bis*-(dimethylboryl)napthalene was found to be capable of abstracting the halide from the competing Lewis acid receptor, demonstrating the role of the chelate effect. The powerful Lewis acidity displayed by this species is described as being a result of steric repulsion between the methyl groups, forcing the boryl groups out of conjugation with the naphthalene ring.

In subsequent work Katz went on to provide the first definitive evidence of a chloride ion bridging between two trigonal boron centres. It was observed that, whilst the hydride sponge was capable of chelating hydride, fluoride and hydroxide anions, it was not a powerful enough Lewis acid to chelate chloride anions. This observation prompted the design of a host capable of chelating chloride and Katz reported 1,8-*bis*-(dichloroboryl)napthalene (Figure 1.11).[20]

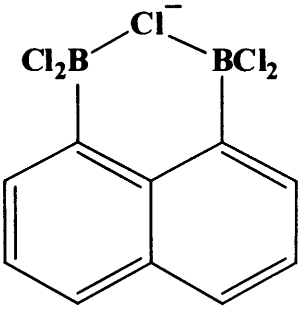

Figure 1.11 Chelation of chloride by 1,8-*bis*-(dichloroboryl)napthalene

Chloride binding studies were performed using [PPh_4]Cl and [PPN]Cl in dichloromethane, and the nature of the chloride-bridged product was confirmed both by X-ray diffraction and ^{11}B NMR. More recent research by Katz has led to the development of the first rigid di-boron host species for di-basic guests. This synthetic study details the synthesis of 1,8-anthracenediethynylbis(catecholboronate) and its role as a host for di-basic guests (Scheme 1.1).[21]

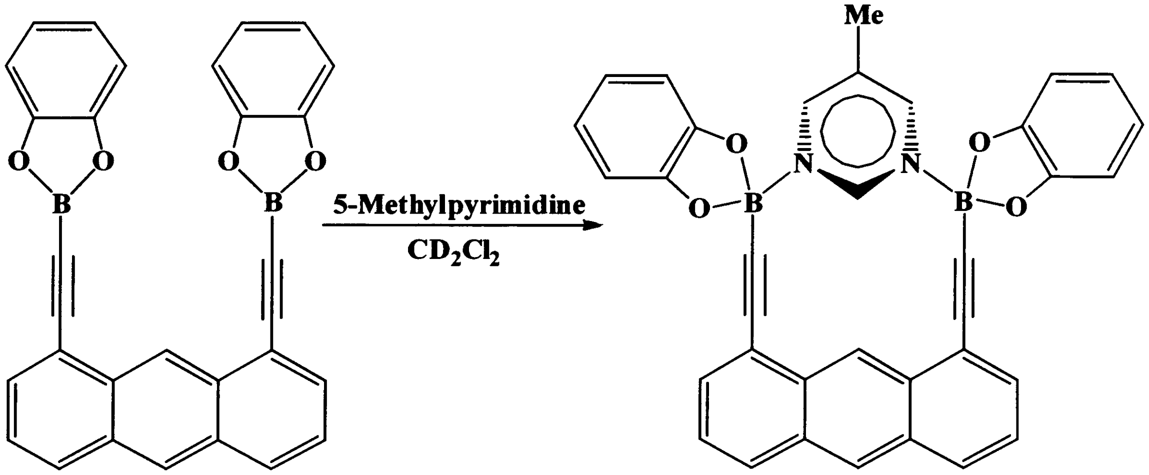

Scheme 1.1 1,8-anthracenediethynylbis(catecholboronate)

The aim of this research was the design of a host species with a larger cavity to support larger guest species, hence the use of the anthracene framework. This very rigid framework offers a boron-boron separation of about 5 Å. Molecular models of 1,8-anthracenediethynylbis(catecholboronate) were made and indicated that with neutral guests such as pyrimidine, featuring two basic sp^2 hybridised atoms in 1,3 positions, binding is almost strain free. Katz investigated the interaction of 1,8-anthracenediethynylbis(catecholboronate) with 5-methylpyrimidine; binding was assayed by ^1H NMR titration in CD_2Cl_2 by monitoring changes in the chemical shifts of the aryl protons. The proton titration of the host treated with 5-methylpyrimidine displayed a distinct slope change after 2.5 equivalents of 5-methylpyrimidine were added. Two binding constants were determined from the NMR data, the first for the 1:1 bridging complex was $K_1 = 130\ M^{-1}$; further addition of 5-methylpyrimidine resulted in the formation of a 2:1 complex, which had a substantially smaller binding constant ($K_2 = 40\ M^{-1}$). Comparative studies were carried out with thiazole (one basic atom) and 4-methylpyrimidine (one sterically hindered basic atom), both of which displayed no bridging interaction with the host from ^1H NMR titration studies, affirming the conclusion that this host was the first rigid Lewis acid-based receptor for dibasic guests.

Jacobson and Pizer have carried out theoretical studies concerning anion binding by macrobicyclic and macrotricyclic organoboron macrocycles. Molecular orbital calculations were undertaken with the intention of clarifying the structures of a range of organoboron species with bound hydride, chloride, fluoride and superoxide (Figure 1.12).[22]

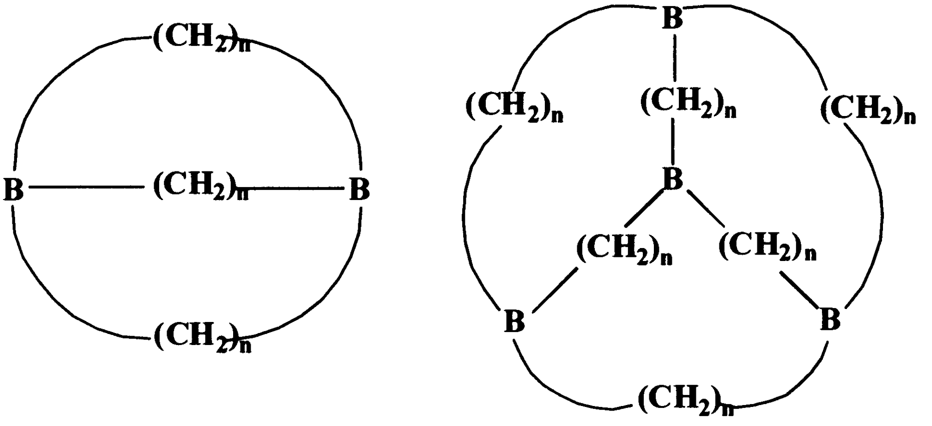

n = 3-10 *n* = 2-4

Figure 1.12 Potential macrobicyclic and macrotricyclic organoboron anion receptors

These investigations led to the interesting conclusion that where the macrobicyclic compounds are concerned, the ionic radii of the anion and its compatibility to a particular cavity size do not *solely* govern specificity of a certain macrocycle for a certain anion. On the basis of calculated standard enthalpies of reaction, the computational results indicated that hydride (2.08 Å), for example, despite being larger than fluoride (1.33 Å) was actually capable of fitting into a smaller cavity. For example, hydride was bound to a comparable extent to hosts featuring n = 4-6, fluoride by hosts with $n = 5$ and 6, chloride by hosts with $n = 6$ and 8 and superoxide to hosts with $n \geq 4$. In the case of this macrobicycle, anions were found to bridge between the two boron centres whereas with the macrotricyclic compound, anions were found to bridge between more than two boron centres. The macrotricyclic host revealed greater selectivity for hydride and superoxide, both of which favoured hosts with $n = 2$. Fluoride and chloride were found to bind predominantly to hosts with $n = 3$. Although a hydride anion bound within a cavity smaller than its own ionic radii is a stable species, a hydride anion bound within a larger cavity has been proven a more stable species; this observation was thought to be as a result of lessened rehybridisation at the boron centre. In all cases it was concluded that anion coordination occurs with a change from sp^2 to sp^3 hybridisation at boron and that charge transfer of electron density from the anion to the Lewis acid centre allows anions to fit into cavities that are smaller than their ionic radii.

The use of borylated-metallocene frameworks as the basis for anion receptor molecules is an exciting area of research although not as thoroughly investigated as some alternative frameworks. Borylation of both the upper and lower cyclopentadienyl rings of a metallocene system provides a receptor that could potentially be tuned, either by substitution at boron, by the use of a specific metallocene that has a precise B•••B separation, or a combination of both of these factors, to provide specificity for a range of anions. A borylated-metallocene based receptor for anions was reported by Herberich, Fischer and Wiebelhaus featuring a bis(boryl)cobaltocenium ion, which displays unusual variability in its interactions with anions (Scheme 1.2).[23]

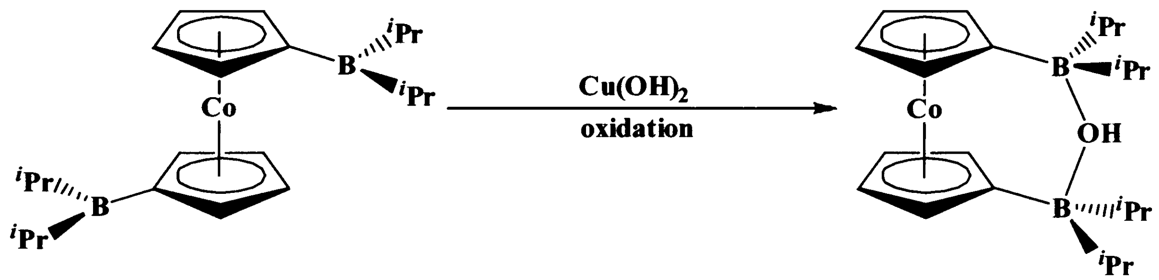

Scheme 1.2 Hydroxide binding by the bis(boryl)cobaltocenium ion

The receptor 1,1'-bis(diisopropylboryl)cobaltocene was prepared by reaction between $C_5H_4B^iPr_2$ with $CoBr_2$.DME in the presence of LiCp. Subsequent oxidation of the product with $Cu(OH)_2$ afforded a host-guest complex featuring an hydroxide anion bridging between two boron centres, as determined via an X-ray diffraction study and NMR spectroscopy (^{1}H and ^{11}B). In contrast, structural characterisation of the oxidation product with C_2Cl_6 revealed an alternative binding mode, in which one chloride anion is bound to one boron centre whilst the remaining boron centre retains its trigonal geometry. ^1H and ^{13}C NMR spectra remain unchanged upon cooling down to –80°C, hence it was concluded that rapid chloride exchange between the two boron centres was occurring on the NMR timescale.

Boron has been widely exploited as a Lewis acid for the binding of anions. Less widely exploited in this application are the alternative Lewis acids such as tin, mercury, silicon and aluminium, both in homo- and heteronuclear systems. An innovative synthetic study detailing the use of tin macrocycles for encapsulation of halide anions was published by Newcombe *et al.* reporting the size selective binding of chloride and fluoride by macrobicyclic hosts containing two Lewis acidic tin binding sites. Results suggested that binding occurs within the cavity (Figure 1.13).[24]

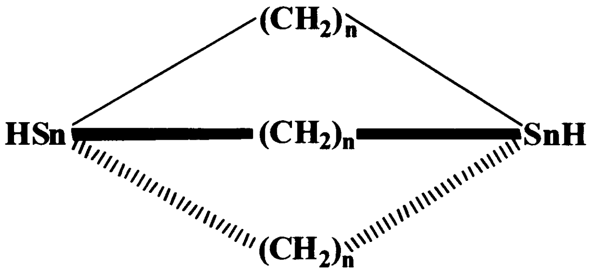

III ***n* = 6**
IV ***n* = 8**

Figure 1.13 Macrobicyclic organotin receptors for halide encapsulation

In this publication by Newcombe *et al.* host **III** (n = 6) was found to have an inappropriate cavity size for chloride encapsulation. On closer inspection of the crystal structure of the host, and observation of a tin – tin separation of 5.25 Å, it was predicted that this species might exhibit size selectivity for the fluoride anion with a complementary diameter of 2.6 Å. The guest was treated with tetrabutylammonium fluoride and the ^{119}Sn NMR spectra indicated a Sn–F interaction. A binding constant for this host-guest complex of 1.2 x 10^4 M^{-1} was determined, a much stronger interaction than that determined for host **IV** ($n = 8$) of 7 M^{-1}. Crystallographic data for host **IV** revealed that chloride and fluoride are bound within the cavity with differing modes of interaction. The X-ray structure of the chloride host-guest complex indicated that the chloride anion is bound with greater strength to one tin atom than the other, forming one trigonal-bipyramidal tin centre with an Sn–Cl separation of 2.61 Å, whilst weakly bound to the other tin atom, which remains in a distorted tetrahedral environment with an Sn–Cl distance of 3.38 Å. The fluoride host-guest complex was found to exhibit roughly equal Sn–F bond lengths (2.12 Å and 2.28 Å) in an almost symmetrical structure. In this host-guest complex both tin atoms are in trigonal bi-pyramidal environments.

A more recent publication by Newcombe *et al.* extends the application of tin macrobicycles within the field of anion binding to incorporate binding of chloride, fluoride and bromide anions.[25]

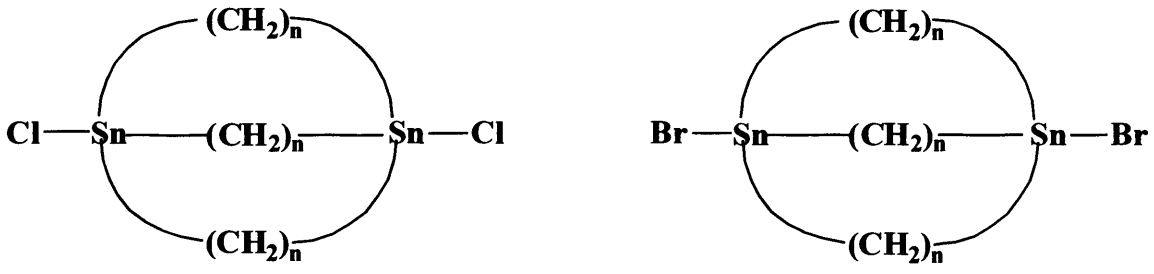

Figure 1.14 Tin macrobicycles for chloride and bromide guest species

($n = 6$ to $n = 12$)

Characterisation of the fluoride and chloride complexes was provided by solid-state ^{119}Sn NMR spectroscopy and X-ray diffraction. Upfield chemical shifts in the ^{119}Sn NMR spectra for the $n = 7$ through $n = 12$ macrobicycles on exposure to tetrahexylammonium chloride were observed, which are symptomatic of increased charge at tin and hence anion coordination. Treatment of the bromide-functionalised hosts with tetrahexylammonium bromide was found to affect a similar upfield shift in the ^{119}Sn NMR spectra, indicating the existence of a bromide bound host-guest species. Job's method was applied to the NMR data to determine a binding stoichiometry of 1:1 in all cases. Temperature dependant dynamic NMR behaviour was observed for the bicyclic hosts, simulations of the spectra measured at various temperatures provided rate constants for both the binding and dissociation of the anionic guest species. Binding constants were found to reflect the complementary fit of chloride and bromide into appropriate cavity sizes, for example the binding equilibrium constant for the chloride $n = 2$ host (0.29 M^{-1}) is much smaller than the binding equilibrium constant for the chloride $n = 12$ host (6.00 M^{-1}), reflecting the increased compatibility between the chloride anion and the binding cavity in the larger ($n = 12$) host.

A synthetic study detailing the anion binding properties of Lewis acidic silicon centres was published by Tamao *et al.*[26] In a later publication the potential of these compounds for fluoride chelation was investigated, detailing the anion binding properties along with calculation of binding constants for ortho-*bis*–(fluorosilyl) benzenes treated with fluoride.[27]

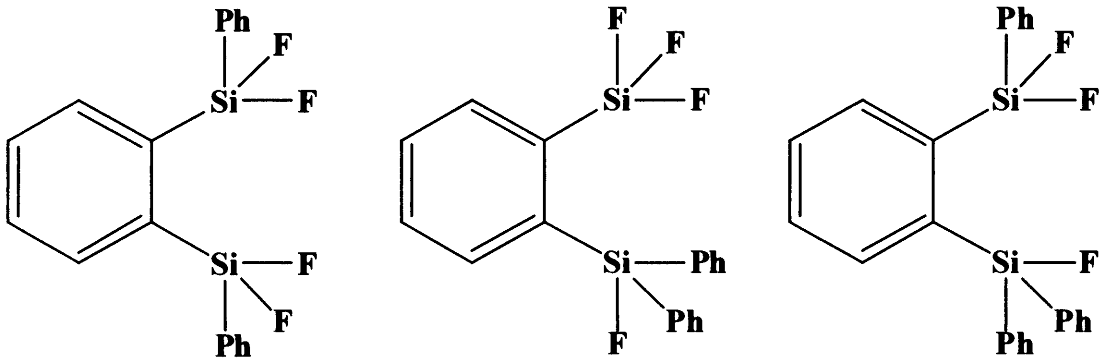

V **VI** **VII**

Figure 1.15 Ortho-*bis*–(fluorosilyl) benzenes

The binding constant of receptor **V** was compared with two alternative receptors **VI** and **VII** to probe the effect of varying the substitution pattern at the silicon centre on fluoride binding properties. The binding constants of these host-guest complexes were measured via ^{1}H and ^{19}F NMR competition experiments with a fluoromonosilane ($PhMeSiF_2$) receptor of known binding constant. The extent of interaction between each host and fluoride was estimated by noting which hosts were capable of competing successfully for fluoride in the presence of fluoromonosilane. Equilibrium constants between each host and $PhMeSiF_2$ were then measured by monitoring the chemical shifts of the $Si–CH_3$ protons of $PhMeSiF_2$. Host **VII** was found to have the weakest binding constant ($K = 5.9 \times 10^5$ M^{-1}), while host **V** was found to have a binding constant of ($K = 5.9 \times 10^7$ M^{-1}) and host **VI** the largest binding constant with fluoride ($K = 1.1 \times 10^9$ M^{-1}). From these results it was concluded that the anion binding ability of the bidentate silanes increases with increasing fluoride substitution at the silicon centres. In the case of hosts **V** and **VI**, where the total number of fluorides is the equal, the asymmetric host (**VI**) is a stronger Lewis acid. This report provided evidence at that time of the strongest binding constant for a host–guest interaction with fluoride.

Hawthorne and Zheng have explored the use of mercury as the Lewis acidic moiety within macrocycles designed specifically as host molecules for anion complexation.[29] These macrocycles featured three or more icosahedral *ortho*-carborane cages with three or more interlinking mercury atoms; examples of these "mercuracarborands" are shown in Figure 1.16.

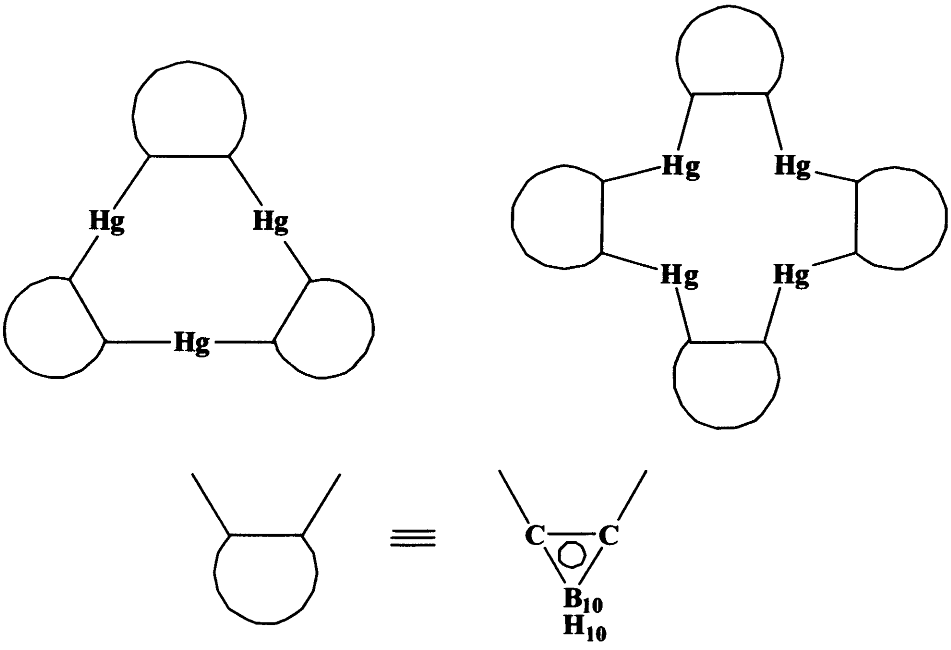

Figure 1.16 Mercuracarborands for halide complexation

Mercury displays many advantageous features that support its utility in the field of anion encapsulation. The linear geometry displayed by some Hg(II) species in cyclic structures provides host species with large binding cavities that can accommodate large anions. Also Hg(II) species are stable in the presence of both air and water, a very beneficial feature for a potential halide receptor. Lastly, it is found that in diorganomercury compounds, Hg(II) forms two σ bonds which are essentially linear, whilst the vacant p-orbitals at Hg(II) remain perpendicular to the plane of the σ-bonds thus retaining substantial Lewis acidity. The tetrameric host has proven capable of binding chloride anions, the encapsulation of two iodide anions was also observed with this host. These halide coordination studies were monitored closely by ^{199}Hg NMR spectroscopy. Anion encapsulation was confirmed by X-ray diffraction studies, from which the bound chloride anion was shown to interact equally with all four mercury centres; the two iodide ions located above and below the plane of the mercuracarborand ring, were also shown to interact with all four mercury centres. Complexation of a molecule of acetonitrile was observed with the trimeric species. The electron withdrawing nature of the carborane cages and the Lewis acidity of the mercury centres combined with the large binding cavity presents a very versatile host for anions.

As previously demonstrated in the work of Hawthorne and Zheng on mercuracarborands, the ability of mercury centres to act as electron acceptors is enhanced with the use of electron withdrawing backbones. This principle is again illustrated in the work of Tschinkl *et al.* in a publication detailing the preparation of 1,2–*bis*(chloromercurio)tetrafluorobenzene and its ability to encapsulate basic substances featuring terminal oxo groups. These studies led to isolation of the first chelate complex between a ketone and a bi-functional Lewis acid (Scheme 1.3).[29]

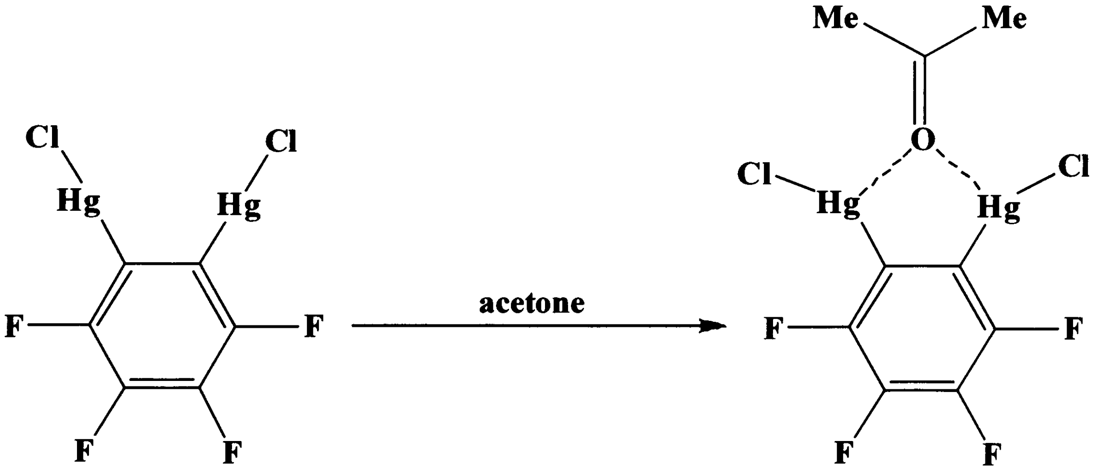

Scheme 1.3 Host-guest chemistry of 1,2–*bis*(chloromercurio)tetrafluorobenzene with acetone

Binding studies were performed in acetone due to low solubility in less polar solvents; DMSO and DMF were added in increments to the solution of 1,2–*bis*(chloromercurio)tetrafluorobenzene. Binding was monitored via ^{199}Hg NMR; a significant downfield shift was observed, indicating the displacement of formerly bound acetone for DMSO and DMF donors. Curves were plotted showing ^{199}Hg NMR shift against concentration of DMSO and DMF, both curves were observed to rapidly reach a plateau; this behaviour is characteristic of the quantitative formation of host – guest complexes. Curves were fitted on the basis of two hypothetical models, one for formation of a 2:1 host – guest complex and the other for formation of a 1:1 host-guest complex. The latter model was found to provide a more stable refinement along with reliable stability constants. Although calculated stability constants were found to be fairly low this was thought to be due to acetone competing with DMSO and DMF for the binding site, since the acetone-bound adduct was obtained as a by–product in crystallisations of the DMSO and DMF adducts from acetone solution [K(DMSO) 8.0 M^{-1} > K(DMF) 1.8 M^{-1}]. These observations follow the relative donor strength associated with each guest species (DMSO > DMF > acetone). Single crystal X-ray diffraction served as further confirmation of the structures of the acetone and DMF host-guest complexes; in both cases the guest species was shown to be bound in a bidentate fashion via the carbonyl oxygen to both Lewis acidic mercury centres.

Tsunoda and Gabbai have extended the use of mercury-based Lewis acidic receptors to polyfunctional organomercurials, in the preparation of a trimeric perfluoro–*ortho*-phenylene mercury receptor for dimethylsulphide (Figure 1.17).[30]

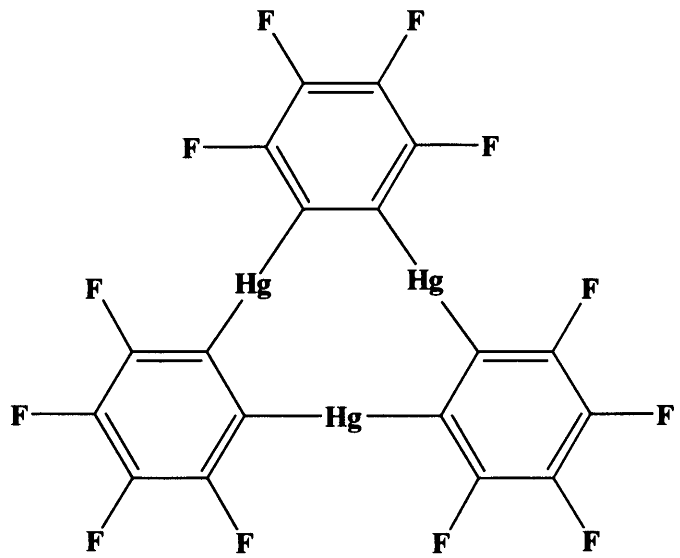

Figure 1.17 Trimeric perfluoro–*ortho*–phenylene mercury receptor

Characterisation of a host-guest complex displaying unusual hexacoordination of dimethylsulphide was reported. X-ray diffraction studies revealed two modes of coordination of the dimethylsulphide molecule to the tridentate receptor. Slow concentration of a dimethylsulphide solution of the receptor yielded crystals featuring four molecules of dimethylsulphide simultaneously bound to the trifunctional Lewis acid; two dimethylsulphide molecules were bound as terminal ligands coordinated each to a single mercury centre, the remaining two dimethylsulphide molecules were bound above and below the plane of the ring, each interacting symmetrically with three mercury centres (**VIII** - Figure 1.18). The receptor was further treated with an excess of dimethylsulphide, followed by slow evaporation of solvent, which yielded an adduct featuring one dimethylsulphide molecule hexacoordinated to two receptor molecules (**IX** - Figure 1.18).

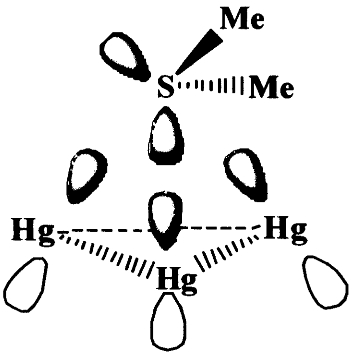

VIII

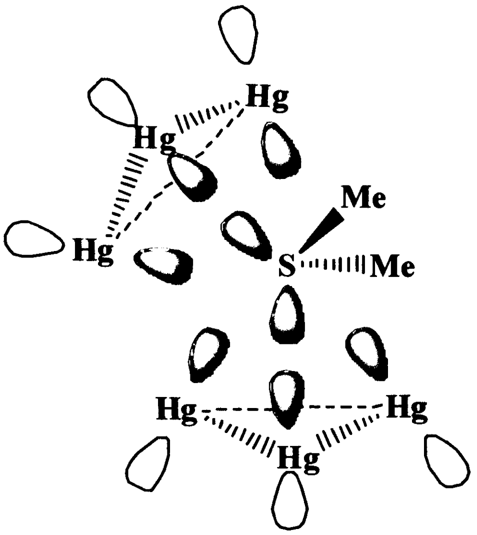

IX

Figure 1.18 The alternative binding modes **VIII** and **IX** of the trimeric perfluoro–*ortho*–phenylene mercury receptor with dimethylsulphide

Dimethylsulphide typically acts as a mono or bidentate bridging ligand, thus these findings give evidence of an unusually high coordination number for a neutral dialkyl sulphide ligand of this type.

1.3 Physical detection of anions by Lewis acidic receptors

Physical detection of anions is an area of research that has been rapidly expanding and there are numerous publications detailing the syntheses of receptors capable of displaying one or more physical outputs upon anion complexation. The word ‘receptor’ refers to a supramolecular structure capable of binding a guest molecule. A receptor is classified as a sensor if it can report the presence of the guest species by some physical means. The illustration below depicts the fundamental role of a sensor (Figure 1.19)

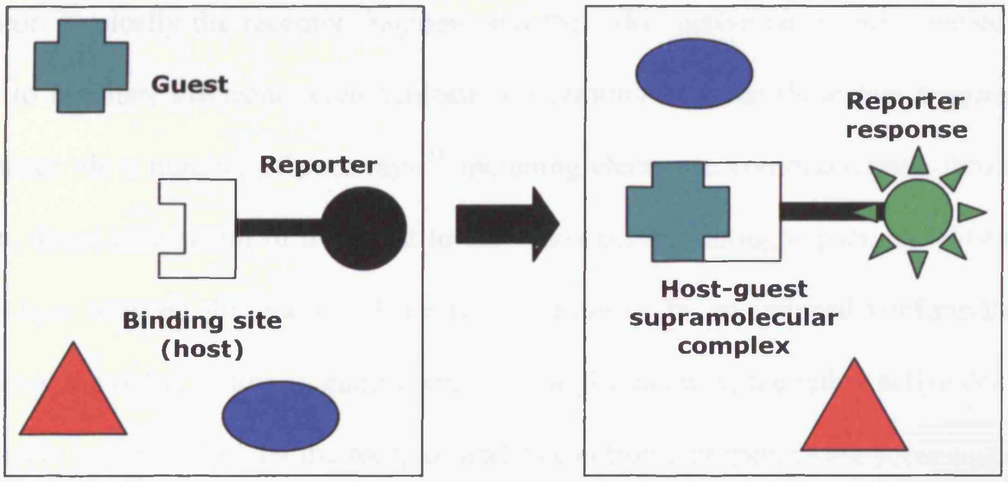

Figure 1.19 Illustration of the role of a sensor.

A common method applied to sensor production involves the incorporation of both a receptor function and a reporter group within the same molecule. The reporter function is chosen according to its specific spectroscopic or electrochemical properties, which are altered upon the binding of a guest to the receptor fragment. For example a response may be generated by quenching the fluorescence of a fluorescent sensor, by inducing a visible colour change or an electronic change detectable by an incorporated redox-active fragment via electrochemical methods. Ideally a sensor must be specific to a particular guest species to ensure that a false response never occurs, i.e. sensors are typically designed to affect specific binding of a certain anion. This section aims to summarise some publications detailing the preparation and functioning of sensors displaying a range of physical outputs.

1.3.1 Electrochemical detection of anions

Electrochemical methods can provide a significant insight into electron transfer processes involved in redox reactions. Sensors that display an electrochemical output can be prepared by attachment of a redox-active moiety to a receptor. Typically the receptor fragment and the redox active centre are coupled in order to facilitate electronic communication. Coupling between these two fragments can occur via a number of pathways,[31] including electronic communication through bonds, direct attachment of the guest to the redox centre, through-space electrostatic interaction between the guest and the redox centre or by an induced conformation change at the redox centre on guest complexation. In this way, the redox active centre can detect anion binding by the receptor and its electronic properties are subsequently altered, affecting a change in the electrochemical features of the redox active centre. Amongst the vast range of redox-active centres ferrocene is by far the most commonly used, having good solubility properties, air/moisture/heat stability and a well understood electrochemical response. A commonly used electrochemical technique for monitoring the redox reactions of ferrocene is cyclic voltammetry; this analytical technique has been applied in many publications detailing ferrocene-based anion sensors.

Ferrocene-based anion receptors using various host-guest interactions have been reported, for example, utilizing both hydrogen-bonding interactions and Lewis acid/base binding motifs. A sensor combining the receptor functionality of calix[4]arene with the redox-active centre of ferrocene has been reported by Beer *et al.*[32] The anion complexation behaviour of the tetra-ureaferrocenecalix[4]arene (Figure 1.20) sensor towards chloride anions was investigated by use of cyclic voltammetry, along with NMR spectroscopy.

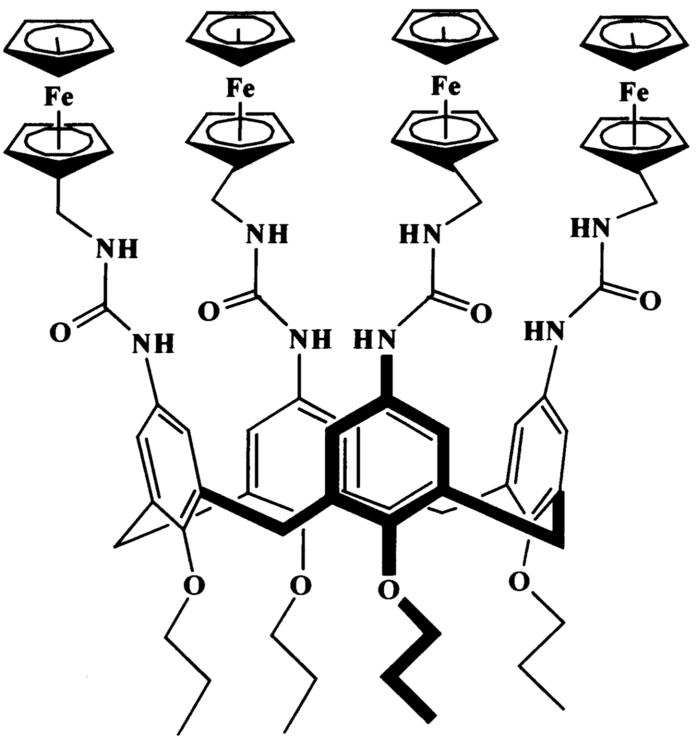

Figure 1.20 Electrochemical tetra-ureaferrocenecalix[4]arene sensor for chloride

Prior to addition of anionic guests, cyclic and square wave voltammetry techniques revealed that this receptor displays a single virtually reversible oxidation, implying that the four ferrocene fragments are independent of each other and are oxidised at the same potential. Sequential addition of anionic guest species resulted in a cathodic shift in the oxidation potential of the ferrocene redox centres. A negative shift in redox potential can in this case be attributed to the binding of an anionic guest species by the NH protons of the urea moiety, which are in close proximity to the ferrocene centre. The absence of the reduction wave on addition of anions was concluded to possibly be a result of the anion-ferrocenium cation interaction. In addition to chloride, the sensor was also treated with benzoate and dihydrogen phosphate anions. Addition of dihydrogen phosphate was found to affect a greater cathodic shift in oxidation potential than those observed with chloride and benzoate.

A series of hydrogen bonding ferrocene receptors for the electrochemical detection of barbiturate and urea neutral guest species was reported by Tucker *et al.*[33] These hosts featured ferrocene backbones, substituted with amidopyridine ligands, either doubly on one cyclopentadienyl ring, or singly on both cyclopentadienyl rings. The hosts were designed to incorporate both hydrogen bond donor and acceptor sites, such that they might bind neutral cyclic organic guests featuring complimentary hydrogen bond donor and acceptor sites, as found in urea derivatives, one combination (host and guest) of the reported series is shown below in Figure 1.21.

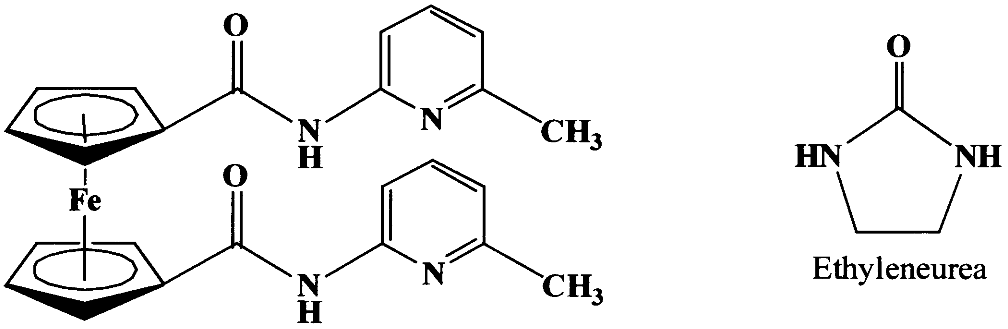

Figure 1.21 Sensor and substrate featured in the electrochemical study by Tucker *et al.*[33]

Cyclic voltammetry studies were performed on the above host in the presence of ≥ 20 molar equivalents of ethyleneurea. Addition of the neutral guest species affected a cathodic shift in the oxidation potential of the ferrocene fragment, from the guest-free species ($E^o = 0.95$ V) to the host-guest complex ($E^o = 0.89$ V), a net cathodic shift of -60 mV (referenced against the Fc^+/ Fc redox couple). The observed cathodic shift is consistent with increased electron density on the receptor due to formation of the hydrogen bond between the amide NH of the receptor and the oxygen donor of the guest, causing the ferrocene redox centre to be oxidised at a lower potential. This report illustrates that cyclic voltammetry can be a powerful analytical tool in investigating the electronic effects of guest binding.

More relevant to the work presented in this thesis however, are Lewis acid/base host-guest interactions. One pertinent example of an electrochemical sensor featuring the Lewis acidic binding site of boron was reported by Shinkai *et al.*[34] The ferroceneboronic acid receptor features the necessary components to achieve effective anion sensing, i.e. the redox active ferrocene moiety coupled to a Lewis acidic boron centre, which is known to have a high affinity for fluoride. The receptor was shown to electrochemically detect fluoride over other halides in high concentration in aqueous solution. The redox properties of the ferrocene centre are significantly altered in the presence of fluoride anions, displaying a cathodic shift of *ca.* −100 mV in water.

1.3.2 Luminescent and colorimetric detection of anions

Certain compounds undergo a visible colour change on addition of a guest species; the design of such compounds is an area that has seen increasing research interest, in particular because this detection method requires nothing more than sight, eliminating the need for any costly instrumentation and/or transduction platforms.

Luminescence is another widely exploited physical detection method applied to sensors for anions, incorporating fluorescence and phosphorescence. Fluorescent techniques are highly sensitive; as such they have been extensively developed for physical detection methods in host-guest chemistry, receiving enormous attention over recent years. These sensors are based on the principle that certain combinations of molecules affect luminescence under certain conditions, typically it is necessary to incorporate both a receptor molecule and an organic or inorganic luminophore, that are in close proximity to one another. Some commonly used fluorophores include anthracene, porphyrins and $Ru(bipy)_3$, and often these will be covalently linked to polyammonium, guanidinium or calixpyrrole receptor molecules,[35] although some examples featuring Lewis acidic receptor molecules are also known. Boron-containing π-electron systems have attracted significant recent attention because of their interesting photophysical properties arising from p_π-π^* conjugation via the vacant p-orbital at the boron centre. One such sensor was reported by Tamao *et al.* featuring a tri(9)anthrylborane, in which the binding of fluoride was found to turn-off the p_π-π^* conjugation resulting in a colour change from orange to colourless.[36] A sensor based on the dibenzoborole backbone has also been reported by Tamao *et al.* in which the p_π-π^*conjugation can be selectively switched-off by exposure to a guest species. This effect is brought about by alteration in the delocalisation of the LUMO, which changes the band gap, resulting in a hypsochromic shift in the spectral band position in the emission and absorption spectra (Figure 1.23).[37]

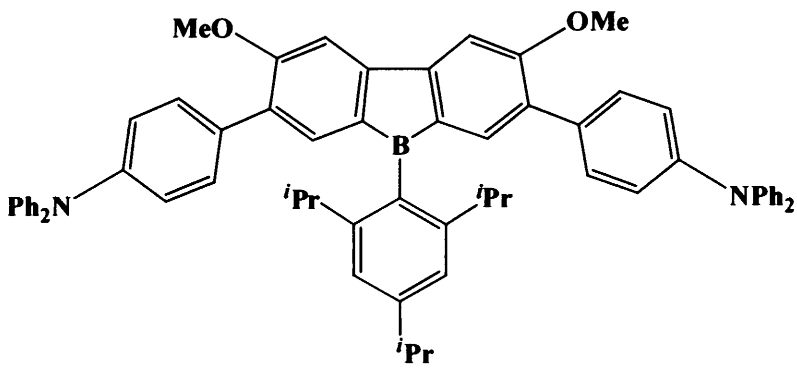

Figure 1.23 Dibenzoborole-based sensor offering 'on-off' control of physical responses to anions.

It was found that the fluorescence properties of this sensor are highly dependant on solvent; the sensor itself has a yellow-orange emission (561 nm) in THF solution. However DMSO coordinates to the receptor, causing the receptor emission band to disappear and a new intense blue band to grow in at λ_{max} = 423 nm. Absorption and fluorescence spectra were then measured before and after addition the of tetra-n-butylammonium fluoride in THF solution. Upon addition of fluoride the absorption spectrum revealed a shift of λ_{max} from 480 to 374 nm, and the fluorescence spectrum showed a similar blue-shift of λ_{max} from 561 to 419 nm. The emission of the fluoride host-guest complex (λ_{max} = 419 nm) is similar to the spectrum observed in DMF solution (λ_{max} = 423 nm). These results illustrate the potential of the dibenzoborole backbone in the fluoride anion sensing applications. In later studies Tamao coupled a triarylborane chromophore with a porphyrin chromophore forming a conjugate system featuring both energy donor and acceptor molecules. When the Lewis acidic boron centre binds an anionic guest, the change in hybridisation from sp^2 to sp^3 interrupts electronic communication, and the formerly cooperative chromophores begin to absorb and emit light independently.[38] This concept was tested experimentally; fluorescence spectroscopy was used to monitor fluoride binding by the triarylborane-porphyrin conjugate (λ_{max} = 670 nm). Prior to addition of fluoride, the sensor showed one emission in the fluorescence spectrum at 670 nm. Upon addition of fluoride the emission band at 670 nm (red) can be seen to decrease in intensity, coupled with an increase in intensity of two bands at 356 nm (triarylborane) and 692 nm (porphyrin) (blue). A colorimetric response was also observed from the purple sensor to the green host-guest complex. However, excitation spectra of the sensor treated with fluoride revealed that the absorbance of the triarylborane still contributes to the porphyrin emission at 692 nm, suggesting that communication between the two functionalities is still possible even when fluoride is bound via the vacant p-orbital at boron. This sensor illustrates the application of a combination of colorimetric and luminescent outputs in detecting fluoride anions.

In a more recent study Gabbaï *et al.* developed a phosphonium borane-based sensor for fluoride. Based on previous studies investigating the use of bidentate boranes for the chelation of fluoride,[39] the use of a cationic borane was thought to offer enhanced fluoride affinity because of the possibility for electrostatic host-guest interactions, coupled with the Lewis acidic binding centre at boron (Figure 1.22).[40]

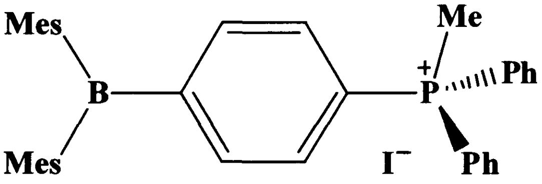

Figure 1.22 A phosphonium borane sensor for fluoride

In addition to the above-mentioned advantages of this system, there is also the potential to monitor the binding process via absorption and emission spectroscopy.

Exposure to fluoride results in quenching of the absorption band of the borane. The emission spectrum of the receptor shows an intense green fluorescence (λ_{max} = 495 nm), which can be observed by the naked eye. This fluorescence band is quenched on formation of the fluoride host-guest complex, thus this sensor provides a range of physical outputs for signalling the presence of fluoride.

One of the most widely investigated luminescent complexes is tris-(2,2'-bipyridyl)ruthenium(II), a complex having chemical stability, as well as suitable redox and luminescence properties. This moiety has been applied to the preparation of a ruthenium-based sensor featuring a quinonehydrazone group, which becomes an azophenol on the binding of a fluoride anion leading to spectroscopic changes and a significant colour change (Scheme 1.4).[41] Incorporation of the $[Ru(bipy)_3]^{2+}$ moiety presents the possibility for enhanced affinity via electrostatic interactions and allows the binding process to be monitored by luminescence spectroscopy.

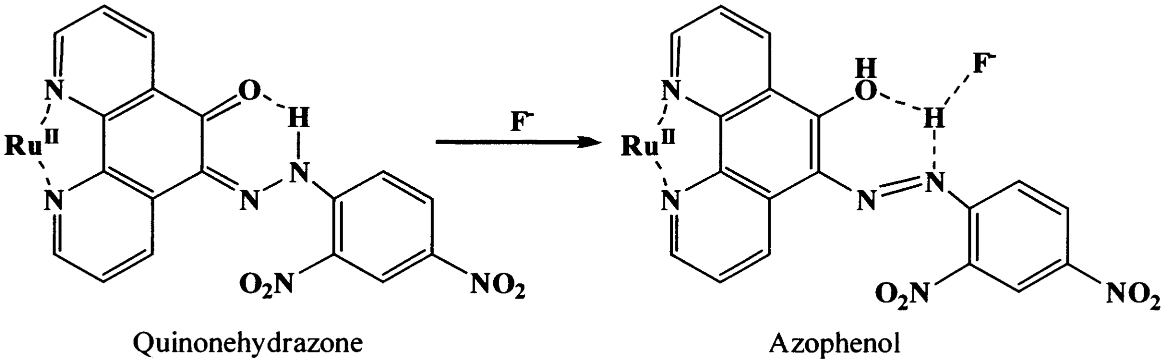

Scheme 1.4 Anion binding by Ru-based sensor.

This sensor was found to be very effective, providing not only a very vivid orange to blue colour change, but also significant enhancement of fluorescence intensities. A test paper for fluoride was prepared by allowing a filter paper to become saturated in a solution of the sensor followed by drying, and was found to be fairly sensitive, detecting fluoride in aqueous solution at a concentration of 10 mg L^{-1}.

Another hydrogen bonding based colorimetric sensor for fluoride, featuring binding sites both for anions and cations was reported by Tucker *et al.*[42] The sensor incorporated a urea-linked nitrobenzene moiety, which has a strong absorption band in the UV region that has been observed to shift to the visible region upon addition of fluoride. This fragment was coupled with a crown-ether binding site for cations. Addition of fluoride resulted in a colourless to yellow colorimetric response; closer inspection via UV/Vis spectroscopy revealed that fluoride binding causes a shift in the absorption maxima of the nitrobenzene moiety from λ = 304 and 332 nm to λ = 288 and 356 nm. Subsequent addition of K^+ was found to result in a further colour change from yellow back to colourless, and NMR studies led to the conclusion that the bound K^+ must interact in some way with the urea group, with the effect that hydrogen bonding to fluoride is weakened.

1.4 Organometallic polymers and oligomers

It was not until the 1950's that transition metal-containing polymers were recognised as a separate class of polymeric compounds, with the free-radical polymerisation of vinylferrocene reported by Arimoto and Haven.[43] Initial preparation of a well characterised transition metal containing polymeric compound was later achieved in the 1970's by Pittman and co-workers.[44] Since these early discoveries the field of transition-metal-containing polymers has attracted enormous research attention, and increasingly important and interesting applications of such compounds have been revealed. These include multi-electron catalysis, optical and electronic applications, electron storage devices, ceramic materials, surface modification of electrodes and sensor intensification. Transition metals may be either σ or π bonded, or both, to the carbon framework of the polymer or side-chain and examples of all three types are discussed below. The majority of research has concentrated on linear polymers, however a number of branched, star and dendritic compounds have also been reported. This section presents a summary of the developments that have brought the chemistry and applications of organometallic polymers to where they are today, including polymers featuring various transition metals and linker groups along with the ferrocene-based polymers, both linear and non-linear.

1.4.1 Ferrocene-based organometallic polymers and oligomers

Metallocenes have been extensively used in the preparation of organometallic polymers, as their capacity to achieve both σ and π metal-carbon bonds enhances their use in some of the above-mentioned applications. Of all metallocenes, by far the most extensively applied to organometallic polymers is ferrocene. Ferrocene containing polymers have been divided into two sub-classes; type **1** polymers featuring ferrocenyl moieties as pendant substituents to the polymer main-chain (for example polyvinylferrocene, Figure 1.23) and type **2** polymers featuring ferrocene as the integral part of the polymer backbone (for example poly(ferrocenylene)s Figure 1.24).

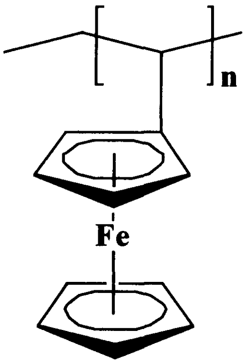

Figure 1.23 A type **1** polymer – Polyvinylferrocene

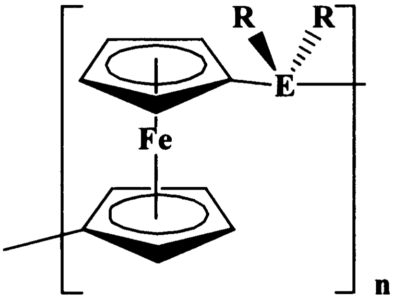

Figure 1.24 A type **2** polymer - Poly(ferrocenylene)

Type **2** polymers featuring the ferrocene moiety coupled with Lewis acidic organoboron centres are especially relevant to the work presented in Chapter Five; polymers of this nature are discussed in much more detail in the relevant chapter.[45] Examples of type **2** polymers vastly outnumber those of type **1**, since it is this class of polymer that has found extensive applications in photo- and electroluminescent devices, liquid crystals, sensor amplification etc. Prior to the well characterised compounds of Pittman and co-workers,[44] poly(ferrocenylsilanes) featuring a main chain of alternating ferrocene and organosilane units had been prepared in the late 1960's via a polycondensation reaction between dilithioferrocene and organodichlorosilanes.[46] However this polymer was prepared in low molecular weight (M_w *ca.* 6000) and was not well characterised. Following these reports, the preparation of poly(1,1'-ferrocenylenes) via an organolithium-organohalide coupling reaction was reported by Neuse *et al.*[47] However this method also afforded polymer of low molecular weight ($M_w < 6200$). It was not until the discovery of the ring-opening polymerisation chemistry of strained [1]ferrocenophanes by Manners *et al.*[48] that the development of poly-ferrocenylenes began to rapidly expand. The reaction was initially tested with a strained cyclic ferrocenylsilane precursor and was found to yield high molecular weight organometallic polymers; this method was subsequently employed in preparation of phosphine and germane derivatives. Figure 1.25 illustrates the preparative scheme for a poly(ferrocenylgermane).

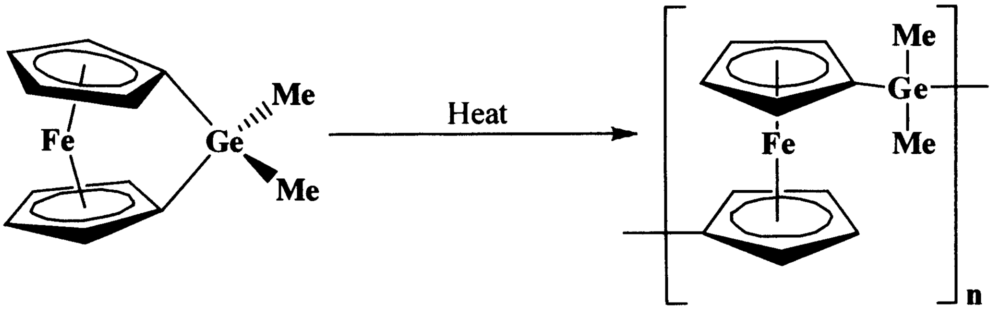

Scheme 1.5 Synthetic route to poly(ferrocenylgermane)

The soluble poly(ferrocenylgermane) product was characterised by NMR (^{1}H and ^{13}C); the molecular weight was estimated via gel permeation chromatography, measured against polystyrene standards, from which values of up to 200,0000 were obtained. In addition, the product was observed to be indefinitely stable to air and moisture. Thus this method was proven to be useful for high-molecular-weight organometallic polymer production, offering versatility in the facile substitution of alternative metal centres. Subsequent work by Manners *et al.* focussed on the analogous ring-opening chemistry of [1]ferrocenylsilane, towards developing a precursor capable of ring-opening polymerisation under more mild conditions. [1]ferrocenylsilane was found to undergo ring-opening polymerisation at room temperature, while previous analogues required heating for reaction to occur. The molecular weight of the product was determined to be *ca.* 130,000.[49] This finding led to studies concentrating on attaining precise control of the regiostructure of the products of polymerisation reaction; control over molecular weight was gained via addition of Et_3SiH, which acts as a chain-terminating group.[50]

Poly(ferrocenylsilene) compounds are thought to display a variety of useful properties as potential precursors for ceramics, also displaying redox properties and novel electronic properties as a result of σ-Si – π-Fe orbital mixing. An analogous hyperbranched polymeric compound, poly(ferrocenylenesilyne), was reported by Sun *et al.*[51] The hyperbranched poly(ferrocenylenesilyne) structure (Figure 1.25) was prepared via a coupling reaction between lithiated-ferrocene and various R-substituted trichlorosilanes, and showed improved solubility and stability along with extended electronic conjugation.

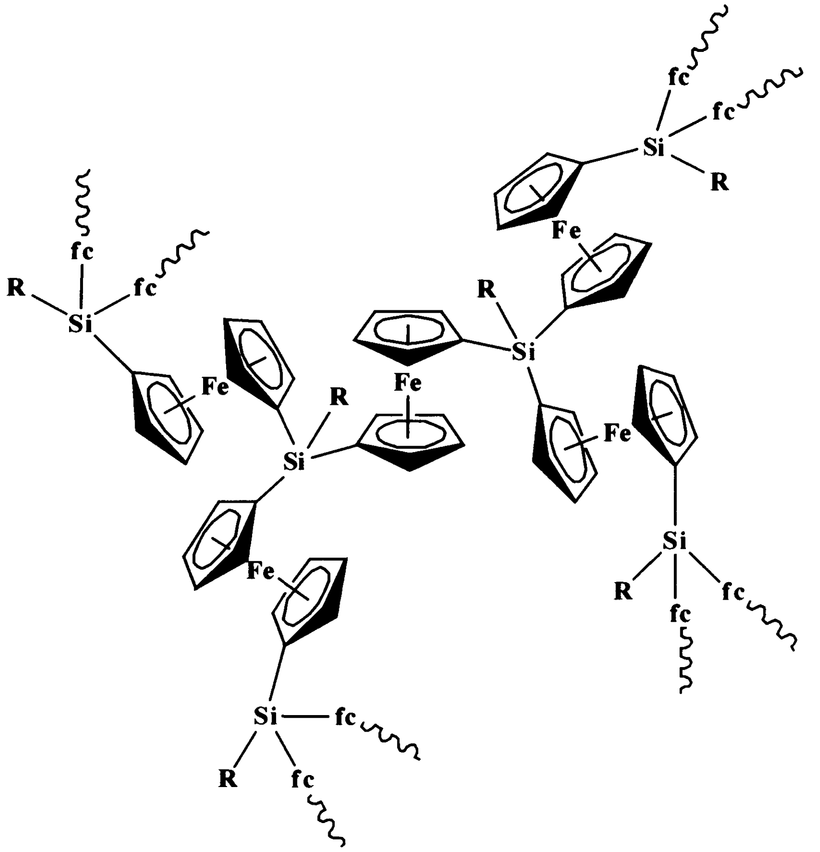

Figure 1.25 A hyperbranched organometallic polymer of poly(ferrocenylenesilyne)

The use of these compounds in the formation of ceramics has been investigated; the thermolysis behaviour of a range of various R-substituted poly(ferrocenylenesilyne)s was investigated using TGA analysis. For example, the methyl-subtituted compound was heated revealing, between 400-500 °C, a rapid thermolytic degradation observed as a sharp drop in the thermogram indicating that the polymer was ceramized by high temperature pyrolysis. The methyl-substituted compound was further investigated by sintering to reduce the pore size by fast evaporation of volatile fragments, making a denser, stronger product.

Earlier examples of hyperbranched oligomeric metallocene aggregates include 'tentacle compounds' featuring a central ferrocene fragment with penta-substituted Cp rings bearing dimethylsilylferrocenes linked via 3-carbon-chains to the central ferrocene, as reported by Batz *et al.* in 1996 (Figure 1.26).[52]

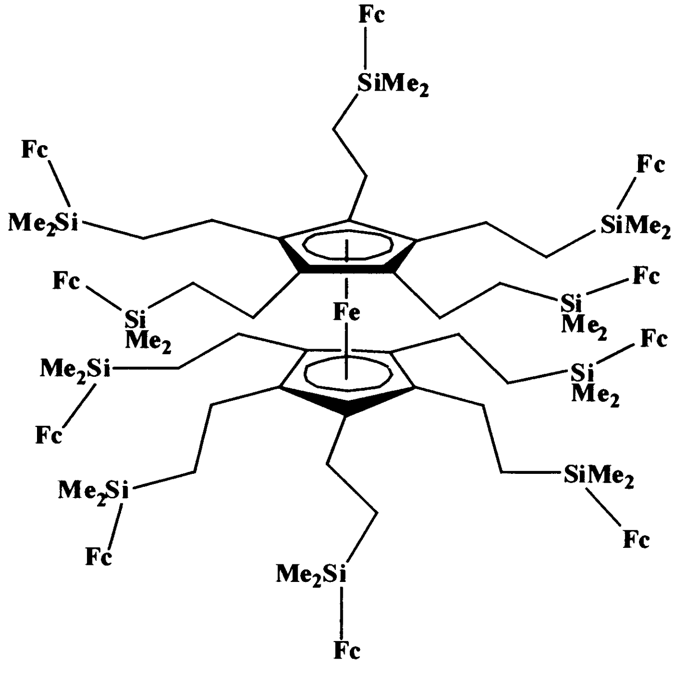

Figure 1.26 Two-dimensional oligonuclear iron complex

Many of the useful applications of organometallic polymers and oligomers stem from their ability to achieve electronic communication along a chain. For example, a polymer or oligomer featuring an electron rich group linked to a fragment bearing a vacant orbital as means of accepting electron density will be capable of propagating an electronic signal. A common method of detecting electronic communication is cyclic voltammetry, since in a communicating molecule the oxidation of one iron centre may have an effect on the oxidation potential of a neighbouring iron centre, and consequently more than one oxidation peak will be observed in the spectrum. Cyclic voltammetry was carried out on the tentacle compound reported by Batz *et al.* in which only one oxidation wave was observed, thereby leading to the conclusion that no electronic communication was occurring between the iron centres. Recent work by Vollhardt *et al.* has focussed on enhancing electronic communication by replacing the electronically "isolating" alkyl chain with directly attached metallocene ligands.[53] This was achieved using a cymantrene core penta-substituted at the Cp ring with five ferrocenyl groups (Figure 1.27).

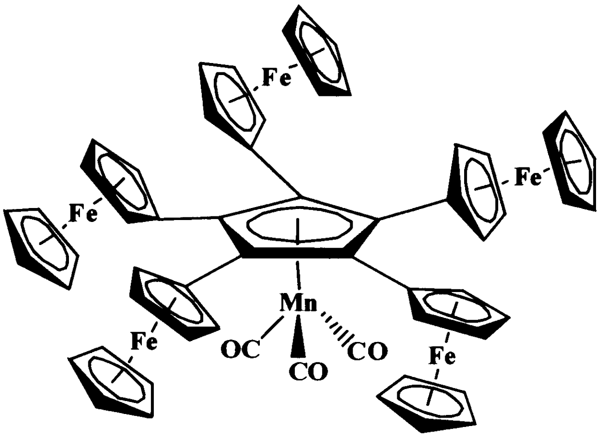

Figure 1.27 Penta(ferrocenyl)cymatrene

Electrochemical studies on this compound revealed a substantial degree of electronic communication, as evidenced by multiple oxidation peaks in the cyclic voltammogram. This compound also has the potential for cluster formation under photolytic conditions.

Organometallic polymers featuring ferrocene fragments within the main-chain are well known, however there are very few example of polymers featuring ferrocene acting as a bridging ligand through interaction of the π-faces. One such recent example reported by Mulvey *et al.* features alkali-metal hexamethyldisilazide (alkali-metal = Li, Na, K, Rb, Cs) linker groups bridged by a facial interaction with the ferrocene π-system (Figure 1.28).[54]

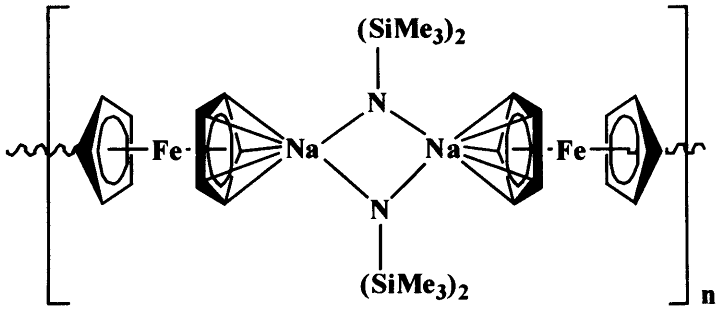

Figure 1.28 A cation-π-interaction-assembled organometallic polymer

The linear polymer featuring sodium cations was characterised both crystallographically and by NMR (^{1}H and ^{13}C), as were the potassium, rubidium and caesium analogues. It was also noted that the rubidium and caesium polymers formed two-dimensional sheet-like structures by intermolecular agostic interactions with neighbouring chains.

1.4.2 Poly(metal acetylide) organometallic polymers

Ferrocene has been extensively used in the preparation of organometallic polymers, however a number of organometallic polymers featuring alternative transition metals (Pt, Pd, Au, Hg, Ag, W for example) have been reported.[55] Of the different σ-bonding transition metal polymer systems, poly(metal acetylides) have dominated the field, being stable materials with interesting electrical and optical properties due to their rigid-rod structures. Following the initial syntheses of polymeric platinum and palladium acetylides by Hagihara *et al.* in the 1970's [56] there has been tremendous interest in metal acetylide polymers; systems have been reported featuring a range of different metal centres. Polymers containing σ-bound conjugated alkynes are most common with platinum and palladium metal centres. Poly(metal acetylide) systems also feature extended π-delocalisation along the polymeric chains as a result of the significant overlap between the π-system of the acetylene linker and the metal d-orbitals, as concluded by theoretical calculations.[57] An organoplatinum polymer featuring an alkynyl-NCN spacer ligand was reported by van Koten *et al.* which was found to polymerise via C≡CH•••ClPt hydrogen bonding interactions (Figure 1.29).[58]

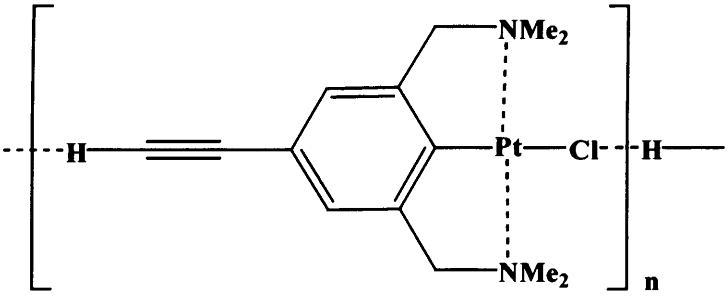

Figure 1.29 Organoplatinum polymer

The NCN ligand was of interest due to its chelating NMe_2 group offering enhanced stability. The short intermolecular hydrogen bonding contact (2.60 Å) was confirmed by an X-ray diffraction study on single crystals of the compound. Subsequent research by the same group led to the development of a dimeric organoplatinum compound, prepared by a coupling reaction between an alternative iodide-substituted alkynyl-NCN ligand and the above platinum alkynyl-NCN fragment (Figure1.30).[59]

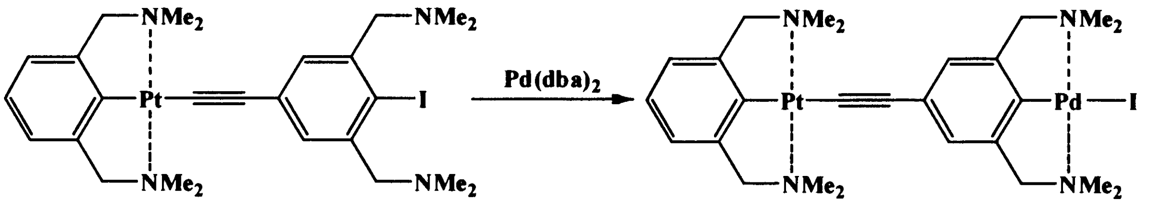

Figure 1.30 Novel precursors for mixed-metal organometallic polymers

The resulting dimeric species underwent oxidative addition to a Pd(0) centre yielding a mixed-metal complex. This report provides a novel strategy for precursors designed for controlled synthesis of rigid-rod metallopolymers.

A subsequent report by Fratoddi *et al.* detailed an alternative synthesis for organometallic square-planar platinum and palladium-containing polymers, featuring a 2,6-diethynyl-4-nitroaniline bridging spacer group.[60] The 2,6-diethynyl-4-nitroaniline spacer group was chosen for its NH_2 and NO_2 groups and their roles in second-order non-linear optical properties, and the two alkynyl groups are especially useful for linking palladium and platinum forming polymer chains (Figure 1.31).

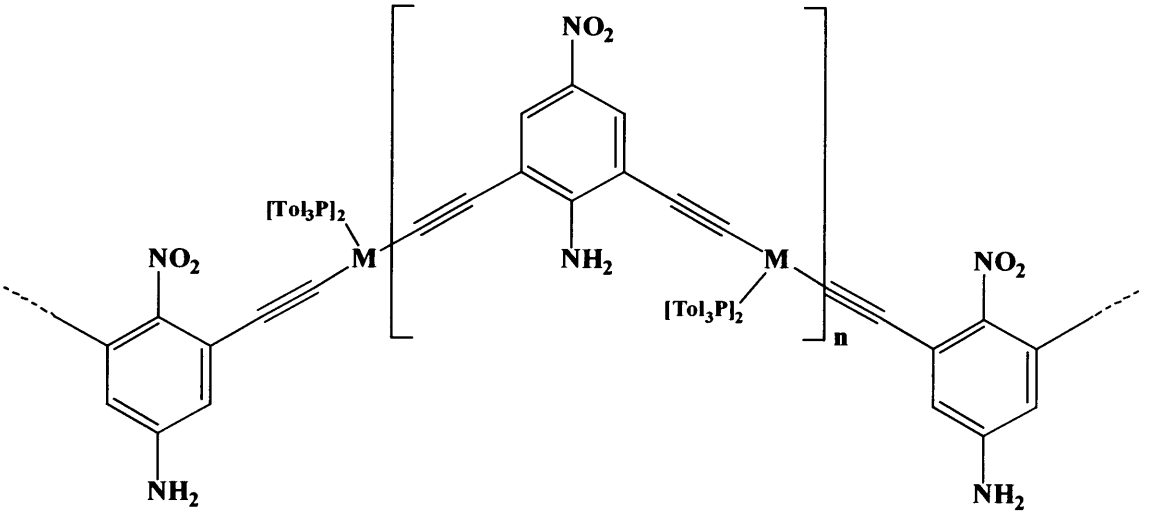

Figure 1.31 Pt(II) and Pd(II) poly-ynes

These platinum and palladium polymers were prepared by reaction of 2,6-diethynyl-4-nitroaniline with *cis*-$[M(PTol_3)_2(C{\equiv}C\text{-}C_6H_5)Cl]$ complexes (where M = Pt or Pd) via a dehydrohalogenation reaction. The products were characterised by IR (specifically looking for the C≡C stretching frequency), and NMR spectroscopy (^1H, ^{13}C and ^{31}P). Molecular weights of the polymeric products were determined from GPC measurements to be 14,600 amu for the Pt polymer (16 repeat units) and 6000 amu for the Pd polymer (8 repeat units). Evidence that the structure of the polymer may not be linear but helical was gained via NOESY experiments, from which correlations between NH_2 and aromatic phosphine protons in the polymer were observed, indicating that these fragments are spatially close.

A more recent report of a rigid-rod organometallic polymer by Leoni *et al.* features a platinum-based cluster fragment alternating with an alkynyl-based linker group.[61] Cluster-containing conjugated structures have proven useful in the field of molecular electronics.[62] This report describes preparation of the first cluster-containing σ-alkynyl polymer (Figure 1.32).

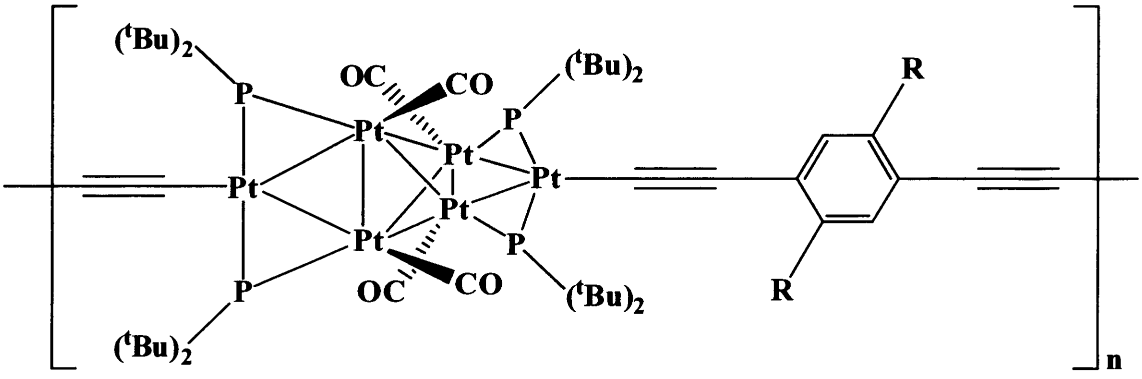

Figure 1.32 Rigid-rod platinum-cluster-containing alkynyl polymer

The polymeric product was characterised by NMR spectroscopy (^{1}H and ^{13}C), and molecular weights of up to *ca.* 65,000 determined by GPC measurements. UV/Vis spectra revealed a red-shift from the dimeric analogue at 449 nm to the polymeric compound (476 nm); this is attributed to extended π-delocalisation along the polymer backbone and through the metal centres of the cluster.

1.4.3 Coordination polymers

The third main area of research contributing to the development of organometallic polymers is that of coordination polymerisation. The field of coordination polymers has rapidly expanded, with very recent efforts aimed at combining the dynamic behaviour of coordination polymers with electronic and/or optical properties. The thermodynamic driving force behind coordination polymerisation is metal-ligand affinity. A range of multidentate pyridine-containing ligands (phenanthroline and terpyridine), and their polymeric products formed on treatment with various transition metals (Ru, Cu and Ag) were reported by Rehahn *et al.* (Figure 1.33).[63]

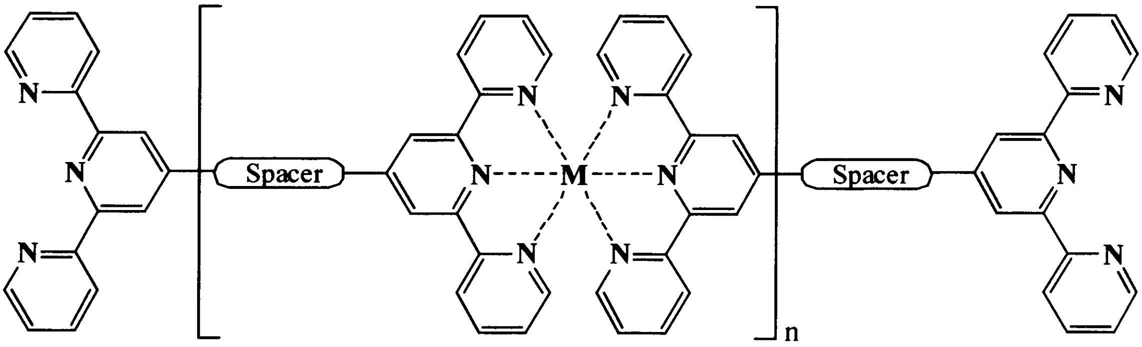

Figure 1.33 A terpyridine coordination polymer

Later work by Chen and MacDonnell has built on Rehahn's studies on terpyridine and phenanthroline-based coordination polymers, developing optically active polymers by copolymerisation of enantiomerically pure Ru complexes (Scheme 1.6).[64]

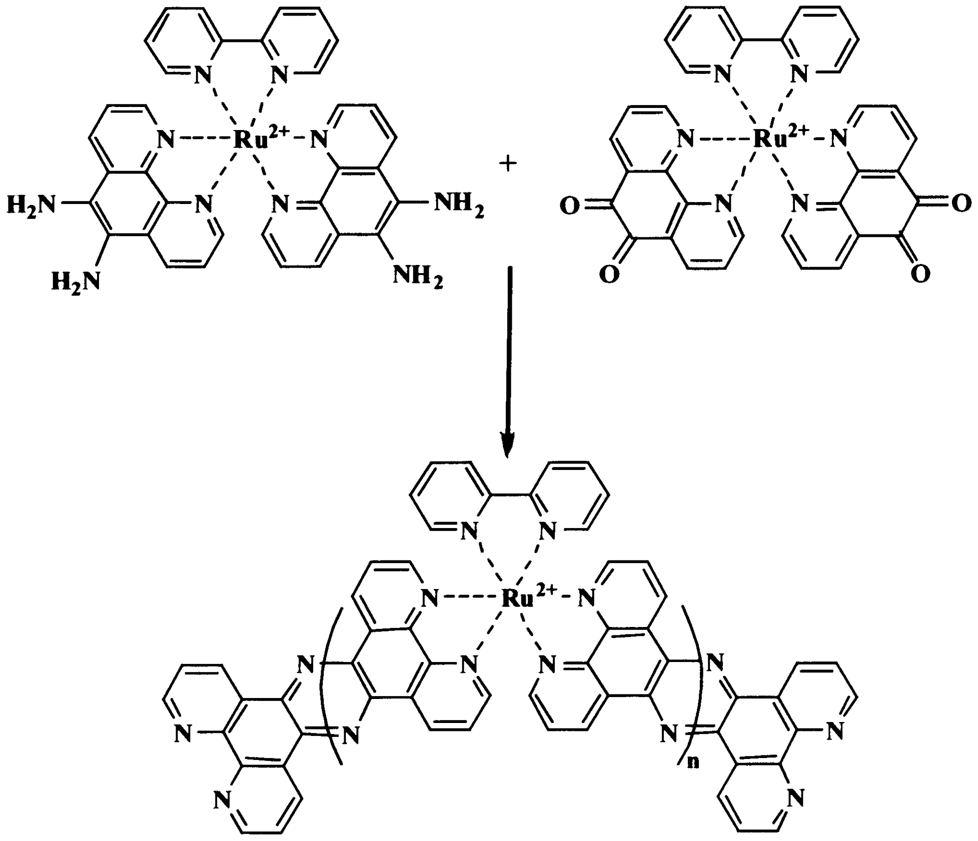

Scheme 1.6 Co-polymerisation of Ru complexes for the synthesis of optically active polymers

One monomer was functionalised with dione groups and the other with diamine groups, the polycondensation reaction produced a non-linear coiled polymer chain that displayed optical activity.

Phosphine donors are commonly used ligands for the synthesis of highly stable coordination polymers especially for late transition metals. Ditopic phosphine spacers have been used in the construction of rhodium-based polymers as reported by

Ding *et al.*[65] The bridging phosphine ligands were reacted with $[Rh(COD)_2]^+ [BF_4]^-$ and the resulting polymeric product (Figure 1.34) was found to act as a recyclable hydrogenation catalyst.

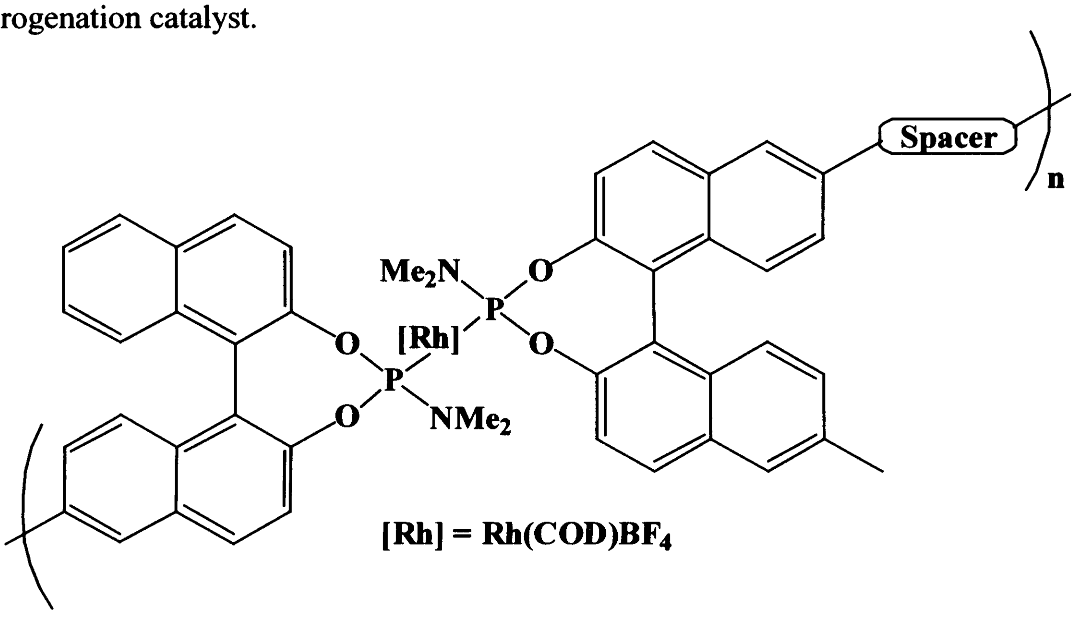

Figure 1.34 Rhodium-based polymeric catalyst for asymmetric hydrogenation

Another branch of coordination polymerisation involves the use of N-heterocyclic carbenes. This is a fairly new area of research despite the tremendous interest in NHC-metal complexes that has been witnessed over several decades. NHCs display high affinities for various transition metals, although the most stable polymers have been those incorporating Pd and Pt metals. One advantage of strongly donating monodentate NHC ligands is that the metal centre may remain coordinatively unsaturated, allowing the complexation of other ligands. This presents the possibility for tuning polymer properties by inclusion of functional groups, such that a particular application may be targeted.[66] One such NHC polymerisation reported by Bielawski and co-workers[67] involved the addition of $PdCl_2$ to an equilibrium mixture of the free carbene and the poly(enetetraamine)s, a product of carbene dimerisation (Scheme 1.7).

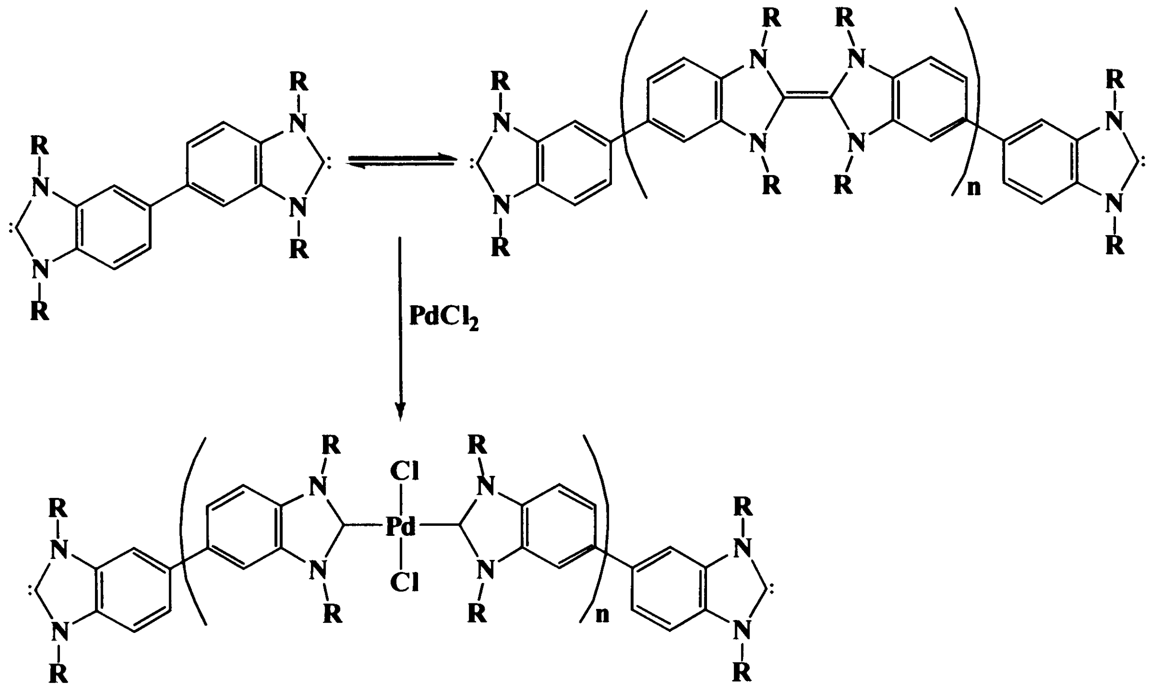

Scheme 1.7 Coordination polymerisation between an NHC and $PdCl_2$

The resulting palladium-containing polymers formed with mixtures of *cis* and *trans* isomers about the metal centre, and were found to be highly air and moisture stable, with molecular weights of up to 10^4 Da determined by GPC measurements (relative to polystyrene standards).

The field of transition metal-containing polymers has received tremendous attention over the past five decades resulting in great development of these compounds. Novel polymerisation methods reported have included the use of both metal-containing monomers and innovative metal-complexing ligands involved in the polymerisation step. Advances in the properties of the organometallic polymers obtained have also been vast. The effects of π-conjugation have been closely examined in the development of polymers displaying novel electronic properties, such that potential applications in molecular wires, photoelectronics, sensory devices and electroluminescent devices have been realised.

1.4.4 Organometallic polymers as fluoride specific sensors

A key aim of the work presented in this thesis is the development of fluoride specific sensors. The field of chemical sensing has recently seen significant advances with novel polymeric, glass and nanostructured sensor materials being developed that display superior sensing properties.[68] As discussed, organometallic polymer-based sensor materials offer amplification of the sensor signal. For example, polymeric sensory materials may display enhanced luminescence, electrochemical or visual responses to smaller aliquots of guest species. Enhanced receptor sensitivity can be critical, in particular allowing very toxic and fast-acting analytes, (e.g. chemical warfare agents), to be detected within a useable timeframe and dose limit.

A σ-conjugated organoboron polymer (Figure 1.35) was reported in 2002 by Miyata and Chujo that was found to bind fluoride anions specifically with an accompanying optical response.[69]

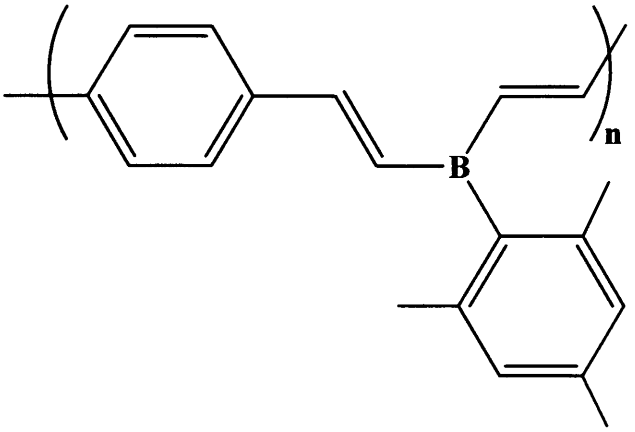

Figure 1.35 Fluoride specific conjugated organoboron polymer

The binding of a fluoride anion by the Lewis acidic boron centre causes a change in hybridisation of the boron atom from sp^2 to sp^3, which interrupts the conjugation along the polymer chain, thereby quenching the emission of the polymer. In addition, fluoride binding was found to cause a significant blue shift in the absorption spectrum. However, this particular polymeric sensor was not found to enhance the emission or absorption spectra significantly, as even 0.1 equiv. of fluoride were not found to be sufficient to produce a significant physical response. Later work by Fujiki *et al.* focussed on the fluoride binding ability of Lewis acidic silicon-based organometallic polymers, including a σ-conjugated poly(3,3,3-trifluoropropylmethylsilane) compound (Figure 1.36) with a very high (nanomolar) sensitivity range.[70]

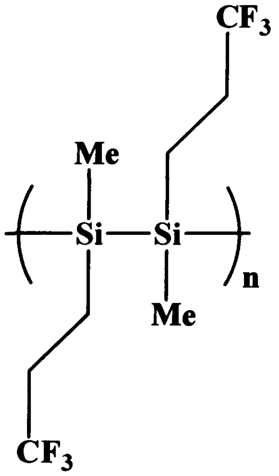

Figure 1.36 A σ-conjugated poly(3,3,3-trifluoropropylmethylsilane) sensor for fluoride

The sensor was found to be specific for fluoride over other halides in THF solution; this specificity was thought to be a result of the underlying affinity of Lewis acidic silicon centres for fluoride anions, and the electron-withdrawing CF_3 groups in the side-chains facilitating fluoride attack on the silicon centres in the main chain. The poly(silane) was found to be a highly emissive material with a high quantum yield. Addition of fluoride to the poly(silane) was found to result in very significant photoluminescence quenching. To determine the sensitivity of the sensor towards fluoride the photoluminescence intensity was measured as a function of fluoride concentration (as the tetra-n-butylammonium salt). From these studies it was determined that the poly(silane) was capable of displaying a significant physical response to parts per billion concentrations of fluoride in THF. The enhanced response to fluoride is thought to be a result of multiple anion-binding sites, if each silicon atom binds a fluoride anion with a specific binding constant, then the binding constant multiplied by the degree of polymerisation ($M_W = 1.13 \times 10^5$, PDI = 3.6) results in a remarkably high overall binding constant.

1.5 Aims of Research

The research objectives described in this thesis can be divided into three main areas as follows:

(i) Following the initial preparation of *mono-* and *bis*-boronate esters based on a ferrocene framework and some very interesting results concerning the anion binding properties displayed by such compounds,[71] it was decided to extend these systems to incorporate *tris-* and *tetrakis-* boronate esters using analogous direct borylation chemistry,[72] as well as extending the range of available *mono*-boronate esters to cover alternative derivatization at boron. The ferrocene backbone offers several advantages: firstly synthetic ease of borylation, secondly ready spectroscopic and electrochemical investigation, and thirdly the potential for further derivatization at the boron centre to allow tuning of the Lewis acidity at boron.

(ii) Considering recent advances in the field of colorimetric recognition of anionic species, it was decided to examine the potential of the above-mentioned multi-functional ferrocene-based boryl compounds to achieve specific and multiple fluoride binding. With the particular aim of improving the prototype bi-functional Lewis acid system[71] to proffer enhanced kinetics and sensitivity of response, a better knowledge of fundamental thermodynamic and kinetic factors behind the oxidation-based colorimetric response to fluoride is sought. A greater knowledge and understanding of such factors should allow specific sensor properties to be tuned *via* simple chemical modification. To this end, the effect of the number and nature of boronic ester groups and additional ligands on the efficiency and rate of colorimetric response will be systematically investigated. Thermodynamic aspects will be assayed by cyclic voltammetry and multi-nuclear NMR spectroscopy whilst the kinetics of response may be assessed by time resolved UV/Vis spectroscopy.

(iii) An extension of classical cation binding by macrocyclic Lewis basic frameworks to encompass macrocyclic Lewis acidic systems for anion binding, which may prove useful synthetic targets in the application of fluoride chelation. Likewise the potential applications of solid-state sensor materials have highlighted organometallic polymers as an exciting class of functional compounds. The development of molecular wires, requires that electronic communication along a polymer chain is possible, this could be achieved in this case by using the vacant p-orbital of boron centres; incorporation of redox-active fragments such as ferrocene provides a convenient means of monitoring electronic communication. Investigation into the factors controlling assembly of boronic ester units into poly-, oligomeric or macrocyclic products is therefore another research objective.

1.6 References

1 C. J. Pederson, *J. Am. Chem. Soc.,* 1967, **89**, 7017.

2 R.W. Alder, P. S. Bowman, W. R. S. Steele, D. R. Winterman, *Chem. Commun.,* 1968, 723.

3 C. H. Park, H. E. Simmons, *J. Am. Chem. Soc.,* 1968, **90**, 2431.

4 P. D. Beer, *Acc. Chem. Res.,* 1998, **31**, 71 and references cited therin.

5 F. P. Schmidtchen, *Angew. Chem. Int. Ed. Engl.,* 1977, **16**, 720.

6 M. A. Hossain, K. Ichikawa, *Tetrahedron. Lett.,* 1994, **35**, 8393.

7 K. Ichikawa, A. Yamamoto, M. A. Hossain, *Chem. Lett.,* 1993, **12**, 2175.

8 J. M. Lehn, E. Graf, *J. Am. Chem. Soc.,* 1976, **98**, 6403.

9 B. Metz, J. M. Rosalky, R. Weiss, *J. Chem. Soc., Chem. Commun.,* 1976, 533.

10 B. Dietrich, J. Guilhem, J. M. Lehn, C. Pascard, E. Sonveaux, *Helv. Chim. Acta,* 1984, **67**, 91.

11 B. Dietrich, J. Guilhem, J. M. Lehn, C. Pascard, *Tetrahedron. Lett.,* 1989, **30**, 4125.

12 R. A. Pascal, J. Spergel, *Tetrahedron. Lett.,* 1986, **27**, 4099.

13 C. R. Bondy, S. J. Loeb, *Coord. Chem. Rev.,* 2003, **240**, 77.

14 a) C. B. Black, B. Andrioletti, A. C. Try, C. Ruiperez, J. L. Sessler, *J. Am. Chem. Soc.,* 1999, **121**, 10438. b) H. Miyaji, P. Anzenbacher Jr, J. L. Sessler, E. R. Bleasdale, P. A. Gale, *Chem. Commun.,* 1999, 1723.

15 S. Camiolo, P. A. Gale, *Chem. Commun.,* 2000, 1129.

16 P. D. Beer, P. A. Gale, D. Hesek, *Tetrahedron. Lett.,* 1995, **36**, 767.

17 For recent reviews on electrostatic and hydrogen bonding receptors see for example (a) P. A. Gale, J. A. Sessler, V. Kral, *Chem. Commun.,* 1998, 1. (b) J. A. Sessler, S. Camiolo, P. A. Gale., *Coord. Chem. Rev.,* 2003, **240**, 17. (c) P. D. Beer, E. J. Hayes., *Coord. Chem. Rev.,* 2003, **240**, 167. (d) P. A. Gale, R. Quesada, *Coord. Chem. Rev.,* 2006, **250**, 3219.

18 D. F. Shriver, M. J. Biallas, *J. Am. Chem. Soc.,*1967, **89**, 1078.

19 H. E. Katz, *J. Org. Chem.*, 1985, **50**, 5027.

20 H. E. Katz, *Organometallics,* 1987, **6**, 5, 1135.

21 H. E. Katz, *J. Org. Chem.*, 1989, **54**, 2179.

22 S. Jacobson, R. Pizer, *J. Am. Chem. Soc.,* 1993, **115**, 11216.

23 G. E. Herberich, A. Fischer, D. Wiebelhaus, *Organometallics*, 1996, **15**, 3106.

24 M. T. Blanda, J. H. Horner, M. Newcombe, P. J. Squattrito, *J. Am. Chem. Soc.,* 1989, **111**, 6294.

25 M. T. Blanda, J. H. Horner, M. Newcombe, *J. Org. Chem.*, 1989, **54**, 4626.

26 K. Tamao, T. Hayashi, Y. Ito, *Organometallics*, 1992, 11, 2099.

27 K. Tamao, T. Hayashi, Y. Ito, *J. Orgmet. Chem.*, 1996, **506**, 85.

28 M. F. Hawthorne, Z. Zheng, *Acc. Chem. Res.*, 1997, **30**, 267.

29 M. Tschinkl, A. Schier, J. Riede, F. P. Gabbai, *Oragnometallics*, 1999, **18**, 1747.

30 M. Tsunoda, F. P. Gabbai, *J. Am. Chem. Soc.,* 2003, 125, 10492.

31 *Supramolecular Chemistry*, P. D. Beer, P. A. Gale, D. K. Smith, OUP, Oxford, 1996.

32 A. J. Evans, S. E. Matthews, A. R. Cowley, P. D. Beer, *J. Chem. Soc., Dalton. Trans.,* 2003, 4644.

33 J. Westwood, S. J. Coles, S. R Collinson, G. Gasser, S. J. Green, M. B. Hursthouse, M. E. Light, J. H. R. Tucker, *Organometallics,* 2004, **23**, 946.

34 C. Dusemund, K. R. A. Sandanayake, S. Shinkai, *J. Chem. Soc., Chem. Commun.,* 1995, 333.

35 F. P. Schmidtchen, M. Berger, *Chem. Rev.,* 1997, **97**, 1609 and references cited therin.

36 S. Yamaguchi, S. Akiyama, K. Tamao, *J. Am. Chem. Soc.,* 2001, **123**, 11372.

37 S. Yamaguchi, T. Shirasaka, S. Akiyama, K. Tamao, *J. Am. Chem. Soc.,* 2002, **124**, 8816.

38 Y. Kubo, M. Yamamoto, M. Ikeda, M. Takeuchi, S. Shinkai, S. Yamaguchi, K. Tamao, *Angew. Chem. Int. Ed.,* 2003, **42**, 2036.

39 S. Solé, F. P. Gabbaï, *Chem. Commun.,* 2004, 1284.

40 M. H. Lee, T. Agou, J. Kobayashi, T. Kawashima, F. P. Gabbaï, *Chem. Commun.,* 2007, 1133.

41 Z. Lin, S. Ou, C. Duan, B. Zhang, Z. Bai, *Chem. Commun.,* 2006, 624.

42 H. Miyaji, S. R. Collinson, I. Prokeŝ, J. H. R. Tucker, *Chem. Commun.,* 2003, 64.

43 F. S. Arimoto, A. C. Haven Jr, *J. Am. Chem. Soc.,* 1955, **77**, 6295.

44 W. J. Patterson, S. P. McManus, C. U. Pittman Jr, *J. Polym. Sci.,* 1974, **12**, 837.

45 For examples of organoboron polymers see: F. Jäkle, *Coord. Chem. Rev.,* 2006, **250**, 1107 and references cited therin.

46 U. S. Pat. 3,426,053, US Dept. of the Air Force: H. Rosenberg; *Chem. Abstr.,* 1969, **70**, P78551v.

47 E. W. Neuse, L. Bednarik, *Macromolecules.,* 1979, **12**, 187.

48 D. A. Foucher, I. Manners, *Makromol. Chem., Rapid. Commun.,* 1993, **14**, 63.

49 Y. Ni, R. Rulkens, J. K. Pudelski, I. Manners, *Macromol. Rapid Commun.,* 1995, **16**, 637.

50 See for example (a) P. Gómez-Elipe, R. Resendes, P. M. Macdonald, I. Manners, *J. Am. Chem. Soc.,* 1998, **120**, 8348. (b) I. Manners, *Chem.*

Commun., 1999, 857. (c) F. Jäkle, Z. Wang, I. Manners, *Macromol. Rapid Commun.*, 2000, **21**, 1291.

51 Q. Sun, K. Xu, H. Peng, R. Zheng, M. Häussler, B. Zhong Tang, *Macromolecules.*, 2003, **36**, 2309.

52 P. Jutzi, C. Batz, B. Neumann, H. G. Stammler, *Angew. Chem. Int. Ed.,*1996, **35**, 2118.

53 Y. Yu, A. D. Bond, P. W. Leonard, K. P. C. Vollhardt, G. D. Whitener, *Angew. Chem. Int. Ed.,* 2006, **45**, 1794.

54 J. J. Morris, B. C. Noll, G. W. Honeyman , C. T. O'Hara, A. R. Kennedy, R. E. Mulvey, K. W. Henderson, *Chem. Eur. J.,* 2007, **13**, 4418.

55 R. J. Puddephatt, *J. Inorg. Organomet. Polym. Mater.*, 2005, **15**, 371.

56 Y. Fujikura, K. Sonogashira, N. Hagihara, *Chem. Lett.,* 1975, **4**, 1067.

57 (a) D. L. Lichtenberger, S. K. Renshaw, R. M. Bullock, *J. Am. Chem. Soc.*, 1993, **115**, 3276. (b) M. Springborg, *J. Solid State Chem.*, 2003, **176**, 311.

58 S. L. James, G. Verspui, A. L. Spek, G. van Koten, *Chem. Commun.*, 1996, 1309.

59 S. Back, M. Albrecht, A. L. Spek, G. Rheinwald, H. Lang, G. van Koten, *Organometallics.*, 2001, **20**, 1024.

60 R. D'Amato, I. Fratoddi, A. Cappotto, P. Altamura, M. Delfini, C. Bianchetti, A. Bolasco, G. Polzonetti, M. V. Russo, *Organometallics,* 2004, **23**, 2860.

61 P. Leoni, L. Marchetti, S. K. Mohapatra, G. Ruggeri, L. Ricci, *Organometallics,* 2006, **25**, 4226.

62 S. P. Gubin, V. Yu. Gulayev, G. B. Khomutov, V. V. Kislov, V. V. Kolesov, E. S. Soldatov, K. S. Sulaimankulov, A. S. Trifonov, *Nanotechnology.*, 2002, **13**, 185.

63 R. Knapp, A. Schott, M. Rehahn, *Macromolecules.,* 1996, **29**, 478.

64 J. Chen, F. M. MacDonnell, *Chem. Commun.,* 1999, 2529.

65 L. Shi, X. Wang, C. A. Sandoval, M. Li, Q. Qi, Z. Li, K. Ding, *Angew, Chem. Int. Ed.,* 2006, **45**, 4108.

66 K. A.Williams, A. J. Boydston, C. W. Bielawski, *Chem. Soc. Rev.,* 2007, **36**, 729.

67 J. W. Kamplain, C. W. Bielawski, *Chem. Commun.,* 2006, 1727.

68 S. W. Thomas, G. D. Joly, T. M. Swager, *Chem. Rev.,* 2007, **107**, 1339.

69 M. Miyata, Y. Chujo, *Polym. J.,* 2002, **34**, 967.

70 A. Saxena, M. Fujiki, R. Rai, S. Y. Kim, *Macromol. Rapid. Commun.,* 2004, **25**, 1771.

71 S. Aldridge, C. Bresner, I. A. Fallis, S. J. Coles, M. B. Hursthouse, *Chem. Commun.*, 2002, 740.

72 T. Renk, W. Ruf, W. Siebert, *J. Organomet. Chem.*, 1976, **120**, 1.

Chapter Two

Experimental Techniques

2.1 Manipulation of air-sensitive materials

Although air stability is a major stipulation of the sensor compounds described in this thesis it has been necessary to employ specific inert and high vacuum techniques as many of the precursors to such compounds are air- and moisture-sensitive and a brief introduction to the techniques involved in handling such compounds is presented below.

2.1.1 Inert atmosphere techniques

The manipulation of air- and-moisture sensitive compounds under an inert atmosphere is a well established technique and common choices of inert gases are argon and nitrogen. Two methods of employing such inert atmosphere techniques have been used in this project: (i) Schlenk line techniques, in which modified glassware is used for the containment of air/moisture sensitive compounds allowing bench-top manipulation of such compounds, and (ii) the use of a glove box, a sealed container accessible by rubber gloves, that is designed to allow the storage and manipulation of objects under an inert atmosphere.

The Schlenk line technique allows the safe and successful manipulation of large or small quantities of air/moisture sensitive chemicals with minimal risk of decomposition. The set-up of the Schlenk line which has been used for all the air/moisture sensitive research reported in this thesis is illustrated in Figure 2.1.

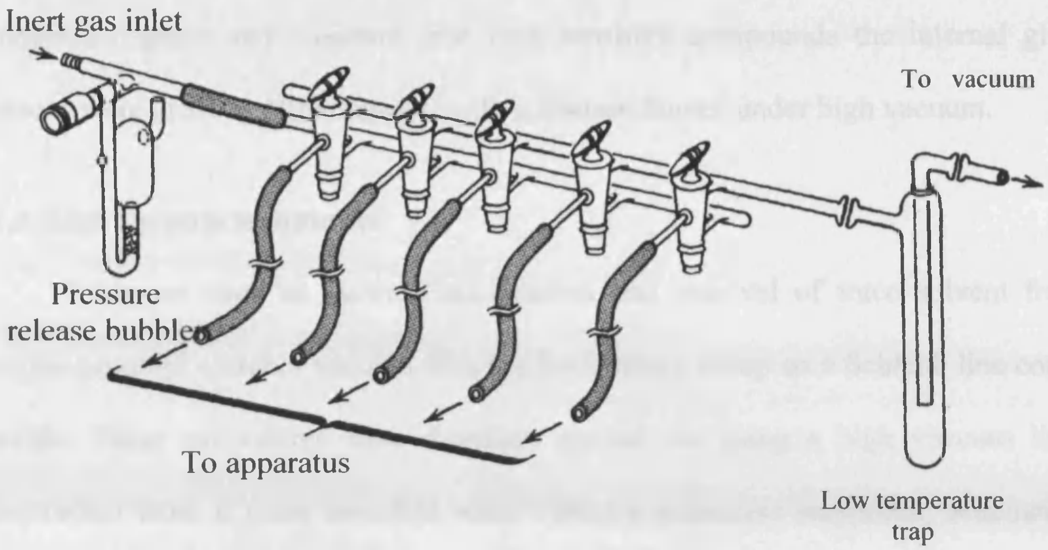

Figure 2.1 A typical Schlenk line.

The Schlenk line consists of a dual manifold with several ports. One manifold is connected to a source of purified inert gas (typically argon) while the other is connected to a high vacuum pump, evacuation was achieved by the use of an oil-sealed rotary pump. The inert gas line is vented through an oil or mercury bubbler depending on the pressure required while solvent vapours and gaseous reaction products are prevented from contaminating the pump through the use of a liquid nitrogen trap. Special three-way stopcocks allow for vacuum or inert gas to be selected without the need for placing the sample on a separate line. The ground glass joints and three-way stopcocks were lubricated with ‘Dow-Corning High Vacuum’ grease which provides a tight seal to prevent the leaking of air under high vacuum. Attachment of a Pirani pressure gauge to the vacuum manifold allowed the pressure of the vacuum to be monitored (typically 10^{-2} Torr). Production of an inert atmosphere within Schlenk glassware requires the apparatus to undergo a ‘pump and purge’ cycle in which glassware is evacuated then filled with inert gas: this cycle is repeated at least three times to achieve an atmosphere which is suitably rid of atmospheric gases and moisture. For very sensitive compounds the internal glass surfaces were dried by 'flaming-out' with a Bunsen burner under high vacuum.

2.1.2 High vacuum techniques

Processes such as vacuum sublimation and removal of trace solvent from samples required a higher vacuum than the basic rotary pump on a Schlenk line could provide. These procedures were therefore carried out using a high vacuum line. Constructed from a glass manifold with Young's greaseless stopcocks, evacuation was achieved by a combination of mercury diffusion and rotary pumps, enabling pressures of ca. 10^{-4} Torr to be reached; a Pirani gauge fitted to the vacuum manifold allowed the pressure of the system to be monitored. Solvent vapours and trace gaseous products were prevented from contaminating the pump through incorporation of a liquid nitrogen trap.

2.2 Physical measurements

2.2.1 NMR Spectroscopy

NMR spectra were measured on a Bruker AM-400 or Jeol Eclipse 300 Plus FT-NMR spectrometer. Residual solvent signals were used for reference with ^{1}H and ^{13}C NMR, whilst a solution of $[^{n}Bu_4N][B_3H_8]$ in $CDCl_3$ was used as an external reference for ^{11}B NMR and $CFCl_3$ was used as an external reference for ^{19}F NMR.

2.2.2 Mass spectrometry

Mass spectra were measured by the EPSRC National Mass Spectrometry Service Centre, University of Wales Swansea and by the departmental services offered by the Cardiff University and the University of Oxford.

Perfluorotributylamine (EI) and polyethylenimine (ES) were used as the standards for high-resolution mass spectra.

2.2.3 Infrared spectroscopy

Infrared spectra were measured by (i) pressing each compound into a KBr disc using a ten-fold excess of dried KBr, (ii) as a solution contained within a solution infrared cell or (iii) as a nujol mull using sodium chloride plates. Where compounds were air-sensitive, KBr discs were prepared in the glove box, in which case the KBr was dried by heating under high vacuum before use. Spectra were recorded on a Perkin-Elmer 1600 Series FTIR spectrometer or a Perkin-Elmer 1000 Paragon FTIR spectrometer.

2.2.4 X-ray crystallography

Data collection was carried out using an Enraf Nonius Kappa CCD diffractometer at Cardiff University or on a similar instrument at the EPSRC National X-ray Crystallography Service Centre, University of Southampton. Structure solution and refinement were carried out by Dr. Liling Ooi (Cardiff University) and Dr. S J Coles (Southampton University).

2.2.5 UV/Vis spectroscopy

UV spectra were measured on a Perkin-Elmer Lambda 20 UV/Vis spectrometer using quartz cells.

2.2.6 Electrochemistry (Cyclic voltammetry)

Electrochemical measurements were performed using dried, distilled dichloromethane or acetonitrile as the solvent and 0.1M tetrabutylammonium hexafluorophosphate as the supporting electrolyte on an Autolab PGSTAT 12 Potentiometer with a Ag/$AgNO_3$ reference electrode (BAS Non-aqueous Reference Electrode Kit). Ferrocene (ethylferrocene where appropriate) was used as an internal standard.

2.2.7 Elemental analysis

Elemental analyses were performed by Warwick Analytical Services, University of Warwick, and by MEDAC Analytical Services.

2.3 Preparation and purification of solvents and reagents

Several compounds prepared during the course of this research were only accessible *via* certain commercially unavailable precursors. Such starting materials have been prepared from readily available reagents as described in the following tables. Some of the commercially available reagents were purchased and used as supplied without further purification, however many starting materials and solvents required purification prior to use. The sources and necessary methods of purification for the various compounds used are found in Table 2.1.

Table 2.1 Chemical suppliers and purification methods.

Compound	**Source**	**Quoted purity**	**Method**
Reagents			
Ferrocene	Alfa Aesar	99 %	Used as supplied
Trans-Stilbene	Lancaster	97 %	Used as supplied
Methane sulphonamide	Avocado	98+ %	Used as supplied
$(DHQD)_2PHAL$	Aldrich	95+ %	Used as supplied
Potassium ferricyanide	Aldrich	99 %	Used as supplied
Potassium carbonate	Aldrich	99 %	Used as supplied
Potassium osmate (VI) dihydrate ($K_2OsO_4.2H_2O$)	Aldrich	Unknown	Used as supplied
Sodium sulphite	B.D.H	96 %	Used as supplied
Sulphuric acid	Fisher	98 %	Used as supplied
Conc. Hydrochloric acid (37 %)	Fisher	Unknown	Used as supplied
Magnesium sulphate	Fisher	99 %	Used as supplied
Triethylamine	Alfa Aesar	99 %	Dried over sodium wire
Boron tribromide	Aldrich	99+ %	Used as supplied
Boron trifluoride etherate	Aldrich	'purified'	Used as supplied
^{n}BuLi (1.6 M in hexanes)	Acros Organics	Unknown	Used as supplied
Tetra-*n*-butylammonium fluoride hydrate	Aldrich	98 %	Used as supplied

Potassium fluoride	Aldrich	99.5 %	Used as supplied
18-Crown-6	Aldrich	99 %	Used as supplied
Ethylferrocene	Aldrich	98 %	Used as supplied
Tetramethylethylene diamine	Aldrich	99 %	Dried over sodium wire
Tri-n-butylborate	Alfa Aesar	98 %	Used as supplied
N-methylmorpholine-N-oxide	Aldrich	Unknown	Used as supplied
Cyclooctadiene	Alfa Aesar	99 %	Used as supplied
Hexamethylenetetramine	Aldrich	99 %	Used as supplied
Methyl iodide	Avocado	99 %	Used as supplied
Silver (I) triflate	Aldrich	99 %	Used as supplied
Silver (I) tetrafluoroborate	Aldrich	99 %	Used as supplied
Ferroceneboronic acid	Aldrich	99 %	Used as supplied
1,2-dibromoferrocene	I. R. Butler	Unknown	Used as supplied
Potassium hydroxide	Fisher	85+ %	Used as supplied
Dihydroxy-para-quinone	Aldrich	98 %	Used as supplied
Chlorotrimethylsilane	Aldrich	99+ %	Used as supplied
Triethoxyborane	Aldrich	99 %	Used as supplied
Granular tin	Aldrich	99+ %	Used as supplied
Silver (I) Fluoride	Aldrich	99 %	Used as supplied
Solvents			
Toluene	Fisher	99+ %	Heated under reflux over sodium followed by distillation
Hexanes	Fisher	99+ %	Heated under reflux over potassium followed by distillation

Dichloromethane	Fisher	99+ %	Heated under reflux over CaH_2 followed by distillation
THF	Fisher	99+ %	Heated under reflux over sodium followed by distillation
Acetonitrile	Fisher	99+ %	Heated under reflux over CaH_2 followed by distillation
Diethyl ether	Fisher	99+ %	Heated under reflux over sodium followed by distillation
2-Methyl-2-propanol	Aldrich	99.5 %	Used as supplied
Ethanol	Fisher	99+ %	Used as supplied
Deuterated Solvents			
Benzene-d_6	Goss	99.6 atom %	Stored under argon over potassium mirror
Chloroform-d	Aldrich	99.8 atom %	Stored under argon over flamed-out molecular sieves
Dichloromethane-d_2	Goss	99.8 atom %	Stored under argon over flamed-out molecular sieves
DMSO-d_6	Avocado	99.5 atom %	Used as supplied
Deuterium Oxide	Goss	99.9 atom %	Used as supplied

2.3.1 Preparation of precursors

Preparation of Dibromoborylferrocene, $FcBBr_2$

Dibromoborylferrocene was prepared by minor amendment of the method published by Ruf, Renk and Siebert.[1] Boron tribromide (5 ml, 52.6 mmol) was added slowly to a solution of ferrocene (9.84 g, 52.6 mmol) in toluene (80 ml) and the resulting mixture was stirred at 45 °C for 3 h. After cooling to room temperature and removal of solvent *in vacuo*, the solid product was extracted into hexanes (3 x 40 ml), combining the washings each time by cannula filtration. Concentration and cooling to –30 °C produced dark red crystals of $FcBBr_2$ in 51 % yield. NMR spectra (^1H and ^{11}B) were in agreement with those reported previously.[1]

Preparation of 1,1'-bis-(dibromoboryl)ferrocene, fc[BBr₂]₂

1,1'-*Bis*-(dibromoboryl)ferrocene was prepared according to the procedure reported by Appel, Noth and Schmidt.[2] Boron tribromide (10.2 ml, 0.108 mmol) was syringed into a slurry of ferrocene (10 g, 53.8 mmol) in dry degassed hexanes (120 ml) and the mixture was heated under reflux for 5 h. Insoluble products were removed by cannula filtration from the hot solution affording a dark red solution. Subsequent concentration and cooling to -30 °C yielded a dark red crystalline solid, isolated in 62 % yield. Characterising data was in the form of ^1H and ^{11}B NMR spectra, which were in accordance with literature reports.[2]

Preparation of 1,1'3,3'-tetrakis-dibromoborylferrocene, fc'[BBr₂]₄

1,1',3,3'-*tetrakis*-(dibromoboryl)ferrocene was prepared according to a procedure reported by Noth *et al.*[2] Boron tribromide (10.2 ml, 108 mmol) was added *via* syringe to solid pre-dried ferrocene (2 g, 10.8 mmol) in a jacketed Schlenk equipped with a stirrer bar. The resulting dark red mixture was heated at reflux (100 °C) with stirring for 36 h. Insoluble products were removed by cannula filtration and washed with portions of toluene (3 x 20 ml). The filtrates were combined and volatiles were removed in vacuo to yield a dark red solid (6.09 g, 65 %). The product was characterised by ^{1}H and ^{11}B NMR spectra which were in agreement with those reported by Noth *et al.*[2]

Preparation of 1',3, 3'-tris-dibromoboryl-1-ethylferrocene, fc'[BBr$_2$]$_3$Et

1,1'3,-*tris*-(dibromoboryl)-3'-ethylferrocene was prepared according to a procedure reported in the thesis of Dörfler.[3] Boron tribromide (6.19 ml, 65 mmol) was added gradually *via* cannula to a stirred solution of ethylferrocene (2.39 ml, 14 mmol) in dry degassed hexanes (150 ml). The resulting dark orange solution was heated to reflux for 24 h. Insoluble products were removed by cannula filtration and the remaining deep red filtrate was cooled to -78 °C. A red powder precipitated from solution, which was isolated by cannula filtration at -78 °C in a yield of 4.18 g, 41 %. Characterising data was in the form of ^{1}H and ^{11}B NMR spectra, which were in accordance with that reported by Dörfler.[3]

Preparation of 1,1'-ferrocene-bis-boronic acid, fc[B(OH)$_2$]$_2$

Ferrocene-*bis*-boronic acid was prepared according to a procedure reported by Knapp and Rehahn.[4] To a stirred solution of ferrocene (10 g, 54 mmol) in diethyl ether (200 ml) at room temperature was added a mixture of TMEDA (18.1 ml, 120 mmol), n-butyllithium (^{n}BuLi) (1.6 M in hexane, 75 ml, 120 mmol) and diethyl ether (100 ml). The reaction mixture was stirred for 6 h at room temperature then added dropwise to a stirred and cooled (-78 °C) solution of tributylborate (35 ml, 130 mmol) in diethyl ether (200 ml). The mixture was stirred at -78 °C for 1 h, then allowed to warm to room temperature and stirred for a further 12 h. After hydrolysis with 10 % aqueous potassium hydroxide (150 ml), the organic phase was extracted with aqueous potassium hydroxide (4 x 100 ml). The combined aqueous layers were cooled in an ice-bath and acidified with dilute sulphuric acid (10 %). The resulting precipitate was isolated by filtration, washed with water (500 ml) and dried under vacuum. The crude material was purified by successive chloroform washings to remove ferroceneboronic acid yielding pure ferrocene-*bis*-boronic acid (2.9 g, 21 %). The product was characterised by ^{1}H, ^{11}B and ^{13}C NMR spectra which were in agreement with those reported by Knapp *et al.*.[4]

Preparation of (S,S)-stilbenediol, (1,2-diphenyl-1,2-ethanediol)

The synthesis of (S,S)-stilbenediol was carried out following the method of Sharpless *et al.*[5] An aqueous solution of potassium ferricyanide (32.3 g, 98 mmol) and potassium carbonate (13.5 g, 33 mmol) was added to a solution of trans-stilbene (6 g, 33 mmol), methane sulphonamide (3.1 g, 33 mmol) and $(DHQD)_2PHAL$ [(S,S)-enantiomer] (255 mg, 0.33 mmol) in tert-butanol (300 ml). The bi-phasic reaction mixture was stirred very vigorously. Potassium osmate(VI) dihydrate (0.049 g, 0.13 mmol) was added and the reaction mixture was stirred for 48 h. To the bright yellow reaction mixture was then added sodium sulphite (4.2 g, 33 mmol) followed by ethyl acetate (180 ml). The organic layer was washed with dilute sulphuric acid (20 ml of a 1 M solution), followed by a solution of sodium hydrogen carbonate (30 ml of a 1 M solution in water) and finally water (3 x 15 ml). Subsequent drying of the organic phase over magnesium sulphate, filtration and removal of solvent yielded a white crystalline solid which was re-crystallised from hot toluene with a yield of 4.2 g, 60 %. Characterising data i.e. ^{1}H and ^{13}C NMR spectra were in agreement with those reported by Sharpless *et al.*[5]

Preparation of 1-(2-napthyl)-1,2-ethanediol

The method of Sharpless *et al.*[5] was employed in the preparation of 1-(2-napthyl)-1,2-ethanediol. An aqueous solution of potassium ferricyanide (32 g, 100 mmol) and potassium carbonate (13.4 g, 100 mmol) in water (160 ml) was added to a solution of 2-vinylnapthalene (5 g, 32.4 mmol) and $(DHQD)_2PHAL$ [(S,S) enantiomer] (253 mg, 0.33 mmol) in tert-butanol (160 ml). The biphasic reaction mixture was stirred vigorously. Potassium osmate (VI) dihydrate (0.047 g, 0.13 mmol) was then added to the stirred reaction mixture followed by vigorous stirring for 48 h. To the bright yellow reaction mixture was then added sodium sulphite (4.2 g, 33 mmol) and the now beige solution was diluted with ethyl acetate (180 ml). The organic layer was then washed with dilute sulphuric acid (20 ml of a 1 M solution), followed by sodium hydrogen carbonate solution (30 ml of a 1 M solution in water) and finally water (50 ml). Subsequent drying of the organic phase over magnesium sulphate, filtration and removal of solvent on a rotary evaporator yielded a white crystalline solid which was recrystallised from hot toluene in 65 % yield. Characterising data was in the form of ^1H and ^{13}C NMR spectra were in agreement with that reported by Sharpless *et al.*[5]

Preparation of (1R,2S,5R,6S)-cyclooctane-1,2,5,6-tetraol

(1R,2S,5R,6S)-Cyclooctane-1,2,5,6-tetraol was synthesised following a procedure reported by Sharpless *et al.*[6] To a solution of cyclooctadiene (2.83 ml, 23 mmol) in acetone (60 ml) was added N-methylmorpholine-N-oxide (5 g, 42 mmol) in water (10 ml). Potassium osmate (VI) dihydrate (0.123 g, 0.33 mmol) was added to the reaction mixture, the reaction vessel was sealed and the contents were stirred for 48 h. A white precipitate formed after 24 h stirring, which was isolated by filtration and recrystallised from 2:1 methanol:acetone in a yield of 1.58 g, 39 %. Characterising data was in the form of ^1H and ^{13}C NMR spectra which were in agreement with that reported by Sharpless *et.al.*[6]

Preparation of 1,2-ferrocene-bis-boronic acid

The synthesis of 1,2-ferrocene-*bis*-boronic acid was achieved using 1,2-dibromoferrocene as the starting material.[7] 1,2-Dibromoferrocene (0.380 g, 11 mmol) was dried in vacuo and dissolved in dry diethyl ether (35 ml). The resulting solution was cooled to –65°C and t-BuLi (1.46 ml of a 1.7 M solution in pentanes) added dropwise. The reaction mixture was warmed to –40°C and stirred for 4 h. The resulting yellow solution was then cooled to –60 °C and triethylborate (1 ml, 5.9 mmol) in diethyl ether (20 ml) added dropwise. The resulting mixture was stirred at –60 °C for 1 h, then warmed to room temperature and stirred for a further 12 h. After extraction with degassed, 10 % aqueous KOH solution (3 x 20 ml at 0 °C), the combined aqueous layer was neutralised with 10 % H_2SO_4 (neutralisation determined using universal indicator paper) and a white precipitate isolated. The orange aqueous layer was filtered and back-extracted into diethyl ether; volatiles removed in vacuo to yield an orange powdery solid (0.136 g, 45 %). Characterising data were in accordance with those provided by I. R. Butler.[8]

Preparation of MeHMTAF, Methylhexamethylenetetramine fluoride dihydrate

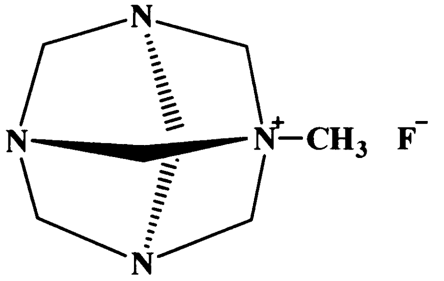

Methylhexamethylenetetramine fluoride dihydrate was prepared according to the procedure reported by Clark and Nightingale.[9] Hexamethylenetetramine (5 g, 36 mmol) was placed in a round-bottomed flask and dissolved in chloroform (70 ml). The flask was fitted with a reflux condenser then cooled in an ice bath before methyl iodide (6.7 ml, 107 mmol) was added. Methylhexamethylenetetramine iodide rapidly formed as a white precipitate. The reaction mixture was stirred overnight, the solution filtered and the resulting solid washed with chloroform and diethyl ether. The resulting white powdery solid was recrystallised from acetonitrile/methanol to yield methylhexamethylenetetramine iodide as white needle-like crystals. The white solid was then dissolved in distilled water (10 ml) and silver fluoride (2.74 g, 21.6 mmol) also as a solution in distilled water (20 ml) added to the methylhexamethylenetetramine iodide solution. The resulting yellow silver iodide precipitate was removed by filtration and water removed from the filtrate to yield a viscous oil which on cooling formed a white solid. After drying in vacuo methylhexamethylenetetramine fluoride dehydrate was isolated as a white free-flowing powder (8.05 g, 80.3 %). Characterising data was in the form of ^{1}H and ^{13}C NMR spectra which were in agreement with those reported by Clark *et al.*[9]

Preparation of 1,2,4,5-tetrahydroxybenzene

1,2,4,5 - Tetrahydroxybenzene was synthesised in quantitative yield according to the method of Hegedus and co-workers.[10] To a suspension of dihydroxy-*para*-quinone (10 g, 0.07 mol) in conc. HCl (200 ml) was added slowly granular tin (10 g), and the mixture heated at reflux for 2 h. Filtration whilst hot and subsequent cooling to 0 °C yielded off-white crystals, which were recrystallised from hot THF to form the pure compound as white crystals. IR and ^{1}H NMR spectra were in accordance with those quoted by Hegedus *et. al.*[10]

Preparation of 1,2,4,5-$(Me_3SiO)_4C_6H_2$

The synthesis of the trimethylsilyl derivative of tetrahydroxybenzene was carried by minor modification of the method reported by Aldridge and co-workers.[11] To a suspension of tetrahydroxybenzene (5 g, 35.2 mmol) in toluene (40 ml) was added via syringe triethylamine (19.6 ml, 0.14 mol) and chlorotrimethylsilane (17.9 ml, 0.14 mol). After stirring at room temperature, the reaction mixture was filtered via cannula, the white $[Et_3NH]Cl$ precipitate washed with toluene (2 x 15 ml) and the combined washings reduced to dryness in vacuo. The resulting solid was extracted into hexanes, filtered and concentrated before recrystallisation at –30 °C. Characterising data in form of ^{1}H and ^{13}C NMR spectra were in agreement with those previously reported by Aldridge *et. al.*[11]

Preparation of 1,2,3,4,5-pentamethylferrocene

To a slurry of $FeCl_2(THF)_{1.5}$ (3.73 g, 15.8 mmol) in THF (35 ml) was added TMEDA (14.4 ml, 15.8 mmol). The resulting slurry was cooled to -30 °C and a slurry of lithium-1,2,3,4,5-pentamethylcyclopentadienide (2.256 g, 15.8 mmol) in THF (50 ml) was added via cannula whilst stirring. The solution was stirred at -30 °C for 48 h, after which a solution of lithium cyclopentadienide (1.14 g, 15.8 mmol) in THF (30 ml) was added via cannula at -30 °C whilst stirring. The resulting solution was warmed to room temperature and stirred for 24 h. Volatiles were removed in vacuo and the dark yellow residue was dried under high vacuum. Recrystallisation from hexanes at -30 °C yielded a yellow crystalline solid. Characterising data in the form of ^{1}H and ^{13}C NMR spectra were in agreement with the expected product.

Preparation of 1,2,3,4,5-pentamethyl-1'-dibromoborylferrocene

To a solution of 1,2,3,4,5-pentamethylferrocene (1.07 g, 4.2 mmol) in toluene (50 ml) was added neat boron tribromide (0.4 ml, 4.2 mmol) via syringe. The dark red mixture was heated to 45 °C for 1.5 h with stirring. Volatiles were removed in vacuo and the red residue was dried under high vacuum for 3 h. The residue was washed with hexanes (2 x 40 ml), concentrated washings were cooled to -30 °C yielding a dark red powder which was isolated by filtration. Characterising data in the form of ^{1}H and ^{13}C NMR spectra were in agreement with those reported by M. Wagner.[12]

Preparation of 1,2,3,4,5-pentamethyl-1',3'-bis-dibromoborylferrocene

To a solution of 1,2,3,4,5-pentamethylferrocene (1.03 g, 4.0 mmol) in hexanes (50 ml) was added neat boron tribromide (1.9 ml, 20 mmol) via syringe. The dark red mixture was heated at reflux for 20 h with stirring. The reaction mixture was filtered, concentrated, and cooled to –30 °C to yield a dark red crystalline solid which was isolated by filtration. Characterising data in the form of ^{1}H and ^{13}C NMR spectra were in agreement with those reported by M. Wagner.[12]

2.4 References

1 T. Renk, W. Ruf, W. Siebert, *J. Organomet. Chem.*, 1976, **120**, 1.

2 A. Appel, H. Nöth, M. Schmidt, *Chem. Ber.*, 1995, **128**, 621.

3 U. Dörfler, PhD thesis, University of Bayreuth, 1994.

4 R. Knapp, M. Rehahn, *J. Organomet. Chem.,* 1993, **452**, 235.

5 K. B. Sharpless, *Chem. Rev.*, 1994, **94**, 2483.

6 A. Gypser, D. Michel, D. S. Nirschl, K. B. Sharpless, *J. Org. Chem.*, 1998, **63**, 7322.

7 I. R. Butler, M. G. B. Drew, *Inorg. Chem. Commun.*, 1999, 234.

8 I. R. Butler, personal communication.

9 J. H. Clark, D. J. Nightingale, *Journal of Fluorine Chemistry.*, 1996, **78**, 91.

10 P. R. Weider, L. S. Hegedus, H. Asada, S. V. D'Andreq, *J. Org. Chem.*, 1985, **50**, 4276.

11 S. Aldridge, R. J. Calder, A. Rossin, A. A. Dickinson, D. J. Willock, C. Jones, D. J. Evans, J. W Steed, M. E. Light, S. J. Coles, M. B. Hursthouse, *J. Chem. Soc., Dalton Trans.*, 2002, **26**, 677.

12 M. Wagner, personal communication.

Chapter Three

The Synthesis and Characterisation of Mono- Tris- and Tetrafunctional Boron-Containing Lewis Acids

3.1 Introduction

The preparation of metallocene systems featuring boron-substituted cyclopentadienyl ligands has attracted much research interest over recent years and such systems have been reported for most elements of the first transition series. These compounds find extensive application in the fields of anion sensing and molecular recognition,[1] in olefin polymerisation catalysis (primarily with group 4 systems), [2,3] and as precursors to organometallic polymers and oligomers of interest due to their remarkable electronic properties.[4,5]

There are two main synthetic approaches that have been established for the preparation of metal complexes bearing borylcyclopentadienyl ligands. The first and less widely used method involves the reaction of a transition metal complex (e.g halide, amide or alkyl) with a cyclopentadienyl ligand precursor containing a pendant boryl function. This approach was utilized by Herberich and co-workers in the preparation of bis(boryl)cobaltocenium ions which were subsequently found to bind various anions depending on the nature of the boryl substituent, R. This series of compounds was prepared by the reaction of an alkali-metal borylcyclopentadienide [M($C_5H_4BR_2$) where M = Li, Na and R = Pr^i] with $CoBr_2$.DME (Scheme 3.1), followed by subsequent oxidation to the corresponding cobaltocenium complex.[6,7]

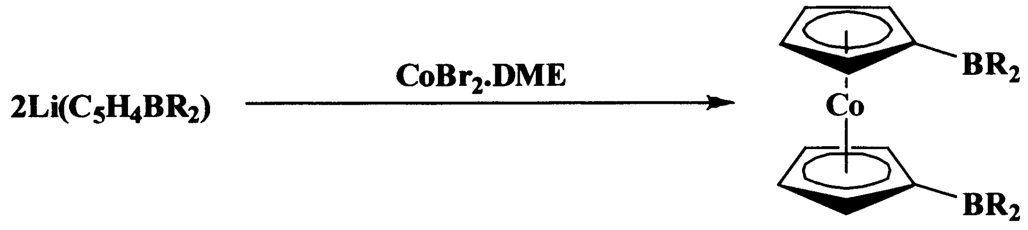

Scheme 3.1 Bis(boryl) substituted cobaltocenes synthesised from pre-assembled borylcyclopentadienyl ligands

The second approach involves introduction of the boron functionality to an existing metallocene fragment, primarily via electrophilic aromatic substitution using boron trihalides. This route has been explored by Siebert *et al.*, for example, to produce both *mono-* and *bis*-dihaloborylferrocenes (Scheme 3.2) *via* electrophillic borylation of ferrocene.[8]

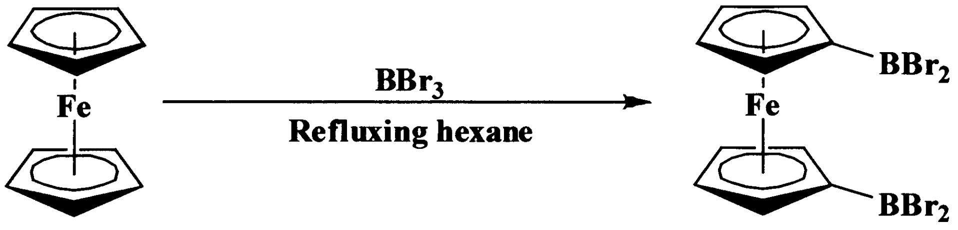

Scheme 3.2 Direct *bis*-borylation of ferrocene with boron tribromide

This chemistry has since been extended in subsequent work by Nöth *et al.* leading to the isolation of the *tris-* and *tetrakis*-dihaloboryl derivatives of ferrocene, ruthenocene and osmocene (Scheme 3.3).

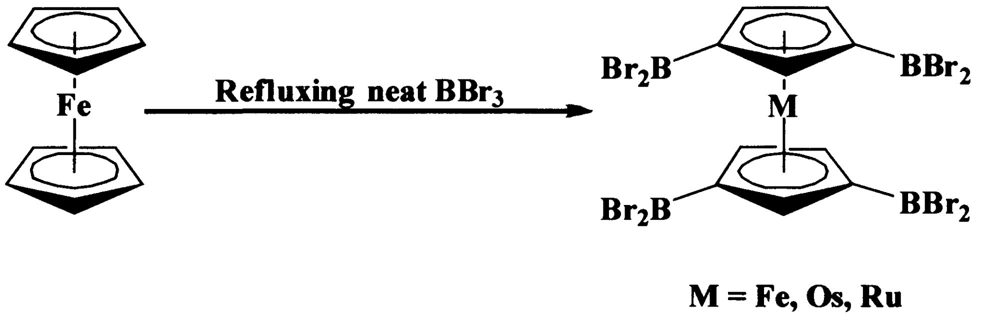

Scheme 3.3 Direct borylation of ferrocene with neat boron tribromide

More severe reaction conditions are required than those used in preparation of the *mono-* and *bis*-dihaloboryl ferrocenes, i.e. the use of neat BBr_3 at reflux temperatures.[9] The resulting complexes feature dihaloboryl units that can be further derivatized *via* boron-centred substitution reactions.[10] A related borylation reaction was applied by Piers *et al.* in the preparation of bis-(pentafluorophenyl)borylferrocene, involving the treatment of ferrocene with bis-(pentafluorophenyl)borane, a highly electrophilic reagent used to introduce a boron-containing fragment.[11]

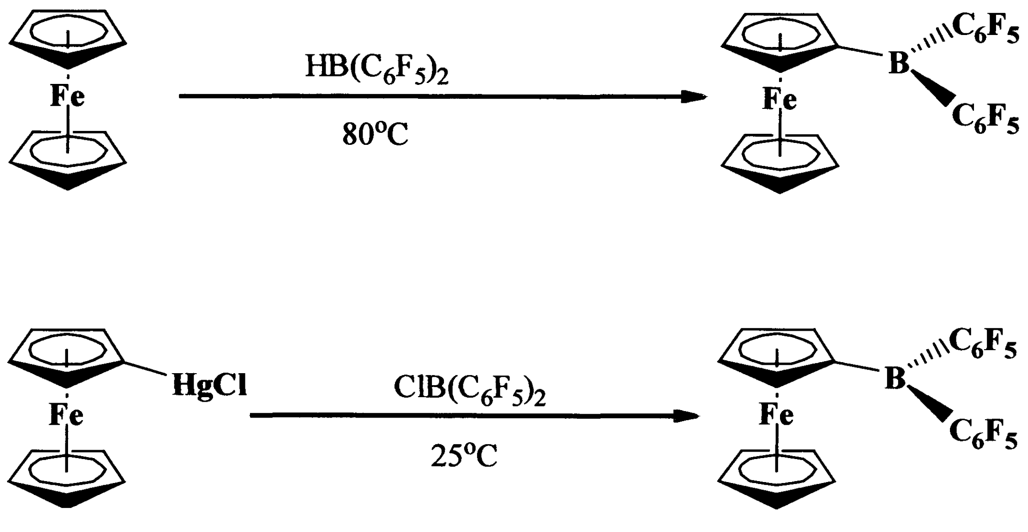

Scheme 3.4 Two alternative syntheses of bis-(pentafluorophenyl)borylferrocene

The authors also reported a second approach to the same compound in which the boron-containing unit is introduced to a metallated ferrocene, (chloromercuric) ferrocene, by treatment with the analogous chloroborane species $ClB(C_6F_5)_2$. A similar process to introduce the boron-containing fragment by reaction of a metallated cyclopentadienyl ring with a boron halide has been reported by Manners *et al.* who reacted a tin-containing ferrocenophane with one equivalent of boron trichloride to introduce a single dichloroboryl moiety.[12]

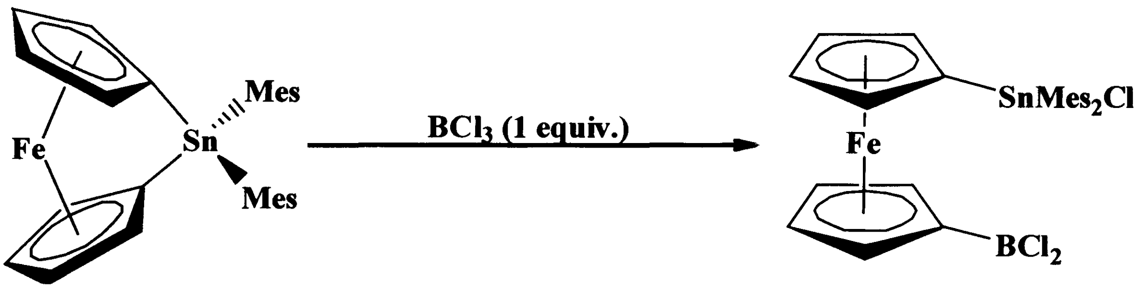

Scheme 3.5 Borylation of a metallated cyclopentadienyl with BCl_3

3.1.1 Aims of present research

Employing the direct borylation methods reported by Siebert and co-workers[8] *mono-* and *bis-*(dihaloboryl)ferrocene systems have been prepared and were further derivatized to synthesize a range of *mono-* and *bis-*boronate esters.[10] The reasons for the choice of ferrocene as the backbone in these compounds were three-fold: firstly synthetic ease of borylation, secondly the ready spectroscopic and electrochemical handles offered by ferrocene-based systems, and thirdly the potential for further derivatization at the boron centre to allow for tuning of the Lewis acidity. Following the initial preparation of ferrocene *mono-* and *bis-*boronate esters and some interesting anion binding properties displayed by such compounds, it was decided (i) to extend this approach to incorporate *tris*- and *tetrakis*- boronate esters using analogous direct borylation chemistry, and (ii) to extend the preparation of *mono*-boronate esters to cover alternative derivatization patterns at boron.

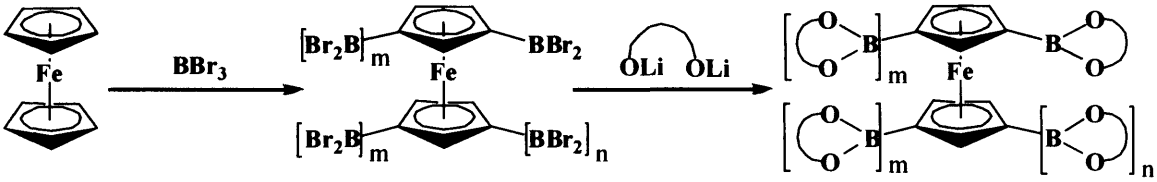

Scheme 3.6 General preparative scheme for *mono* and multi-functional boryl metallocenes (where n = 0, 1 and m = 0, 1)

3.2 Experimental

Preparation of mono-ethanediolatoborylferrocene (**1a**)

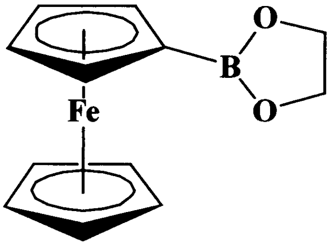

Ethane-1,2-diol (1.2 ml, 2.15 mmol) was dried under vacuum for 3 h and dissolved in toluene (30 ml). Triethylamine (0.6 ml, 4.27 mmol) was then added to the stirred diol solution followed by a solution of dibromoborylferrocene (0.75 g, 2.1 mmol) in toluene (30 ml). The resulting cloudy orange solution was stirred for twelve 12 h. The ^{11}B NMR spectrum at this point revealed the presence of boric acid at δ_B 22 ppm along with the desired product at δ_B 32 ppm. The orange solution was filtered and volatiles removed in vacuo to produce a bright yellow powder in 32 % yield, which was further dried in vacuo. The yellow powder was washed with dry hexane; the washings were filtered and placed in the freezer. Slow evaporation of benzene from a solution afforded orange block-like crystals suitable for X-ray diffraction. ^{1}H NMR (400 MHz, [D]chloroform, 20 °C): δ 4.08 [s, 5H, C_5H_5], 4.26 [s, 4H, CH_2CH_2 of chelate], 4.34 [m, 4H, C_5H_4]. ^{13}C{^{1}H} NMR (75.5 MHz, [D]chloroform, 20 °C): δ 65.8 [CH_2CH_2 of chelate], 68.5 [C_5H_5], 72.2 [C_5H_4], 73.7 [C_5H_4]. ^{11}B{^{1}H} NMR (96 MHz, [D]chloroform, 20 °C): δ 32.7. IR (KBr disc, cm^{-1}): ν 2973 w, 2911 md, 1497 md, 1473 s, 1312 s, 1384 md, 1184 md, 1129 s, 990 s. UV/Vis (chloroform): λ_{max} 444 nm, ε = 135 cm^{-1} mol^{-1} dm^3. MS(EI): M^+ = 256 (100 %), exact mass (calc.) *m/z* 256.0353, (obs.) 256.0352. Crystal data: $C_{12}H_{13}BFeO_2$, orthorhombic, $P\,2_1\,2_1\,2_1$, a = 5.81790(10) Å, b = 9.9233(2) Å, c = 18.4741(5) Å, V = 1066.56(4) Å^3, Z = 4, D_{calc} = 1.594 Mg m^{-3}, μ(MoKα) = 1.391 mm^{-1}. A suitable crystal was covered in pre-dried mineral oil and mounted at 150(2) K. 2138 unique reflections were collected ($3.6 < \theta < 26.3°$). Final R-factor: R_1 = 0.034.

Preparation of (pinanediolatoboryl)ferrocene (**1b**)

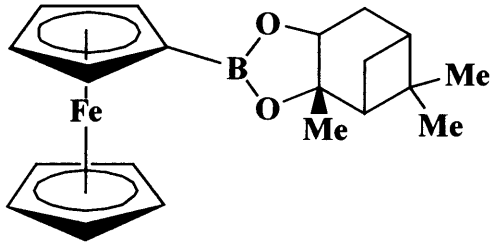

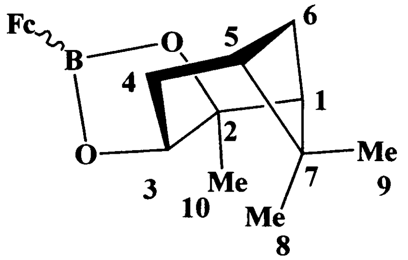

(1S,2S,3R,5S)-(+)-Pinane diol (0.461 g, 2.7 mmol) was dried in vacuo for 4 h and dissolved in toluene (25 ml), the diol solution cooled to –78°C and n-butyllithium (3.52 ml of a 1.6 M solution in hexanes, 5.6 mmol) added drop-wise via syringe. The dilithiate solution was warmed to room temperature and stirred for 2 h whereupon a solution of dibromoborylferrocene (1.002 g, 1.2 mmol) in toluene (50 ml) was added drop-wise via cannula. The resulting orange reaction mixture was stirred for 48 h and the orange solution was filtered from the precipitate. Toluene was removed in vacuo to yield a bright orange powdery solid, which was further dried in vacuo, taken into a minimum volume of hexane and placed in the freezer (-30 °C). An orange solid crashed out of hexane, was isolated, dried in vacuo and re-dissolved in acetonitrile. Slow evaporation of solvent from an acetonitrile solution afforded orange block-like crystals of the product. Yield of orange solid: 379 mg, 37.1 %. ^{1}H NMR (400 MHz, [D]chloroform, 20 °C): δ 0.42 [s, 3H, H-8], 0.93 [s, 3H, H-9], 1.21 [s, 3H, H-10], 1.33 [d J = 10 Hz, 1H, H-6a], 1.55 [m, 1H, H-5], 1.89-2.08 [overlapping m, 4H, H-1, H-4a, H-4b, H-6b], 4.03 [s, 5H, C_5H_5], 4.10 [m, 2H, C_5H_4], 4.11 [d J = 2 Hz, 1H, H-3], 4.58 [d J = 1.6 Hz, 2H, C_5H_4], atom numbering scheme shown above. ^{13}C{^{1}H} NMR (75.5 MHz, [D]chloroform, 20 °C): δ 22.5, 25.5, 25.7, 27.9, 34.7, 36.8, 38.5, 50.4, 73.1, 76.7 [pinane backbone], 67.5 [C_5H_5], 70.9 [C_5H_4], 73.0 [C_5H_4]. ^{11}B{^{1}H} NMR (96 MHz, [D]chloroform, 20 °C): δ 30.1. IR (KBr disc, cm^{-1}): ν 2930 md, 1501 md, 1482 s, 1382 s, 1324 s, 1261 md, 1189 w, 1130 s, 1034 md, 909 w, 816 s, 702 w, 688 md, 598 w. UV / Vis (chloroform): λ_{max} 446 nm, ε = 134 mol^{-1} cm^{-1} dm^3. MS (EI): M^+ = 364.1 (100%), exact mass (calc.) *m/z* 362.1292, (obs.) 364.1290. Crystal data: $C_{20}H_{25}BFeO_2$, tetragonal, P_42, a = 16.8050(16) Å, b = 16.8050(16)Å, c = 6.3272(4)Å, V = 1786.9(3) Å^3, Z = 4, D_{calc} = 1.353 Mg m^{-3}, μ(MoKα) = 0.852 mm^{-1}. A suitable crystal was covered in pre-dried mineral oil and mounted at 150(2) K. 3179 unique reflections were collected (3.6 < θ < 26.3°). Final R-factor: R_1 = 0.084.

Preparation of 1,1',3-tris-(ethanediolatoboryl)-3'-ethyl ferrocene (**3a**)

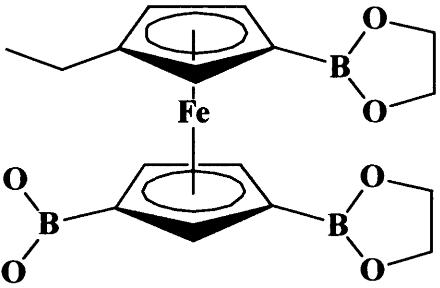

Ethane-1,2-diol (0.31 ml, 5.56 mmol) was dried in vacuo for 6 h and dissolved in toluene (50 ml), and triethylamine (1.54 ml, 10.9 mmol) added via syringe. 1,1',3-*tris*-(dibromoboryl)-3'-ethyl ferrocene (1.33 g, 1.83 mmol) in toluene (50 ml) was then added drop-wise via cannula and the resulting orange solution stirred for 12 h. After filtration, the solvent was removed in vacuo to yield an orange powdery solid. Recrystallisation from hexanes at –30 °C yielded an orange oil which was dried under high vacuum to yield an orange solid: 318 mg (41 %). ^{1}H NMR (400 MHz, [D]chloroform, 20 °C): δ 0.91 [t J = 7 Hz, 3H, CH_3 of Et], 2.26 [broad quartet, 2H, CH_2 of Et], 4.22 [m, 1H, C_5H_3], 4.24 [s, 1H, C_5H_3], 4.26 [b s, 12H, CH_2CH_2 of chelate], 4.45 [m, 1H, C_5H_3], 4.51 [m, 2H, C_5H_3]. ^{13}C{^{1}H} NMR (75.5 MHz, [D]chloroform, 20 °C): δ 14.6, 21.7 [Et], 64.7 [CH_2 of chelate, 2 overlapping signals (ca. 2:1) at 64.72 and 64.46], 65.77 [CH_2 of chelate], 72.7, 74.3, 74.4, 78.4, 78.6, 81.7 [CH of C_5H_3]. ^{11}B NMR (96 MHz, [D]chloroform, 20 °C): δ 32.6. IR (KBr disc, cm^{-1}): ν 2924 s, 1460 s, 1376 s, 1298 md, 1198 md, 1084 w, 1064 md, 991 md, 42 md, 850 w, 722 md, 686 w. UV/Vis (chloroform): λ_{max} 454 nm, ε = 199 mol^{-1}cm^{-1}dm^3. MS(EI): M$^+$ = 424 (100%), exact mass (calc.) *m/z* 424.1118, (obs.) 424.1119.

Preparation of 1,1',3-tris-(stilbenediolatoboryl)-3'-ethyl ferrocene **(3b)**

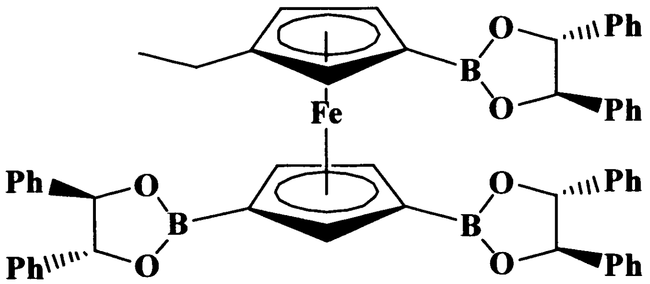

(S,S)–Stilbenediol (1.18g, 5.51 mmol) was dried in vacuo for 2 h and dissolved in toluene (70 ml), the solution was cooled to –78 °C and n-butyllithium (6.89 ml of a 1.6 M solution in hexanes, 11.0 mmol) was added drop-wise via syringe. After warming to room temperature and stirring for 1 h, 1,1',3-*tris*-(dibromoboryl)-3'-ethyl ferrocene (1.33 g, 1.83 mmol), in toluene (50 ml) was added drop-wise via cannula. A white precipitate was formed and the resulting cloudy orange solution stirred for 12 h before filtration. Volatiles were then removed in vacuo to yield an orange oily product which was further dried under high vacuum to produce an orange powdery solid. The orange solid was extracted into hexane, and precipitated at -30°C, the solid was isolated by filtration. An acetonitrile solution of the resulting solid, layered with water in an NMR tube yielded orange plate-like crystals. Yield of orange solid: 672 mg, 46%. ^{1}H NMR (400 MHz, [D]chloroform, 20 °C): δ 1.08 [t J = 3.3 Hz, 3H, CH_3 of Et], 2.38 [q, 2H, CH_2 of Et], 4.47 [s, 1H, CH of chelate], 4.50 [s, 1H, CH of chelate], 4.55 [s, 1H, CH of chelate], 4.63 [s, 1H, CH of chelate], 4.85 [s, 1H, CH of chelate], 5.01 [s, 1H, CH of chelate], 5.13 [m, 2H, C_5H_3], 5.14 [m, 2H, C_5H_3], 5.22 [s, 1H, C_5H_3], 5.25[s, 1H, C_5H_3], 7.25-7.67 [m, 30H, aromatic CH]. $^{13}C\{^{1}H\}$ NMR (75.5 MHz, [D]chloroform, 20 °C): 14.0, 21.1 [Et], 72.6, 73.6, 74.1, 77.7, 78.5, 81.0 [CH of chelate], 125.0, 125.2, 125.3, 127.0, 127.1, 127.2, 127.5, 127.6, 127.7 [aromatic CH], 138.7, 138.8, 139.3 [aromatic quarternary]. $^{11}B\{^{1}H\}$ NMR (96 MHz, [D]chloroform, 20 °C): δ 34.1. IR (KBr disc, cm^{-1}): v 2923 s, 1463 s, 1376 s, 1274 s, 1209 md, 1078 w, 1059 md, 986 md, 844 w, 759 md, 697 s, 650 w, 611 w. UV/Vis (chloroform): λ_{max} 454 nm, $\varepsilon = 253$ mol^{-1} cm^{-1} dm^{3}. MS(EI): $M^+ = 880$ (100%), exact mass (calc.) *m/z* 880.2996, (obs.) 880.2997. Crystal data: $C_{54}H_{47}B_3FeO_6$, orthorhombic, P 2_1 2_1 2_1, a = 9.26740(10) Å, b = 15.9758(2) Å, c = 30.0231(4) Å, V = 4445.04(9) Å^3, Z = 4, D_{calc} = 1.315 Mg m^{-3}, μ(MoKα) = 0.392 mm^{-1}. A suitable crystal was covered in pre-dried mineral oil and mounted at 150(2) K. 8873 unique reflections were collected (3.6 < θ < 26.3°). Final R-factor: $R_1 = 0.071$.

Preparation of 1,1',3-tris-(pinanediolatoboryl)-3'-ethyl ferrocene (**3c**)

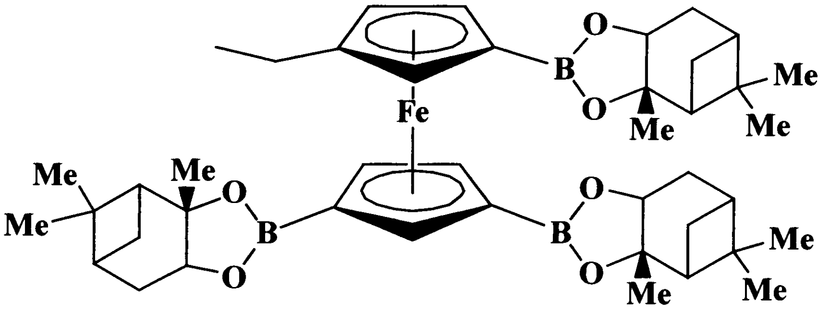

(1S,2S,3R,5S)-(+)-Pinanediol (0.784 g, 5.49 mmol), was dried in vacuo for 2 h and dissolved in toluene (40 ml), the diol solution cooled to –78 °C and n-butyllithium (6.86 ml of a 1.6 M solution in hexanes, 10.9 mmol) added drop-wise via syringe. After warming to room temperature and stirring for 2 h, 1,1',3-*tris*-(dibromoboryl)-3'-ethyl ferrocene (1.33 g, 1.83 mmol) in toluene (50 ml) was added drop-wise. The resulting cloudy orange solution was stirred for 12 h, filtered, and volatiles removed in vacuo to yield an orange powdery solid. The solid was dissolved in a minimum volume of hexane, cooled to –30°C, and an orange oily solid isolated by filtration and further dried under high vacuum. Yield of orange solid: 523 mg (38 %). ^{1}H NMR (400 MHz, [D]chloroform, 20 °C): δ 0.82 [s, 9H, C-10], 1.09 [t *J* = 5 Hz, 3H, C-12], 1.24 [s, 9H, C-9], 1.20 [m, 3H], 1.41 [overlapping signals, 9H, C-8], 1.87 [m, 6H], 2.04 [m, 3H], 2.31 [m, 3H], 2.33 [m, 5H], 4.15-4.52 [overlapping m, 9H, C_5H_3 and H-3]. $^{13}C\{^1H\}$ NMR (75.5 MHz, [D]chloroform, 20 °C): δ 12.9 [Et, C12], 21.9 [Et, C11], 24.1, 26.7 [three overlapping signals], 27.2, 29.0, 35.7 [three overlapping signals], 38.2, 39.7, 51.4 [three overlapping signals] 77.8 [three overlapping signals], 85.6 [three overlapping signals, pinane backbones], 73.4, 77.4, 77.7, 78.2, 81.9, 82.5 [CH of C_5H_3]. $^{11}B\{^1H\}$ NMR (96 MHz, [D]chloroform, 20 °C): δ 32.8. IR (KBr disc, cm^{-1}): ν 2923 s, 1716 w, 1462 s, 1375 s, 1304 md, 1233 md, 1122 md, 1078 md, 1061 w, 1025 w, 989 w, 937 w, 722 md. UV/Vis (chloroform): λ_{max} 454 nm, ε = 218 mol^{-1} cm^{-1} dm^3. MS(EI): M^+ = 754 (100%), exact mass (calc.) *m/z* 754.4044, (obs.) 754. 4045.

Preparation of 1,1',3,3'- Tetrakis(ethanediolatoboryl)ferrocene (**4a**)

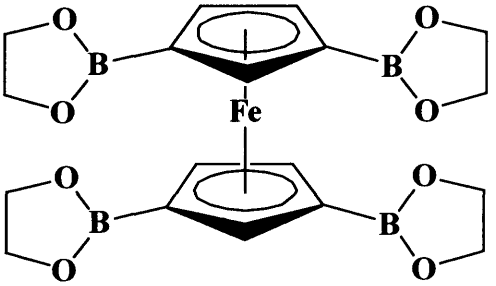

To a solution containing ethane-1,2-diol (0.42 ml, 7.52 mmol) and triethylamine (2.11 ml, 15 mmol) in toluene (30 ml) was added a solution of 1,1',3,3'-tetrakis(dibromoboryl) ferrocene (1.633g, 1.18 mmol), also in toluene (30 ml). An orange precipitate formed and the ^{11}B NMR spectrum at this point revealed the presence of boric acid (δ_B 22 ppm) along with the product peak (δ_B 32 ppm). The orange solution was filtered via cannula and the orange precipitate was washed with toluene and the washings were filtered, and combined. Toluene was removed in vacuo to yield a dark orange solid, which was washed with hexane and sonicated. The pale yellow hexane washings were dried in vacuo and the yellow solid was taken into deuterated benzene for NMR, yield of yellow solid: 264 mg (31 %). Benzene was allowed to slowly evaporate from the NMR sample and orange rod-like crystals grew over a two week period. Yield of crystals: 25.6 mg, 3.0 %. ^{1}H NMR (400 MHz, [D]chloroform, 20 °C): δ 4.35 [s, 16H, CH_2CH_2 of chelate], 4.53 [s, 4H, C_5H_3], 4.65 [s, 2H, C_5H_3]. $^{13}C\{^1H\}$ NMR (75.5 MHz, [D]chloroform, 20 °C): δ 64.8 [chelate], 77.7, 80.8 [C_5H_3], quaternaries of C_5H_4 not observed. $^{11}B\{^1H\}$ NMR (96 MHz, [D]chloroform, 20 °C): δ 32.3. IR (KBr disc, cm^{-1}): ν 3404 md, 1495 s, 1398 md, 1340 md, 1300 s, 1262 md, 1199 s, 1068 s, 992 md, 943 md, 860 w, 802 md, 691 md, 583 w, 500w. UV/Vis (chloroform): λ_{max} 442 nm, ε = 79 mol^{-1} cm^{-1} dm^3. MS(EI): M$^+$ = 466 (100%), exact mass (calc.) *m/z* 466.1031, (obs.) 466.1029. Crystal data: $C_{18}H_{22}B_4FeO_8$, monoclinic, P 2_1/n, a = 5.8495(3) Å, b = 9.8627(5) Å, c = 17.0345(11) Å, β= 96.899(2)°. V = 975.64(9) Å^3, Z = 2, D_{calc} = 1.584 Mg m^{-3}, μ(MoKα) = 0.819 mm^{-1}. A suitable crystal was covered in pre-dried mineral oil and mounted at 150(2) K. 1987 unique reflections were collected (3.6 < θ < 26.3°). Final R-factor: R_1 = 0.055.

Preparation of 1,1',3,3'-tetrakis(stilbenediolatoboryl)ferrocene (**4b**)

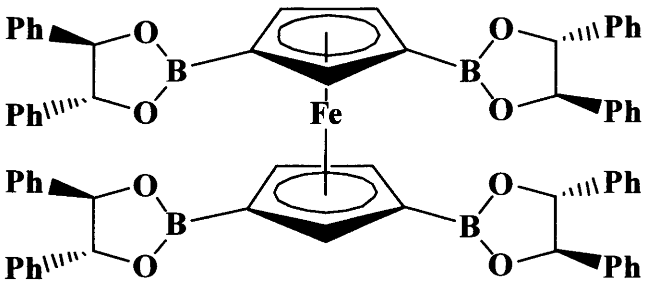

(S,S)-Stilbene-diol (1.48 g, 6.91 mmol) was dried in vacuo for 2 h, dissolved in toluene (50 ml) cooled to –78°C and n-butyllithium (8.65 ml of a 1.6M solution in hexanes, 13.8 mmol) was added drop-wise *via* syringe. The dilithiate was stirred for 48 h at room temperature before 1,1',3,3'-tetrakis(dibromoboryl)ferrocene (1.507g, 1.7 mmol) in toluene (50 ml) was added dropwise *via* cannula. The resulting orange solution was filtered and toluene was removed in vacuo to yield an orange viscous oily product. The product was dried in vacuo and washed with hexane but was only very sparingly soluble. A toluene solution of the product layered with hexanes afforded large orange block-like crystals. Yield of crystals: 698 mg, 38 %. ^{1}H NMR (300 MHz, [D$_8$]toluene, 20°C): δ 5.20 [m, 2H, C_5H_3], 5.23 [s, 4H, CH of chelate], 5.30 [m, 2H, C_5H_3], 5.34 [s, 4H, CH of chelate], 5.64 [s, 2H, C_5H_3], 7.01-7.24 [m, 40H, aromatic CH]. ^{13}C{^{1}H} NMR (75.5 MHz, [D$_6$]benzene, 20°C): δ 81.4, 81.8, 84.1 [C_5H_3], 88.4, 88.5 [CH of chelate], 127.7, 128.1, 129.8, 129.9, 138.6 (2 overlapping signals) [aromatic CH], 146.3, 146.5 [aromatic quaternary]. ^{11}B{^{1}H} NMR (96 MHz, [D$_6$]benzene, 20°C): δ 33.2 (b). IR (KBr disc, cm^{-1}): ν 3033 w, 1605 w, 1496 s, 1276 s, 1213 md, 1192 md, 1146 w, 1061 s, 988 s, 802 w, 760 md, 698 s, 538 md. UV/Vis (chloroform): λ_{max} 472 nm, ε = 667 mol^{-1} cm^{-1} dm^3. MS(EI): M^+ = 1074 (100%), exact mass (calc.) *m/z* 1074.3535, (obs.) 1074.3546. Crystal data: $C_{66}H_{54}B_4FeO_8$, orthorhombic, C 222_1, a = 12.3580(2) Å, b = 15.4190(2) Å, c = 29.7570(5) Å, V = 5670.14(15) Å^3, Z = 4, D_{calc} = 1.258 Mg m^{-3}, μ(MoKα) = 0.322 mm^{-1}. A suitable crystal was covered in pre-dried mineral oil and mounted at 150(2) K. 5619 unique reflections were collected (3.6 < θ < 26.3°). Final R-factor: R_1 = 0.051.

Preparation of 1,1',3,3'-tetrakis(pinanediolatoboryl)ferrocene (**4c**)

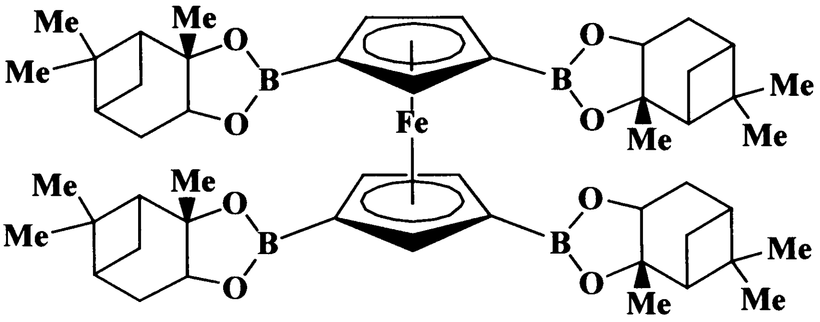

(1S,2S,3R,5S)-(+)-Pinane diol (0.784 g, 4.6 mmol) was dried in vacuo for 2 h, dissolved in toluene (40 ml), the solution was cooled to –78°C and n-butyllithium (5.75 ml of a 1.6 M solution in hexanes, 9.2 mmol) added drop-wise via syringe. The dilithiate solution was warmed to room temperature and stirred for 2 h, whereupon a solution of 1,1',3,3'-tetrakis(dibromoboryl)ferrocene (1.003 g, 1.2 mmol) in toluene (50 ml) was added drop-wise via cannula. The resulting orange solution was filtered, and toluene was removed in vacuo to yield an orange solid which was further dried under high vacuum. Recrystallisation from acetonitrile produced orange plate-like crystals. Yield of orange solid: 488 mg (47 %). ^{1}H NMR (400 MHz, [D]chloroform, 20 °C): δ 0.80 [s, 12H, H-10], 1.24 [s, 12H, H-9], 1.42 [s, 12H, H-8], 1.88 [overlapping m, 12H], 2.02 [t $J = 5$ Hz, 4H], 2.16 [m, 4H], 2.29 [m, 4H], 4.30 [t $J = 7$ Hz, 4H, H-3], 4.50 [m, 4H, C_5H_3], 4.56 [m, 2H, C_5H_3], 5.22 [m, 4H, H-3]. $^{13}C\{^{1}H\}$ NMR (75.5 MHz, [D]chloroform, 20 °C): δ 23.8, 26.9, 29.1, 35.8, 37.9, 39.7, 51.6, 51.7,81.8, 85.6 [pinane backbone], 78.0 [C_5H_5], 78.2 [C_5H_3], 79.0 [C_5H_3]. $^{11}B\{^{1}H\}$ NMR (96 MHz, [D]chloroform, 20 °C): δ 32.3. IR (KBr disc, cm^{-1}): ν 3434 w, 2913 s, 2868 md, 2358 w, 1491 s, 1397 md, 1305 s, 1224 md, 1148 w, 1062 s, 988 w, 922 md, 692 s, 539 md. UV/Vis (chloroform): λ_{max} 472 nm, $\varepsilon = 203$ mol^{-1} cm^{-1} dm^{3}. MS(EI): $M^{+} = 898$ (100%), exact mass (calc.) *m/z* 898.4787, (obs.) 898.4796. Crystal data: $C_{50}H_{70}B_4FeO_8$, orthorhombic, P 2_1 2_1 2_1, a = 11.969(2) Å, b = 11.964(2) Å, c = 32.749(7) Å, V = 4689.6(15) Å^3, Z = 4, D_{calc} = 1.272 Mg m^{-3}, μ(MoKα) = 0.375 mm^{-1}. A suitable crystal was covered in pre-dried mineral oil and mounted at 150(2) K. 5184 unique reflections were collected (3.8 < θ < 23.5°). Final R-factor: R_1 = 0.106.

Preparation of 1,1'3,3'-tetrakis(2-napthyl-ethanediolatoboryl)ferrocene **(4d)**

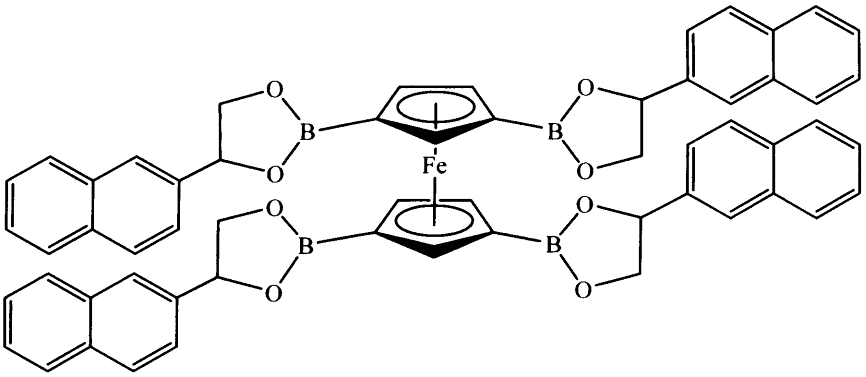

(2S)-Napthyl-ethane-1,2-diol (0.039 g, 0.21 mmol) was dried under vacuum for 2 h, dissolved in toluene (50 ml), the solution cooled to –78 °C and n-butyllithium (2.6 ml of a 1.6 M solution in hexanes, 4.2 mmol) added drop-wise via syringe. After stirring for 12 h at room temperature, 1,1',3,3'-tetrakis(dibromoboryl)ferrocene (452 mg, 0.52 mmol) in toluene (50 ml) was added dropwise via cannula and the resulting cloudy orange solution stirred for a further 12 h. After filtration through a frit containing celite, solvent was removed in vacuo to yield an orange oily product, which was dried under high vacuum for 12 h. The resulting orange solid was recrystallised from hexanes at –30°C. Yield of orange solid: 251 mg (50 %). ^{1}H NMR (400 MHz, [D]chloroform, 20 °C): δ 4.13 [overlapping m, 4H, CH_2 of chelate], 4.42 [m, 2H, CH of chelate], 4.65 [m, 2H, CH of chelate], 4.74 [d, J = 1.2 Hz, 2H, C_5H_3], 4.80 [d, J = 1.3 Hz, 2H, C_5H_3], 4.95 [s, 2H, C_5H_3], 5.62 [t, J = 8 Hz, 2H, CH_2 of chelate], 5.69 [t, J = 8 Hz, 2H, CH_2 of chelate], 7.39 [m, 12H, aromatic CH], 7.74 [m, 16H, aromatic

CH]. $^{13}C\{^1H\}$ NMR (75.5 MHz, [D]chloroform, 20 °C): δ 70.9 [C_5H_3], 71.0 [C_5H_3], 76.5 [CH_2 of chelate], 76.6 [CH_2 of chelate], 76.8 [CH of chelate], 77.1 [CH of chelate], 80.4 [C_5H_3], 121.0, 121.4, 122.7, 123.0, 124.2, 125.8, 126.1, 126.7, 126.8, 131.1, 131.2, 131.3, 136.0, 136.5 [napthyl CH]. $^{11}B\{^1H\}$ NMR (96 MHz, [D]chloroform, 20 °C): δ 32.4. IR (KBr disc, cm^{-1}): ν 2923 s, 1625 w, 1462 s, 1376 s, 1063 md, 855 w, 814 w, 722 md. UV/Vis (chloroform): λ_{max} 461 nm, ε = 347 mol^{-1} cm^{-1} dm^3. MS(EI): M^+ = 970 (100%), exact mass (calc.) *m/z* 970.2909, (obs.) 970.2908.

Alternative synthesis of (ethanediolatoboryl)ferrocene (**1a**) *from ferroceneboronic acid*

Ferroceneboronic acid (0.776 g, 33.8 mmol) was weighed into a pressure tube, dissolved in acetone (30 ml) and ethane-1,2-diol (0.210 g, 33.8 mmol) added. The pressure tube was sealed, placed in an oil bath and heated to 70 °C for 20 h with stirring. The resulting orange solution was filtered and volatiles removed in vacuo to yield an orange powdery solid which was recrystallised from hot dichloromethane, yield 0.676 g, 75 %. Characterising data were the same as those quoted above for compound **1a**.

Alternative synthesis of pinanediolatoborylferrocene (**1b**) *from ferroceneboronic acid*

Ferroceneboronic acid (0.388 g, 16.9 mmol) was weighed into a pressure tube and dissolved in acetone (30 ml), (1S,2S,3R,5S)-(+)-pinanediol (0.288 g, 16.9 mmol) added. The pressure tube was sealed, placed in an oil bath and heated to 70 °C for 20 h with stirring. The resulting orange solution was filtered and volatiles were removed in vacuo to yield an orange powdery solid which was recrystallised from hot dichloromethane. Yield: 0.444 g, 72 %. Characterising data were the same as those quoted above for compound **1b**.

Alternative synthesis of 1,1'-bis(stilbenediolatoboryl)ferrocene (**2a**) *from ferrocenebis-boronic acid*

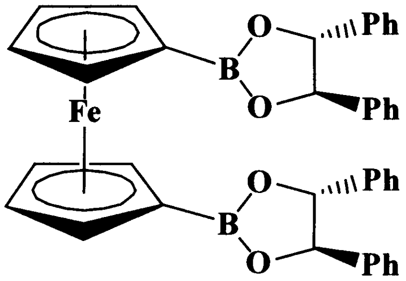

Ferrocene*bis*-boronic acid (0.481 g, 19.9 mmol) and (S,S)-stilbene diol (0.852 g, 39.8 mmol) dissolved in acetone (40 ml) in a thick-walled pressure tube. The pressure tube was sealed and heated to 70 °C for 24 h with stirring. The resulting orange solution was filtered and volatiles removed in vacuo to yield an orange powdery solid. The crude product was extracted with dichloromethane (40 ml), filtered and solvent was removed under vacuum to yield an orange solid (1.00g, 80 %). ^{1}H NMR (400 MHz, [D$_6$]benzene, 20°C): δ 4.39 [m, 2H, C_5H_4], 4.44 [m, 2H, C_5H_4], 4.88 [m, 2H, C_5H_4], 4.99 [m, 2H, C_5H_4], 5.30 [s, 4H, CH of chelate], 7.04 – 7.26 [m, 20H, C_6H_5]. ^{13}C{^{1}H} NMR (75.5 MHz, [D$_6$]benzene, 20°C): δ 72.9, 73.5, 75.1, 75.5 [CH of C_5H_4], 86.9 [CH of chelate], 126.2, 128.4, 128.8 [aromatic CH], 140.1 [aromatic quaternary]. ^{11}B{^{1}H} NMR (96 MHz, [D]chloroform, 20 °C): δ 34.0. MS(EI): M^+ = 630 (100%), exact mass (calc.) *m/z* 630.1836, (obs.) 630.1834.

Alternative synthesis of 1,1'(bis-pinanediolatoboryl)ferrocene **(2b)** *from ferrocenebis-boronic acid*

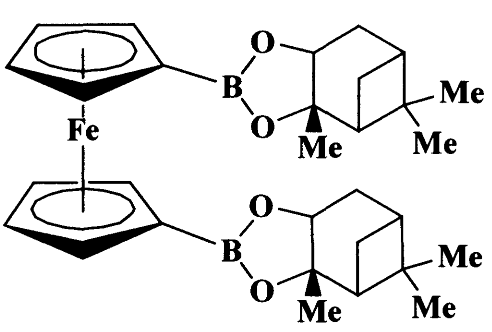

Ferrocene*bis*-boronic acid (0.710 g, 29.3 mmol) was weighed into a pressure tube, equipped with a stirrer bar and dissolved in acetone (40 ml) and (1S,2S,3R,5S)–(+)–pinanediol (1.00 g, 58.7 mmol) added. The pressure tube was sealed and heated to 70 °C for 24 h with stirring. The resulting orange solution was cooled to room temperature and crystalline **2a** isolated on cooling by filtration (0.693 g, 43 %). ^{1}H NMR (400 MHz, [D]chloroform, 20 °C): δ 0.83 [s, 6H, H-8], 1.25 [s, 6H, H-9], 1.28 [d J = 10 Hz, 2H, H-6a], 1.42 [s, 6H H-10], 1.89 [overlapping m, 4H, H-2, H-4a, H-5, H-7], 2.07 [t J = 5 Hz, 2H, H-1], 2.21 [m, 2H, H-6b], 2.35 [2H, m, H-4b], 4.32 [m, 4H, CH of C_5H_4], 4.34 [m, 2H, H-3], 4.35 [m, 2H, CH of C_5H_4], 4.37 [m, 2H, CH of C_5H_4]. $^{13}C\{^1H\}$ NMR (75.5 MHz, [D]chloroform, 20 °C): δ 24.2, 26.7, 27.2, 29.1, 35.9, 38.3, 39.7, 51.4, 77.9, 85.8 [pinane backbone], 72.5, 72.6, 74.2, 74.3 [CH of C_5H_4]. $^{11}B\{^1H\}$ NMR (96 MHz, [D]chloroform, 20 °C): δ 32.2. IR (KBr disk, cm^{-1}): ν 3155 w, 2924 st, 2253 st, 1794 w, 1647 w, 1560 w, 1480 st, 1383 st, 1323 st, 1312 st, 1277 md, 1261 md, 1237 md, 1209 w, 1189 w, 1128 st, 1096 md, 1021 md, 916 st, 712 st. UV/Vis (chloroform): λ_{max} = 462 nm, ε = 101 cm^{-1} mol^{-1} dm^3. MS(EI): M^+ = 542 (100%), exact mass (calc.) *m/z* 542.2457, (obs.) 542.2456.

***Attempted preparation of 1,2-bis(stilbenediolatoboryl)ferrocene* (6a)**

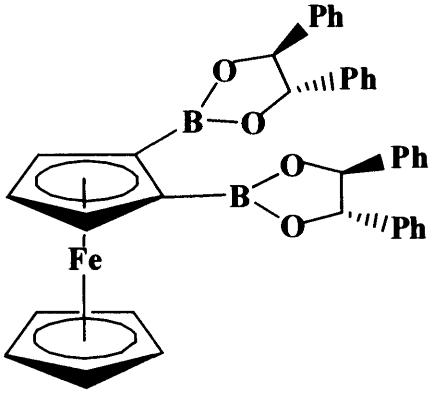

1,2-Ferrocene*bis*-boronic acid (0.093 g, 3.4 mmol) and (S,S)-stilbene diol (0.145 g, 6.8 mmol) dissolved in acetone (40 ml) in a thick-walled pressure tube. The pressure tube was sealed and heated to 70 °C for 24 h with stirring. The resulting orange solution was filtered and volatiles removed in vacuo to yield an orange powdery solid. The crude product was washed with dichloromethane (40 ml), the dichloromethane solution was filtered and solvent was removed under vacuum to yield an orange solid (0.069 g, 32.6 %). ^{11}B NMR (96 MHz, [D]chloroform, 20 °C): δ 32.8. MS(EI): $M^+ = 630.3$ (100%), 486.1 (80 %), 408.2 (20 %). The orange solid was found by mass spectrometry to be a mixture of products, which separated into three bands after filtration of a chloroform solution through a small silica column. The first band was found to contain the mono-stilbene compound (**1c**), the remaining two bands were found still to comprise a mixture of components. Alternative separation methods proved unsuccessful. A cleaner synthesis may be required to achieve full characterisation of the product.

Preparation of 1'-mono-(stilbenediolatoboryl)-1,2,3,4,5-pentamethylferrocene (**5a**)

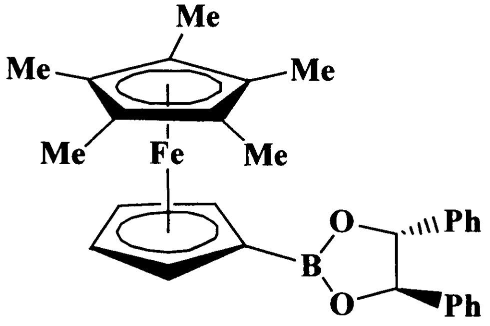

To a solution of (S,S)-stilbene diol (0.6 g, 2.78 mmol) in toluene (30 ml) was added n-butyllithium (3,5 ml of a 1.6 M solution in hexanes, 5.56 mmol) dropwise via syringe at –78°C. The reaction mixture was warmed to room temperature and a solution of 1,2,3,4,5-pentamethyl-1'-(dibromoboryl)ferrocene (1.18 g, 2.78 mmol) in toluene (30 ml) added dropwise via cannula. The resulting cloudy orange solution was filtered, and volatiles removed in vacuo to yield a orange powder that was further dried under high vacuum. 56 % yield after recrystallisation from hexanes (air-stable orange crystalline solid). ^{1}H NMR (400 MHz, [D$_6$]benzene, 20°C): δ 2.02 [s, 15H, Cp*], 4.03 [m, 1H, C_5H_4], 4.05 [m, 1H, C_5H_4], 4.45 [m, 1H, C_5H_4], 4.48 [m, 1H, C_5H_4], 5.43 [s, 2H, CH of chelate], 7.19-7.25 [m, 6H, C_6H_5], 7.42-7.45 [m, 4H, C_6H_5]. ^{13}C{^{1}H} NMR (75.5 MHz, [D$_6$]benzene, 20°C): δ 11.3 [CH_3 of Cp*], 71.2 [b, C_5H_4 quaternary], 76.0 (two overlapping signals), 76.7, 77.4 [CH of C_5H_4], 80.4 [Cp* quaternary], 86.6 [CH of chelate], 126.4, 127.2, 128.6 [aromatic CH], 140.2 [aromatic quaternary]. ^{11}B{^{1}H} NMR (96 MHz, [D$_6$]benzene, 20°C): δ 33.3. IR (KBr disk, cm^{-1}): ν 3423 md, 2962 md, 2904 md, 2854 w, 1636 w, 1496 md, 1479 st, 1451 md, 1382 st, 1325 md, 1315 md, 1301 md, 1261 w, 1208 w, 1174 w, 1125 st, 1027 st, 988 w, 818 w, 802 w, 762 w, 700 md, 686 w, 537 w, 482 w. UV/Vis (chloroform): λ_{max} = 445 nm, ε = 193 cm^{-1} mol^{-1} dm^3. MS(EI): M$^+$ = 478 (5%), exact mass (calc.) *m/z* 477.1797, (obs.) 477.1791.

Preparation of 1',3'-bis-(stilbenediolatoboryl)-1,2,3,4,5-pentamethylferrocene **(5b)**

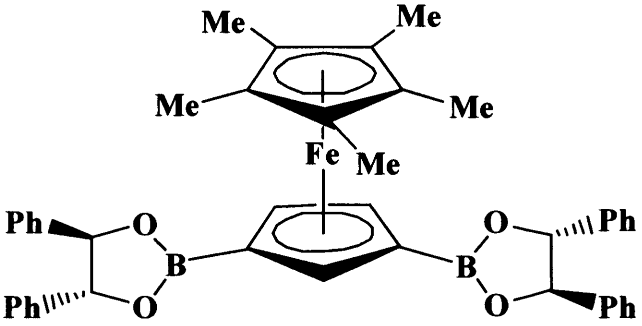

By an analogous method **5b** was prepared by reaction between (S,S)-stilbenediol in toluene with a solution of 1,2,3,4,5-pentamethyl-1',3'-bis(dibromoboryl)-ferrocene also dissolved in toluene. Filtration of the cloudy orange solution followed by removal of volatiles in vacuo yielded an orange powder. 58 % yield after recrystallization from hexanes (air-stable orange crystalline solid). ^{1}H NMR (400 MHz, [D$_6$]benzene, 20 °C): δ 2.18 [s, 15H, Cp*], 4.77 [m, 1H, C_5H_3], 4.79 [m, 1H, C_5H_3], 5.33 [s, 1H, C_5H_3], 5.47 [s, 4H, CH of chelate], 7.23-7.32 [m, 12H, C_6H_5], 7.45-7.47 [m, 8H, C_6H_5]. ^{1}H NMR ([D]chloroform, 20°C): δ 1.88 [s, 15H, Cp*], 4.27 [m, 1H, C_5H_3], 4.32 [m, 1H, C_5H_3], 4.55 [s, 1H, C_5H_3], 5.23 [s, 4H, CH of chelate], 7.27-7.34 [m, 20H, C_6H_5]. ^{13}C{^{1}H} NMR (75.5 MHz, [D$_6$]benzene, 20°C): δ 11.3 [CH_3 of Cp*], 65.9 [b, C_5H_4 quaternary], 80.7 [CH of C_5H_3], 80.9 [Cp* quaternary], 81.6, 83.7 [CH of C_5H_3] 86.6 [CH of chelate], 126.4, 128.6 [aromatic CH], 140.2 [aromatic quaternary]. ^{11}B{^{1}H} NMR (96 MHz, [D]chloroform, 20 °C): δ 32.7. IR (KBr disk, cm^{-1}): ν 3436 md, 3063 w, 3031 w, 2964 md, 2901 md, 1634 w, 1484 st, 1454 md, 1382 w, 1335 md, 1274 st, 1209 w, 1188 md, 1139 w, 1080 md, 1058 st, 1030 md, 985 md, 803 md, 760 md, 697 st, 650 w, 607 w, 534 w, 493 w. UV/Vis (chloroform): λ_{max} = 453 nm, ε = 217 cm^{-1} mol^{-1} dm^3. MS(EI): M$^+$ = 700 (5%), exact mass (calc.) *m/z* 698.2686, (obs.) 698.2690.

3.3 Results and discussion

3.3.1 Mono(boronic ester) ferrocene-based Lewis acids

Dibromoboryl ferrocene was prepared by the direct borylation of ferrocene with boron tribromide as previously discussed.[8] Subsequent reaction of with a diol-dilithiate proceeds via elimination of two equivalents of lithium bromide to successfully yield mono-functional boronic esters containing ferrocene backbones (Scheme 3.7). All compounds were isolated as orange-yellow air-stable solids, typically in yields of about 40%.

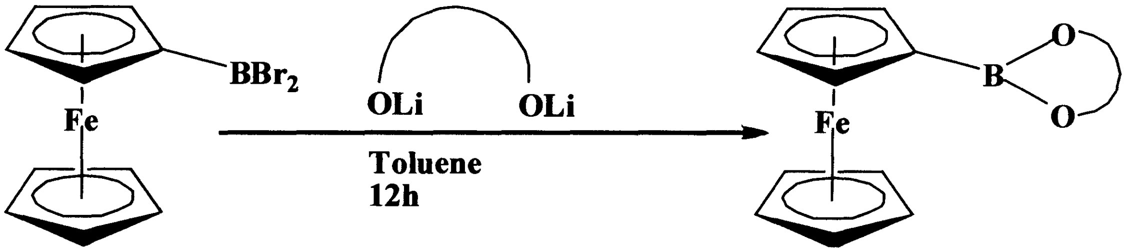

Scheme 3.7 Synthetic route to *mono*-borylferrocenes (**1a** and **1b**)

Preliminary confirmation of the identity of the desired products (**1a** and **1b**) was obtained via inspection of the ^{11}B NMR spectrum of the reaction mixture, which in each case is found to be too broad to conclusively rule out the presence of impurities; further characterising data from ^{1}H and ^{13}C NMR measurements were acquired on crystalline products. The ^{1}H NMR spectra corroborate the proposed structures, exhibiting singlet resonances for the unsubstituted Cp ligand and the expected pattern of signals for the boryl-substituted Cp ligand i.e. multiplets for each of the two sets of chemically equivalent CHs in the 2 and 3 positions. In the ^{1}H NMR spectrum of compound **1a** a singlet resonance (4H) is observed for the CH_2 groups of the chelate backbone and the ^{13}C NMR reveals just four signals in total, one signal for the chelate backbone, one for the un-substituted cyclopentadienyl ring and a further two signals for the mono-substituted ring: no quaternary carbons are observed in the spectrum presumably due to broadening by the presence of unresolved coupling to the quadrupolar ^{11}B (I = 3/2) and ^{10}B (I = 3) nuclei of the boryl substituent. In the case of compound **1a** a broad singlet is observed in the ^{11}B NMR spectrum at 32.1 ppm characteristic of a cyclic boronate ester, and similar to the chemical shift observed for **1c** (34.0 ppm). Mass spectrometry data confirmed the expected molecular ion peak along with the correct isotope pattern. Slow evaporation of a solution of **1a** in deuterated chloroform in an NMR tube yielded single orange crystals suitable for X-ray diffraction. The solid-state structure of this species is illustrated in Figure 3.1; selected bond lengths and angles are listed in Table 3.1.

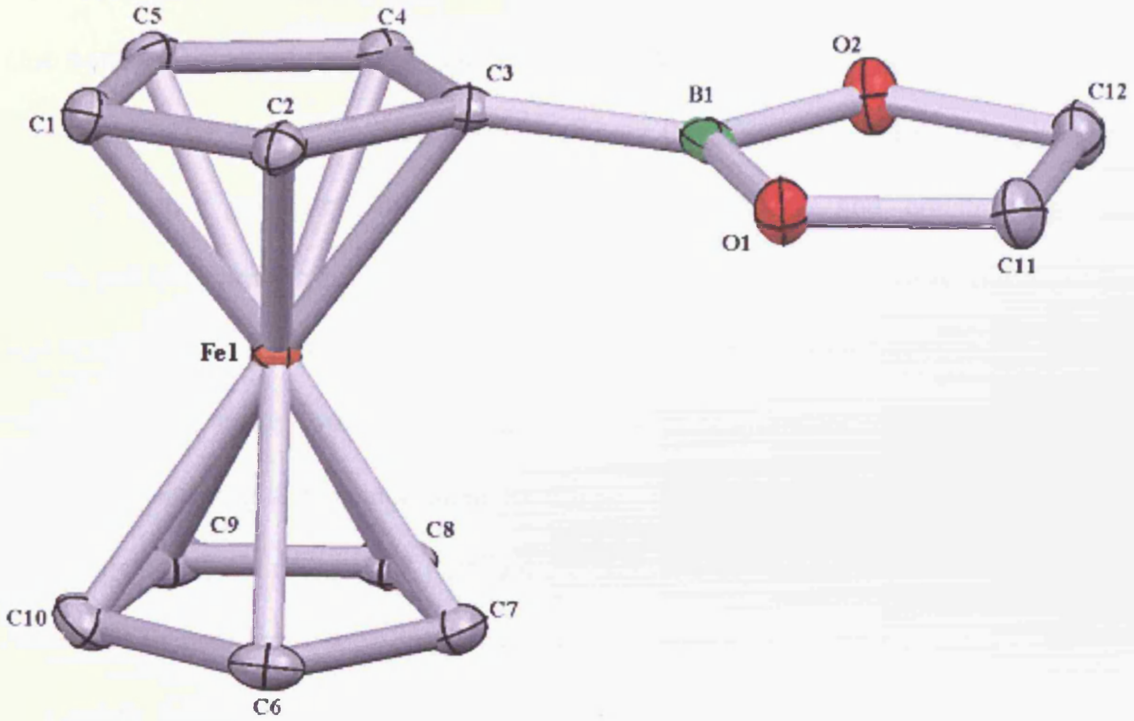

Figure 3.1 Molecular structure of (ethanediolatoboryl)ferrocene (**1a**). ORTEP ellipsoids set at the 50 % probability level. Hydrogen atoms omitted for clarity.

Table 3.1 Bond lengths [Å] and angles [°] for **1a**.

C(1)-Fe(1)	2.048(3)	C(11)-O(1)	1.446(3)
C(2)-C(3)	1.445(4)	C(11)-C(12)	1.527(4)
C(3)-B(1)	1.538(4)	C(12)-O(2)	1.444(3)
C(3)-Fe(1)	2.060(2)	O(1)-B(1)	1.371(4)
C(6)-C(10)	1.412(4)	O(2)-B(1)	1.363(4)
C(4)-C(3)-B(1)	125.3(3)	B(1)-O(2)-C(12)	107.9(2)
B(1)-O(1)-C(11)	107.4(2)	O(1)-C(11)-C(12)	105.5(2)
O(2)-B(1)-O(1)	114.0(2)	O(2)-C(12)-C(11)	105.2(2)
O(2)-B(1)-C(3)	122.0(3)	C(2)-C(3)-B(1)	128.2(3)
O(1)-B(1)-C(3)	124.0(3)	C(1)-C(5)-C(4)	107.9(2)

One notable feature of the solid-state structure of **1a** is the O-B-O bond angle, which was found to be 114.0(2) °. This is slightly lower than that expected for an idealised trigonal planar geometry, due to the chelating backbone and constraining 5-membered heteroatom ring. The sum of angles about the boron centre is found to be 359.9(8)° indicative of a perfectly trigonal planar geometry. These bond angles are consistent with those found for previously made analogous *mono*-boronic ester of ferrocene, featuring a propanediolato backbone.[13] B-O bond lengths are also within the predicted region of *ca.* 1.37 Å,[16] and are comparable with those observed for the related stilbenediolato substituted compound (Figure 3.2); many other salient parameters listed in Table 3.2 are comparable to those observed for the *mono*-stilbenediolato compound.

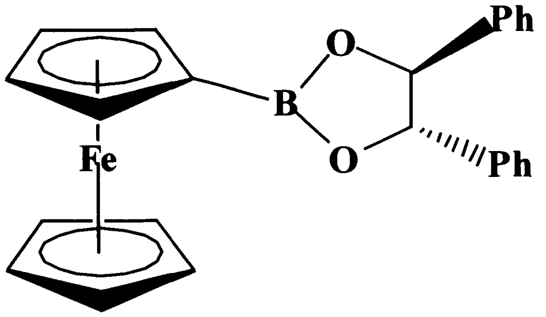

Figure 3.2 (Stilbenediolatoboryl)ferrocene (**1c**)

Table 3.2 Bond lengths [Å] and angles [°] for **1c**.

B(1)-O(1)	1.379(6)	O(1)-C(11)cyclic boronate	1.434(5)
C(Cp)-B(1)	1.538(7)	O(2)-C(12)cyclic boronate	1.438(5)
B(1)-O(2)	1.369(6)		
O(1)-B(1)-O(2)	113.1(4)	B(1)-O(1)-C(1)cyclic boronate	108.6(3)
C(Cp)-B(1)-O(2)	124.8(4)	B(1)-O(2)-C(2)cyclic boronate	107.7(3)
C(Cp)-B(1)-O(1)	122.0(4)		

It has been noted by Wagner and others[14] for related *mono*-functional compounds that the boryl moiety is tilted out of the plane of the Cp ligand towards the iron centre, a particularly large tilt angle being measured for the mono-borylferrocene system featuring a catecholate boronic ester function (13.3°). However the tilt angle observed for compound **1a** is much smaller being only 5.0°. This observation will be discussed presently in more detail.

The corresponding compound featuring a pinanediolato boronic ester (**1b**) was prepared by analogous reaction of dibromoborylferrocene with one equivalent of the di-lithiate of (1S,2S,3R,5S)-(+)-pinanediol to yield **1b** as a very crystalline orange air-stable solid in 37 % yield. ^{11}B NMR analysis substantiates a formulation containing a three-coordinate boryl group with a broad signal being observed at δ_B 30 ppm, effectively coincident with the chemical shift observed for compound **1a**. ^{1}H and ^{13}C NMR spectra confirm that the desired product has been formed. The non-equivalence of all hydrogens of the chiral pinane fragment brings about some complex coupling patterns in the ^{1}H NMR spectrum; the atom numbering scheme for the pinane fragment of **1b** in the chair conformation is shown in Figure 3.3. The methyl signals are easily assigned to the three singlets all around 1 ppm (C8, C9 and C10). The singlet in the Cp region is easily assigned to the unsubstituted cyclopentadienyl ring and the mono-substituted Cp ring shows the characteristic AB pattern. The CH of the chelate (C3) gives rise to a distinctive signal owing to its high shift at 4.11 ppm; the remainder of the pinane fragment shows a complex overlapping pattern between 1.3 and 2.1 ppm. The mass spectrometry data corroborates the proposed structure, displaying the expected molecular ion peak and isotopic pattern, further verified by an accurate mass measurement.

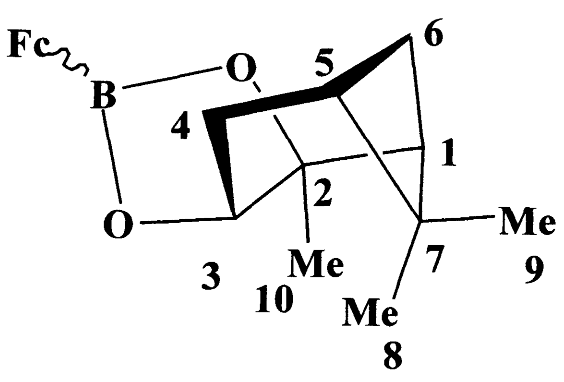

Figure 3.3 Atom numbering scheme quoted in NMR discussion for **1b**

X-ray diffraction data further confirms the expected structure, which is represented pictorially in Figure 3.4. Relevant bond lengths and angles are noted in Table 3.3.

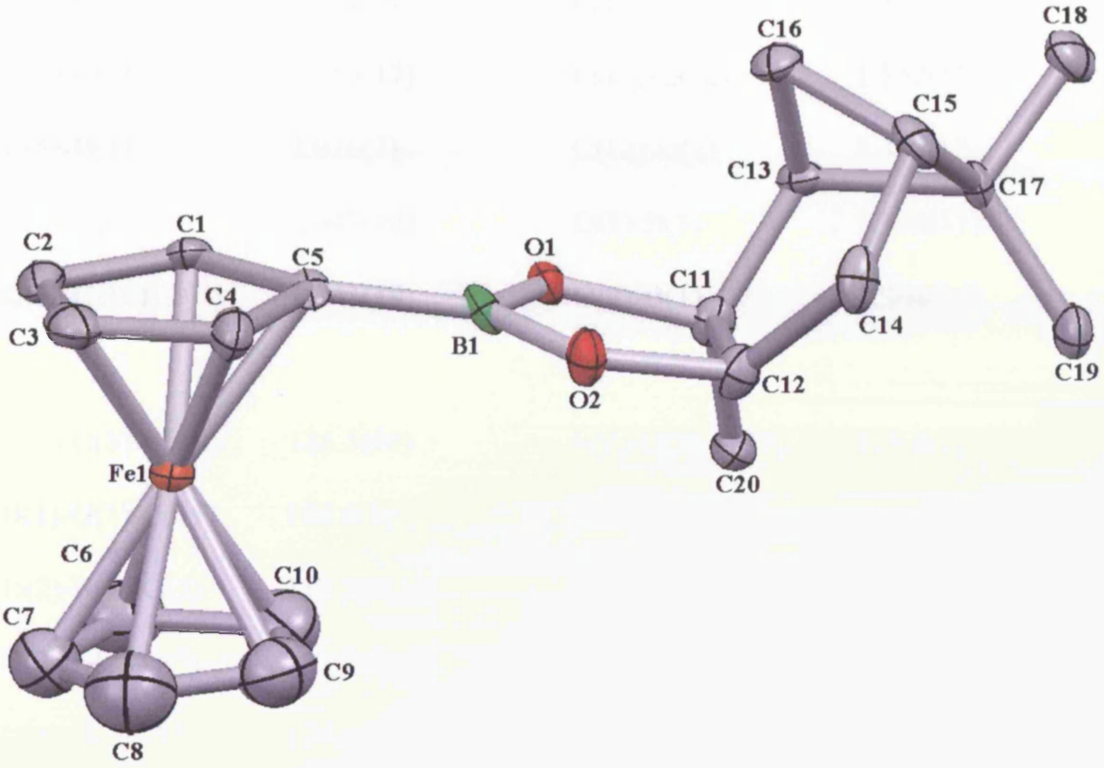

Figure 3.4 Molecular structure of (pinanediolatoboryl)ferrocene (**1b**). ORTEP ellipsoids set at the 30 % probability level. Hydrogen atoms omitted for clarity.

Table 3.3 Bond lengths [Å] and angles [°] for **1b**.

C(1)-Fe(1)	2.014(9)	C(11)-O(1)	1.475(10)
C(2)-C(3)	1.459(17)	C(11)-C(12)	1.562(11)
C(5)-B(1)	2.026(7)	C(12)-O(2)	1.426(10)
C(3)-Fe(1)	2.047(10)	O(1)-B(1)	1.366(11)
C(6)-C(10)	1.343(19)	O(2)-B(1)	1.364(11)

C(1)-C(5)-B(1)	126.5(10)	B(1)-O(2)-C(12)	110.4(7)
B(1)-O(1)-C(11)	108.6(6)	O(1)-C(11)-C(12)	103.7(6)
O(2)-B(1)-O(1)	112.7(8)	O(2)-C(12)-C(11)	104.6(7)
O(2)-B(1)-C(5)	122.7(8)	C(4)-C(5)-B(1)	126.2(8)
O(1)-B(1)-C(5)	124.6(8)	C(1)-C(5)-C(4)	106.1(8)

The structural parameters for **1b** are all within the expected ranges; the O-B-O bond angle (112.7(8)$^{\circ}$) are akin to that observed for **1a** (114.0(2)$^{\circ}$), in addition the B-O bond lengths of 1.364(11) and 1.366(11) Å is comparable to those found for **1a** (*ca.* 1.37 Å). When comparing the geometric parameters associated with mono-boronic ester Lewis acid systems it is interesting to note the tilt angles. The diagram below (Figure 3.5) shows compound **1b** with the tilt angle illustrated; the Cp centroid-C(Cp)-B angle is measured as 169.41°, and so the tilt angle is calculated to be 10.59°.

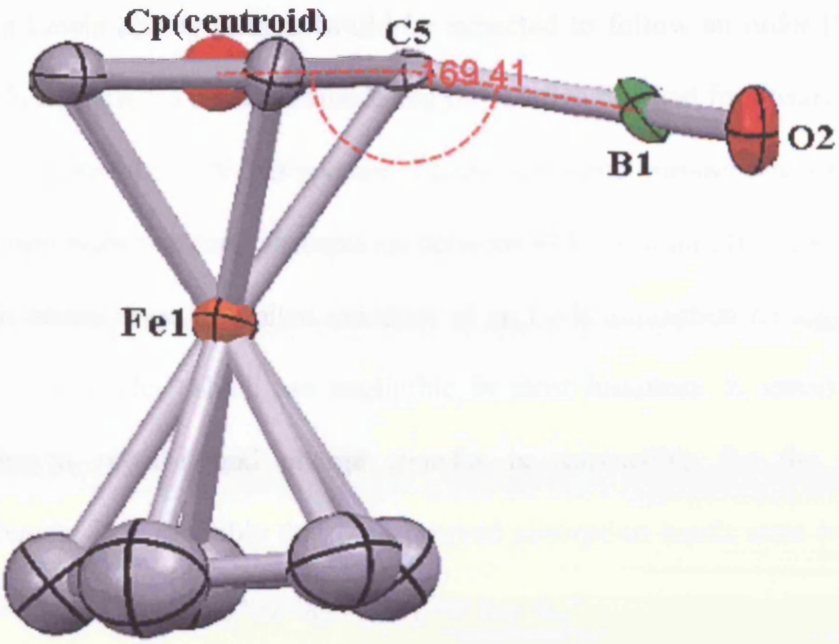

Figure 3.5 Compound **1b** with the tilt angle illustrated and the pinane fragment omitted for clarity.

In each case the trigonal planar boryl moiety is tilted out of the plane of the cyclopentadienyl ligand to a varying extent depending on a donor/acceptor interaction between filled molecular orbitals on the iron centre and the vacant p_z-orbital at boron. This bending of the boryl group towards the iron centre has been previously observed in the crystal structures of fc[BBr_2]$_2$ and FcBBr_2 in which the tilt angles were found to be 10.2° and 17.7° respectively. These observations were corroborated by electronic spectra, in which intense absorptions were observed and conclusively assigned *via* experimental and computational methods to a symmetry allowed metal-ligand charge transfer from the occupied Fe dz^2/ dx^2-y^2 orbitals to the formally vacant p-orbital at boron.[14,17] The corresponding angles measured for **1a**, **1b** and FcB$(OH)_2$ were found to be 5.0°, 10.6° and 3.6° respectively . These figures likely reflect a difference in the crystal packing of these compounds, but may also reflect a difference in Lewis acidity, which would be expected to follow an order [$FcBBr_2$ > $fc[BBr_2]_2$ > $FcB(OH)_2$ > **1b** > **1a**] considering the relative demand for electron density at each boron centre. The UV/Vis spectra of these ferrocene boronic esters have been found to exhibit weak/medium absorptions between 444 - 472 nm, (ε = 79-667 mol^{-1} cm^{-1} dm^{3}). It seems there is limited evidence of an Fe-B interaction as suggested by the observed tilt angles which are negligible in most instances. It seems unlikely therefore that a metal-ligand charge transfer is responsible for the observed absorption bands; it is probable that the observed absorption bands arise from other d→d transitions, for example, a_{1g}-e_{2g}, a_{1g}-$e_{1g}*$ or e_{2g}- $e_{1g}*$.

Initial synthesis of these mono-boronate Lewis acids was achieved via a dibromoborylferrocene precursor, followed by salt elimination of lithium bromide or triethylammonium bromide depending on which base was used. This route was found to provide an average yield of a moderately impure product, perhaps due to the very sensitive nature of the reactants and (where triethylamine is used) difficulty in separating the product from the $NEt_3H^+Br^-$ salt by-product of the reaction. However the alternative preparation of **1a** and **1b** by a condensation reaction between ferroceneboronic acid with the respective diol provided very pure products in high yields of about 70 %. This method has the further advantage that reactants and products are air stable and this route was used in preference over the dibromoborylferrocene route for all subsequent preparations of **1a** and **1b**.

3.3.2 *Bis*(boronic ester) ferrocene-based Lewis acids

The initial preparation of bi-functional boron-containing ferrocene based Lewis acids by Bresner,[10] and subsequent investigation of their unique fluoride binding capabilities has provided the foundation upon which the work presented in this chapter aims to build, and the original findings provide valuable comparison with more recently prepared mono-, tris- and tetrakis-functional analogues. *Bis*boronic esters of ferrocene were prepared using direct metallocene borylation chemistry[8] to give $-BBr_2$ derivatives followed by subsequent salt elimination reaction with various diol-dilithiates. Of the many air-stable bis-substituted compounds prepared the most widely investigated and thus the most useful for comparative purposes is 1,1'-*bis*-(stilbenediolatoboryl)ferrocene (**2a**), shown in Figure 3.6. Relevant bond lengths and angles are noted in Table 3.4.

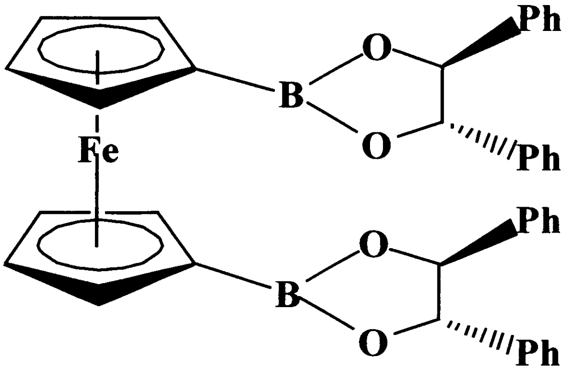

Figure 3.6 1,1'-*bis*-(stilbenediolatoboryl) ferrocene (**2a**).

Table 3.4 Bond lengths [Å] and angles [°] for **2a**.

B(1)-O(1)	1.378(3)	B(2)-O(3)	1.372(3)
C(Cp1)-B(1)	1.538(4)	B(2)-O(4)	1.369(4)
B(1)-O(2)	1.378(3)	C(Cp2)-B(2)	1.533(4)
O(1)-B(1)-O(2)	113.4(2)	O(3)-B(2)-O(4)	113.6(2)
C(Cp1)-B(1)-O(2)	122.0(2)	B(1)-O(2)-C(6)cyclic boronate	106.3(2)
C(Cp2)-B(2)-O(4)	123.5(2)	B(2)-O(3)-C(26)cyclic boronate	107.5(2)
B(1)-Cp(centroid)-Cp(centroid)-B(2)		52.6	

The B-O bond lengths and O-B-O bond angles associated with **2a** are all similar to those observed for **1a**, **1b** and **1c**. It was noted of the crystal structure of **2a** that the intramolecular boron-boron separation [3.790(4) Å] is much larger than the Cp-Cp centroid distance [3.304(5) Å] because the boryl groups are not eclipsed but are twisted away from each other, (torsion angle of 52.6(6)°). The corresponding B•••B distance in an eclipsed conformation was calculated to be *ca.* 2.87 Å, which is ideal to chelate fluoride based on standard B-F distances for B-F-B units (*e.g ca.* 1.5 Å in $[F_3B\text{-}F\text{-}BF_3]^-$),[15] assuming that it is possible to achieve an eclipsed geometry by rotation about the Cp-Fe-Cp axis. Moreover, on steric grounds the torsion angle might be expected to be significantly larger, i.e. approaching 180° to minimize repulsive interactions between boryl groups, as has been witnessed with analogous *bis*-systems.[16] The measured torsion angle of 52.6° was thought to be a result of crystal packing.

3.3.3 *Tris*(boronic ester) ferrocene-based Lewis acids

The preparation of a tri-functional boron-containing ferrocene Lewis acid was undertaken using the direct borylation chemistry as reported by Siebert *et al.*[8] Preparation of a tri-functional Lewis acid via this direct borylation chemistry first requires the preparation of a *tris*(dibromoboryl)ferrocene species, an example of which was first reported by Nöth and co-workers.[9] In theory isolation of *tris*(dibromoboryl)ferrocene can be accomplished in two ways, firstly by reaction of ferrocene with an excess of boron tribromide under reflux conditions and by termination of this reaction at an appropriate time i.e. between the formation of *bis*(dibromoboryl)ferrocene (requiring a 5 h reflux) and *tetrakis*-(dibromoboryl)ferrocene (requiring a 36 h reflux). However, this route does not represent a viable method for the isolation of usable amounts of *tris*(dibromoboryl)ferrocene, the critical drawback being that the reaction mixture at this point comprises a mixture of *mono*, *bis*, *tris* and *tetrakis* species, which is very difficult to separate. The second method to these compounds requires blocking of one CH site of the parent ferrocene to prevent borylation occurring at this site. This was achieved by using an alkylferrocene derivative;[17] reaction of ethylferrocene, for example, with a slight excess of boron tribromide in hexanes under reflux conditions for 24 h results in the formation of the desired product in 41 % yield. Subsequent reaction of *tris*(dibromoboryl)ethylferrocene with a diol-dilithiate and elimination of lithium bromide (triethylammonium bromide in the case of **3a**) leads to the formation of the tri-functional Lewis acids **3a**, **3b** and **3c**.

1,1',3-*tris*-(ethanediolatoboryl)-3'-ethylferrocene (**3a**), shown in Figure 3.7, was prepared by reaction between ethane-1,2-diol and 1,1',3-*tris*-(dibromoboryl)-3'-ethylferrocene to yield an orange powdery air-stable solid in yields of 41 %.

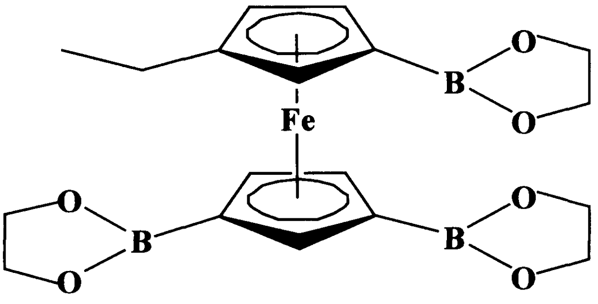

Figure 3.7 1,1',3-*tris*(ethanediolatoboryl)-3'-ethylferrocene (**3a**)

Evaluation of the ^{11}B NMR spectrum of **3a** reveals a single broad peak (δ_B 32 ppm), despite the chemical in-equivalence of each boron centre. In general, the observed shift is consistent with what is known for a three-coordinate boron centre bonded to two oxygen donors and a cyclopentadienyl ligand. The ^{1}H NMR spectrum of **3a** reveals that all the backbone CH_2 protons are coincidently equivalent despite the in-equivalence that the ethyl group brings to the molecule. The upper and lower cyclopentadienyl rings are however found to be inequivalent in the ^{1}H NMR spectrum as evidenced by the four signals observed. The ^{13}C NMR spectrum displays two overlapping signals for the chelate backbone carbons (ca. 2:1) at 64.7 and 64.4 ppm; consistent with the inequivalence of the upper and lower cyclic boryl moieties. Mass spectrometry results confirm the expected molecular ion peak, further verified by an accurate mass measurement. Crystal growth proved unsuccessful using various techniques and solvent systems, however the spectroscopic evidence and comparison with structurally characterised **3b** supports the proposed structure.

Compound **3b**, 1,1',3-*tris*-(stilbenediolatoboryl)-3'-ethylferrocene, shown in Figure 3.8, was synthesised by the reaction of the dilithiate of (S,S)-stilbene diol with

1,1',3-*tris*(dibromoboryl)-3'-ethylferrocene to yield an orange powdery air-stable solid in a 46 % yield.

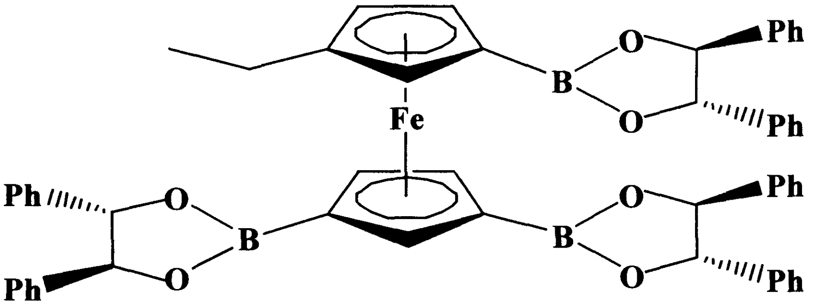

Figure 3.8 1,1',3-*tris*-(stilbenediolatoboryl)-3'-ethylferrocene (**3b**)

The ^{11}B NMR spectrum of **3b** reveals a single broad peak (δ_B 34 ppm), although each boron centre is expected to show a different shift owing to the inequivalence provided by the ethyl group. It seems likely that what is observed in the ^{11}B NMR spectrum of **3b** is a broad signal comprising several overlapping resonances of very similar chemical shift. The observed shift is coherent with a three-coordinate boron centre with two appended oxygen donors and a cyclopentadienyl ligand. Scrutiny of the ^{1}H NMR spectrum of **3b** confirms the inequivalence of the Cp CHs on the upper and lower Cp rings, these being observed as four singlets. The CH groups of the chelate rings are observed as six distinct singlets. The ^{13}C NMR data further substantiates the proposed structure with unique signals being observed for each of the Cp CHs and for each of the CH groups of the three unique chelate rings. Mass spectrometry measurements gave the expected molecular ion peak, endorsed by accurate mass measurement. The extensive solubility of **3b** in a wide range of solvents complicated the crystallisation procedure. However orange plate-like crystals suitable for X-ray diffraction were eventually grown from an acetonitrile/water layering at room temperature. The suppositions based on spectroscopic data are confirmed by the X-ray diffraction studies (Figure 3.9). Relevant bond lengths and angles are noted in Table 3.5.

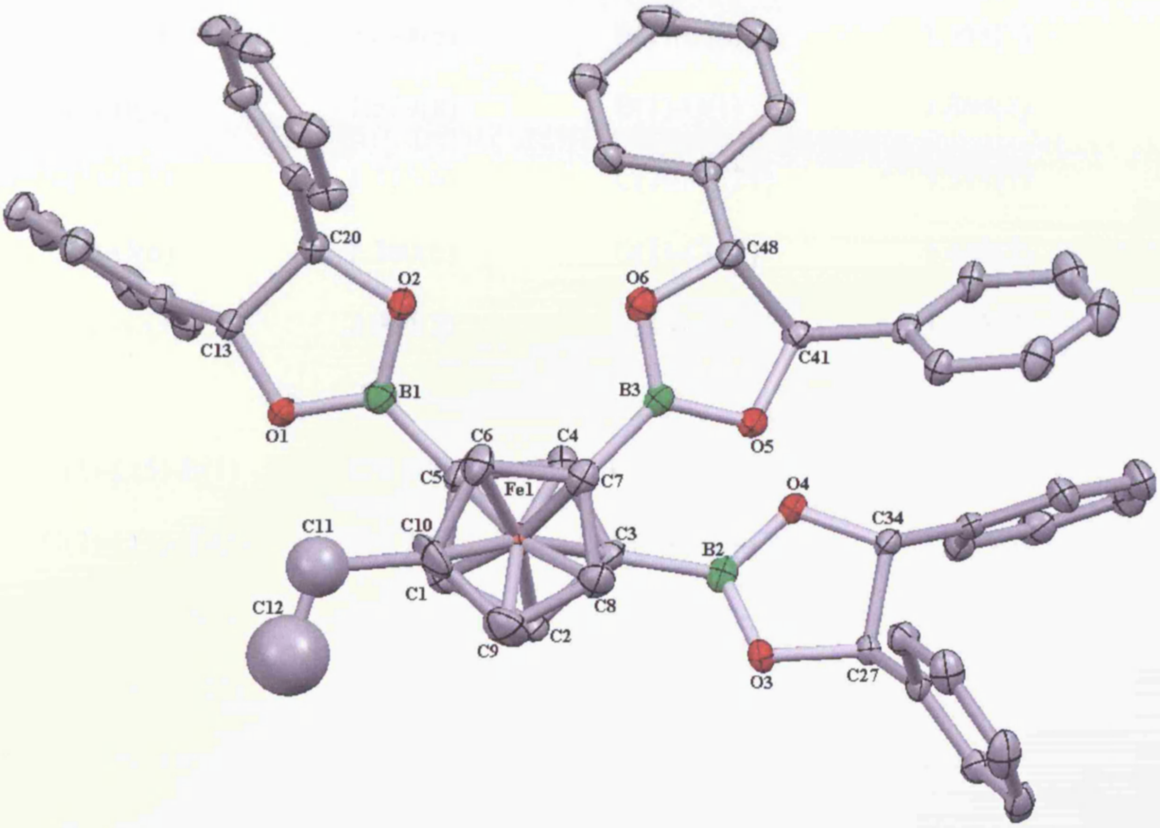

Figure 3.9 Molecular structure of 1,1',3-*tris*-(stilbenediolatoboryl)-3'-ethylferrocene (**3b**). ORTEP ellipsoids set at the 30 % probability level. Hydrogen atoms omitted for clarity. C11 and C12 remain isotropic due to a high degree of disorder and the difficulty modelling these atoms anisotropically.

Table 3.5 Bond lengths [Å] and angles [°] for **3b**.

C(10)-C(11)	1.564(13)	C(3)-B(2)	1.547(7)
C(11)-C(12)	1.302(18)	B(2)-O(3)	1.361(7)
C(9)-C(10)	1.409(10)	B(2)-O(4)	1.375(7)
C(10)-Fe(1)	2.074(6)	B(1)-O(2)	1.361(7)
C(7)-B(3)	1.529(8)	B(1)-O(1)	1.369(7)
B(3)-O(5)	1.375(6)	C(20)-C(21)	1.511(7)
B(3)-O(6)	1.360(6)	O(1)-C(13)	1.442(5)
Fe(1)-C(3)	2.064(5)	C(13)-C(20)	1.558(7)

C(1)-C(5)-B(1)	126.7(5)	O(1)-B(1)-C(5)	123.1(5)
C(2)-C(3)- B(2)	126.7(5)	O(3)-B(2)-C(3)	123.9(5)
C(6)-C(7)-B(3)	125.5(5)	O(5)-B(3)-C(7)	122.7(4)
O(1)-B(1)-O(2)	113.2(5)	C(14)-C(13)-C(20)	111.4(4)
O(3)-B(2)-O(4)	113.5(4)	C(21)-C(20)-C(13)	111.4(4)
O(5)-B(3)-O(6)	113.7(5)	C(9)-C(10)-C(11)	130.3(7)
O(1)-C(13)-C(20)	103.9(4)	C(9)-C(10)-C(6)	108.9(6)
C(10)-C(11)-C(12)	112.8(12)	B(3)-O(5)-C(41)	107.1(4)
B(2)-Cp(centroid)-Cp(centroid)-B(3)	56.03		

The O-B-O angles in the solid state structure of **3b** are found to be 113.2(5)°, 113.5(4)° and 113.7(5)°. These O-B-O bond angles are consistent with that observed in **1a** (114.0(2)°). The sum of angles about the boron centre is found to be 359.9(14)°

in all three cases, confirming that the boron centres are in a trigonal planar environment These observations are consistent with those found for the mono-boronic ester systems **1a**, **1b** and **1c** and the previously reported bis-boronic ester system **2a**.[10] In the case of **3b**, there are now multiple boron centres, which introduces some more interesting features for discussion, one being the intramolecular B•••B distances [3.775(7) (B2-B3) and 4.745(7) (B1-B3) Å], which are significant because it is this feature that will determine whether chelation of a fluoride anion is possible, although the B•••B separation will vary by rotation about the Cp(centroid)-Fe-Cp(centroid) axis. This boron-boron distance is comparable with that known for compound **2a** [3.790(4) Å] and, like **2a**, this boron-boron distance is somewhat larger than distance between the cyclopentadienyl rings [3.326 Å] due to the fact that the boronic ester groups are not eclipsed but rotated away from each other about the Cp(centroid)-Fe-Cp(centroid) axis. The torsion angle [B-Cp(centroid)-Cp(centroid)-B] was calculated at 56.0°, similar to that measured for **2a** [52.6°]. The distinction between these two species with respect to torsion angles being that **3b** is a tetra-substituted ferrocene and there is a limit to how large the torsion angle can extend and in this case the torsion angle [56.0°] represents the maximum possible separation between upper and lower boryl/ethyl groups, while the torsion angle of compound **2a** could be extended up to 180° to gain maximum boryl-boryl separation. Given the intramolecular B•••B distance for a torsion angle of *ca.* 56°; the corresponding B•••B distance in an eclipsed conformation is calculated to be *ca.* 2.88 Å, similar to **2a** (*ca.* 2.87 Å), also an ideal distance to potentially chelate fluoride. One unusual and prominent aspect of this compound is the remarkably large tilt angle for the boryl group attached to the Cp ring bearing the ethyl moiety of 15.8°, whereas the tilt angles associated with the Cp ring featuring two boryl groups are much smaller (*ca.*

3.7°). This bending of the boryl group towards the iron centre has been formerly observed in the crystal structures of fc[BBr_2]$_2$ and $FcBBr_2$ in which the tilt angles were found to be 10.2° and 17.7° respectively[14,17] and also noted in the crystal structures of **1a** and **1b** but not to such a great extent. On closer examination of the structure **3b** it is apparent that the large tilt angle of the one boryl ligand is coupled with a shortened Fe-B distance of 2.985 Å, which can be compared with the corresponding Fe-B distances within the same molecule of *ca.* 3.168 Å. Furthermore, a similar tilt angle of 16° was reported for an analogous borylmetallocene compound featuring pentafluorophenyl ligands by Piers *et. al.* with a similar shortening of the Fe-B distance also noted (2.924 Å).[11] In addition to these observations the authors also note a shortening of the C(Cp)-B distance to 1.501(4) Å, a value intermediate between those known for B-C double bond (1.44 Å in $LiCH_2{=}B(Mes)_2$)[18] and the B-C single bond (1.58 Å in BPh_3).[19] This observation gives evidence of electron donation from the Cp ligand as well as from the Fe centre into the vacant p-orbital at boron. In the structure of **3b**, specifically the tilted boryl group, a very slight shortening of the C(Cp)-B bond length is observed (1.529(8) Å) compared to the other boryl groups e.g. 1.547(7) Å but this value provides no statistically significant evidence of electron donation from the Cp ligand into the vacant p-orbital of boron.

1,1',3-*tris*(pinanediolatoboryl)-3'-ethylferrocene (**3c**), pictured in Figure 3.10, was prepared by the corresponding reaction of the dilithiate of (1S,2S,3R,5S)-(+)-pinanediol with 1,1',3-*tris*(dibromoboryl)-3'-ethylferrocene to yield a bright orange powdery air-stable solid which was isolated in yields of 38%.

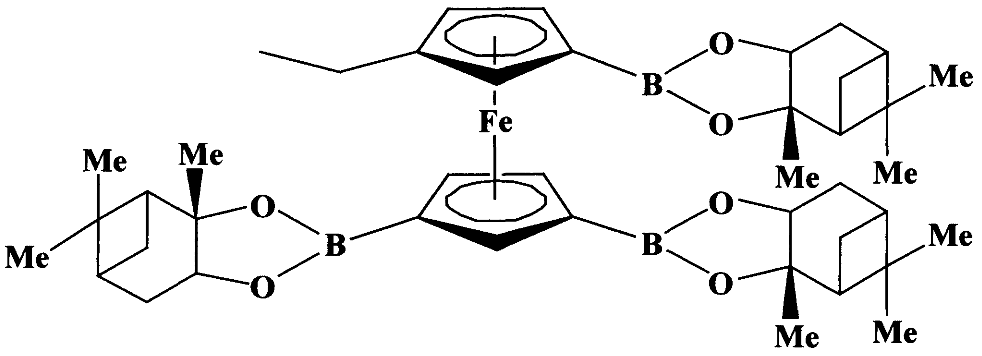

Figure 3.10 1,1',3-*tris*-(pinanediolatoboryl)-3'-ethylferrocene (**3c**)

The ^{11}B NMR spectrum of **3c** shows a single broad, presumably multi-component peak (δ_B 32 ppm), which is consistent with shifts observed for the analogous compounds **3a** and **3b**. The ^{1}H NMR spectrum becomes very complex in the case of compound **3c**; the pinane fragment gives rise to convoluted overlapping resonances and the spectrum becomes yet more involved in the presence three inequivalent pinane moieties. The only distinctive signals in the ^{1}H NMR spectrum are the ethyl signals and three methyl singlets each integrating to the nine total methyl protons. The ^{13}C NMR spectrum is also complex, and as the NMR spectra are not definitive in compound characterisation, other data (in particular mass spectrometry) have been utilized. Mass spectra for **3c** display the molecular ion peaks as expected, with accurate mass measurement confirming the identity of the ion. As with compound **3a**, crystal growth of **3c** has been unsuccessful over a range of techniques and solvent systems, however the spectroscopic data are in agreement with the structure depicted in Figure 3.10.

3.3.4 *Tetrakis*(boronic ester) ferrocene-based Lewis acids

Preparation of a tetra-functional boron-containing ferrocene Lewis acid has also proved successful, once again using the direct borylation methodology reported by Siebert *et al.*[8] followed by subsequent derivatization of the Lewis acidic group to yield of a range of air-stable tetra-functional boron-containing ferrocene Lewis acids. These syntheses first require the preparation of the intermediate 1,1',3,3'-*tetrakis*(dibromoboryl)ferrocene.[9] Synthesis of this intermediate is achieved by reaction of ferrocene with a ten-fold excess of neat boron tribromide under reflux conditions for 36 h in yields of ca. 40 %. Subsequent reactions of this intermediate with various diols has led to the isolation of a range of tetra-functional Lewis acids **4a**, **4b**, **4c** and **4d**.

Compound **4a** (1,1'3,3'-*tetrakis*(ethanediolatoboryl)ferrocene), shown in Figure 3.11, was prepared by reaction of four equivalents of ethane-1,2-diol in the presence of excess triethylamine with one equivalent of 1,1',3,3'-*tetrakis*-dibromoborylferrocene to produce **4a** as an orange powdery air-stable solid which was isolated in yields of 31 %.

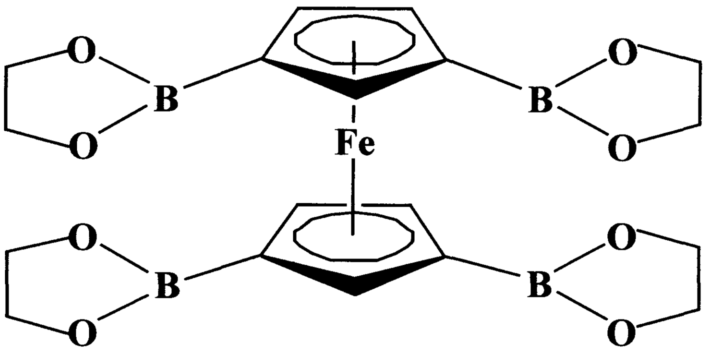

Figure 3.11 1,1',3,3'-*tetrakis*-(ethanediolatoboryl)ferrocene (**4a**)

Assessment of the ^{11}B NMR spectrum of **4a** revealed a single broad peak (δ_B 32 ppm), this chemical shift being entirely consistent with ^{11}B NMR shifts observed for the analogous *mono-*, *bis-* and *tris*-functional species, and with compounds in general containing a three-coordinate boron centre with two pendant oxygen donors. The ^{1}H NMR spectrum is very simple, featuring only three signals: a singlet resonance for the sixteen protons of the chelate backbone and two singlet resonances (2:1) of the substituted cyclopentadienyl rings. The ^{13}C NMR also presents only three signals, one for the chelating backbone and two for the cyclopentadienyl carbons: quaternary carbons were not observed in this spectrum despite acquisition of > 2000 scans with increased pulse delays. The expected molecular ion peak was confirmed by mass spectrometry and verified by an accurate mass measurement. Orange rod-like crystals suitable for X-ray diffraction were grown by slow evaporation of benzene from a concentrated solution of **4a**, and assumptions based on spectroscopic data were confirmed by the X-ray diffraction studies. The structure of **4a** is represented pictorially in Figure 3.12. Relevant bond lengths and angles are listed in Table 3.6.

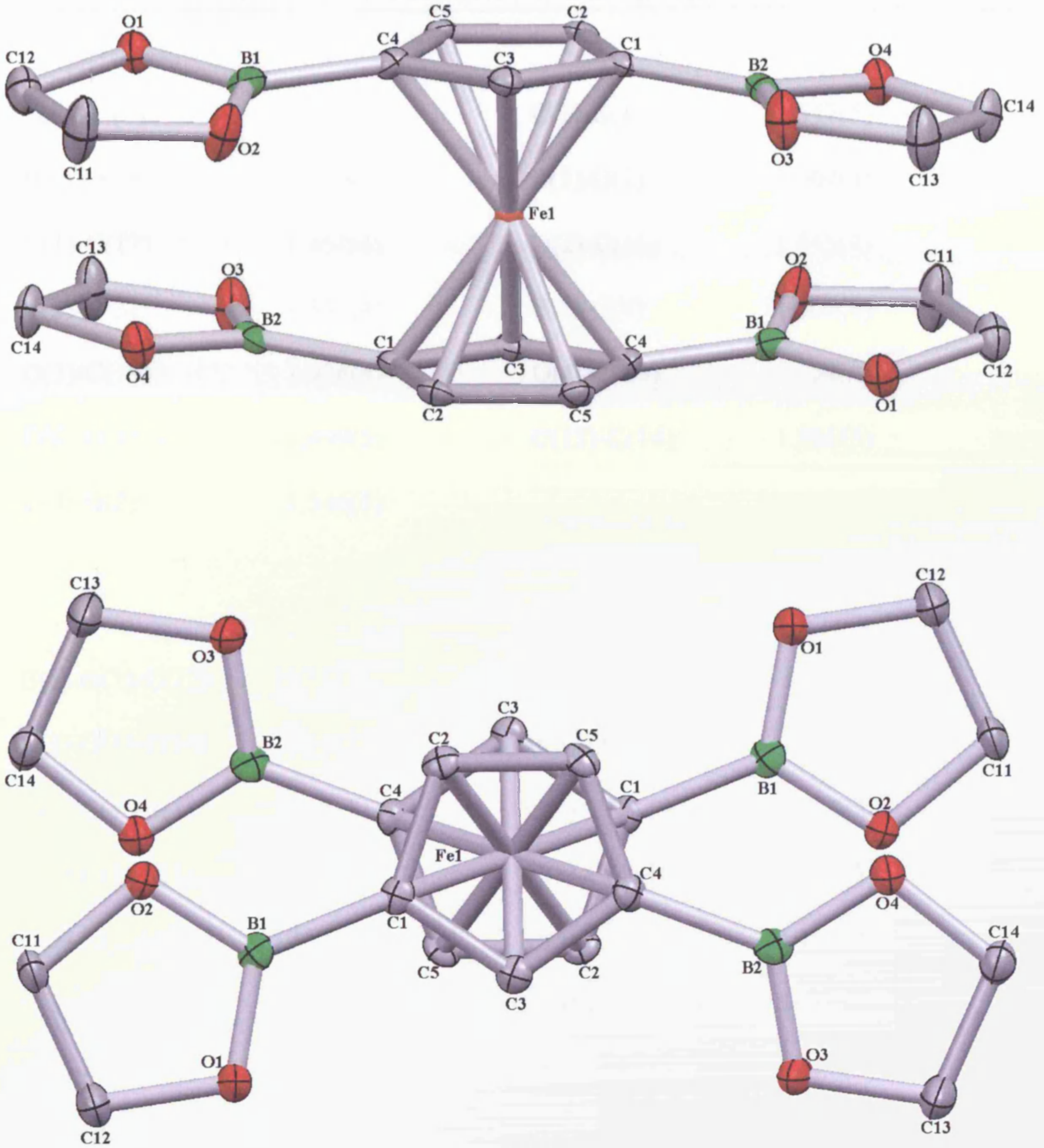

Figure 3.12 Molecular structure of 1,1',3,3'-*tetrakis*(ethanediolatoboryl)ferrocene (**4a**). ORTEP ellipsoids set at the 30 % probability level. Hydrogen atoms omitted for clarity.

Table 3.6 Bond lengths [Å] and angles [°] for **4a**

Fe(1)-C(1)	2.065(3)	C(1)-B(1)	1.547(5)
B(1)-O(1)	1.362(4)	B(1)-O(2)	1.367(4)
O(1)-C(12)	1.452(4)	O(2)-C(11)	1.445(4)
B(2)-O(3)	1.357(4)	B(2)-O(4)	1.361(4)
O(3)-C(13)	1.436(4)	O(4)-C(14)	1.454(4)
C(11)-C(12)	1.499(5)	C(13)-C(14)	1.501(5)
C(4)-B(2)	1.546(5)		

B(1)-O(1)-C(12)	107.6(3)	B(1)-O(2)-C(11)	107.0(3)
B(2)-O(4)-C(14)	107.0(3)	B(2)-O(3)-C(13)	108.2(3)
C(2)-C(1)-B(1)	130.6(3)	C(3)-C(1)-B(1)	123.3(3)
C(3)-C(4)-B(2)	123.0(3)	C(5)-C(4)-B(2)	130.1(3)
O(3)-C(13)-C(14)	105.4(3)	O(4)-C(14)-C(13)	105.6(3)
O(3)-B(2)-C(4)	121.3(3)	O(3)-B(2)-O(4)	113.7(3)
O(2)-B(1)-C(1)	125.5(3)	O(1)-B(1)-C(1)	120.8(3)
O(4)-B(2)-C(4)	125.0(3)		

B(1)-Cp(centroid)-Cp(centroid)-B(2) 39.95

Compound **4a** contains a centre of symmetry and thus the asymmetric unit contains only half of the molecule. Bond lengths and angles determined from the crystal structure of **4a** are analogous to those noted for *mono-*, *bis-* and *tris-*functional compounds **1**, **2** and **3**; for example the O-B-O angles in the solid state structure of **4a** are found to be 113.6(3)° and 113.7(3)°. The sum of angles about each boron centre is found to be 359.9(9)°, representative of a boron centre in a trigonal planar environment. The torsion angle calculated is unusually small [40.0°] compared to those measured for analogous compounds, for example the torsion angle observed for **3b** [56.0°]. It is likely that the small angle observed is an artifact of the crystal packing system. Tilt angles are negligible in this case, being just 6.0° and 4.8°, similar to that for compound **1a**, which also features the ethanediolate backbone. A B•••B separation of 3.626(4) Å is entirely consistent with those previously observed.

1,1',3,3'-*tetrakis*(stilbenediolatoboryl)ferrocene (**4b**, Figure 3.13) was synthesised by reaction of four equivalents of (S,S)-stilbene diol with eight equivalents of n-butyllithium and subsequent reaction of the resulting lithiate with one equivalent of 1,1',3,3'-*tetrakis*(dibromoboryl)ferrocene to produce an orange solid which was isolated in yields of 38 %.

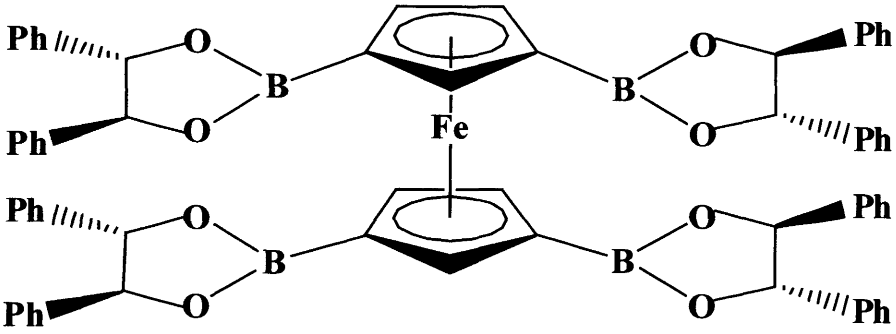

Figure 3.13 1,1',3,3'-*tetrakis*(stilbenediolatoboryl)ferrocene (**4b**)

The ^{11}B NMR spectrum of **4b** revealed the characteristic single broad peak (δ_B 33 ppm), characteristic of a cyclic boronate ester. In the case of **4b**, NMR measurements at room temperature in d_8-toluene are consistent with a more symmetrical structure than that of approximate (non-crystallographic) C_2 symmetry determined in the solid state (vide infra). NMR measurements made in d-chloroform shows coincidental equivalence which complicates interpretation. VT-NMR measurements made in d_8-toluene however imply that rotation about the centroid-Fe-centroid axis (Figure 3.14) becomes slow on the NMR timescale at temperatures below -60°C. Thus, for example, the two singlet resonances due to the prochiral methine protons of the boronic ester chelate rings are split into four distinct signals at -90°C, which sharpen on further cooling. By simulating the experimental data a barrier to rotation of $\Delta_G^‡$ =. 13.0 kcal mol^{-1} for the 'cogged' rotation of the η^5-$C_5H_3[B(OR)_2]_2]$ boronic ester units can be calculated, which compare with similar values of 11.0 and 13.1 kcal mol^{-1} calculated for the 1,1',3,3'-tetra(trimethylsilyl) and 1,1',3,3'-tetra-(*tert*-butyl)-ferrocenes.[20]

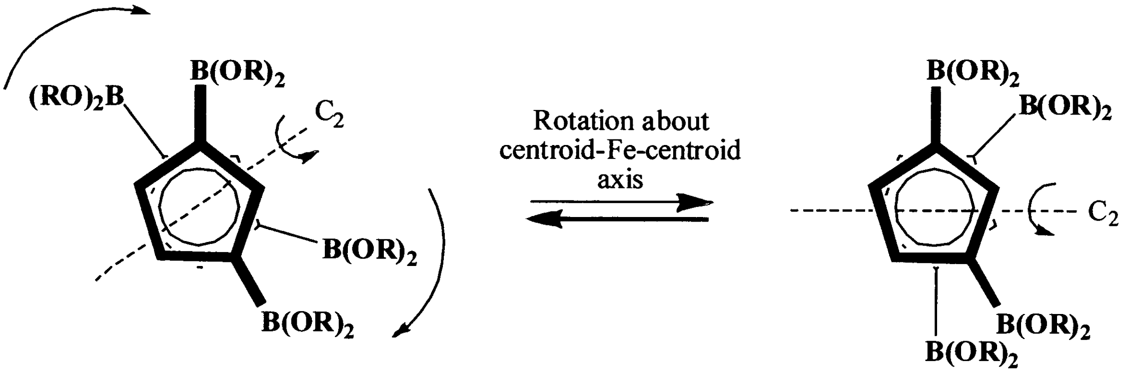

Figure 3.14 C_2 symmetry of **4b** and rotation about the centroid-Fe-centroid axis

The predicted molecular ion peak was observed in the mass spectrum and its identity confirmed by accurate mass measurement. **4b** was found to be a very crystalline material and orange, block-like crystals suitable for X-ray diffraction were grown from a toluene/hexane layering. The expected structure is confirmed by the X-ray diffraction studies, the structure of **4b** being represented pictorially in Figure 3.15; relevant bond lengths and angles are listed in Table 3.7.

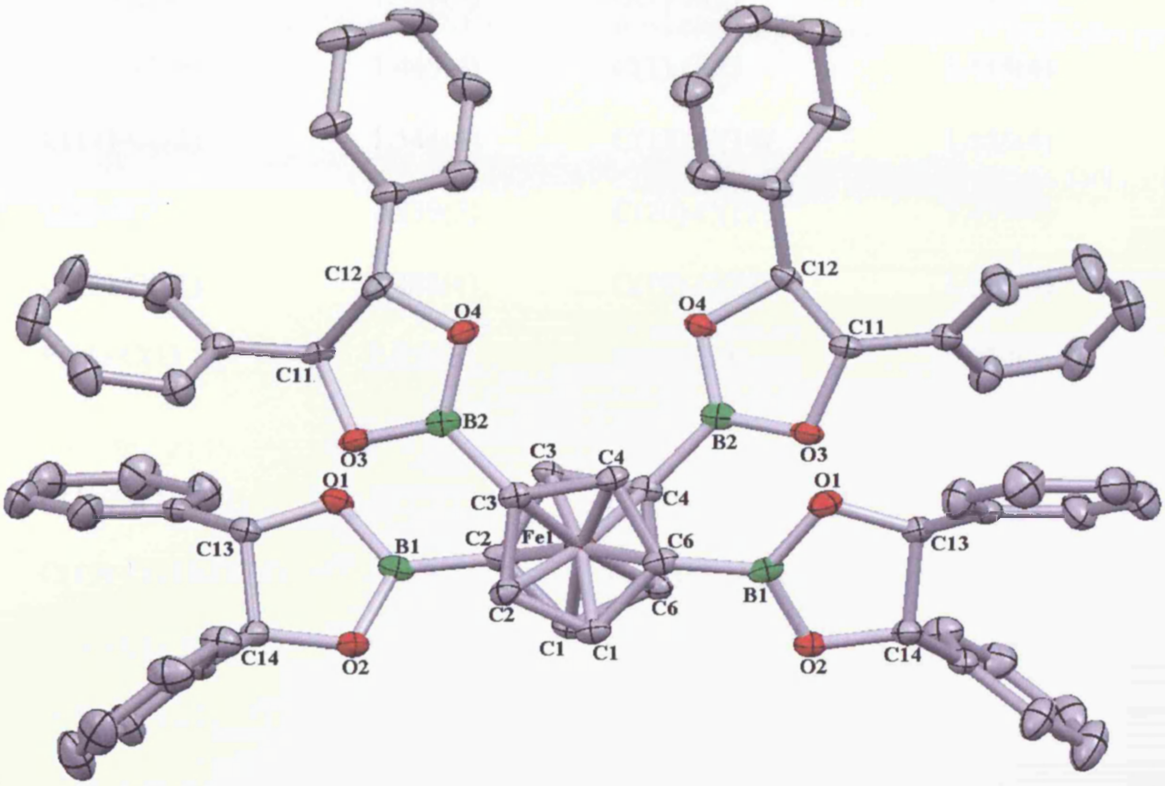

Figure 3.15 Molecular structure of 1,1'3,3'-*tetrakis*-(1,2-diphenylethanediolatoboryl)ferrocene (**4b**). ORTEP ellipsoids set at the 30 % probability level. Hydrogen atoms omitted for clarity.

Table 3.7 Bond lengths [Å] and angles [°] for **4b**

O(2)-B(2)	1.371(4)	O(3)-C(14)	1.444(4)
O(3)-B(1)	1.373(4)	O(3)-C(11)	1.455(4)
O(4)-C(12)	1.448(3)	O(1)-B(2)	1.371(4)
O(1)-C(13)	1.445(4)	C(1)-C(2)	1.414(4)
C(11)-C(12)	1.544(4)	C(13)-C(14)	1.558(4)
C(6)-B(2)	1.539(5)	C(20)-C(12)	1.495(4)
C(19)-C(11)	1.488(4)	C(19)-C(29)	1.387(5)
Fe(1)-C(1)	2.030(3)	Fe(1)-C(3)	2.054(3)
C(1)-Fe(1)-C(2)	40.75(13)	C(20)-C(49)-C(59)	120.6(4)
C(19)-C(11)-C(12)	113.5(3)	C(19)-C(30)-C(47)	120.8(3)
C(20)-C(12)-C(11)	116.5(3)	O(3)-C(11)-C(19)	113.0(2)
O(3)-C(11)-C(12)	102.5(2)	O(4)-C(12)-C(11)	112.2(3)
B(2)-O(2)-C(14)	108.4(2)	B(1)-O(3)-C(11)	106.2(2)
B(2)-O(1)-C(13)	107.9(2)	B(1)-O(4)-C(12)	106.2(2)
B(2)-O(2)-C(6)	124.0(3)	B(2)-O(1)-C(6)	122.9(3)
O(3)-B(1)-O(4)	113.6(3)	O(1)-B(2)-O(2)	113.0(3)
B(1)-Cp(centroid)- Cp(centroid)-B(2)		50.48	

As with **4a** the asymmetric unit contains only half of a molecule of **4b**. From the crystal data the O-B-O angles were found to be 113.6(3) and 113.0(3)°, and the sum of angles about the boron centre found to be 360.0(9)°. B-O bond lengths were measured 1.371(4) and 1.373(4) Å, which is standard compared with analogous compounds. The intra-molecular B•••B distance of 3.800(4) Å is within the expected range and a torsion angle B(1)-Cp(centroid)- Cp(centroid)-B(2) of 50.48° is similar to those noted for compounds **2a** and **3b**. Calculated tilt angles are not of notable magnitude in this case [5.52° and 8.28°], as expected for a weakly Lewis acidic boronic ester moiety. It is notable that the boryl groups do not actually lie coplanar to Cp ligand but are twisted out of the plane by angles of between 17.8°-19.7°, suggesting that electron donation into the vacant p_Z-orbital at boron comes predominantly from the neighbouring oxygen donors rather than the Cp ligand. Such large out-of-plane twists are observed particularly where the stilbene group is present, are probably due to steric effects.

Compound **4c** (1,1',3,3'-*tetrakis*(pinanediolatoboryl)ferrocene, Figure 3.16) was prepared by the reaction of four equivalents of (1S,2S,3R,5S)-(+)-pinanediol with eight equivalents of butyl-lithium and further reaction of the resulting diol-dilithiate with 1,1',3,3'-*tetrakis*(dibromoboryl)ferrocene to yield a bright orange solid which was isolated in yields of 47 %.

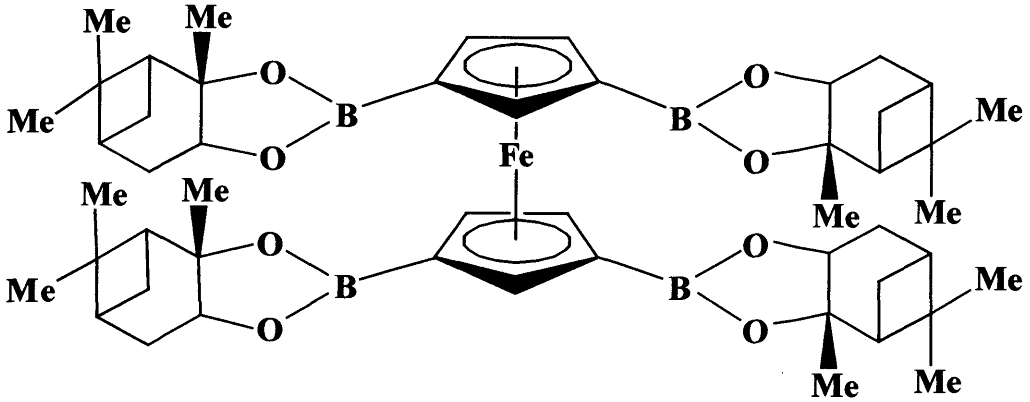

Figure 3.16 1,1',3,3'-*tetrakis*(pinanediolatoboryl)ferrocene (**4c**)

The ^{11}B NMR spectrum shows a single broad peak (δ_B 32 ppm), indicating the presence of boron in a single chemical environment or of closely overlapping resonances; this shift is consistent with analogous compounds **4a** and **4b**. As with the previously made *mono*(pinanediolatoboryl) derivative (**1b**), *bis*(pinanediolatoboryl)[16] and *tris*(pinanediolatoboryl) species (**3c**), the ^{1}H NMR spectrum of **4c** is very complex. The three methyl groups provide characteristic signals namely three singlets (each 12H) below 1.5 ppm. The four CH groups of the boronic ester chelate ring also display a very distinctive singlet, because of the proximity to the two oxygen centres; the remainder of the spectrum is very complex with overlapping signals, however in total the peaks integrate to the correct number of protons. The ^{13}C spectrum is equally convoluted, there are ten signals for the pinane fragment that cannot be reliably assigned using just the 1-D ^{13}C spectrum, and three more distinct C_5H_3 signals at higher shifts. The predicted molecular ion peak was observed by mass spectrometry, with its identity verified by an accurate mass measurement. Compound **4c** is a very crystalline material (as with many other compounds containing the pinane fragment) and orange plate-like crystals were grown by slowly cooling an acetonitrile solution from 80°C to room temperature. The expected structure was confirmed by X-ray diffraction studies and the structure of **4c** is represented pictorially in Figure 3.17; relevant bond lengths and angles are listed in Table 3.8.

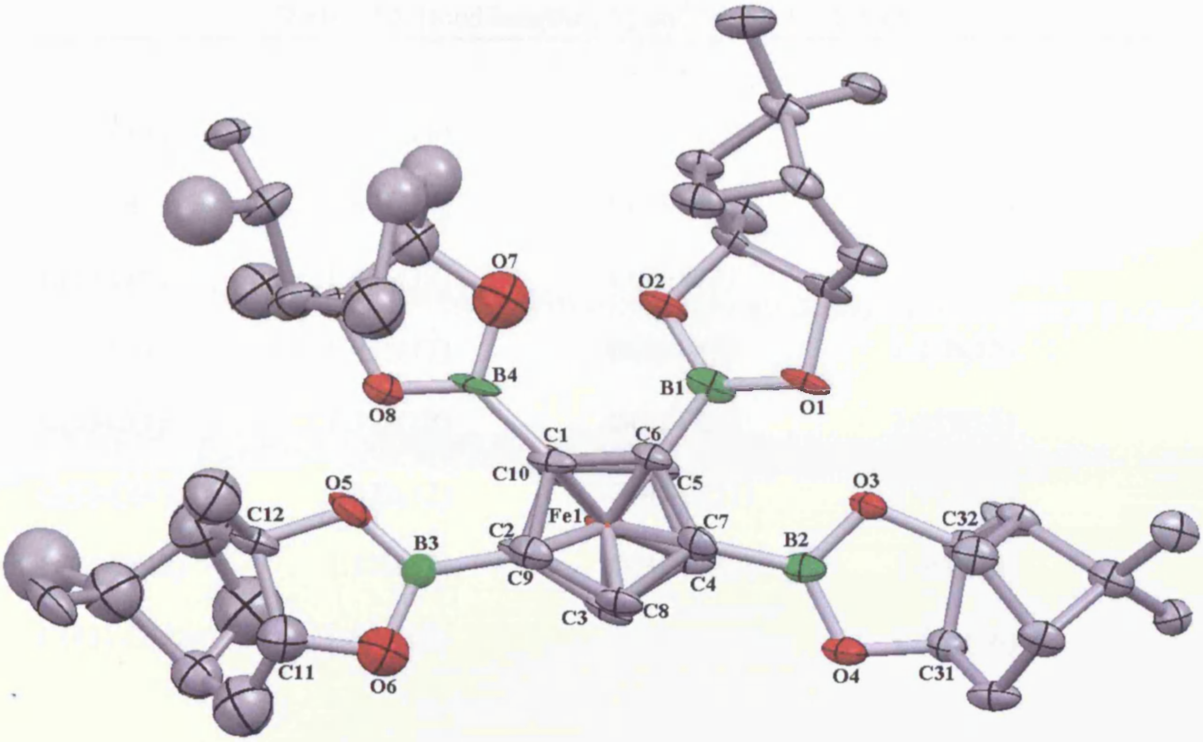

Figure 3.17 Molecular structure of 1,1'3,3'-*tetrakis*(pinanediolatoboryl)ferrocene (**4c**). ORTEP ellipsoids set at the 30 % probability level. Hydrogen atoms omitted for clarity. Isotropic atoms are to due a degree of disorder in the pinane fragment and difficulty in modelling these atoms anisotropically.

Table 3.8 Bond lengths [Å] and angles [°] for **4c**

B(1)-O(1)	1.378(18)	C(5)-Fe(1)	2.005(10)
B(1)-O(2)	1.371(17)	C(7)-Fe(1)	2.162(12)
B(1)-C(5)	1.453(17)	C(7)-B(2)	1.549(19)
C(5)-C(4)	1.435(17)	B(2)-O(3)	1.276(15)
C(5)-C(1)	1.399(18)	B(2)-O(4)	1.337(15)
O(1)-C(41)	1.372(12)	O(4)-C(31)	1.442(14)
O(2)-C(42)	1.373(12)	O(3)-C(32)	1.490(14)
C(41)-C(42)	1.606(19)	C(31)-C(32)	1.451(16)
O(1)-B(1)-O(2)	120.5(10)	O(2)-C(42)-C(45)	106.7(9)
C(5)-B(1)-O(1)	127.1(13)	B(2)-O(3)-O(4)	108.2(12)
C(5)-B(1)-O(2)	112.3(13)	C(7)-B(2)-O(4)	128.9(11)
B(1)-O(2)-C(42)	101.6(10)	C(7)-B(2)-O(3)	122.8(11)
B(1)-O(1)-C(41)	104.4(10)	B(2)-O(4)-C(31)	112.9(9)
O(1)-C(41)-C(42)	104.1(9)	B(2)-O(3)-C(32)	112.5(9)
B(1)-C(5)-C(1)	125.6(12)	B(2)-C(7)-C(6)	129.9(10)
B(1)-C(5)-Fe(1)	121.4(9)	B(2)-C(7)-Fe(1)	123.2(8)

B(1)-Cp(centroid)- Cp(centroid)-B(2) 67.53

B(3)-Cp(centroid)- Cp(centroid)-B(4) 58.17

B•••B distances are larger in the case of compound **4c**, 4.42(17) Å [B1•••B2] and 4.45(17) Å [B3•••B4] than those found for analogous tetrafunctional compounds. The boryl groups are bending further away from each other due to the sizeable steric bulk of the pinane fragment, as evidenced by the increased torsion angles calculated B(1)-Cp(centroid)- Cp(centroid)-B(2) 67.53° and B(3)-Cp(centroid)- Cp(centroid)-B(4) 58.17°. Tilt angles in this case are insignificant and the sum of angles about each boron centre is found to be 359.9(36)°.

A *tetrakis*-functionalised system featuring a napthalene-substituted boronic ester function (**4d**), as shown in Figure 3.18, was also prepared by an analogous procedure to **4b** and **4c**, yielding an air stable orange solid in *ca.* 50 % yield.

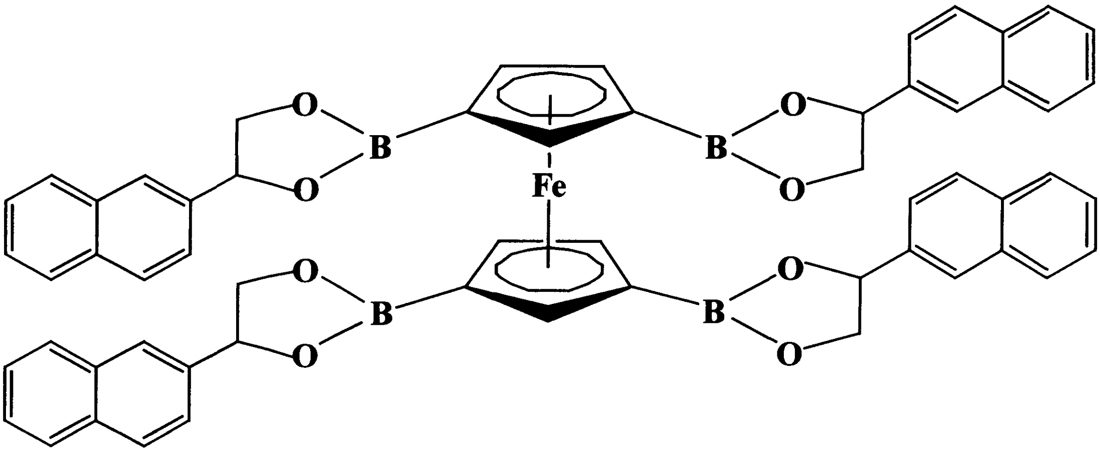

Figure 3.18 1,1'3,3'-*tetrakis*(2S-napthylethanediolatoboryl)ferrocene (**4d**)

Attempts to grow single crystals, suitable for X-ray diffraction, proved unsuccessful despite the use of varied solvent systems and a number of techniques (layering, diffusion and cooling of concentrated solutions). However the product was characterised by a number of spectroscopic techniques, including ^{11}B NMR spectroscopy (δ_B 32 ppm), which gives a resonance similar to related structurally characterised analogous compounds. ^{1}H NMR corroborates the proposed structure, although the aromatic region is very convoluted the mid-field region displays distinctive peaks: two 2H doublets and a 2H singlet for the Cp CHs and two overlapping multiplets for the chelate CH and CH_2 groups. ^{13}C NMR shows two distinctive signals in the Cp region for the C_5H_3 CHs and four signals for the chelate CH and CH_2 groups and again the aromatic region is very complex. Mass spectrometry (including accurate mass determination) analyses confirm the expected molecular ion peak and are consistent with the structure represented in Figure 3.18.

3.4 Modifications towards more efficient anion binding

3.4.1 Introduction

The main application perceived for these multi-functional boronic esters of ferrocene is in the selective binding of fluoride anions; the *mono-* (**1c**) and *bis*-functionalised systems (**2a**) previously mentioned have been shown by a range of techniques to achieve selective fluoride binding. This and the anion binding results for the corresponding *tris-* and *tetrakis*-compounds will be discussed at length in chapter four. Some modifications to existing compounds have been made in an attempt to enhance performance in the task for which they have been made.

3.4.2 Attempted preparation of a 1,2-di(boryl) ferrocene system

The main purpose of the ferrocene boronic ester systems discussed in this chapter is the binding of fluoride anions. Furthermore the chelation of fluoride is an even more advantageous target; however evidence to date (namely ^{19}F NMR) strongly suggests that chelation of fluoride is not occurring when 1,1'-diborylated systems are treated with a source of fluoride. With the aim of improving "first generation" ferrocene systems to promote chelation of fluoride, the use of 1,2-disubstituted ferrocene systems has been investigated. Initial preparation of 1,2-dibromoferrocene was carried out by Dr. I. R. Butler (Univ. of Wales, Bangor) according to a published route.[21]

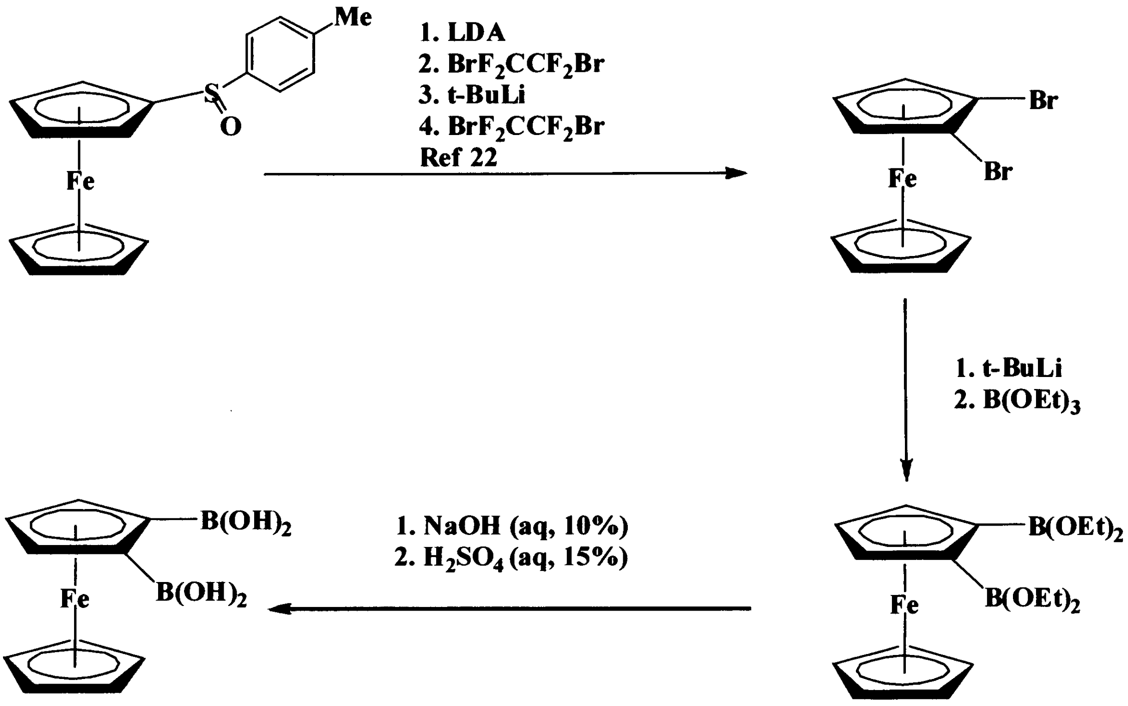

Scheme 3.9 Preparative scheme for ferrocene-1,2-bis(boronic acid)

From the 1,2-dibromoferrocene starting material, preparation of 1,2-ferrocenediboronic acid was attempted *via* reaction with t-butyllithium and triethoxyborate to prepare 1,2-diethoxyboryl ferrocene, followed by hydrolysis of the ethoxy groups with aqueous sodium hydroxide and sulphuric acid solutions. A subsequent condensation reaction with (S,S)-stilbene diol, in which the boronic acid is heated with the diol and acetone in a sealed pressure tube at 80°C for 24h, was carried out in an attempt to synthesise 1,2-*bis*-(diphenylethanediolatoboryl) ferrocene (**6a**) as shown below in Scheme 3.10.

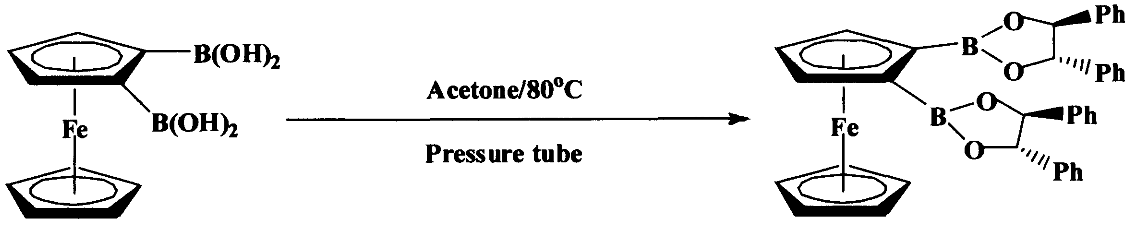

Scheme 3.10 Preparative scheme for 1,2-*bis*-diphenylethanediolatoborylferrocene (**6a**)

After removal of solvent the product was isolated as an orange, air-stable solid in a yield (crude) of 69.5 mg, 32.6 %. However mass spectrometry results indicated that the product comprised a mixture of compounds, (i) the desired product observed at m/z = 630.2, (ii) a compound featuring one stilbenediolatoboryl and one bromide group pendant to ferrocene at m/z = 486.0 and (iii) the *mono*(stilbenediolatoboryl) compound (**1c**) at 408.1.The solid was re-dissolved in chloroform and filtered through a small silica column and three clearly separated bands were isolated. The first band was found to contain the *mono*-stilbenediolatoboryl compound (**1c**) confirmed by ^{1}H NMR and mass spectrometry. The second and third bands were still found to consist of a mixture of products by mass spectrometry, although the third band appeared to contain less of the *mono*-substituted compound. Concerning NMR spectroscopy, the ^{1}H NMR spectrum was expected to be slightly more complex than those previously discussed, but without a suitable separation method it is impossible to reliably assign the peaks. The peak in the ^{11}B NMR is within the expected region at δ_B 34.3 ppm, however. Separation of these compounds has been attempted through fractional crystallisation and by slow evaporation of various solvents, but these attempts failed. It appears that these compounds are of too similar solubility for this method to succeed. A cleaner synthesis may be required to achieve clean samples of the desired product.

3.4.3 Preparation of Pentamethylferrocene derived boronic esters

Further modification was made to the existing ferrocene boronic ester systems involving the use of the more strongly electron donating Cp* ligand; the *mono-* and *bis*-stilbene compounds featuring a Cp* ligand (**5a** and **5b**) were prepared by C. Bresner as shown in Scheme 3.11.[22]

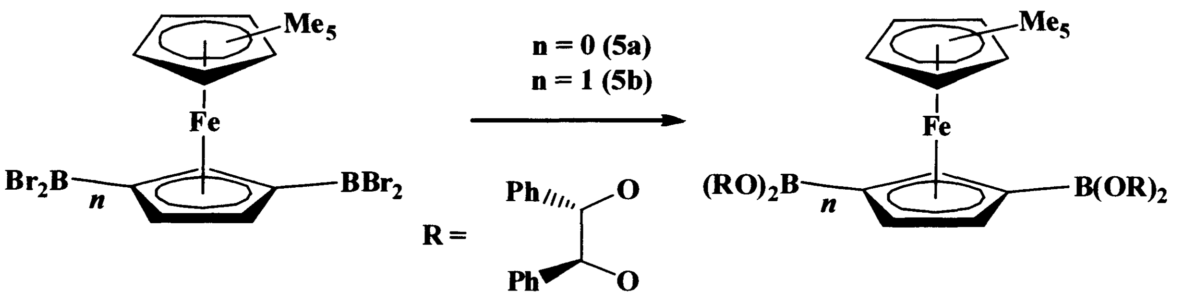

Scheme 3.11 Syntheses of pentamethyferrocene-based Lewis acids containing one or two pendant boronic ester functions (**5a** and **5b**).

These compounds were prepared with a view to improving the response time associated with colorimetric sensing of fluoride. The additional electron donation from the methyl groups of the Cp* ligand should enhance the kinetics of the system, making the electron-transfer process more rapid by making oxidation more thermodynamically favourable (Marcus theory). Compounds **5a** and **5b** were prepared by reaction 1,2,3,4,5-pentamethyl-1'-(dibromoboryl)ferrocene and 1,2,3,4,5-pentamethyl-1',3'-bis(dibromoboryl)-ferrocene respectively, with 1 and 2 equiv. of the lithiate of (S,S)-stilbene diol respectively, yielding yellow air-sensitive powders.

3.5 Conclusions and suggestions for future research

The synthesis of mono-functional boronic ester derivatives (**1a, 1b**) has been achieved in excellent yields and very high purities *via* condensation chemistry, to extend the series of known mono-functional compounds of this type. Comparison of the X-ray structures of **1a** and **1b** with that of the known compound **1c** has revealed no significant structural differences.

The successful preparation of the analogous multi-functional boronic ester derivatives (**3a-5a**) has allowed for further comparison of structural and chemical parameters with the corresponding mono-functional compounds. Most of these compounds were found to be extremely crystalline materials, allowing not only for ease of purification, but also for crystallographic analyses. However the *tris*(ethanediolatoboryl) (**3a**) and *tris*(pinanediolatoboryl) (**3c**) compounds proved problematic in terms of crystal growth, with no single crystals grown despite numerous attempts.

With respect to improvement of the syntheses used in the preparation of *tris*- and *tetrakis*-functional boronic esters of ferrocene, it would be valuable investigating synthetic routes to *tris*- and *tetrakis*-boronic acids of ferrocene as precursors for the condensation reaction with diols, given the ease of synthesis, greatly improved yields and very high purity of the products.

Successful isolation of pure 1,2-stilbenediolatoborylferrocene (**6a**) would be very beneficial to the advancement of this project, with the boryl groups brought into closer proximity of each other it is possible that chelation of fluoride will be the most favoured mode of binding and will present a more stable, and perhaps more crystalline, host-guest complex which will hence allow for more extensive characterisation of the fluoride-bound product.

3.6 References

1 H. Yamamoto, A. Ori, K. Ueda, C. Dusemund, S. Shinkai, *Chem Commun*, 1996., 407.

2 M. Bochmann, S. J. Lancaster, O. B. Robinson, *Chem. Commun.*, 1995, 2081.

3 K. A. Rufanov, V. V. Kotov, N. B. Kazenova, D. A. Lemonovskii, E. V. Avtomonov, J. Lorberth, *J. Organomet. Chem.*, 1996, **525**, 287.

4 H. Braunschweig, R. Dirk, M. Müller, P. Nguyen, R. Resendes, D. P. Gates, I. Manners, *Angew. Chem. Int. Ed. Engl.*, 1996, **36**, 2338.

5 F. Jäckle, K. Polhorn, M. Wagner, *Chem. Ber.*, 1996, **129**, 603.

6 G. E. Herberich, A. Fischer, *Organometallics.*, 1996, **15**, 58.

7 G. E. Herberich, A. Fischer, D. Wiebelhaus, *Organometallics.*, 1996, **15**, 3106.

8 T. Renk, W. Ruf, W. Siebert, *J. Organomet. Chem.*, 1976, **120**, 1.

9 A. Appel, H. Nöth, M. Schmidt, *Chem. Ber.*, 1995, **128**, 621.

10 S. Aldridge, C. Bresner, I. A. Fallis, S. J. Coles, M. B. Hursthouse, *Chem. Commun.*, 2002, 740.

11 B. E. Carpenter, W. E. Piers, M. Parvez, G. P. A. Yap, S. J. Rettig, *Can. J. Chem.*, 2001, **79**, 857.

12 F. Jäckle, A. Berenbaum, A. J. Lough, I. Manners, *Chem. Eur. J.*, 2000, **6**, 2762.

13 C. Bresner, S. Aldridge, I. A. Fallis, unpublished results.

14 A. Appel, F. Jäckle, T. Priermeier, R. Schmid, M. Wagner, *Organometallics.*, 1996, **15**, 1188.

15 K. Akiba, M. Yamshira, Y. Yamamoto, S. Nagase, *J. Am. Chem. Soc.*, 1999, **121**, 644.

16 S. Aldridge, I. A. Fallis, N. D. Coombs, unpublished results.

17 B. Wrackmeyer, U. Dörfler, W. Milius, M. Herberhold, *Polyhedron.*, 1995, **14**,1425.

18 M. M. Olmstead, P. P. Power, K. J. Weese, R. J. Doedens, *J. Am. Chem. Soc.,* 1987, **109**, 2459.

19 F. Zettler, H. D. Hausen, H. J. Hess, *J. Organomet. Chem.,* 1974, **72**, 157.

20 (a) D. W. Luke, A. Streitwieser Jr, *J. Am. Chem. Soc.,* 1981, **103**, 3241. (b) J. Okuda, E. Herdtweck, *J. Organomet. Chem.,* 1989, **373**, 99.

21 I. R. Butler, M. G. B. Drew, *Inorg. Chem. Commun.*, 1999, 234.

22 C. Bresner, I. A. Fallis, S. Aldridge, unpublished results.

Chapter Four

Fluoride Binding by Mono-, *Bis*-, *Tris*- and *Tetrakis*-functional Boron–Containing Lewis Acids

4.1 Introduction

4.1.1 Chemical warfare agents

The selective recognition of chemical warfare agents (CWAs) is a rapidly expanding area of chemical research interest and its relevance to health and environmental issues is largely driven by current global political situations. More specifically, the use of CWAs as weapons in terrorist or military action present growing concerns, and sensors for such potential weapons may find application in the supply of personal monitors for military personnel and in decontamination. Sensors for nerve and blister CWAs are among the most highly researched. A potent class of nerve agents are the G agents, organophosphonate esters, which are similar in structure to some insecticides. The critical feature of these polar organic liquids is the phosphorus-oxygen double bond, which binds irreversibly to acetylcholinesterase, the enzyme that is responsible for effective neurotransmitter function. When nerve agents irreversibly bind to acetylcholinesterase, it can no longer stimulate and control nerve impulses. The nerve gases GB (Sarin) and GD (Soman) are highly toxic, typically causing death within one minute after ingestion (0.01 mg per kg body weight), and slow debilitation in lower doses. Detection of such species requires that unique features of the behaviour of nerve agents be exploited, for example, fluorophosphonate esters are known to hydrolyse spontaneously in air to produce HF gas (Scheme 4.1).

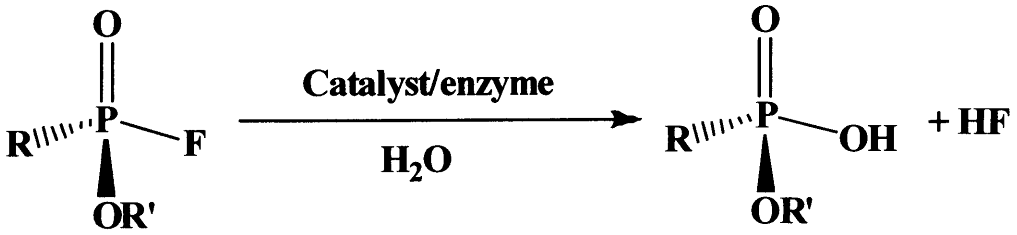

Scheme 4.1 Hydrolysis of a fluorophosphonate ester (Sarin; R = Me, R' = ^{i}Pr)

4.1.2 Background to the field of colorimetric fluoride sensing

In developing a useable sensor for Sarin (GB), the chemically specific recognition of HF must be possible; furthermore the binding event should be coupled by a fluorescence, colorimetric, or electrochemical response to have use in the sensing application. To this end, sensors which specifically bind fluoride and undergo a change in photophysical properties as a result of the binding event are a key goal of the work presented in this chapter; it is also a subject of wide and varied research interest. Fluoride anions demonstrate a specific affinity for Lewis acidic boron-based receptors,[1] and this feature has been exploited by many research groups in the design of the boron-based receptors. Since there are very few benign compounds that spontaneously release HF gas, the possibility of a sensor for Sarin giving a 'false-positive' response is very small and the detection of HF should provide a sensor exclusive to Sarin.

If a redox active centre is incorporated in the design of anion specific receptors, electrochemistry can provide a convenient method of monitoring and analysing the fluoride binding ability of the receptor. The ferrocene fragment can provide such advantages and the selective recognition of fluoride by ferroceneboronic acid has been achieved by Shinkai *et al.*[2] (Figure 4.1).

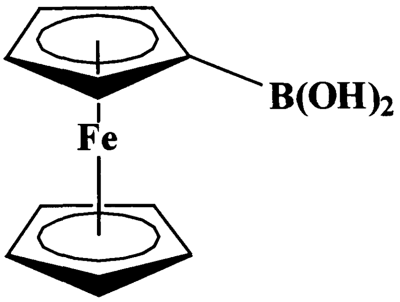

Figure 4.1 Ferroceneboronic acid

Boronic acids have a high affinity for fluoride anions and in ferroceneboronic acid the Lewis acid binding site has a pendant ferrocene fragment, enabling the binding process to be monitored by cyclic voltammetry. Specifically the shift in the redox potential of the ferrocene moiety as a result of anion complexation can be used to detect fluoride. The redox properties of ferroceneboronic acid are drastically altered on addition of fluoride; even in water a cathodic shift is observed in the CV of *ca.* −100 mV, consistent with the formation of the electron-donating four-coordinate boronate anion. Furthermore, the receptor was shown to electrochemically detect fluoride in water even in the presence of other halides in high concentrations, thus specificity for fluoride was displayed.

The conversion of binding information into comprehensible fluorescent outputs has been the target of many research groups.[3] Again exploiting the high affinity of boronic acids for fluoride, James *et al.* carried out fluorescence titrations of phenylboronic acid and 2-napthylboronic acid with KF and reported a decrease in fluorescence intensity upon addition of KF.[4] When a three-coordinate boron centre binds a fluoride anion there is a change in hybridisation from sp^2 to sp^3 at the boron centre.[5] The fluorescence intensity decreases as a result of formation of this sp^3 four-coordinate boronate anion, which is known to quench the fluorescence of directly attached fluorophores by a mechanism of photo-induced electron-transfer.[6] This report represented the first example where fluorescence had been used as an analytical technique to monitor fluoride binding.

Colorimetric fluoride ion sensing has been investigated by Tamao *et al.* in developing the boron-containing π-electron system of dimesityl-boryl substituted trianthrylborane (Figure 4.2).[7] The π-conjugation in this system extends through the vacant p-orbital at the boron centres resulting in characteristic absorption properties in the UV/Vis spectrum. Thus fluoride binding can be closely monitored by this spectroscopic technique because complexation of a fluoride anion at the boron centre will interrupt the extended π-conjugation, thereby causing a marked change in λ_{max}. The authors report the fluoride sensing ability of dimesityl-boryl-substituted trianthrylborane to be characterised by a red to orange colour change, monitored by UV/Vis spectroscopy.

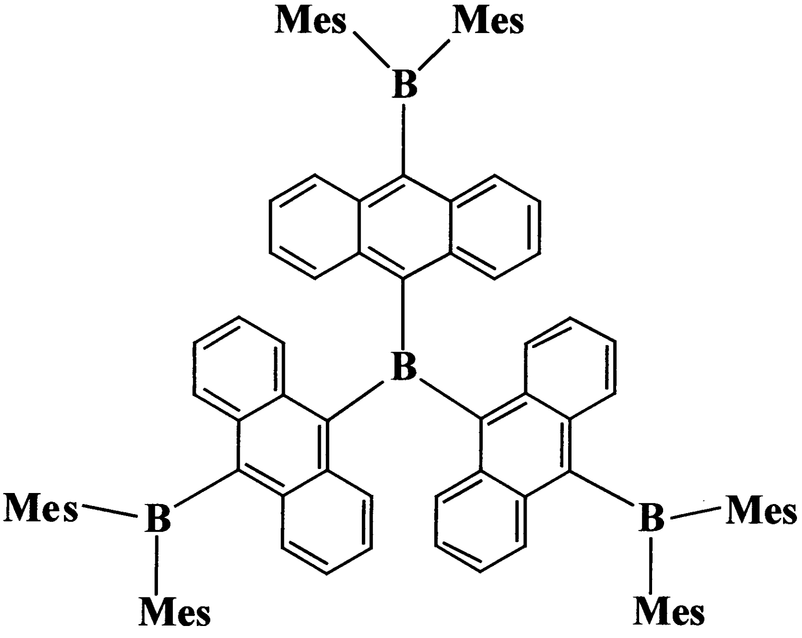

Figure 4.2 Dimesityl-boryl substituted trianthrylborane

Fluoride complexation by this receptor was accompanied by a decrease in intensity of the absorption band of the parent compound (474 nm) and the growth of a new absorption band at 570 nm. This shift was interpreted as the mono-fluoride guest-host complex, which was later confirmed by X-ray diffraction studies. Upon addition of subsequent portions of fluoride further shifts in the absorption bands in the UV/Vis spectrum were observed. These spectral changes were construed as complexation of two additional equivalents of fluoride to the second and third boron centres, the final spectrum looking similar to that of the fluoride-free compound except red-shifted by *ca.* 25 nm. Thus the authors conclude that fluoride complexation does not occur at the central boron atom.

Phosphorescence as an analytical tool for monitoring anion binding remains a limited area of research, although Gabbaï *et al.* recently reported the use of a heteronuclear bidentate Lewis acid as a phosphorescent fluoride sensor (Scheme 4.2).[8]

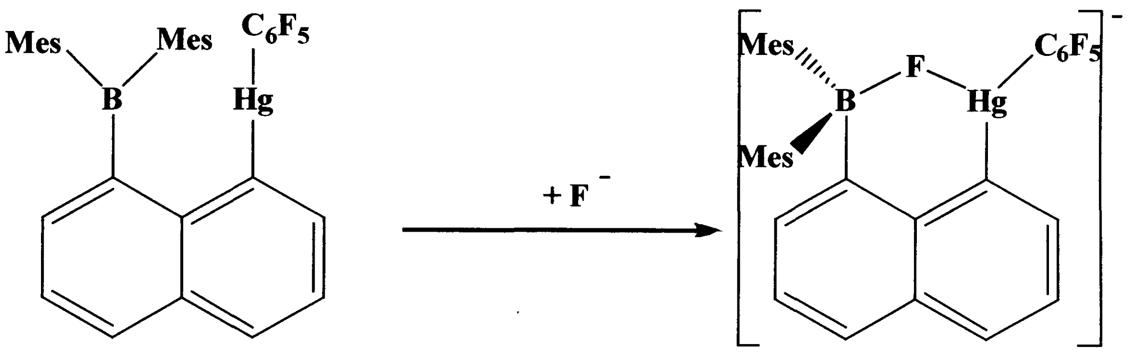

Scheme 4.2 A heteronuclear bidentate Lewis acidic phosphorescent fluoride sensor

This heteronuclear B/Hg bidentate Lewis acid features napthalenediyl and mesityl substituents, hence π-conjugation extends through the vacant p-orbital at boron between these two substituents, as seen in the UV/Vis spectrum as a broad absorption band at 361 nm. Furthermore, heavy atoms such as mercury are known to enhance spin-orbit coupling in organic molecules, which in spectroscopic terms can lead to enhanced phosphorescence emission, and solid-state photoexcitation of this species gives rise to an emission at λ_{max} = 531 nm, which is observed as a red glow. This bifunctional Lewis acid was found to chelate fluoride anions, evidence of which was gained from ^{19}F and ^{199}Hg NMR, which are comparable to previously characterised fluoride-bridged boron species.[8] When fluoride chelation occurs the formerly vacant p-orbital at boron becomes populated and conjugation between the napthalenediyl and mesityl substituents is no longer mediated. As a result the absorption band in the UV/Vis spectrum is seen to progressively decrease upon incremental addition of fluoride, until the baseline is reached after addition of exactly 1 equiv. implying formation of a 1:1 guest-host complex. Photoexcitation of the fluoride-bound guest-host complex gives rise to a new intense emission at 480 nm, which is green in colour, indicating that the loss of conjugation isolates the napthalenediyl chomophore, which readily phosphoresces. These results prove that fluoride binding has no effect on the spin-orbit coupling induced by the mercury atom.

In a recent publication Gabbaï *et al.* reported a fluoride-selective sensor based on a cationic *ortho*-ammonium borane, which was found to display distinct photophysical changes on the binding of fluoride (Figure 4.3).[9]

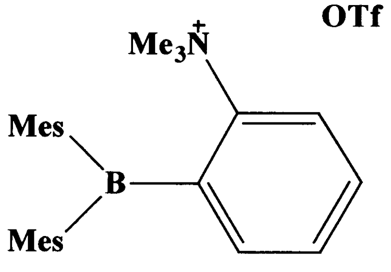

Figure 4.3 A cationic borane as a fluoride-selective sensor

Addition of a source of fluoride to the sensor in aqueous solution was found to induce rapid quenching of the UV/Vis absorption band at 321 nm, followed by precipitation of the fluoride-bound complex. From the fluoride-binding UV/Vis data a binding constant of 910 M^{-1} was calculated. Experimental and DFT studies have implied that the *ortho*-trimethylammonium group leads to increased Lewis acidity, since the *para*-analogue was found to bind cyanide anions exclusively whilst treatment with fluoride resulted in no spectral changes in the UV/Vis spectrum. DFT results show that the energy of the LUMO in the *ortho*-isomer is lower than in the *para*-isomer. Steric crowding was thought to be one reason for the observed selectivity of this receptor for fluoride. Addition of Al^{3+} ions to a solution of the fluoride-bound host-guest complex was found to result in regeneration of the fluoride-free receptor, indicated by changes in the UV/Vis spectrum.

4.1.3 Preliminary work

In previous studies towards the development of a sensor for fluoride anions made within the group, the mono-functional boronic ester **1c** was found to act as a selective receptor for fluoride in chloroform solution. Electrochemical studies then revealed that the binding event was accompanied by a cathodic shift in the oxidation potential of the ferrocene centre of ca. –530 mV (from +131 to –403 mV with respect to ferrocene/ferrocenium).[10] Conclusive evidence of formation of the four-coordinate adduct $[FcB(OR)_2F]^-$ was gained *via* multi-nuclear (^1H, ^{11}B and ^{19}F) NMR and electro-spray mass spectrometry, and a relatively weak binding constant ($K = 35 \pm 9$ $mol^{-1}\ dm^3$) was determined by use of a ^1H NMR titration curve. This weak host-guest interaction was thought to be responsible for the high degree of selectivity for fluoride displayed. Despite the relatively large electrochemical shift observed on binding fluoride the thermodynamics of oxidation for compound **1c** are not sufficiently favourable that atmospheric oxygen is able to oxidise the orange ferrocene compound to the corresponding green ferrocenium compound, hence this compound does not behave as a colorimetric sensor for fluoride. In subsequent investigations to facilitate colorimetric sensing, modifications to the existing sensor were made. Such modifications included the addition of an extra boryl group into the system, which is now capable of binding two equivalents of analyte, and consequently bringing about a larger electrochemical shift (*ca.* 1 V) on fluoride coordination. The *bis*-fluoride adduct is now oxidised by atmospheric oxygen affecting a visual colour change from orange to green and the bi-functional Lewis acid system featuring a stilbenediolate backbone (**2a**), as shown Scheme 4.3, has been reported to act as a fluoride specific colorimetric sensor molecule.[11] The ferrocene to ferrocenium oxidation process, which accompanies fluoride binding, is characterised in the UV/Vis spectrum by the decay of bands at 341 and 449 nm and growth of features at 428 and 633 nm. Cyclic voltammetry results indicate a cathodic shift from the parent compound at +206 mV (with respect to ferrocenium/ferrocene) with two redox waves observed with net shifts of -590 and -960 mV. The former shift is similar to that measured for the mono-stilbene fluoride-bound adduct [**1c•F**]$^-$ and was hence assigned to oxidation of the mono-fluoride adduct, whilst the larger shift (and the observed oxidation in the presence of air) was thought to be strongly suggestive of the *bis*-fluoride adduct.

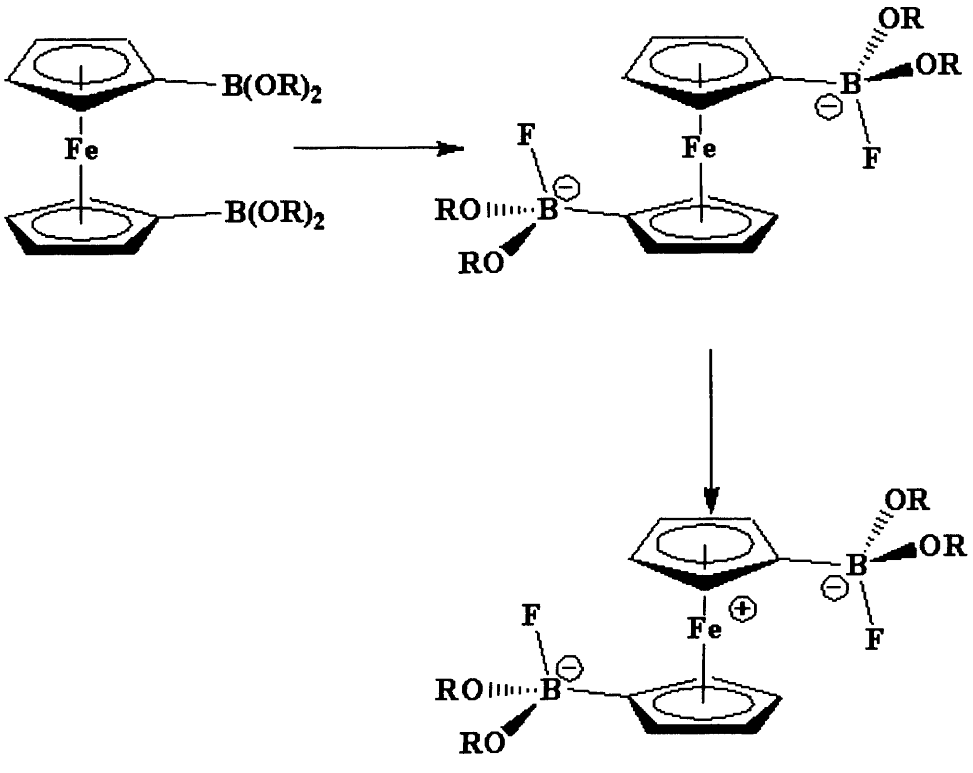

Scheme 4.3 Colour change and chemical mode of action for a *bis*-functional boronic ester as a colorimetric fluoride ion sensor in chloroform solution.

Subsequent studies on these systems led to the development of a receptor featuring a boron-based binding site with a Lewis basic component incorporated in the within the molecular framework, to facilitate whole acid binding, either of an intact HF molecule or as distinct H^+ and F^- components. The interaction of this receptor with three equivalents of HF in MeCN solution led to the isolation of a zwitterionic species $[(\eta^5\text{-}C_5H_5)Fe\{\eta^5\text{-}C_5H_3(BF_3)(CH_2NMe_2H)\}]$, characterised spectroscopically and by X-ray diffraction (Figure 4.5). The intermolecular H-F interaction was found to be relatively weak as evidenced by a separation of 2.204 Å (0.92 Å for gaseous HF).[12]

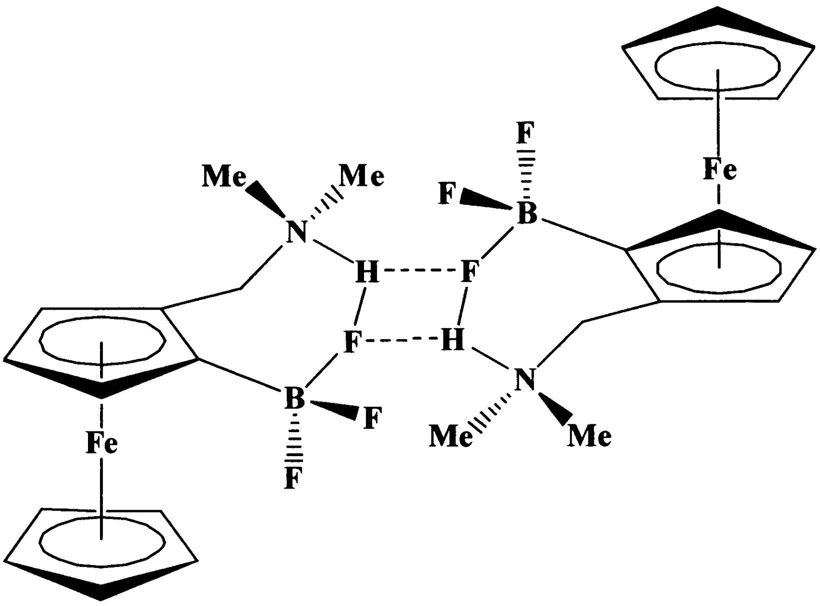

Figure 4.5 Mixed Lewis acid/Lewis base system for whole acid binding

The key feature of this whole acid binding systems is the high selectivity for HF over other acids, demonstrated electrochemically in the presence of HCl. Addition of HF to the receptor revealed a cathodic shift of –80 mV consistent with transformation of a three-coordinate boronic acid group into an electron-donating four-coordinate boronate. By contrast, addition of HCl caused a significant anodic shift (+149.5 mV), consistent with protonation of the amine moiety, with no significant Lewis base coordination at the boron centre.

4.1.4 Aims of Research

Considering recent advances in the field of colorimetric recognition of specific anionic species, it was decided to examine the potential of Lewis acidic binding of fluoride anions using the multi-functional ferrocene-based boryl compounds synthesised in chapter three. With the specific aim of advancing the prototype bi-functional Lewis acid system to proffer enhanced kinetics and sensitivity of response, a better knowledge of fundamental thermodynamic and kinetic factors behind the oxidation-based colorimetric response to fluoride was sought. A greater knowledge and understanding of such factors should allow particular sensor properties to be tuned *via* simple chemical modification. To this end, the effect of the number and nature of boronic ester groups and additional ligands on the efficiency and rate of colorimetric response have been systematically investigated. Thermodynamic aspects have been evaluated by use of cyclic voltammetry and multi-nuclear NMR spectroscopy whilst the kinetics of response was assessed by time resolved UV/Vis spectroscopy.

4.2 Experimental

4.2.1 *Electrochemical (CV) analysis of multi-functional borylmetallocenes*

Electrochemical analysis was carried out under the following conditions: electrolyte, 0.1 M $[^{n}Bu_4N][PF_6]$ in dry dichloromethane or acetonitrile; reference electrode standard, 0.1 M $[^{n}Bu_4N][PF_6]$, 0.01 M silver nitrate in acetonitrile. Initially the electrolyte solution was degassed with argon to remove any dissolved oxygen before background cyclic voltammetry (CV) scans were recorded to guarantee the purity of the electrolyte solution prior to addition of the compound. Once a clean flat background CV had been measured a small sample of the Lewis acid (*ca* 2-5 mg) was added and the solution was further degassed to purge the solution of any additional dissolved oxygen and to dissolve the compound by agitation before spectral acquisition. Further CV scans were measured after of addition of ferrocene/ethylferrocene as the reference compound. This procedure was carried out for compounds **1a**, **1b**, **3b**, **4b** and **4c**.

4.2.2 *Electrochemical (CV) analyses of multi-functional borylmetallocenes treated with fluoride*

Electrochemical analysis was carried out under analogous conditions to those quoted in section 4.3.1. Once a clean flat background CV had been measured a small sample of the Lewis acid (*ca* 2-5 mg) was added and the solution was further degassed to purge the solution of any additional dissolved oxygen and to dissolve the compound by agitation before spectral acquisition. Further CV scans were measured after addition of portions of solid [^{n}Bu$_4$N]F and on addition of ferrocene/ethylferrocene as the reference compound. This procedure was carried out for compounds **1a**, **1b** and **4b**.

4.2.3 *Chemical Oxidations*

Chemical oxidation of **1b**

A solution of **1b** (0.2 g, 5.49 mmol) in dichloromethane (50 ml) was added to a solution of silver (I) tetrafluoroborate (0.107 g, 5.49 mmol) also in dichloromethane (50 ml). A very rapid colour change from orange to blue was observed and the resulting dark blue solution was stirred for a further 12 h. After filtration to remove silver metal, solvent was removed in vacuo to yield a dark blue oily residue which was extracted into toluene. The toluene solution was concentrated, layered with hexanes and stored at –30 °C, whereupon crystals of [**1b**]$^+$[BF$_4$]$^-$ suitable for X-ray diffraction were grown over a 24 h period. ^{11}B NMR (96 MHz, CDCl$_3$): δ 44.1. UV/Vis (chloroform): λ_{max} = 627 nm, ε = 97.6 mol^{-1} cm^{-1} dm^3. Crystal data: $C_{20}H_{25}B_2F_4FeO_2$, orthorhombic, P 2_1 2_1 2_1, a = 9.0670(3) Å, b = 10.0542(3) Å, c = 22.8151(9) Å, V = 2079.86(12) Å^3, Z = 4, D_{calc} = 1.440 Mg m^{-3}, μ(MoKα) = 0.773 mm^{-1}. A suitable crystal was covered in pre-dried mineral oil and mounted at 150(2)

K. 4171 unique reflections were collected ($3.57 < \theta < 26.37^\circ$). Final R-factor: R_1 = 0.0906.

Chemical oxidation of **1c**

By an analogous method to that used for $[\mathbf{1b}]^+[BF_4]^-$, **1c** (0.2 g, 4.9 mmol) was oxidised with silver (I) triflate (0.125 g, 4.9 mmol) in dichloromethane solution (50 ml). An immediate colour change from orange to dark green was observed. Layering of the concentrated dark green solution with hexanes at –30°C yielded blue plate-like crystals of $[\mathbf{1c}]^+[CF_3SO_3]^-$ suitable for X-ray diffraction. ^{11}B NMR (96 MHz, $CDCl_3$) δ 44.5. Crystal data: $C_{50}H_{42}B_2F_6Fe_2O_{10}S_2$, monoclinic, P 2, a = 10.1599(5) Å, b = 9.4937(5) Å, c = 12.7481(10) Å, V = 1175.17(13) Å^3, Z = 1, D_{calc} = 1.575 Mg m^{-3}, μ(MoKα) = 0.791 mm^{-1}. A suitable crystal was covered in pre-dried mineral oil and mounted at 150(2) K. 4339 unique reflections were collected ($3.72 < \theta < 26.37^\circ$). Final R-factor: R_1 = 0.0689.

Chemical oxidation of **2b**

By an analogous method to those listed above, **2b** (0.2 g, 3.69 mmol) was oxidised with silver (I) triflate (0.095 g, 3.7 mmol) in dichloromethane solution (50 ml). An immediate colour change from orange to dark green was observed. Layering of the concentrated dark green solution with hexanes at –30°C yielded blue plate-like crystals of $[\mathbf{2b}]^+[CF_3SO_3]^-$ suitable for X-ray diffraction. ^{11}B NMR (96 MHz, $CDCl_3$) δ 43.2. UV/Vis (chloroform): λ_{max} = 631 nm, ε = 107.6 mol^{-1} cm^{-1} dm^3. MS(ES): M$^+$ = 542.4 (100%). Crystal data: $C_{30}H_{40}B_3F_4FeO_4$, orthorhombic, P 2_1 2_1 2_1, a = 11.243(3) Å, b = 13.871(4) Å, c = 19.773(5) Å, V = 3083.9(15) Å^3, Z = 4, D_{calc} = 1.355 Mg m^{-3}, μ(MoKα) = 0.547 mm^{-1}. A suitable crystal was covered in pre-dried mineral oil and mounted at 120(2) K. 6208 unique reflections were collected ($4.0 < \theta < 29.4^\circ$). Final R-factor: $R_1 = 0.0688$.

4.2.4 *NMR analyses of fluoride binding to mono- and multi-functional Lewis acids* **1a**, **1b**, **4a**, **4b** and **4c**

A sample of mono/multi-functional Lewis acid (typically approximately 20 mg) was weighed into a Young's NMR tube under an argon atmosphere, dissolved in dry, degassed CD_3Cl, and the purity of the compound checked by ^{11}B and ^1H NMR preceding fluoride addition. Tetra-n-butyl ammonium fluoride trihydrate (1 equiv. *ca.* 10 mg) was added to the Young's NMR tube under an inert atmosphere. A 10-minute period was allowed for mixing before the ^{11}B and ^1H NMR were measured again. Subsequent equivalents of $[^nBu_4N]F$ were added until the starting material was undetected in the ^{11}B NMR spectrum.

Spectroscopic data for **1a** + $[^nBu_4N]F$

^{11}B NMR (96 MHz, $CDCl_3$) δ_B 9.75 (br); ^{19}F NMR ([D]chloroform, 283 MHz, 20°C), δ_F -133.39.

Spectroscopic data for **1b** + MeHMTAF

^{11}B NMR (96 MHz, $CDCl_3$) δ_B 8.92 (br); ^{19}F NMR ([D]chloroform, 283 MHz, 20°C), δ_F -137.29.

Spectroscopic data for **4b** + $[^nBu_4N]F$

^{11}B NMR (96 MHz, $CDCl_3$) δ_B 6.30 (br); ^{19}F NMR ([D]chloroform, 283 MHz, 20°C), δ_F -134.0.

Spectroscopic data for **4c** + $[^nBu_4N]F$

^{11}B NMR (96 MHz, $CDCl_3$) δ_B 5.11 (br); ^{19}F NMR ([D]chloroform, 283 MHz, 20°C), δ_F -135.1.

4.2.5 *Binding stoichiometry of multi-functional borylmetallocenes* **3b, 4b** *and* **4c** *by UV/Vis spectroscopy determined via Job's Method.*

Into nine sample vials were weighed varying masses (0 to 40 mg in 5 mg increments) of a multi-functional boryl-metallocene (**3b, 4b** and **4c**) and each dissolved in chloroform (8.4 ml). $[^nBu_4N]F.3H_2O$ was added to each sample vial in varying amounts so as to keep the overall concentration constant (4.4×10^{-3} mol dm^{-3}). After one hour was allowed for thorough mixing of the solution and dissolution of oxygen into the system, the UV/Vis spectrum of each solution was recorded. A subsequent plot of absorbance of the ferrocenium peak against molar ratio provided a curve from which a binding stoichiometry can be ascertained.

4.2.6 *UV Kinetic Studies*

An aliquot containing a known excess of tetra-n-butylammonium fluoride trihydrate was added via syringe to 2.5 cm^3 of a stock solution of the boronic ester (17.5 mM) contained within the UV cell. The absorbance in the UV spectrum for the band at *ca.* 630 nm, associated with the ferrocenium product was then recorded at 1s intervals for a period of 2400 s. Each boronic ester has a specific wavelength associated with its ferrocenium oxidation product; these values are displayed with the corresponding UV spectrum.

4.3 Results and Discussion

4.3.1 Electrochemical and chemical oxidation of mono- and multi-functional ferroceneboronic esters

Electrochemical methods have long provided a valuable insight into the mechanisms of electron transfer reactions involved in redox processes and the ferroceneboronic esters described in chapter three were designed with this convenient method of analysis in mind. Cyclic voltammetry measurements have been carried out on compounds **1a**, **1b**, **3a**, **4b** and **4c** with a view to analysing the electronic effects of the number and nature of the pendant boryl groups boryl groups. Measurements were carried out in either dichloromethane or acetonitrile solution depending on solubility, and in all cases ferrocene was used as a reference compound, except in the case of **3b** where ethylferrocene was used as the reference compound. The cyclic voltammograms of compounds **1a**, **1b**, **3b**, **4b** and **4c** are shown in Figures 4.6- 4.10 and a summary of relevant information is given in Table 4.1.

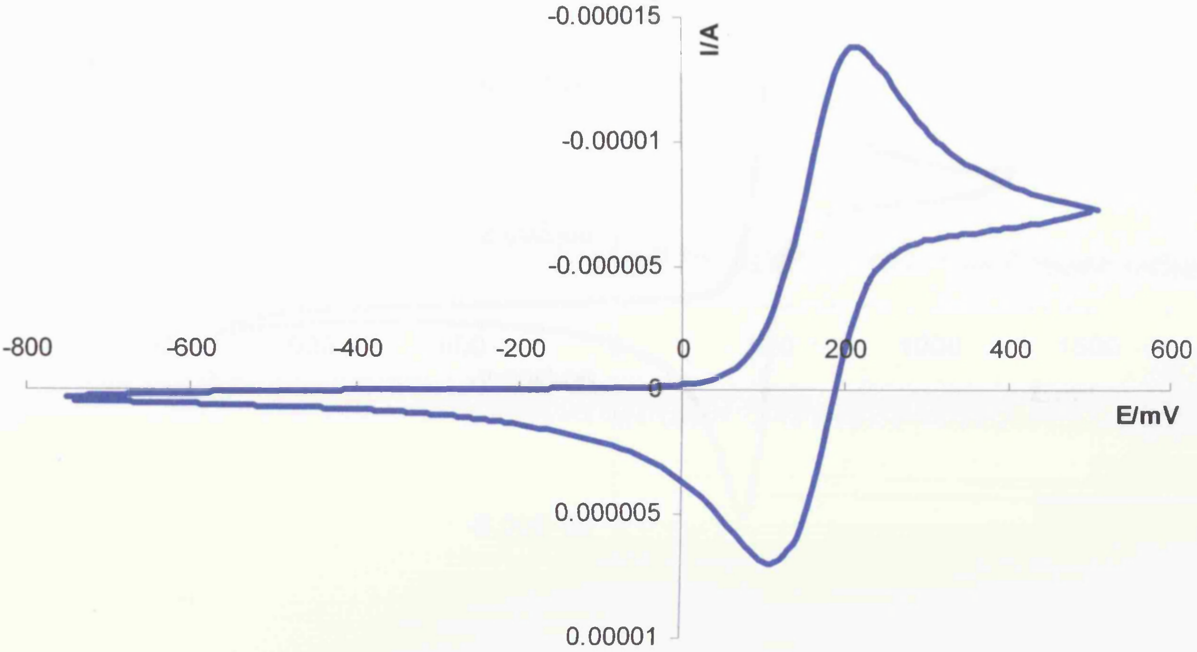

Figure 4.6 Cyclic Voltammogram of compound **1a**.

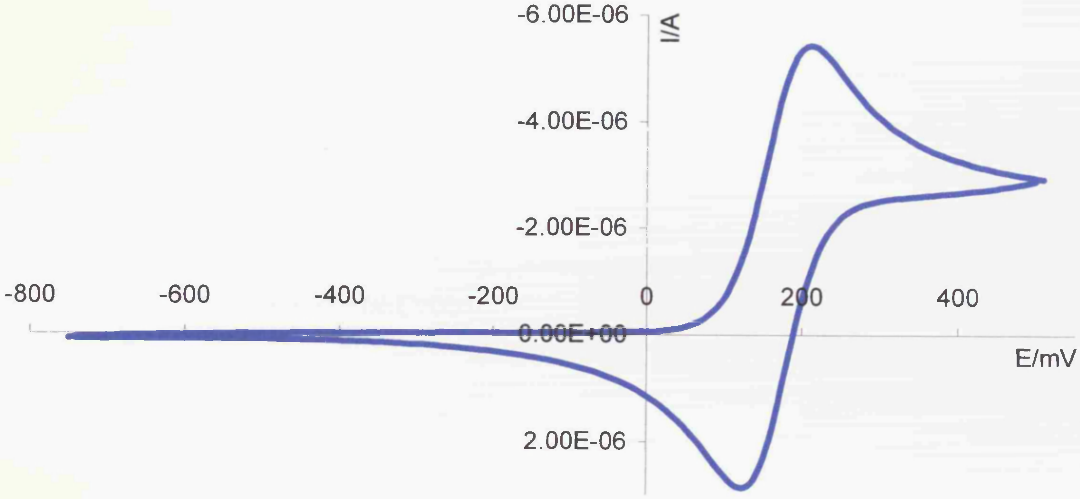

Figure 4.7 Cyclic Voltammogram of compound **1b**.

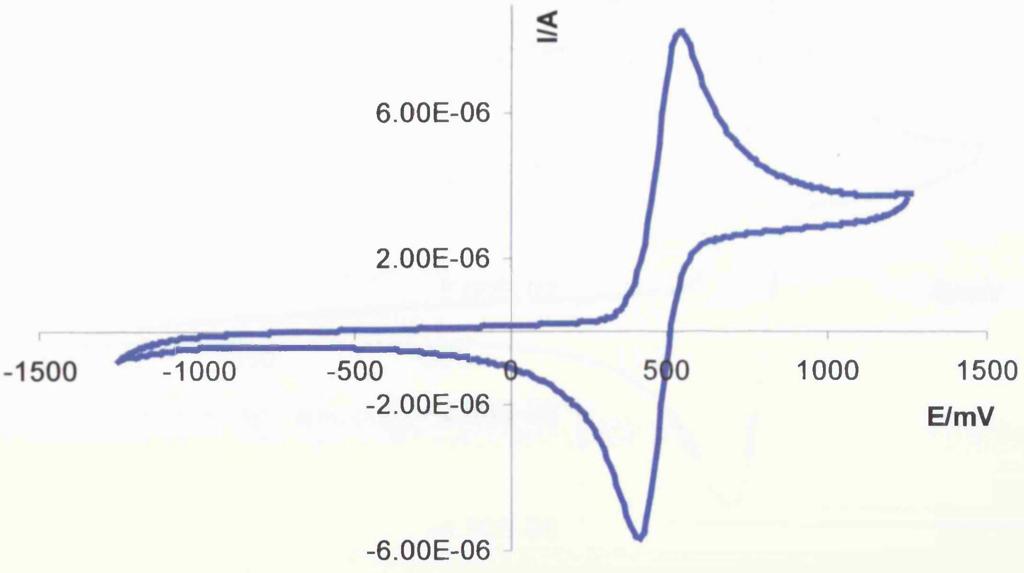

Figure 4.8 Cyclic Voltammogram of compound **3b**.

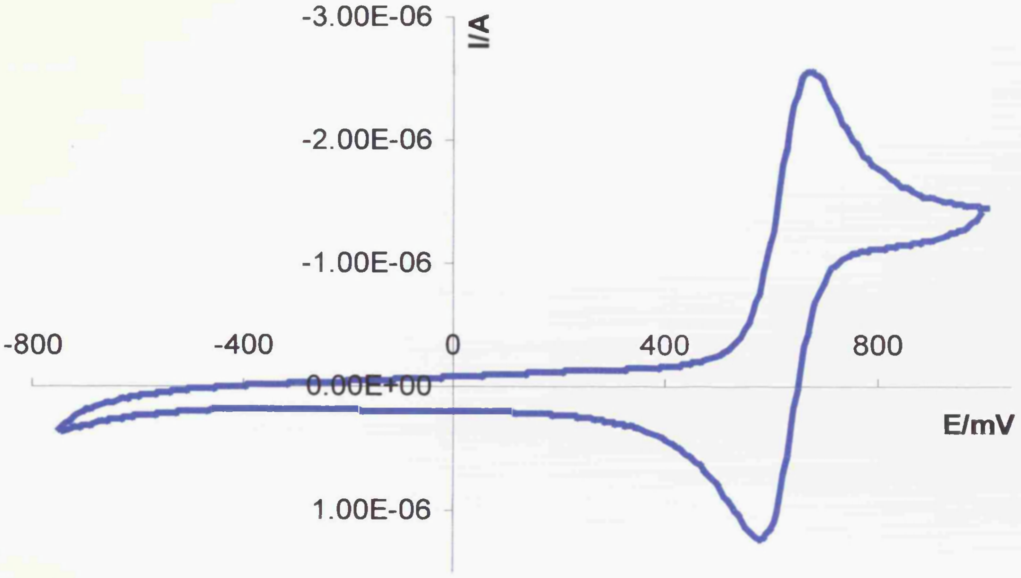

Figure 4.9 Cyclic Voltammogram of compound **4b**.

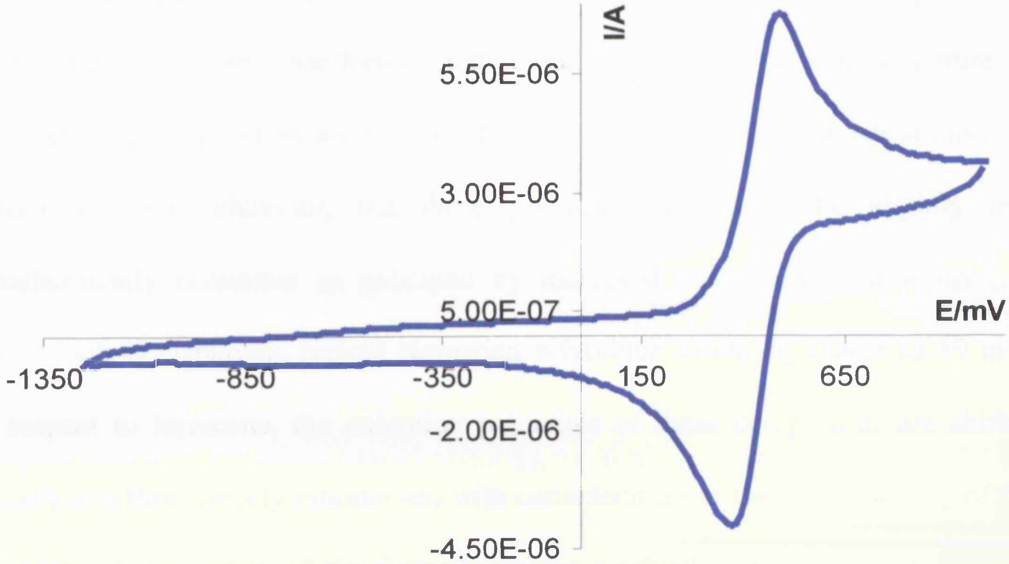

Figure 4.10 Cyclic voltammograms of compound **4c**.

Compound	Solvent	Oxidation Potential (mV)	Peak-Peak separation (mV)	Potential Relative to FcH (Ref.) (mV)
1a	MeCN	+216	100	+29
1b	MeCN	+206	90	+90
3b*	Dichloromethane	+544	107	+305*
4b	Dichloromethane	+680	90	+430
4c	Dichloromethane	+501	149	+280
1c	Dichloromethane	+317	91	+131

Table 4.1 Electrochemical data for borylferrocene systems **1a**, **1b**, **3b***, **4b**, **4c** and **1c** (***3b** referenced against ethylferrocenium/ethylferrocene).

All compounds (**1a**, **1b**, **3b**, **4b** and **4c**) exhibit reversible oxidation processes characteristic of the ferrocene/ferrocenium redox couple. The reversible nature of these electrochemical processes implied by the observed peak-peak separations is approaching ideal behaviour, but these processes appear to be slightly less electrochemically reversible as indicated by increased peak-peak separations (*ca.* 95mV) which if displaying typical Nernstian behaviour would be closer to 59 mV. With respect to ferrocene, the oxidation potentials of these compounds are shifted anodically and this is easily rationalised with consideration of the Lewis acidity of the boron centre. Conjugation of the formally vacant p-orbital at boron causes electron withdrawal from the π-orbitals of the cyclopentadienyl aromatic system; hence the iron centre becomes less electron rich and less easily oxidised compared with ferrocene. The effect becomes more pronounced as additional boryl groups are introduced to the system as evidenced by the increasingly anodic shifts observed for *tris*- (+305 mV cf. EtFcH) and *tetrakis*-functionalised systems (+430 mV cf. FcH), compared to shifts observed for *mono*-borylmetallocenes (+90 mV cf. FcH) and *bis*-borylmetallocenes (+206 mV cf. FcH). Electrochemical shifts observed for the novel *mono*-compounds (**1a** and **1b**) are slightly lower (*ca.* 100 mV) than that observed for the previously reported *mono*-compound **1c** as shown in Table 4.1, it is likely that solvent effects are responsible for the difference in shifts, **1a** and **1b** were run in acetonitrile where **1c** was run in dichloromethane.

As discussed, *tris*- and *tetrakis*-boronic esters are shifted anodically compared to *mono*- and bi-functional compounds; this is consistent with the π-electron withdrawing nature of the boronic ester fragment, and is shown pictorially in Figure 4.12 in which the cyclic voltammograms for *mono*-, *bis*-, *tris*- and *tetrakis*-stilbene compounds (**1c**, **2a**, **3b** and **4b**) have been overlaid.

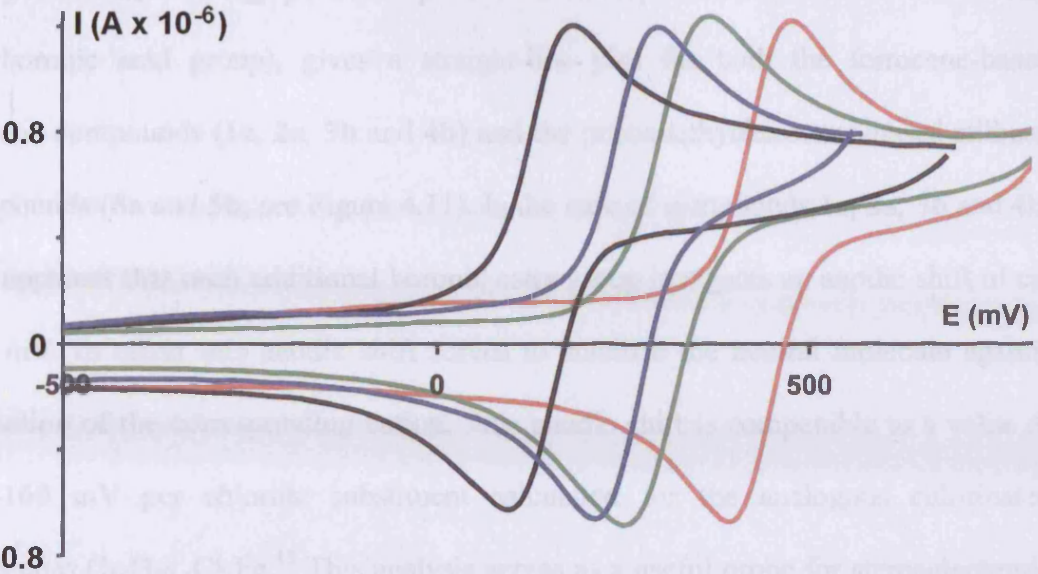

Figure 4.12 Cyclic voltammograms comparing **1c** (black trace), **2a** (blue trace), **3b** (green trace) and **4b** (red trace), referenced against ferrocenium/ferrocene (**1c**, **2a**, **4b**), ethylferrocenium/ethylferrocene (**3b**).

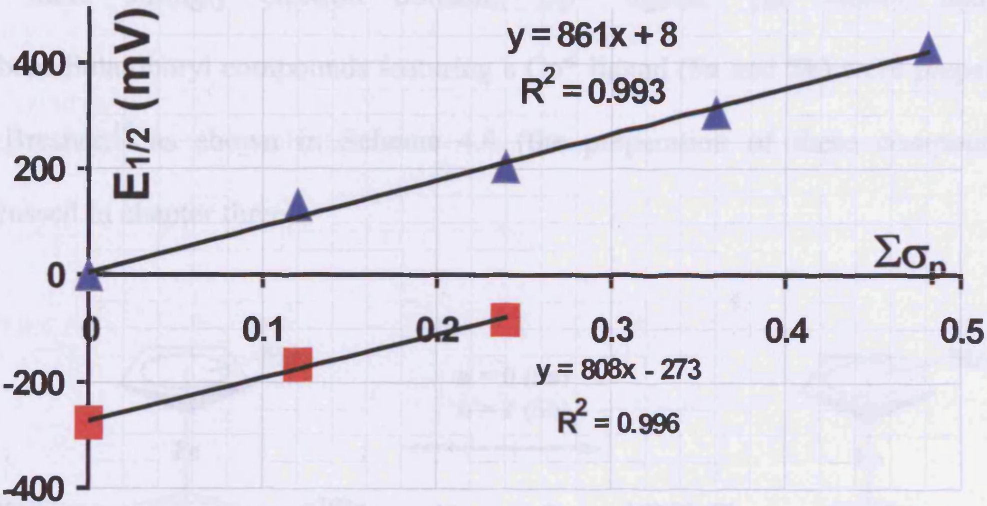

Figure 4.13 Plot of $E_{1/2}$ against the Hammett parameter summed for each additional boronic ester group in **1c**, **2a**, **3b** and **4b** (blue triangles), **5a** and **5b** (*Vide infra,* red squares).

The plot of $E_{1/2}$ versus $\sum\sigma_p$ (where σ_p is the Hammett *para* coefficient associated with the boronic acid group), gives a straight-line plot for both the ferrocene-based stilbene-compounds (**1c**, **2a**, **3b** and **4b**) and the pentamethylferrocene-based stilbene compounds (**5a** and **5b**, see Figure 4.11). In the case of compounds **1c**, **2a, 3b** and **4b**, it is apparent that each additional boronic ester group instigates an anodic shift of ca. 110 mV, in effect this anodic shift serves to stabilise the neutral molecule against formation of the corresponding cation. This anodic shift is comparable to a value of 120-160 mV per chloride substituent calculated for the analogous chlorinated ferrocenes $C_{10}H_{10-x}Cl_xFe$.[13] This analysis serves as a useful probe for stereoelectronic effects at work in these systems; in this case we observe a linear plot of $E_{1/2}$ Vs σ_p and this evidence serves as proof that the multiple boryl groups act independently of each other.

Further modification was made to the existing systems involving the use of the more strongly electron donating Cp* ligand. The *mono-* and *bis-*stilbenediolatoboryl compounds featuring a Cp* ligand (**5a** and **5b**) were prepared by C. Bresner,[14] as shown in Scheme 4.4 (the preparation of these compounds is discussed in chapter three).

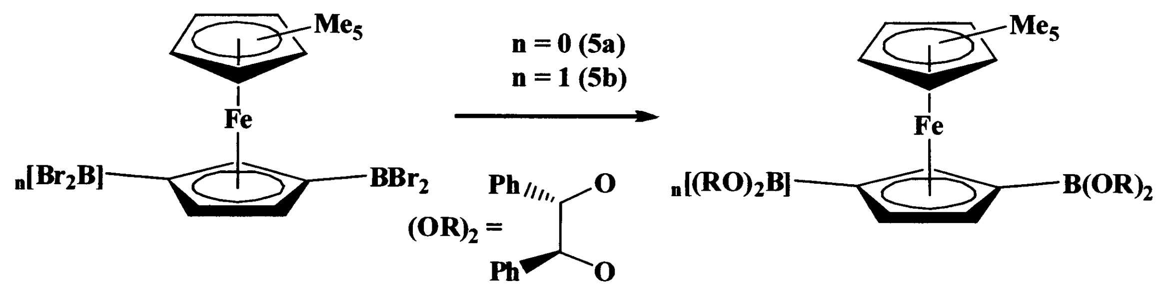

Scheme 4.4 Syntheses of pentamethyferrocene-based Lewis acids containing one or two pendant boronic ester functions (**5a** and **5b**)

These compounds were prepared with a view to improving the response time associated with colorimetric sensing of fluoride. The electron donating methyl groups of the Cp* ligand should enhance the kinetics of the system because the iron centre is more electron rich, making oxidation more thermodynamically favourable according to Marcus theory. This effect is clear in the cyclic voltammograms of the *mono*-substituted compounds **5a** (black trace) and **1c** (blue trace), in which a cathodic shift of *ca.* -300 mV is observed on permethylation of the Cp ligand (Figure 4.11).

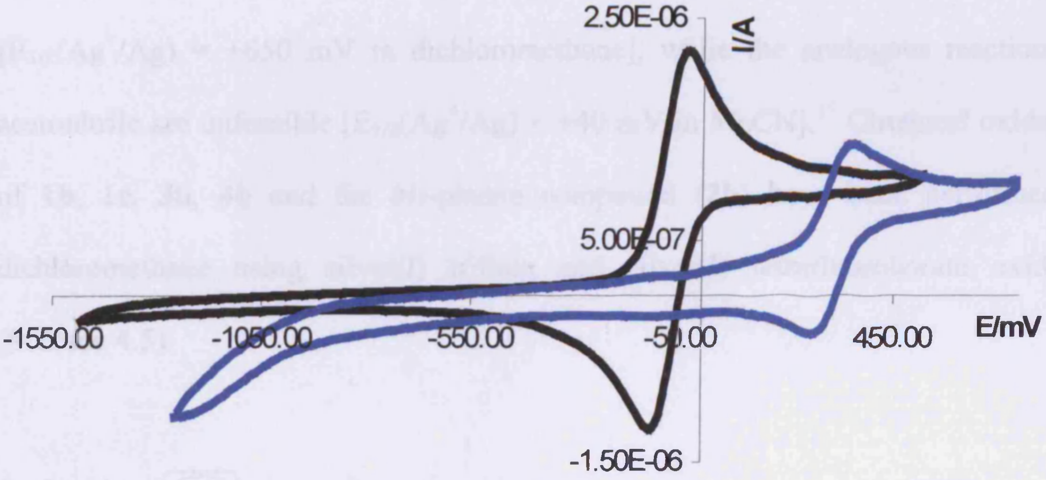

Figure 4.11 Cyclic voltammograms of **1c** (blue trace) and **5a** (black trace) overlaid.

Compound	Solvent	Oxidation Potential (mV)	Peak-Peak separation (mV)	Potential Relative to FcH (Ref.) (mV)
5a	Dichloromethane	-126	91	-169
5b	Dichloromethane	-32.3	100	-83
1c	Dichloromethane	+317	91	+131

Table 4.2 Electrochemical data for borylferrocene systems **1c**, **5a** and **5b**

Chemical oxidation of ferroceneboronic esters has also been undertaken using silver(I) oxidants; thus isolation of ferroceniumboronic esters in the absence of fluoride has been possible. Silver(I) salts are very widely used as one-electron oxidants, however it is worthwhile to note that the oxidation potential of such oxidants depends greatly on the solvent; whereas silver(I) salts can be considered strong oxidants in dichloromethane solution, they are considered weak oxidants in acetonitrile solution. Consistent with these findings, the chemical oxidation of ferroceneboronic esters was easily achieved by the use of a silver(I) oxidant [$E_{1/2}(Ag^+/Ag)$ = +650 mV in dichloromethane], while the analogous reactions in acetonitrile are unfeasible [$E_{1/2}(Ag^+/Ag)$ = +40 mV in MeCN].[15] Chemical oxidation of **1b**, **1c**, **3b**, **4b** and the *bis*-pinane compound (**2b**) have been performed in dichloromethane using silver(I) triflate and silver(I) tetrafluoroborate oxidants (Scheme 4.5).

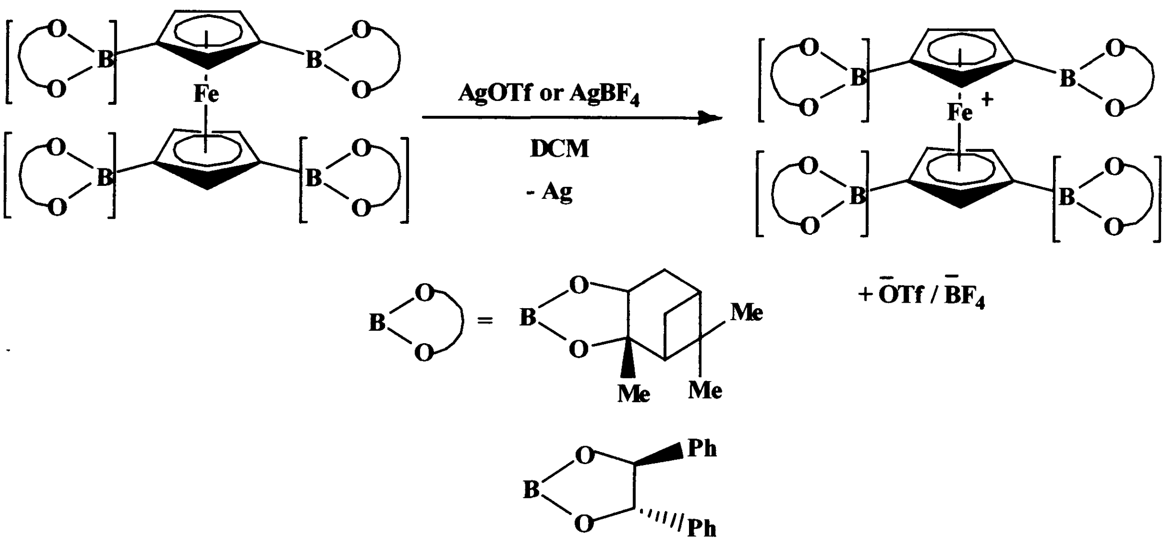

Scheme 4.5 General preparative scheme for ferroceniumboronic esters.

In all cases a very rapid orange-green/blue colour change is observed on addition of the oxidant accompanied by precipitation of silver metal, which is subsequently removed by filtration. Compound **1b** was oxidised with one equivalent of silver(I) tetrafluoroborate to yield a blue solution, from which crystals suitable for X-ray diffraction were grown after layering with hexane. The solid-state structure of $[\mathbf{1b}]^+[\mathbf{BF_4}]^-$ is illustrated in Figure 4.14; selected bond lengths and angles are listed in Table 4.3.

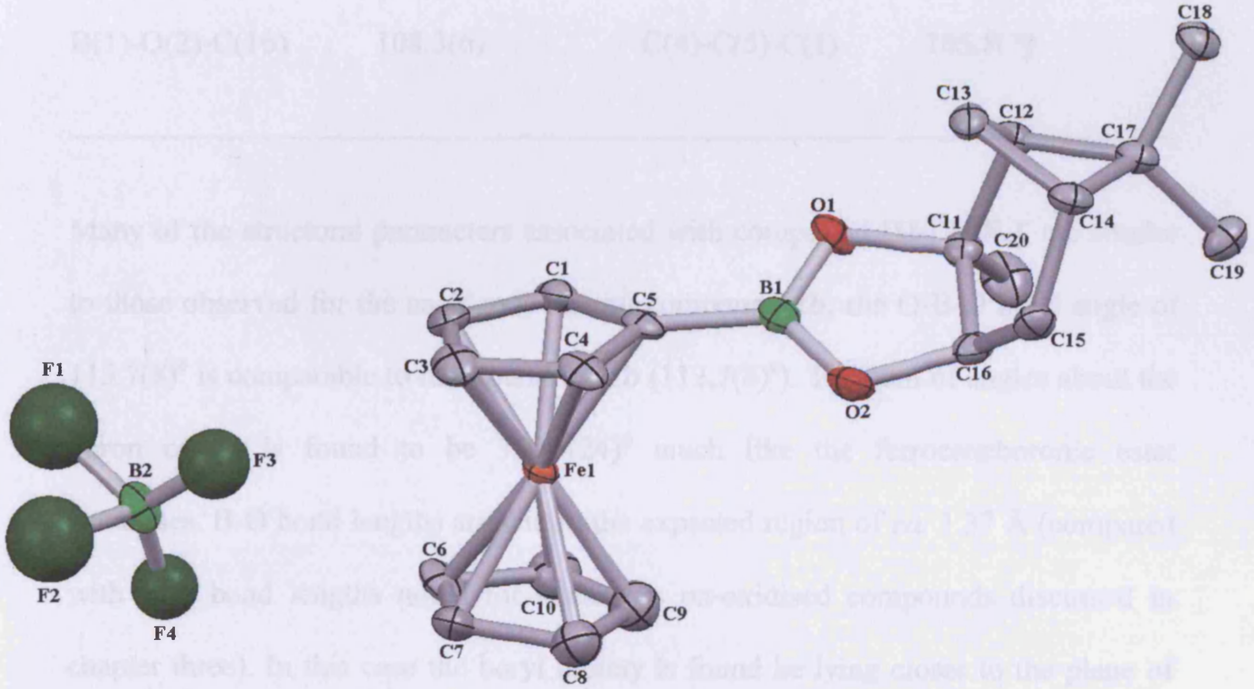

Figure 4.14 Molecular structure of $[\mathbf{1b}]^+[\mathbf{BF_4}]^-$. ORTEP ellipsoids set at the 50 % probability level. Hydrogen atoms omitted for clarity. Fluoride atoms of the tetrafluoroborate counter ion remain isotropic due to a high degree of disorder and difficulty in modelling these atoms anisotropically.

Table 4.3 Bond lengths [Å] and angles [°] for **1b$^+$BF$_4$**.

O(1)-B(1)	1.350(11)	O(2)-B(1)	1.350(12)
C(5)-B(1)	1.554(13)	C(5)-Fe(1)	2.135(7)
C(11)-O(1)	1.491(10)	C(16)-O(2)	1.457(10)
O(1)-B(1)-O(2)	115.7(8)	O(2)-B(1)-C(5)	122.5(8)
O(1)-B(1)-C(5)	121.9(8)	B(1)-O(1)-C(11)	107.4(6)
B(1)-O(2)-C(16)	108.3(6)	C(4)-C(5)-C(1)	105.8(7)

Many of the structural parameters associated with compound [**1b**]$^+$[**BF$_4$**]$^-$ are similar to those observed for the analogous neutral compound **1b**; the O-B-O bond angle of 115.7(8)° is comparable to that found for **1b** (112.7(8)°). The sum of angles about the boron centre is found to be 359.9(24)° much like the ferroceneboronic ester analogues. B-O bond lengths are within the expected region of *ca.* 1.37 Å (compared with B-O bond lengths noted for analogous un-oxidised compounds discussed in chapter three). In this case the boryl moiety is found be lying closer to the plane of the Cp ligand, the tilt angle being only 1.9° where in the parent compound (**1b**) the tilt angle is 10.6°, perhaps this is because the iron centre now has less electron density to interact with the vacant p-orbital at the boron centre, hence the boryl fragment is tilted less towards the iron centre. There are two further features to note, firstly the Cp rings are perfectly eclipsed and secondly the boryl fragment is twisted out of the plane of the Cp ligand by an angle of (27.4°) where it lies virtually planar in the parent compound, these features are likely to be result of the crystal packing system.

In a similar fashion compound **1c** was oxidised with one equivalent of silver(I) triflate in dichloromethane solution, to yield a green solution, from which crystals suitable for X-ray diffraction were grown after layering with hexane at –30°C. The solid-state structure of **[1c]$^+$[CF$_3$SO$_3$]$^-$** is illustrated below in Figure 4.15; selected bond lengths and angles are listed in Table 4.4.

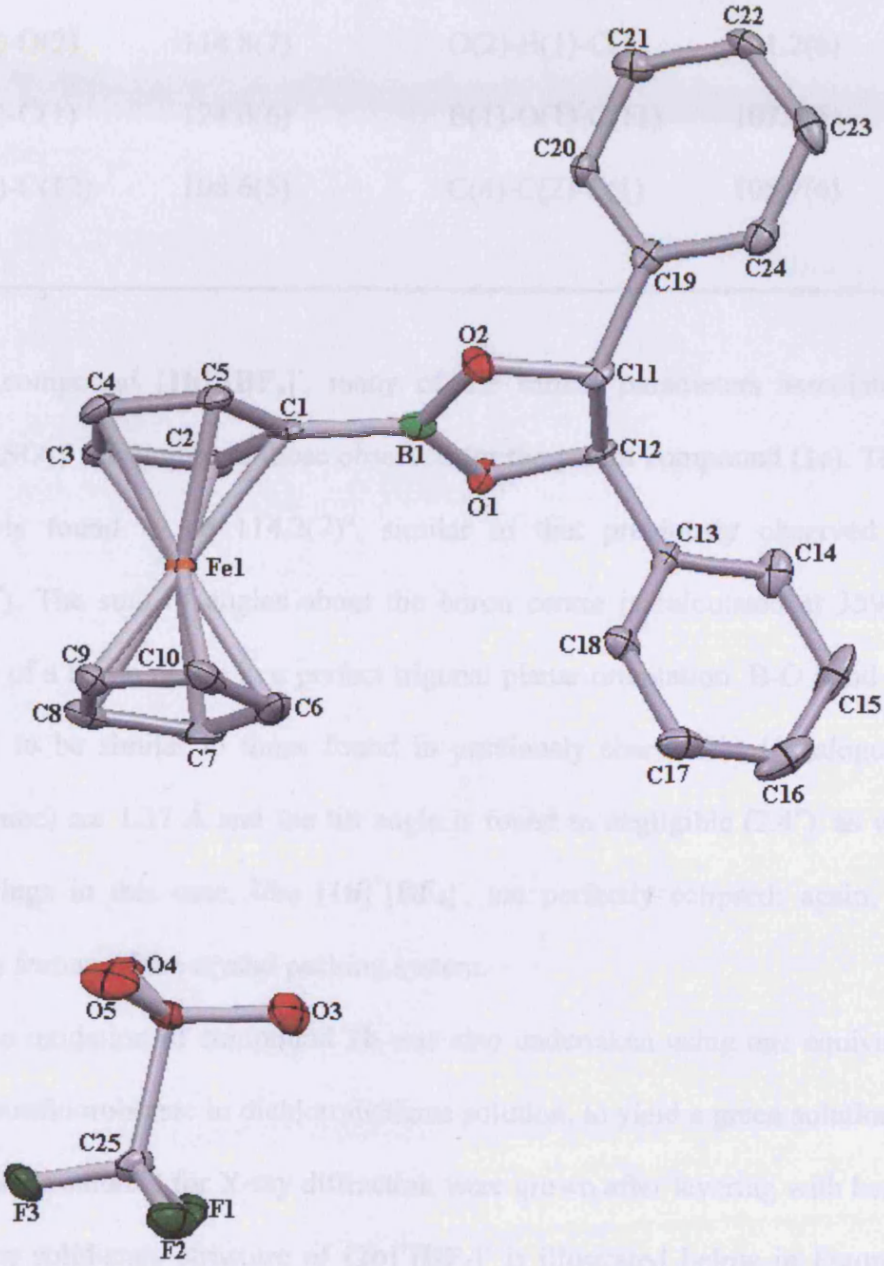

Figure 4.15 Molecular structure of **[1c]$^+$[CF$_3$SO$_3$]$^-$**. ORTEP ellipsoids set at the 50 % probability level. Hydrogen atoms omitted for clarity.

Table 4.4 Bond lengths [Å] and angles [°] for **[1c]**$^+$**[CF$_3$SO$_3$]**$^-$.

O(1)-B(1)	1.352(9)	O(2)-B(1)	1.380(9)
C(1)-B(1)	1.555(11)	C(1)-Fe(1)	2.096(7)
C(12)-O(1)	1.447(7)	C(11)-O(2)	1.429(8)
O(1)-B(1)-O(2)	114.8(7)	O(2)-B(1)-C(1)	121.2(6)
O(1)-B(1)-C(1)	124.0(6)	B(1)-O(1)-C(11)	107.5(5)
B(1)-O(2)-C(12)	108.6(5)	C(4)-C(2)-C(1)	105.7(6)

As with compound **[1b]**$^+$**[BF$_4$]**$^-$, many of the salient parameters associated with **[1c]**$^+$**[CF$_3$SO$_3$]**$^-$ are similar to those observed for the parent compound (**1c**). The O-B-O angle is found to be 114.2(7)°, similar to that previously observed for **1c** (113.1(4)°). The sum of angles about the boron centre is calculated at 359.9(19)°, indicative of a boron centre in a perfect trigonal planar orientation. B-O bond lengths are found to be similar to those found in previously characterised analogues (see Chapter three) *ca.* 1.37 Å and the tilt angle is found to negligible (2.4°), as with **1c**. The Cp rings in this case, like **[1b]**$^+$**[BF$_4$]**$^-$, are perfectly eclipsed; again, this is probably a feature of the crystal packing system.

The oxidation of compound **2b** was also undertaken using one equivalent of silver(I) tetrafluoroborate in dichloromethane solution, to yield a green solution, from which crystals suitable for X-ray diffraction were grown after layering with hexane at –30°C. The solid-state structure of **[2b]**$^+$**[BF$_4$]**$^-$ is illustrated below in Figure 4.16; selected bond lengths and angles are listed in Table 4.5.

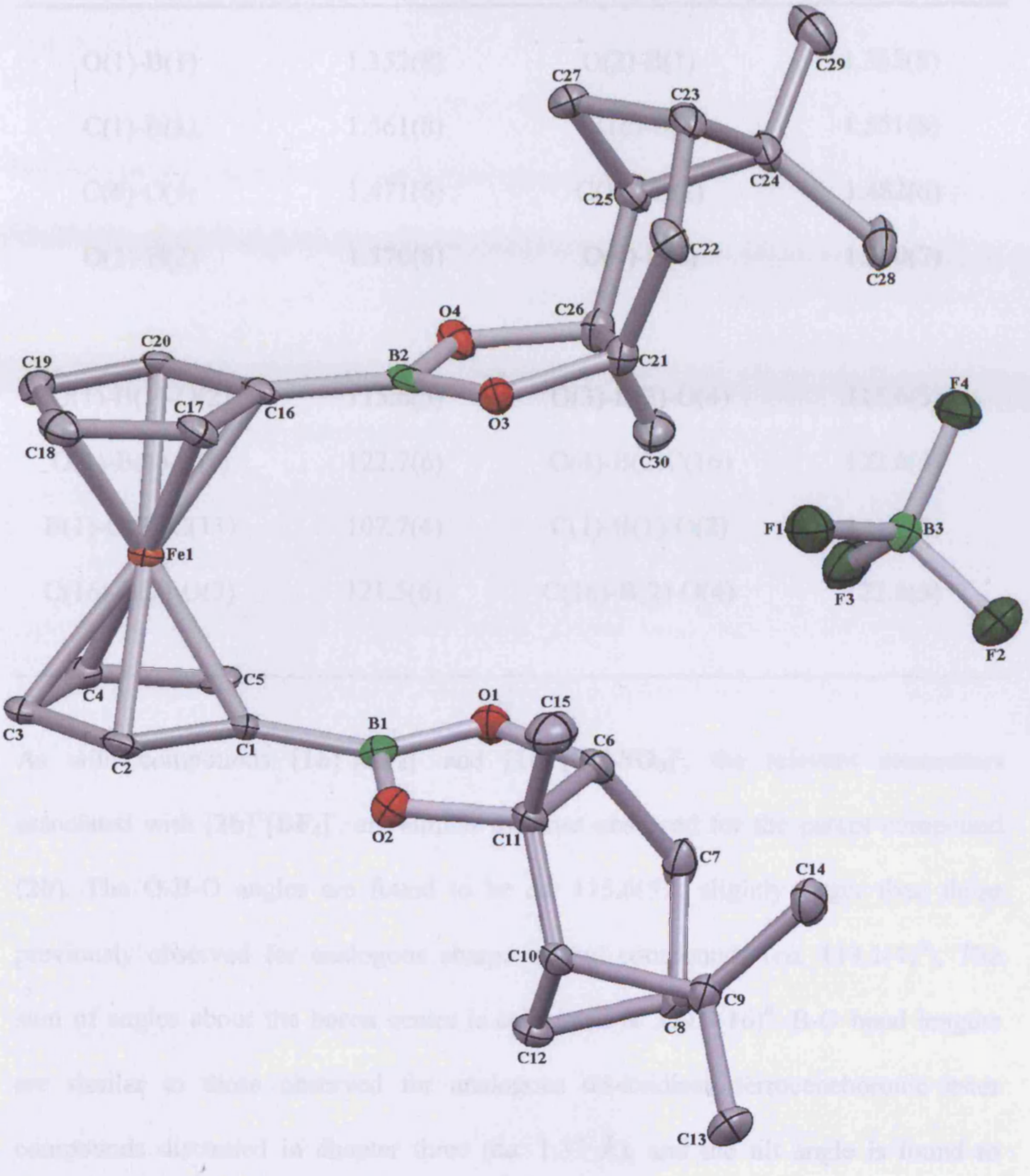

Figure 4.16 Molecular structure of **$[2b]^+[BF_4]^-$**. ORTEP ellipsoids set at the 30 % probability level. Hydrogen atoms omitted for clarity.

Table 4.5 Bond lengths [Å] and angles [°] for **[2b]**$^+$**[BF$_4$]**$^-$.

O(1)-B(1)	1.352(8)	O(2)-B(1)	1.355(8)
C(1)-B(1)	1.561(8)	C(16)-B(2)	1.551(8)
C(6)-O(1)	1.471(6)	C(11)-O(2)	1.482(6)
O(3)-B(2)	1.370(8)	O(4)-B(2)	1.360(7)

O(1)-B(1)-O(2)	115.6(5)	O(3)-B(2)-O(4)	115.6(5)
O(1)-B(1)-C(1)	122.7(6)	O(4)-B(2)C(16)	122.6(5)
B(1)-O(2)-C(11)	107.7(4)	C(1)-B(1)-O(2)	121.6(6)
C(16)-B(2)-O(3)	121.5(6)	C(16)-B(2)-O(4)	122.6(5)

As with compounds **[1b]**$^+$**[BF$_4$]**$^-$ and **[1c]**$^+$**[CF$_3$SO$_3$]**$^-$, the relevant parameters associated with **[2b]**$^+$**[BF$_4$]**$^-$. are similar to those observed for the parent compound (**2b**). The O-B-O angles are found to be *ca.* 115.6(5)°, slightly larger than those previously observed for analogous charge neutral compounds (*ca.* 113.1(4)°). The sum of angles about the boron centre is calculated at 359.9(16)°. B-O bond lengths are similar to those observed for analogous un-oxidised ferroceneboronic ester compounds discussed in chapter three (*ca.* 1.37 Å), and the tilt angle is found to negligible (0.2°), smaller tilt angles have been consistently observed with ferroceniumboronic esters. The Cp rings in this case are actually staggered, unlike the Cp rings in the oxidised analogues **[1b]**$^+$**[BF$_4$]**$^-$ and **[1c]**$^+$**[CF$_3$SO$_3$]**$^-$. The torsion angle in this case is 36.8°, which is small considering the steric bulk of the pinane fragment and the likely steric repulsion between the two pinane fragments. In the parent compound (**2b**) the torsion angle was found to be 162.2°, this is likely to be simply a feature of the crystal packing system rather than a result of the oxidation of this compound.

Chemical oxidation of *tris*-functionalised ferroceneboronic esters was also undertaken, using the silver(I) triflate and tetrafluoroborate oxidants in dichloromethane solution has yielded blue/green solutions, which after subsequent layering with hexanes at –30°C yields powdery orange solid after *ca.* 24 h, which was confirmed by mass spectrometry to be the un-oxidised starting material. Chemical oxidation of the *tetrakis*-functionalised ferroceneboronic esters was also undertaken but proved unsuccessful, with the blue oxidised compounds also being reduced back to un-oxidised starting material after layering. The silver (I) oxidant has a redox potential of +0.65 V in DCM (with respect to ferrocene), thus it is a strong enough oxidant to oxidise *tris*- and *tetrakis*-functionalised compounds (oxidation potential of **3b** = +305 mV and oxidation potential **4b** = +430 mV, both with respect to ferrocene). It is apparent that the combined effect of oxidation and the electron-withdrawing boryl groups create a highly electron poor iron centre which is stable only for a limited time, before it is reduced. Oxidation of *tetrakis*-functional ferroceneboronic esters has also been attempted using the very strong oxidant, nitrosonium tetrafluoroborate. The NO^+ ion is generally considered a non-innocent chemical oxidant since it tends to display coordinative behaviour and is believed to perform inner-sphere electron-transfer processes, indeed this ion proved to be non-innocent, causing complete degradation of the starting material.[16]

4.3.2 Analysis of fluoride binding by NMR

The complexity of NMR spectra of the *tris-* and *tetrakis*-functional boronic esters of ferrocene (**3b**, **4b** and **4c**) has meant that the effectiveness of NMR as an analytical technique to monitor fluoride binding by *tris-* and *tetrakis*-functional boronic esters is drastically reduced. Spectra, particularly ^{1}H NMR spectra, become ever more complex where there are > 2 binding sites for fluoride anions and it is not possible to reliably monitor the movement of a single peak in the ^{1}H NMR spectrum for the purpose of plotting a ^{1}H NMR titration curve. Determination of the mode, stoichiometry and thermodynamics of binding for the *tris-* and *tetrakis*-functional boronic esters is of much importance in terms of their application in the field of anion sensing. As discussed, the NMR spectra of the *tris-* and *tetrakis*-functional boronic esters become too complex to determine a binding constant or mode of binding *via* construction of a ^{1}H NMR titration curve, possibly due to in-equivalent binding and/or slow exchange between binding sites. However, NMR investigations have been performed, mainly using ^{11}B and ^{19}F NMR techniques to study fluoride binding, although the results are really only sufficient to confirm interaction with fluoride.

In the case of compounds **1a** and **1b**, treatment with excess quantities of fluoride as [^{n}Bu$_4$N]F or methylhexamethylenetetramine fluoride (MeHMTAF) in chloroform solution (methanol/acetonitrile where MeHMTAF is the fluoride source) under anaerobic conditions, leads to an upfield shift in ^{11}B NMR spectra, from the fluoride-free species (δ_B 32.7 ppm) to a broad resonance at δ_B 9.8 ppm (**1a**) and δ_B 8.9 ppm (**1b**). The spectra of the *tetrakis*-functional compounds **4b** and **4c** reveal a similar effect. Treatment of **4b** and **4c** with excess fluoride as [^{n}Bu$_4$N]F in chloroform solutions under anaerobic conditions leads to an upfield shift in the ^{11}B NMR spectra, from the free receptors (δ_B 33.1 (**4b**) and δ_B 32.7 (**4c**) ppm) to a broad resonance at δ_B

6.3 ppm (**4b**) and δ$_B$ 5.1 ppm (**4c**). These shifts are consistent with the binding of an anionic donor to three-coordinate boron and are comparable to the upfield shift of *ca.* 25 ppm observed after treatment of **2a** (*bis*-(stilbenediolatoboryl) compound) with excess [^{n}Bu$_4$N]F in chloroform (δ$_B$ 34.0 ppm to δ$_B$ 9.4 ppm). The ^{19}F NMR spectra of compounds **1a**, **1b**, **4b** and **4c** treated with fluoride reveal shifts distinctly different from the shifts of the individual fluoride sources themselves, δ$_F$ -133.4 ppm (**1a**), δ$_F$ -137.2 ppm (**1b**), δ$_F$ -134.0 ppm (**4b**) and δ$_F$ -135.1 ppm (**4c**), compared with the standard fluoride sources used; [^{n}Bu$_4$N]F (δ$_F$ -122.7) and MeHMTA$^+$F$^-$ (δ$_F$ -150.0).

This data is strongly suggestive of some form of Lewis acid-fluoride interaction taking place; however determination of the mode of binding and binding stoichiometry requires further investigation. Regarding the multi-functional boronic esters, there are two simple possible modes of anion binding: chelation of a fluoride anion to two boron centres, or mono-dentate coordination of a single fluoride anion which is then fluxional between a pair of boron centres (Figure 4.17).

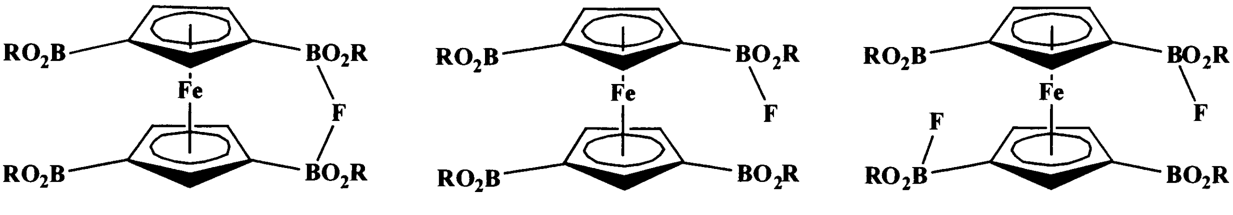

Figure 4.17 The three possible modes of fluoride binding for *tetrakis*-functional ferrocene boronic esters

4.3.3 Analysis of fluoride binding of multi-functional borylmetallocenes 3b, 4b and 4c by UV/Vis spectroscopy

It was observed in initial studies that *tris*- and *tetrakis*-borylmetallocenes **3b**, **4a**, **4b** and **4d** achieved the selective binding of fluoride anions over other anions (Cl$^-$, Br$^-$, BF$_4^-$, PF$_6^-$) in solution, and undergo a similar orange to green colour changes on exposure to fluoride in air as the prototype *bis*-borylmetallocene compound (Figure 4.18). This colour change occurs with apparently very different kinetics i.e. much more rapidly with the *tris*- and *tetrakis*-functional compounds. By eye, a very rough estimate of time taken for a colour change to occur was noted for *bis*- and *tetrakis*-functionalised receptors (*ca.* 30 minutes and *ca.* 30 seconds respectively). This interesting observation provided confirmation that response to fluoride could indeed be tuned to meet specific requirements by simple chemical modification. From this observation arose the palpable question of binding stoichiometry, i.e. how many equivalents of fluoride are being bound to affect such rapid response.

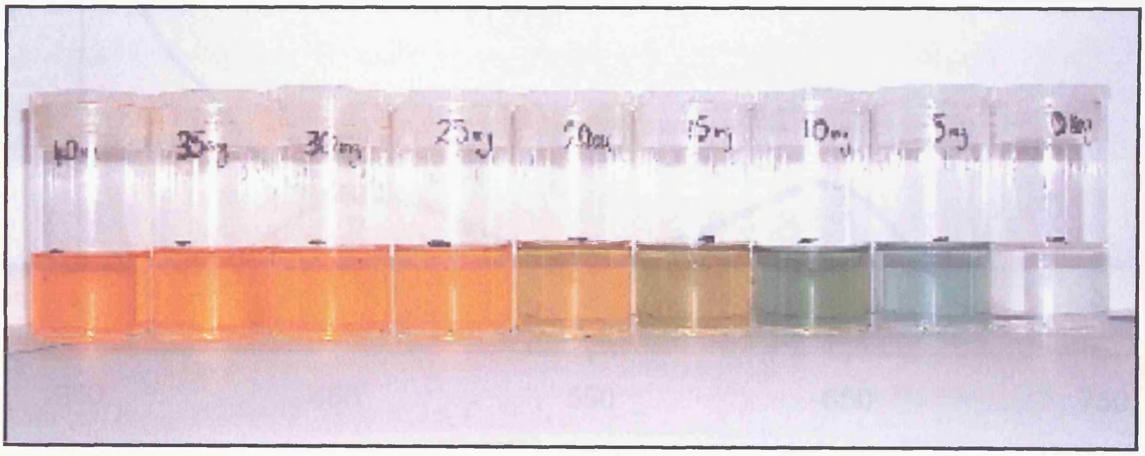

Figure 4.18 Samples prepared for the Job Plot of **4b** displaying the colour change observed on addition of fluoride to a chloroform solution, under aerobic conditions.

UV/Vis spectroscopy provides a convenient means of monitoring the orange-green colour change, and is strongly suggestive that the colorimetric response is associated with formation of a ferrocenium ion, with a new band growing in at *ca.* 640 nm. This band is similar in energy and intensity to that observed in the spectrum of ferrocenium itself (617 nm), which has been attributed to a $^2E_{2g}$ – $^2E_{1u}$ LMCT charge transfer process.[17] Compounds **3b** and **4b** both display absorptions at 454 nm and 472 nm respectively, and like ferrocene itself, display no significant absorptions above 530 nm. These bands are quantitatively replaced by new features at 640 nm (**4b**) and 654 nm (**3b**) upon aerobic addition of excess [^{n}Bu$_4$N]F (Figure 4.19).

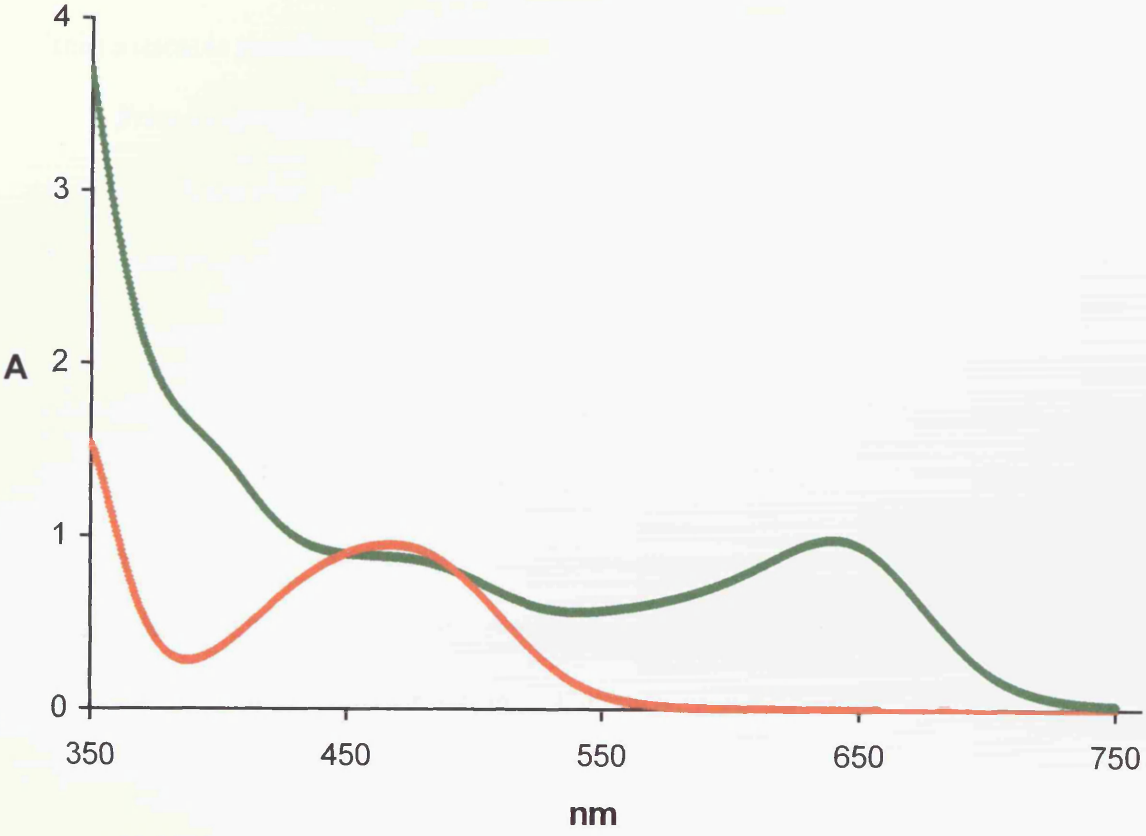

Figure 4.19 UV/Vis spectra of **4b** (orange trace), and **4b** plus excess [^{n}Bu$_4$N]F (green trace) in chloroform solution.

Similar anion binding studies were performed on the *tetrakis*-functional ferroceneboronic ester featuring the pinane backbone (**4c**). Interestingly it was found that a solution of **4c** in chloroform underwent an extremely slow orange-green colour change after the addition of excess [^{n}Bu$_4$N]F and exposure of the solution to atmospheric dioxygen. Addition of alternative sources of fluoride (MeHMTA$^+$F$^-$ and KF/18-crown-6) in various solvents affected the same result. Response time is key in the design and manufacture of colorimetric sensors for GB (Sarin), as the action of Sarin as a nerve agent is extremely rapid, and a potential sensor must be capable of detection on a smaller timescale. This observation precludes the potential use of **4c** as a colorimetric sensor for such fluoride-containing analytes, as the response time is not within a useable timeframe.

Prior to investigation into the kinetics at work in the system, it was decided to attempt to determine a binding stoichiometry by construction of a Job plot *via* UV/Vis spectroscopy. Job's method can be used to identify a binding stoichiometry and a provisional binding constant and is generally carried out by UV/Vis spectrophotometry. UV analysis is performed on samples containing various equimolar quantities of host and guest species, each solution maintains a constant final concentration. The results are plotted in a graph of host-guest complex absorbance versus molar fraction, the maximum of which determines the binding stoichiometry. Conditional formation constants can be calculated using equations proposed by Likussar and Boltz,[18] however this method has not been used to determine a binding constant in this case. For this analysis, which was carried out on compounds **3b** and **4b**, varying masses of boryl-metallocene were weighed into sample vials and dissolved in chloroform, the fluoride source [^{n}Bu$_4$N]F was weighed in the corresponding varying masses as to keep the overall concentration of each solution constant (4.4 x 10^{-3} mol dm^{-3}). Each solution was exposed to the air for one hour to allow for oxygen dissolution into the system, after which the UV/Vis spectrum of each solution was run. The results were plotted as follows:

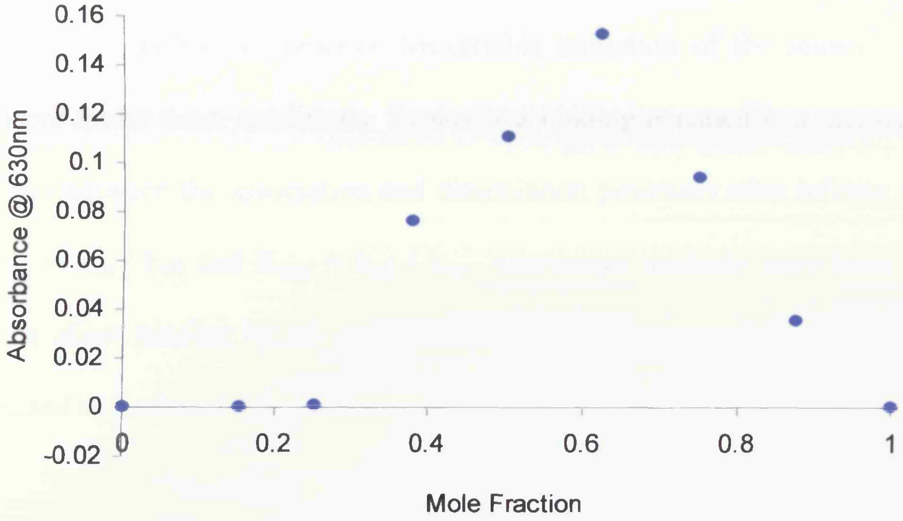

Figure 4.20 Job plot of tri-functional boryl-metallocene **3b**

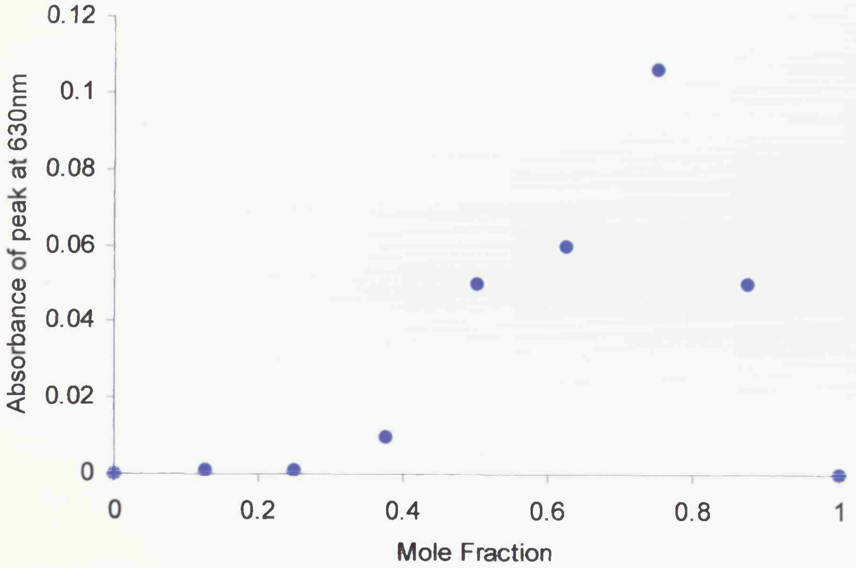

Figure 4.21 Job plot of tetra-functional boryl-metallocene **4b**

As can be clearly seen from the graphs, a conclusive binding stoichiometry cannot be determined from these plots as the maximum spans the region of 2, 3 and 4 equivalents of fluoride. Thus these graphs cannot be used to determine a binding constant using Likussar and Boltz's method. However it is relevant to note that these receptors do not behave as classical sensors, in that the binding of fluoride in this case is not truly an equilibrium process. Irreversible oxidation of the sensor molecule would occur under these conditions. Typically a binding constant is a measure of an equilibrium between the association and dissociation processes after infinite reaction time; $K_{ass} = k_{on} / k_{off}$ and $K_{diss} = k_{off} / k_{on}$. Alternative methods have been used to investigate anion binding by tri- and tetra-functional boryl-metallocenes further and are discussed in section 4.4.5.

4.3.4 Analysis of fluoride binding by electrochemical methods

In much the same way that cyclic voltammetry (CV) has been used to analyse the electronic effects of the boryl group, it is also a convenient analytical method for monitoring the process of fluoride binding by these systems. The effect of fluoride binding on the oxidation potential of the ferrocene moiety is very pronounced in the CV spectrum as a result of the electronic changes that take place at the boron centre. Prior to fluoride binding the boryl groups act as net electron withdrawing groups as evidenced by the increasing anodic shift of the ferrocene moiety observed as the number of pendant boryl groups increases. This effect is reversed on the binding of fluoride as the resulting four-coordinate borate moiety acts as an electron-donating group. Consequently the ferrocene fragment becomes more electron rich and hence is oxidised at a lower potential. In previous anion binding studies the mono-functional ferroceneboronic ester **1c** was found to act as a selective receptor for fluoride, with the binding event being accompanied by a cathodic shift in oxidation potential of the iron centre from +131 mV to –403 mV, a total shift of -534 mV. In subsequent anion binding studies made on novel mono-functional ferroceneboronic esters (**1a** and **1b**); similar cathodic shifts of ca. –460 mV were observed in dichloromethane solution. The CV scan for **1a** treated with solid [^{n}Bu$_4$N]F in dichloromethane solution is shown in Figure 4.22, with the CV scan for the parent compound overlaid.

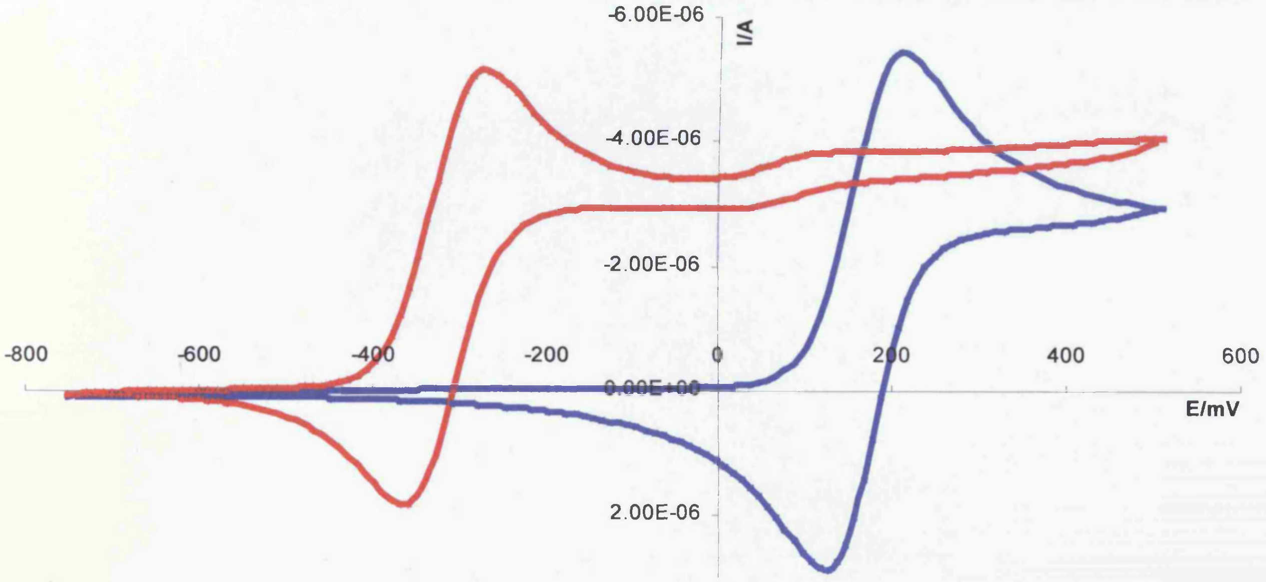

Figure 4.22 Cyclic voltammogram of **1a** (blue trace) and **1a** plus ≥ 1 equivalent of [^{n}Bu$_4$N]F (red trace) in dichloromethane.

In the case of the previously reported compound **2a**, featuring two boryl groups, the receptor is capable of binding two equivalents of fluoride, with the effect that the iron centre becomes so electron rich that it is oxidised by atmospheric di-oxygen. This is evident from the CV scan, in which two distinct binding events are observed in the presence of excess fluoride; these are measured at –384 and –746 mV (with respect to ferrocene/ferrocenium) and represent net shifts of –590 and –1002 mV compared to the parent compound as shown in Table 4.6. The former shift is similar to that observed for **1c** treated with fluoride, and is therefore assigned to the mono(fluoride) adduct [**2a**•F]$^-$; the larger shift is logically indicative of the formation of the *bis*(fluoride) adduct [**2a**•2F]$^{2-}$, considering also the observed aerobic oxidation of this adduct. The CV scan of **2a** treated with solid [^{n}Bu$_4$N]F in dichloromethane solution is shown in Figure 4.23, with the CV scan for the parent compound overlaid.

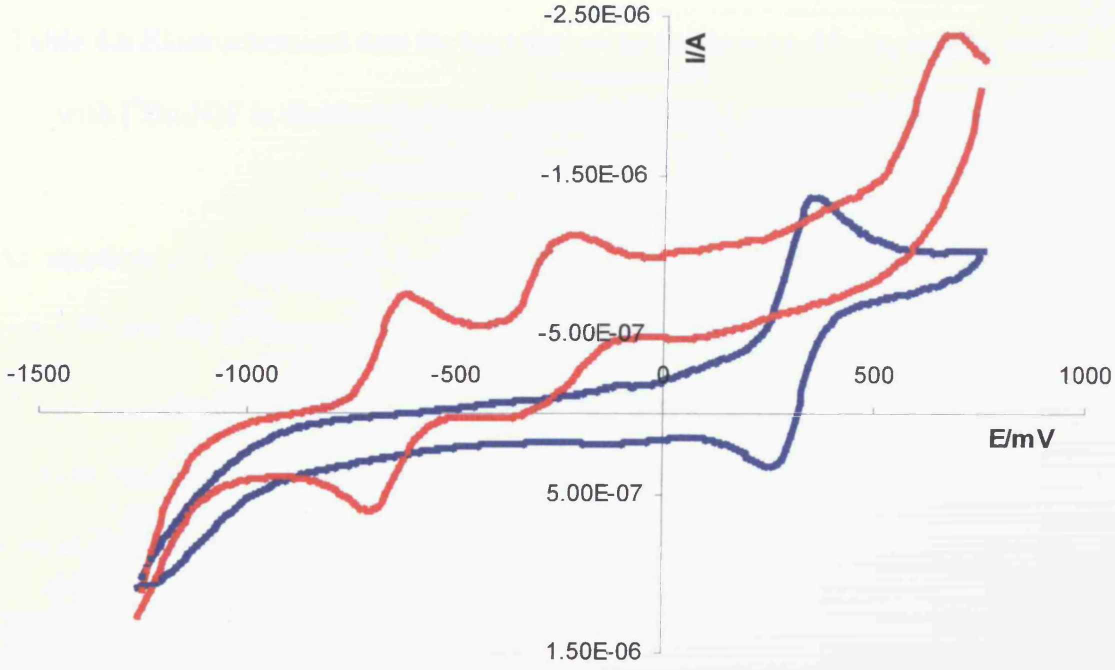

Figure 4.23 Cyclic voltammogram of **2a** (blue trace) and **2a** plus ≥ 2 equivalents of [^{n}Bu$_4$N]F (red trace) in dichloromethane.

Compound	**Initial oxidation potential (mV)**	**F^- adduct potential relative to FcH (mV)**	**Cathodic shift (mV)**
1a	+216	-237	-482
1b	+206	-146	-442
1c	+317	-403	-534
2a	+448	-746	-1002

Table 4.6 Electrochemical data for borylferrocene systems **1a**, **1b**, **1c**, and **2a** treated with [$^nBu_4N$]F in dichloromethane referenced against ferrocene/ferrocenium.

As mentioned in section 4.4.3, *tris-* and *tetrakis*–functionalised ferroceneboronic esters **3b** and **4b** undergo a similar (although much more rapid) orange-green colour change on exposure to fluoride in air. CVs of **3b** and **4b** in the presence of excess fluoride are however indicative of *irreversible* electrochemical processes. The CV scan of **4b** treated with excess [$^nBu_4N$]F in dichloromethane is shown in Figure 4.24.

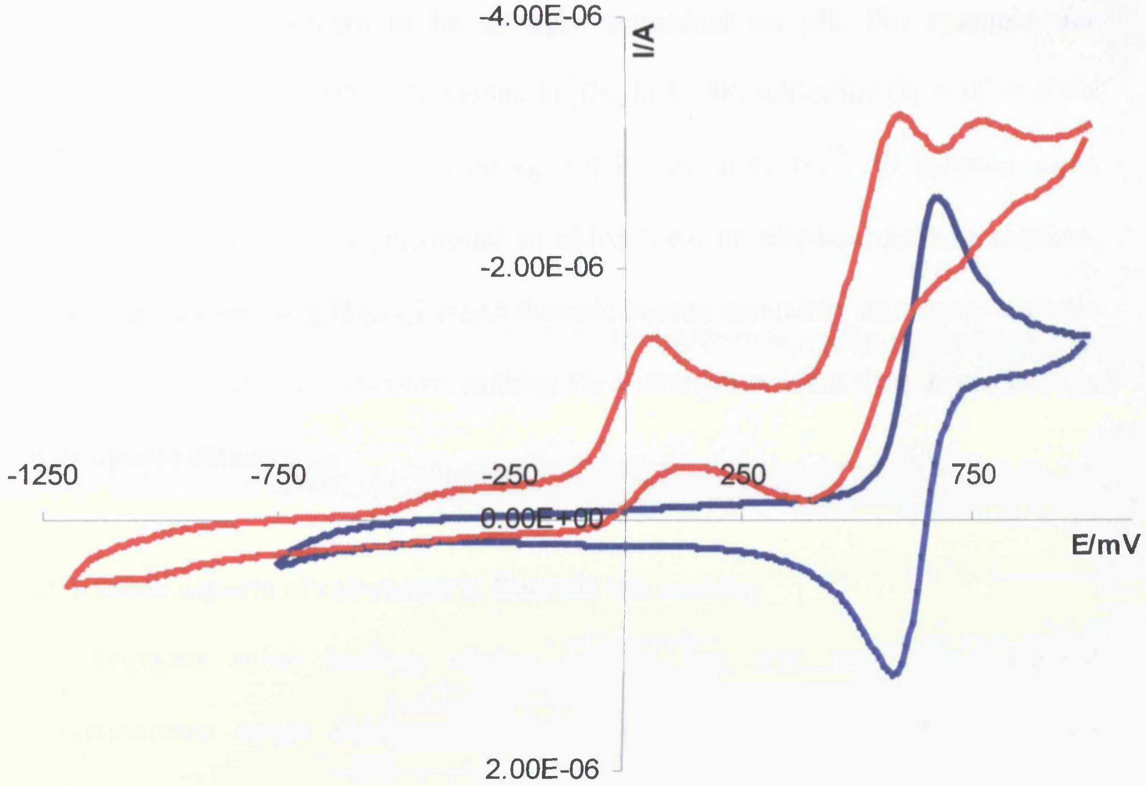

Figure 4.24 Cyclic voltammogram of **4b** (blue trace) and **4b** plus ≥ 4 equivalents of [^{n}Bu$_4$N]F (red trace) in dichloromethane.

The CV scan features an oxidation wave at a +69 mV (red trace), a net shift of –622 mV from the parent compound, which features an oxidation wave at –680mV (blue trace). This is similar to the cathodic shift in oxidation potential observed for bis(fluoride) adduct **[2a**•2F]$^-$ of –590 mV. However this oxidation wave cannot be reliably assigned to the **[4b**•2F]$^-$ adduct as the wave is irreversible and there are other features at higher oxidation potentials in the CV. The rapid orange-green colour change observed on aerobic exposure to fluoride is indicative of formation of at least the *bis*(fluoride) adduct, as thermodynamically the shift typically associated with formation of such a dianion would be the minimum required for oxidation by atmospheric dioxygen. The potential associated with the O_2/O_2^- redox couple in non-aqueous solution is known to be strongly dependant on pH. For example, for $O_2 + e^- \rightarrow O_2^-$, $E_{1/2}$ = -1000 mV versus Fc^+/Fc in DMF, while for $O_2 + H^+ + e^- \rightarrow HO_2$, $E_{1/2}$ = -280 mV also referenced against Fc^+/Fc in DMF.[19] All solution anion binding studies have been performed in chloroform or dichloromethane solution, however the use of the $[^nBu_4N]F\mathit{x}H_2O$ fluoride source inevitably introduces a protic component to the reaction mixture, making O_2 a stronger oxidant than it would be in strictly aprotic solution.

4.3.5 Kinetic aspects of colorimetric fluoride ion sensing

Previous anion binding studies suggest that *tris-* and tetra-functional ferroceneboronic esters bind two or more equivalents of fluoride. Thus the colorimetric response to fluoride and the maximum observed in the Job plot (although broad) both imply the binding of ≥ 2 equivalents of fluoride. Monitoring the rate of colorimetric response as a function of fluoride concentration offers a means of assessing fluoride binding.

The kinetics of colorimetric response have been evaluated by UV/Vis spectroscopy, following the observation that anion binding proceeds with accompanying growth of a ferrocenium band in the UV/Vis spectrum. The intensity of the ferrocenium band was monitored as a function of time for various ferroceneboronic esters treated with fluoride. Initial studies have highlighted the critical dependence of the kinetic response on the oxidant. It was found that under strictly anaerobic conditions, in the absence of dissolved dioxygen, a solution of **4b** in chloroform shows no colorimetric response to $[^nBu_4N]F$, and the ferrocenium band at ca. 640 nm is absent. The effect of pre-saturating the chloroform solvent with dioxygen was found to be negligible as reactions carried out in bench chloroform and chloroform pre-saturated with dioxygen were found to undergo aerobic oxidation with similar absorption/time profiles. In addition, chloroform solutions pre-saturated with argon but exposed to air on addition of the fluoride source, demonstrate how the sensor response is limited by the rate of diffusion of dioxygen into the system, in that the initial rate is reduced by approximately 70 % (from 1.6×10^{-2} to 4.6×10^{-3} s^{-1}). The graph below shows the kinetics of oxidation of **4b** in chloroform solution under different degrees of oxygenation (Figure 4.25).

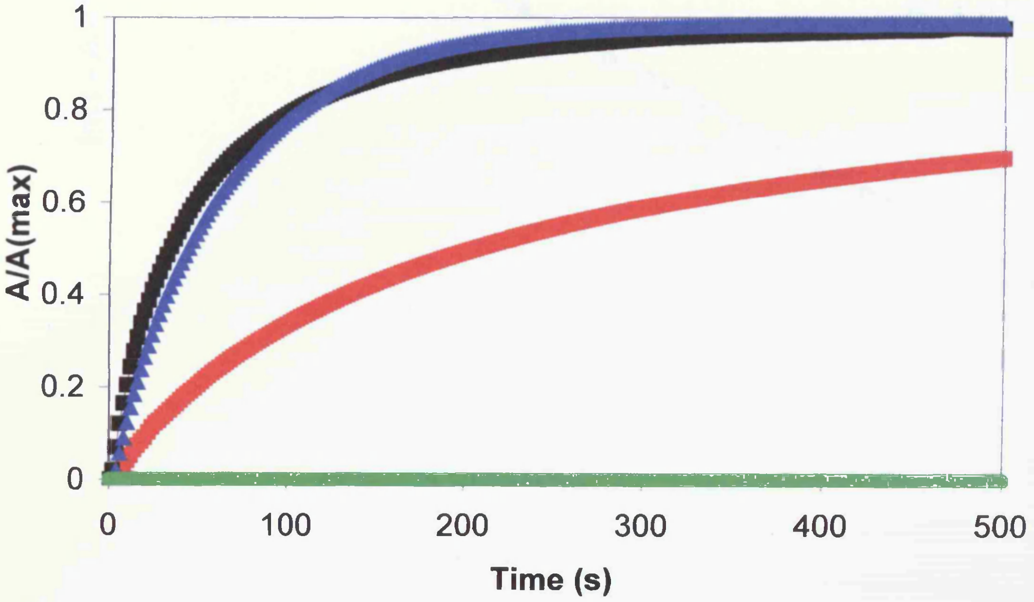

Figure 4.25 Plot of normalized absorbance vs. time for ferrocenium band at 640 nm formed on addition of 15 equiv. [^{n}Bu$_4$N]F to **4b** in chloroform solution (17.5 mM) under different degrees of oxygenation green: strictly anaerobic conditions; red: solvent pre-saturated with argon but exposed to air during measurement; blue: untreated bench solvent; black: solvent pre-saturated with dioxygen.

The logarithmic plot (Figure 4.26) proves the initial rate of response to fluoride to be pseudo first-order and demonstrates the much-reduced initial rate in the absence of excess oxygen.

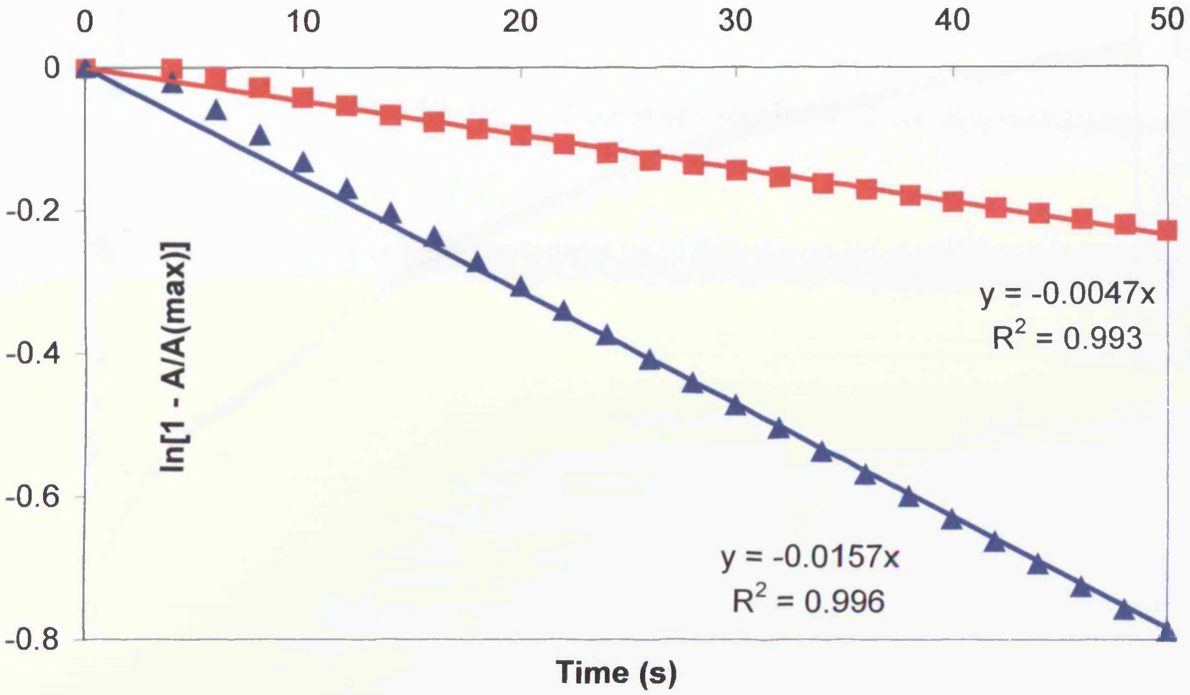

Figure 4.26 Pseudo first-order fits for red (solvent pre-saturated with argon but exposed to air during measurement) and blue data (untreated bench chloroform solvent) for $t < 30$ s.

UV/Vis monitoring of bands associated with the respective ferrocenium products of **2a**, **3b** and **4b** treated with fluoride proves consistent with substantial variation in reaction kinetics depending on the number of boronic ester binding sites. The plots of normalised absorbance, A/A(max), against time for *bis*, *tris* and *tetrakis* stilbene diolate-functionalised receptors **2a**, **3b** and **4b** are shown below in Figure 4.27. All measurements were performed under standardised conditions and are not limited by fluoride concentration or availability of oxidant (15 equiv. fluoride, bench chloroform, 20°C).

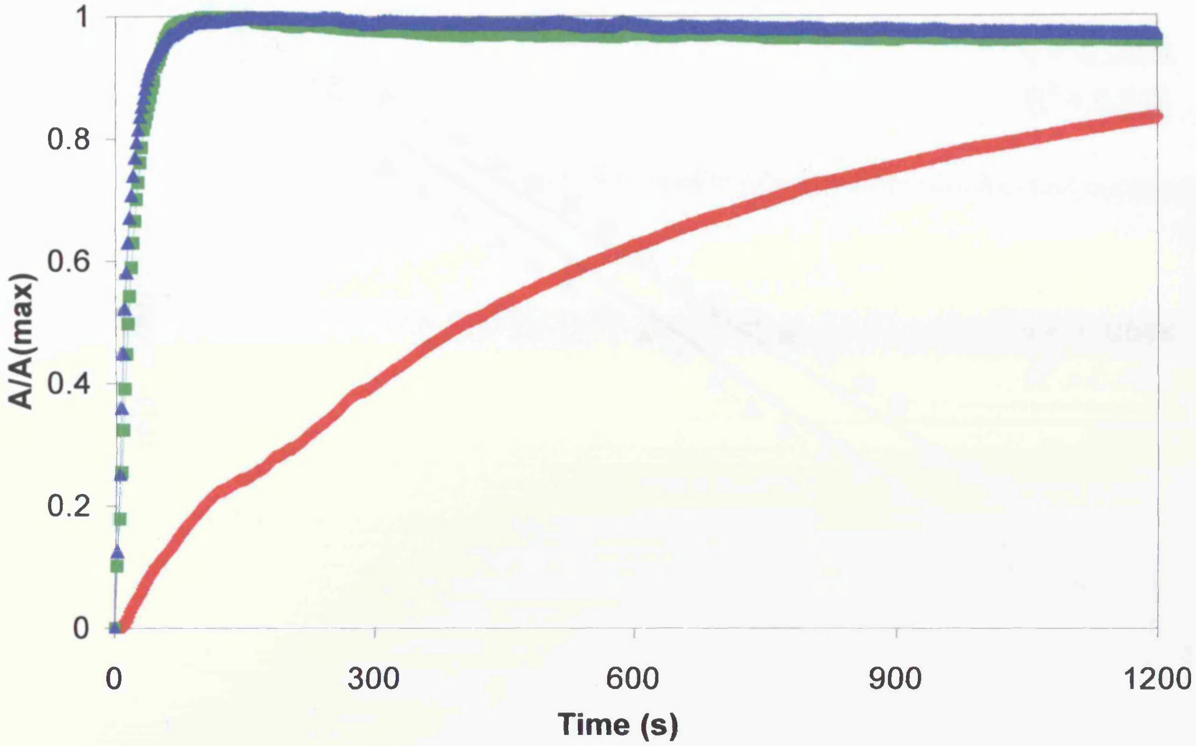

Figure 4.27 Plot of normalized absorbance against time for the band at ca. 630 nm associated with the oxidized ferrocenium species formed on addition of [^{n}Bu$_4$N]F (15 equiv.) to the receptors **2a**, **3b** and **4b** (17.5 mM). Red: **2a** (monitored at 633 nm); green: **3b** (654 nm); blue: **4b** (640 nm).

This graph substantiates the initial observation made that the response of *tris-* and *tetrakis*-functionalised ferroceneboronic esters to fluoride follows vastly different kinetics than that of *bis*-functionalised system. The very steep initial curve for **3b** and **4b** compared to **2a** clearly indicates that the rate of formation of the ferrocenium product is significantly enhanced for the *tris-* (**3b**) and *tetrakis*-functionalised (**4b**) compounds, compared with the *bis*-functionalised (**2a**) analogue.

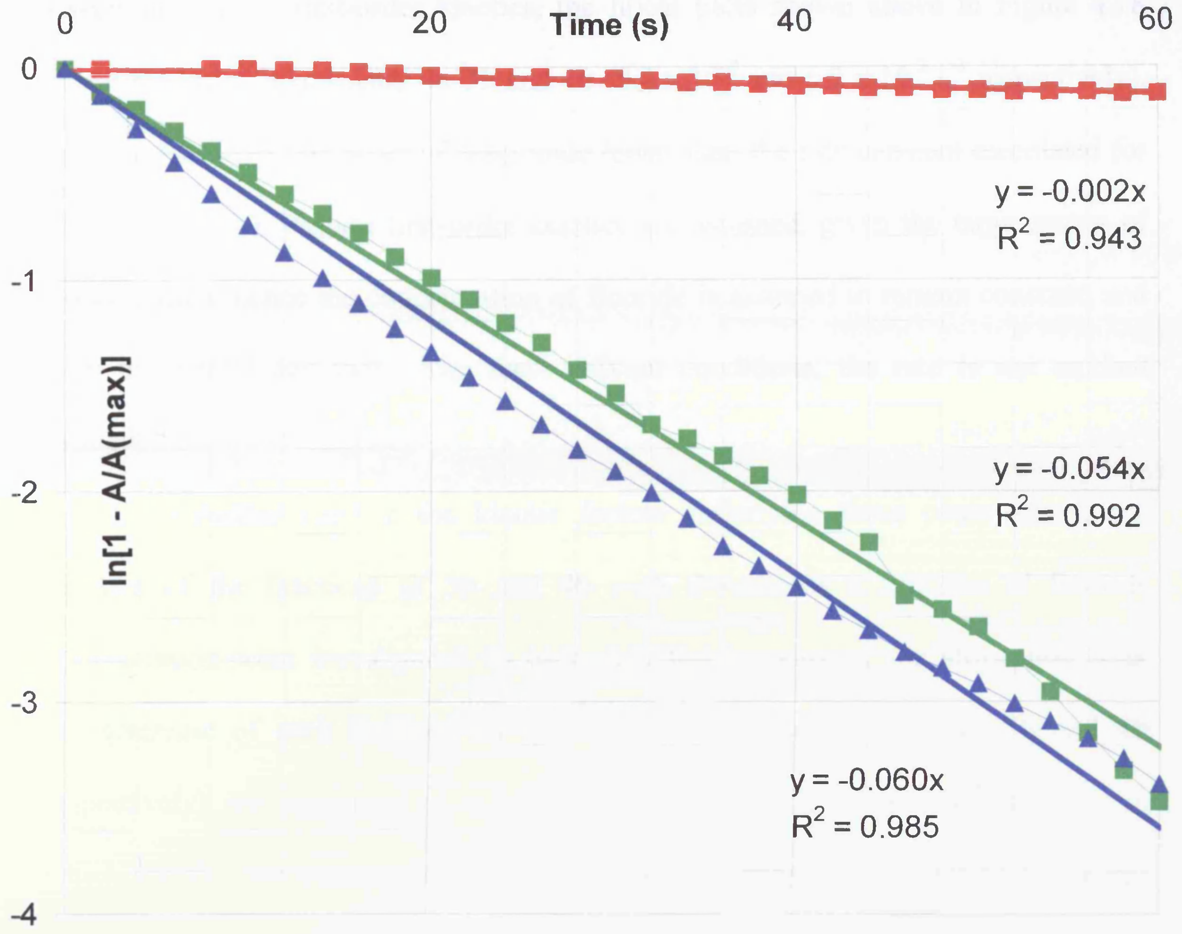

Figure 4.28 Logarithmic plot to determine pseudo first-order rate constants. Red: **2a**; green: **3b**; blue: **4b**.

Assuming pseudo first-order kinetics, the linear plots shown above in Figure 4.28 reveal similar rate constants for **3b** and **4b** (5.4×10^{-2} and 6.0×10^{-2} s^{-1} respectively), which are at least one order of magnitude larger than the rate constant calculated for **2a** (2×10^{-3} s^{-1}). Pseudo first-order kinetics are assumed, given the large excess of fluoride used, hence the concentration of fluoride is assumed to remain constant, and with the knowledge that under these solvent conditions, the rate is not oxidant limited.

To further explore the kinetic factors underlying these observations, the kinetics of the reactions of **3b** and **4b** with fluoride as a function of fluoride concentration were investigated. In each case the intensity of the absorption peak characteristic of each ferrocenium species (654 nm and 640 nm for **3b** and **4b** respectively) was measured as a function of time for a number of kinetic runs in which the fluoride concentration was systematically varied. Estimates of the initial rate, v_i, for each run were obtained by fitting a linear function to the absorbance/time data for $t \leq 20$ s. Using the method of initial rates,[20] the order of reaction with respect to fluoride was obtained from the gradient of the linear plot of $\ln(v_i)$ against $\ln[F^-]$. The results are shown below in Figure 4.29 and 4.30 (**3b**) and Figure 4.31 and 4.32 (**4b**).

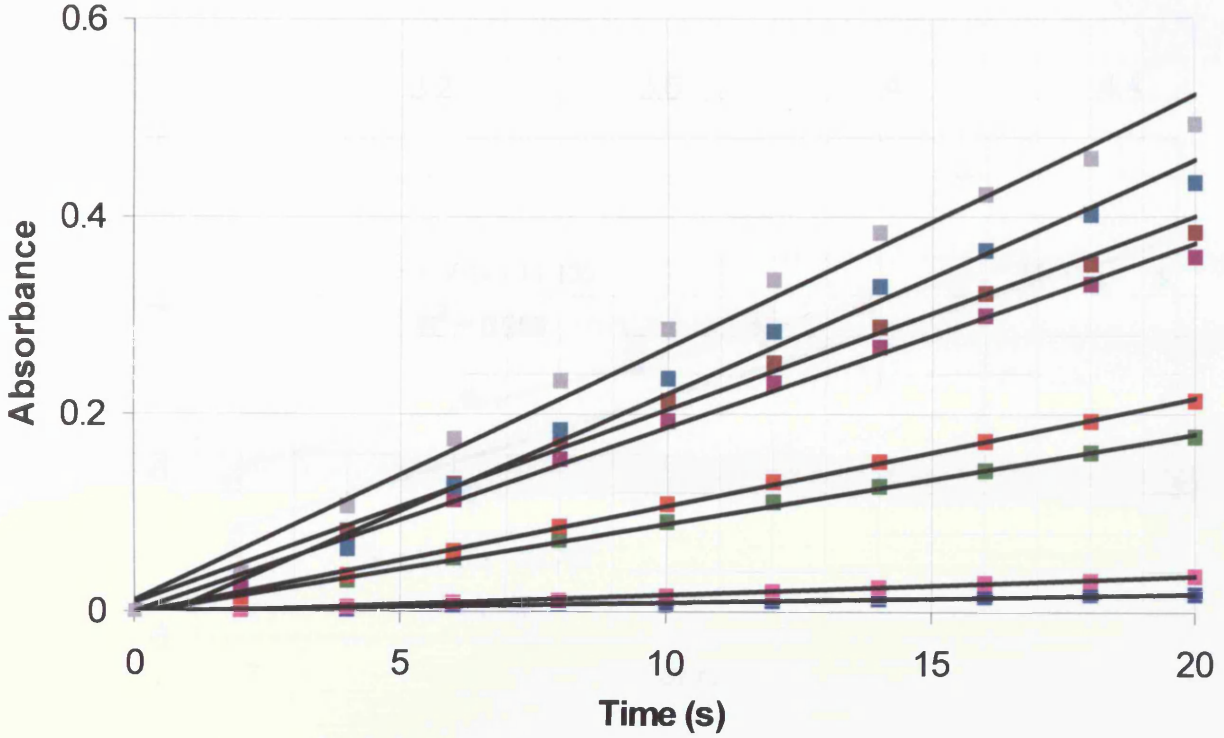

Figure 4.29 Plot of absorbance against time for the growth of the band at 654 nm associated with the ferrocenium species formed on oxidation of **3b** (17.5 mM) in the presence of different concentrations of [^{n}Bu$_4$N]F. The eight traces (bottom to top) were obtained for [^{n}Bu$_4$N]F concentrations of 17.5, 26.3, 35.0, 43.8, 52.5, 61.3, 78.8 and 87.5 mM, and initial rates (ν_i) obtained by fitting the data to a linear expression in time.

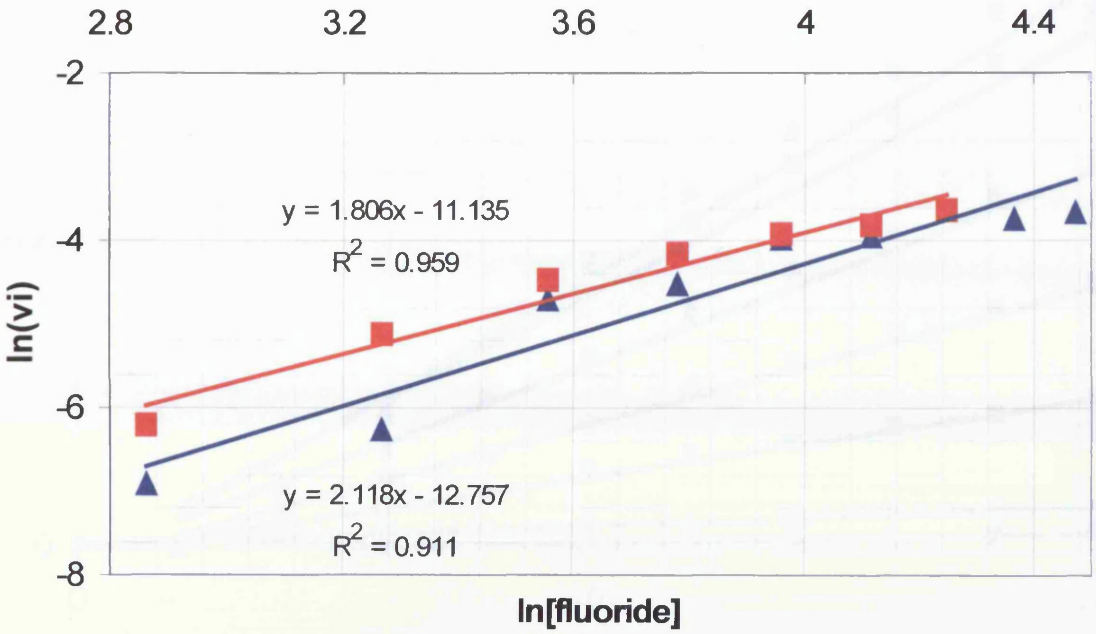

Figure 4.30 Plot of ln(ν_i) against ln(fluoride concentration) for the generation of the ferrocenium species formed on oxidation of **3b** in the presence of different concentrations of [^{n}Bu$_4$N]F. Two independent sets of data are plotted, that represented by the blue triangles corresponding to the kinetic runs described by the upper figure.

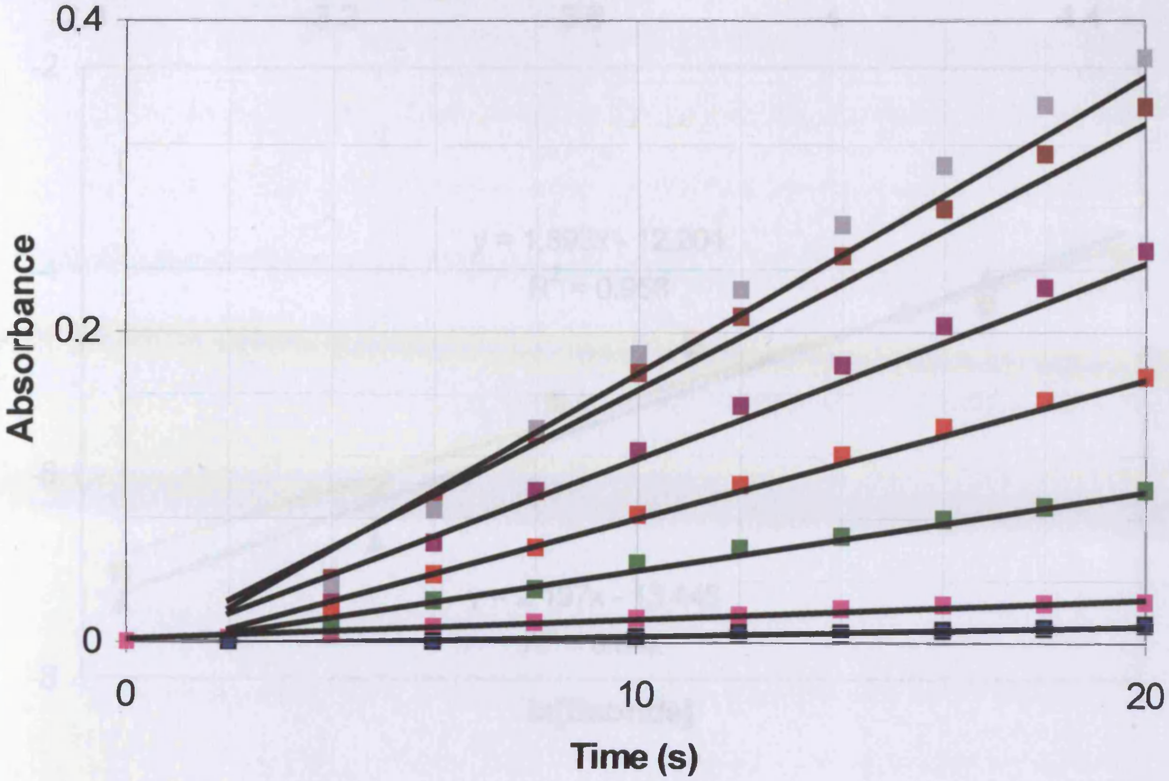

Figure 4.31 Plot of absorbance against time for the growth of the band at 640 nm associated with the ferrocenium species formed on oxidation of **4b** (17.5 mM) in the presence of different concentrations of [^{n}Bu$_4$N]F. The seven traces (top to bottom) were obtained for [^{n}Bu$_4$N]F concentrations of 17.5, 26.3, 35.0, 43.8, 61.3, 70 and 87.5 mol dm^{-3}, and initial rates (ν_i) obtained by fitting the data to a linear expression in time.

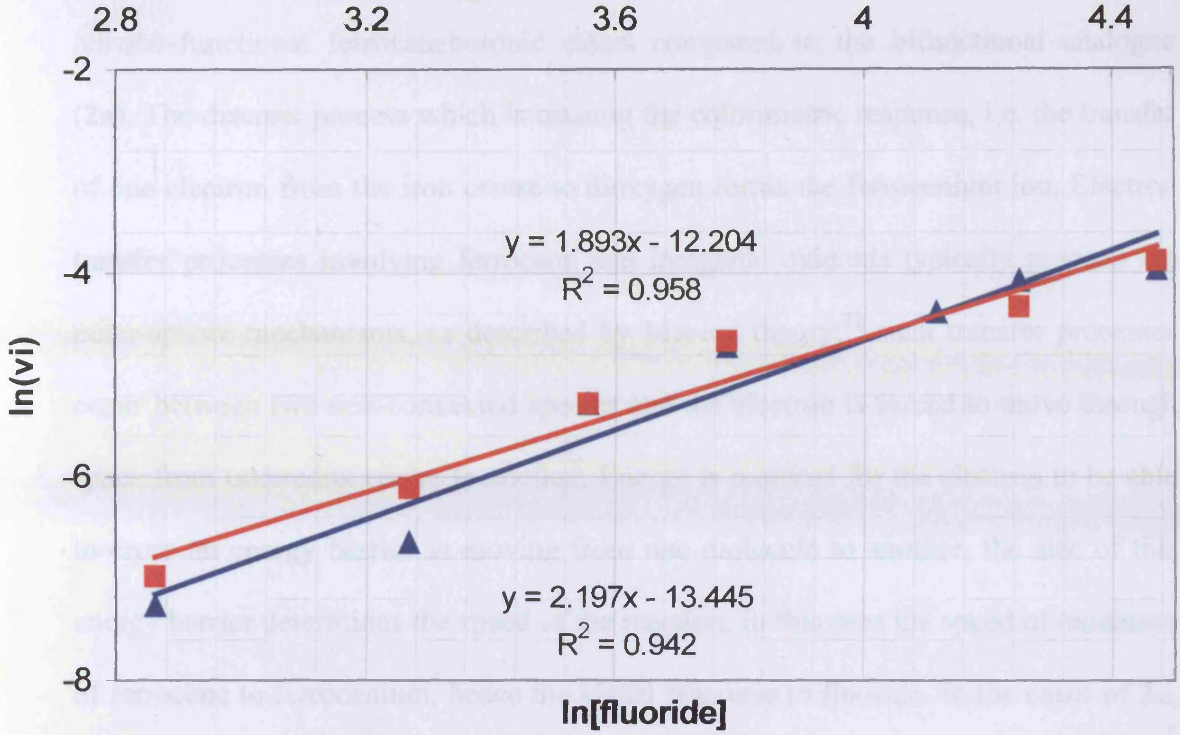

Figure 4.32 Plot of ln(ν_i) against ln(fluoride concentration) for the generation of the ferrocenium species formed on oxidation of **4b** in the presence of different concentrations of [^{n}Bu$_4$N]F. Two independent sets of data are plotted, that represented by the blue triangles corresponding to the kinetic runs described by the upper figure.

In each case the data shows the order of reaction with respect to fluoride to be second order (from the gradient of the linear plot of ln(ν_i) against ln[F$^-$]), consistent with a mechanism whereby two equivalents of fluoride are bound by one equivalent of the receptor. This observation is also in keeping with electrochemical studies, which have showed that the conversion of at least two electron-withdrawing boronic ester groups to electron-donating boronates is necessary to affect a colorimetric response to fluoride. The kinetic results present an interesting question: if *tris*- and tetra-functional ferroceneboronic esters are, like the *bis*- analogues, binding only two equivalents of fluoride, why is the response to fluoride so much faster with *tris*- and *tetrakis*-functional ferroceneboronic esters compared to the bifunctional analogue (**2a**). The discreet process which is causing the colorimetric response, i.e. the transfer of one electron from the iron centre to dioxygen forms the ferrocenium ion. Electron transfer processes involving ferrocene and inorganic oxidants typically proceed via outer-sphere mechanisms, as described by Marcus theory;[21] such transfer processes occur between two non-connected species and the electron is forced to move through space from one redox centre to another. Energy is required for the electron to be able to cross an energy barrier in moving from one molecule to another, the size of this energy barrier determines the speed of the reaction, in this case the speed of oxidation of ferrocene to ferrocenium, hence the visual response to fluoride. In the cases of **2a**, **3b** and **4b** the rates of oxidation to ferrocenium appear to be controlled by different factors; the thermodynamics of oxidation of [**3b**•2F]$^{2-}$ and [**4b**•2F]$^{2-}$ would be expected to be less favourable than that for [**2a**•2F]$^{2-}$, since in the former two compounds there remain uncomplexed pendant boryl groups which will withdraw electron density from the metal centre, which would make the iron centre less easy to oxidise. Thus it could be rationally assumed that the kinetics of oxidation of the [**3b**•2F]$^{2-}$ and [**4b**•2F]$^{2-}$ species would be *slower* than that for [**2a**•2F]$^{2-}$, however the observed results invalidate these predictions. It is possible that the remaining (uncomplexed) three-coordinate boron centre(s) in [**3b**•2F]$^{2-}$ and [**4b**•2F]$^{2-}$ provide a facile route for electron transfer from the electron rich ferrocene to the dioxygen oxidant. Three-coordinate boron centres possessing vacant p-orbitals are known to offer a facile route for electron transfer.[22] Perhaps it is feasible that dioxygen is capable of forming a transitory interaction with the vacant p-orbital at boron, thus effectively providing the means of achieving a rapid inner-sphere electron transfer process. Alternatively, it is possible that the additional pendant boronic ester groups present in the [**3b**•2F]$^{2-}$ and [**4b**•2F]$^{2-}$ complexes offer a mechanism for fluoride chelation, since the boron centre becomes much more Lewis acidic in the ferrocenium species, this effect would increase the binding energy and hence the overall thermodynamic driving force behind the aerobic oxidation and the Marcus-predicted rate. Thus the lack of an uncomplexed boronic ester group in the [**2a**•2F]$^{2-}$ complex may offer an explanation as to the notably slower oxidation process, where the oxidation thermodynamics are not enhanced by formation of a stable fluoride chelate complex (Figure 4.33)

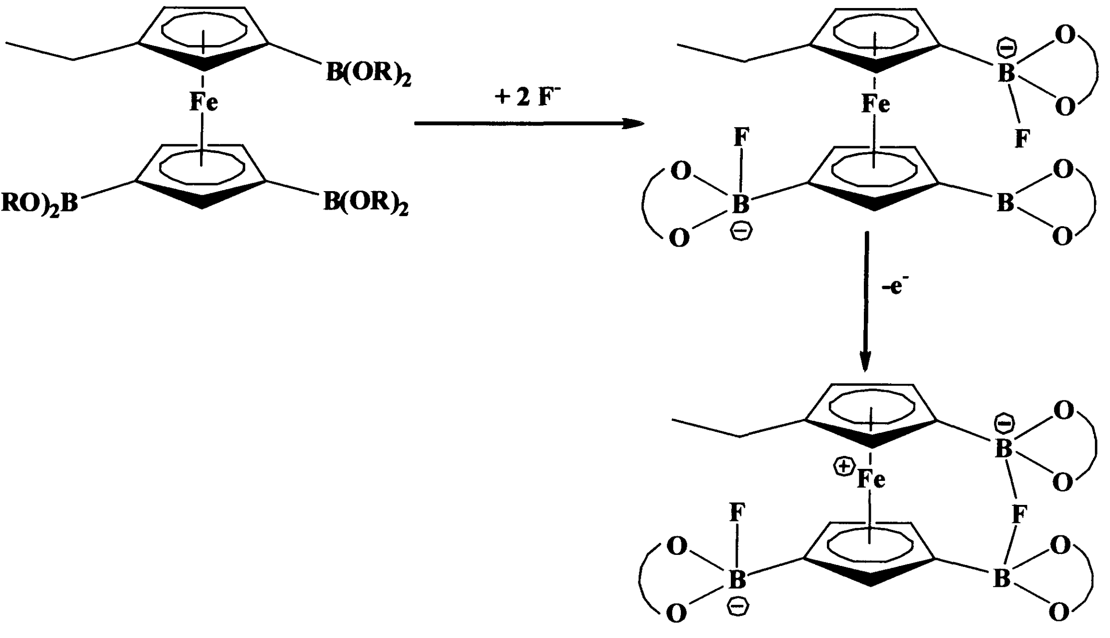

Figure 4.33 Potential fluoride chelation in *tris*-functional compounds

Finally, to explore the effect of the boronic ester backbone on the kinetic response to fluoride the response of the *tetrakis*-functionalised ferroceneboronic esters featuring the pinanediolatoboryl and napthalenediolatoboryl backbones have been compared with the *tetrakis*(stilbenediolatoboryl) analogue. It has been previously noted that the pinanediolatoboryl-functionalised receptors show markedly slower colorimetric responses to fluoride. Equimolar solutions of each compound were prepared in bench chloroform and excess fluoride added to each. The results are shown in the graphs below (Figures 4.34 and 4.35).

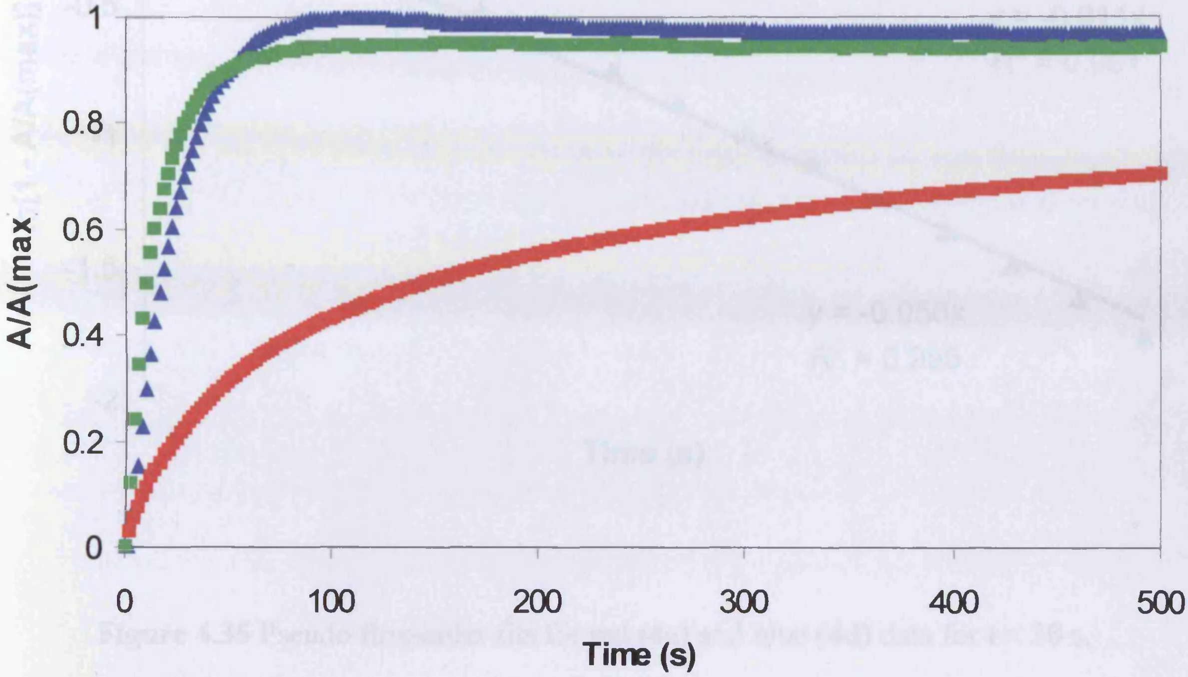

Figure 4.34 Plot of normalized absorbance against time for the band at 640 nm associated with the oxidized ferrocenium species formed on addition of 15 equiv. [^{n}Bu$_4$N]F to the *tetrakis* boronic ester receptors **4b**, **4c** and **4d** (each 17.5 mM in chloroform). Red: **4c**; green: **4b**; blue: **4d**

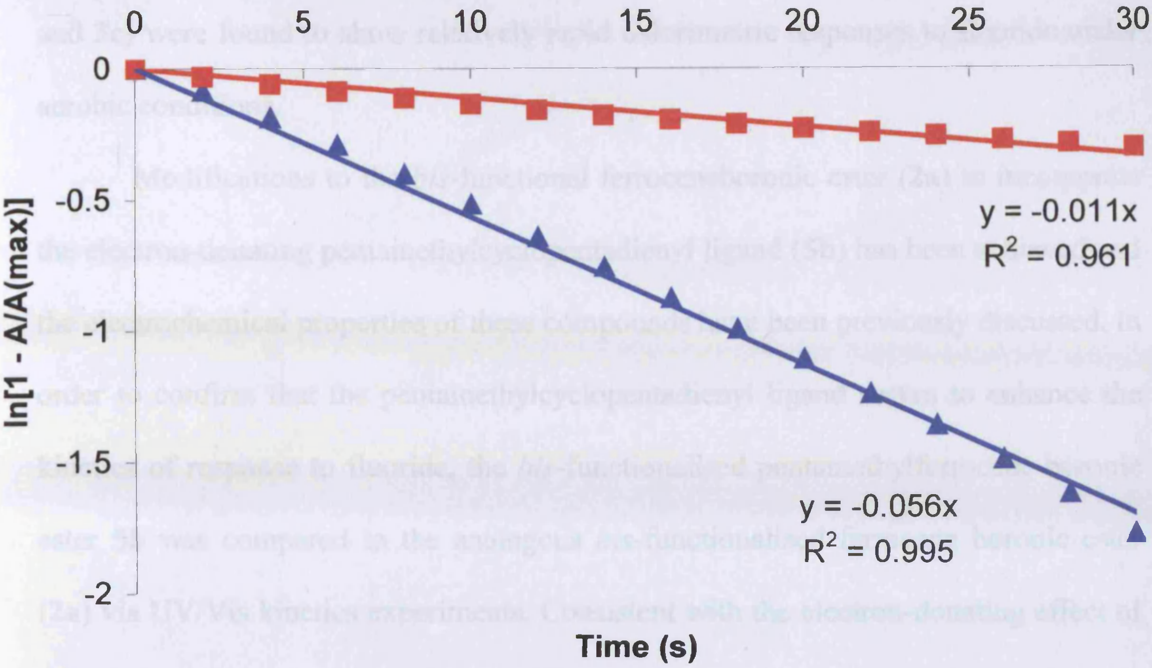

Figure 4.35 Pseudo first-order fits for red (**4c**) and blue (**4d**) data for t < 30 s.

As previously mentioned, a visual colorimetric response to fluoride is not immediately observed with the *tetrakis*-pinane compound (**4c**), consistent with this observation the calculated rate constant is *ca.* five times slower than **4b**. The pinane fragment is very sterically hindering, it is possible that in this case, where there are four closely spaced pinanediolatoboryl moieties, the steric bulk of the ligands is hindering the fluoride anions ability to reach the binding site at the boron centre. The pinane fragment is also saturated and is unlikely to be delocalised with the oxygen donors, decreasing the Lewis acidity of the boron centre by enhancing electron-donation from the adjacent oxygen donors to the boron centre. It is apparent from anion binding studies that steric bulk is not hindering anion complexation where there are just two or three pinanediolatoboryl ligands, as the analogous *bis*- and *tris*-functionalised ferroceneboronic esters featuring the pinanediolatoboryl backbone (**2b** and **3c**) were found to show relatively rapid colorimetric responses to fluoride under aerobic conditions.

Modifications to the *bis*-functional ferroceneboronic ester (**2a**) to incorporate the electron-donating pentamethylcyclopentadienyl ligand (**5b**) has been achieved and the electrochemical properties of these compounds have been previously discussed. In order to confirm that the pentamethylcyclopentadienyl ligand serves to enhance the kinetics of response to fluoride, the *bis*-functionalised pentamethylferrocene boronic ester **5b** was compared to the analogous *bis*-functionalised ferrocene boronic ester (**2a**) via UV/Vis kinetics experiments. Consistent with the electron-donating effect of the pentamethylcyclopentadienyl ligand the kinetic response to fluoride of **5b** is found to be *ca.* double that measured for **2a**. This is a result of the electron-donating Cp^* ligand making oxidation thermodynamically more favourable according to Marcus theory. The kinetic data for **2a** and **5b** are shown in the graphs below in Figures 4.36 and 4.37.

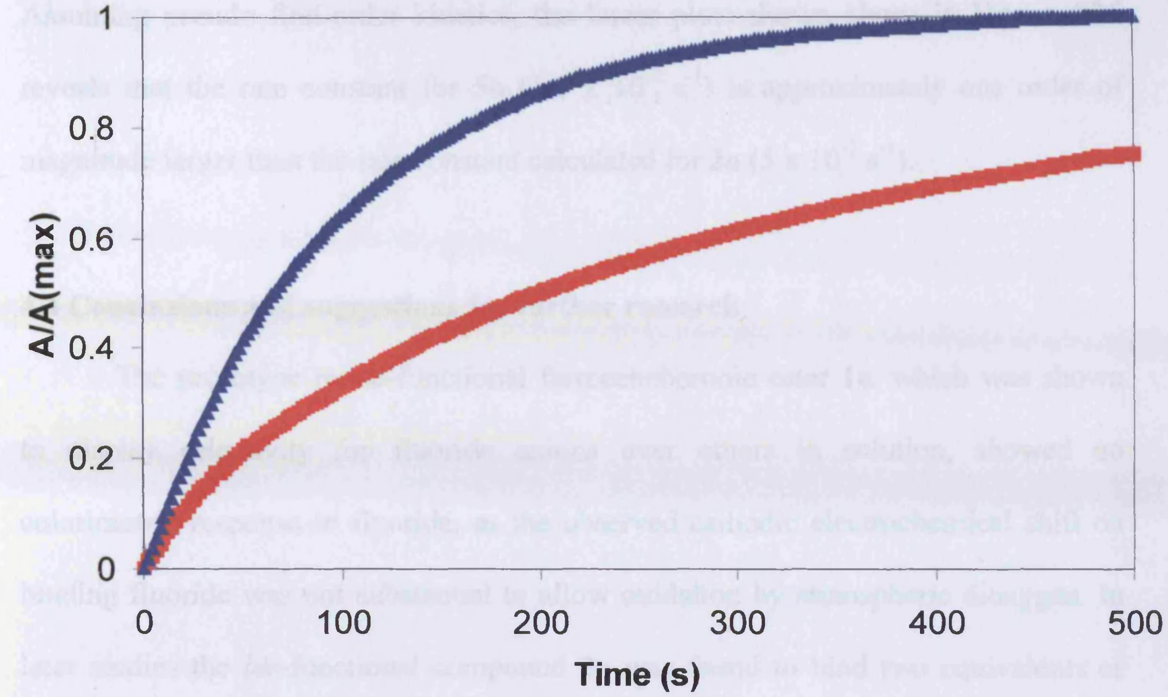

Figure 4.36 Plot of normalized absorbance against time for the band at ca. 630 nm associated with the ferrocenium species formed on addition of 15 equiv. of [^{n}Bu$_4$N]F to **2a** and **5b** (each 17.5 mM in chloroform). Red: **2a** (monitored at 633 nm); blue: **5b** (722 nm).

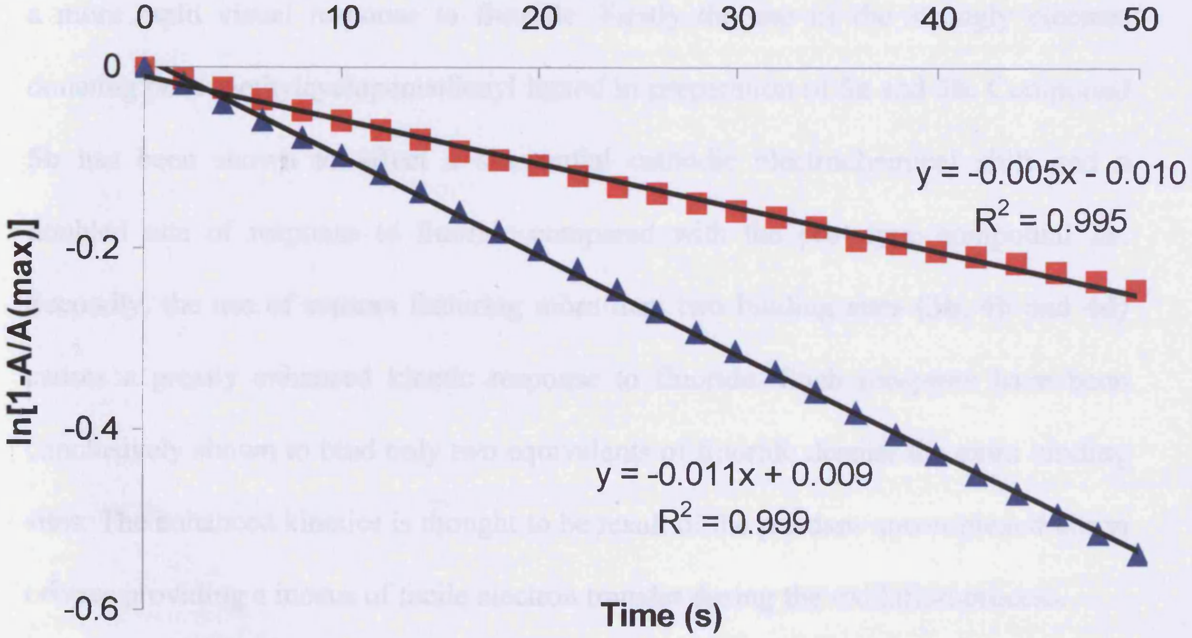

Figure 4.37 Pseudo first-order fits for red (**2a**) and blue (**5b**) data for t < 50 s.

Assuming pseudo first-order kinetics, the linear plots shown above in Figure 4.36 reveals that the rate constant for **5b** (1.1 x 10^{-2} s^{-1}) is approximately one order of magnitude larger than the rate constant calculated for **2a** (5 x 10^{-3} s^{-1}).

4.4 Conclusions and suggestions for further research

The prototype mono-functional ferroceneboronic ester **1c**, which was shown to display selectivity for fluoride anions over others in solution, showed no colorimetric response to fluoride, as the observed cathodic electrochemical shift on binding fluoride was not substantial to allow oxidation by atmospheric dioxygen. In later studies the *bis*-functional compound **2a** was found to bind two equivalents of fluoride, thereby causing a significant cathodic electrochemical shift the result being that oxidation by dioxygen was possible.

Two successful chemical modifications have since been made to these prototype systems in designing enhanced colorimetric sensors for fluoride capable of a more rapid visual response to fluoride. Firstly the use of the strongly electron donating pentamethylcyclopentadienyl ligand in preparation of **5a** and **5b**. Compound **5b** has been shown to affect a substantial cathodic electrochemical shift and a doubled rate of response to fluoride compared with the prototype compound **2a**. Secondly, the use of sensors featuring more than two binding sites (**3b**, **4b** and **4d**) causes a greatly enhanced kinetic response to fluoride. Such receptors have been conclusively shown to bind only two equivalents of fluoride despite the extra binding sites. The enhanced kinetics is thought to be result of the pendant uncomplexed boron centres providing a means of facile electron transfer during the oxidation process.

The rate of sensor response (by UV/Vis measurements) is found to be critically dependant on the availability of oxidant. This observation is particularly relevant to the preparation of solid-state sensor devices, where the incorporation of a suitable redox-matched solid-state oxidant would be required in order to facilitate a useable colorimetric response over a realistic timeframe. Incorporation of an oxidant pendant to the ferroceneboronic ester, for example, perhaps a quinone-based oxidant, may prove advantageous and eliminate the dependence of kinetic response on the availability of oxidant.

Fluorescence spectroscopy has proven a very useful analytical tool for monitoring fluoride binding and has employed by many research groups.[23] The tetra-functional ferroceneboronic ester compound featuring a pendant napthalene group (**4d**) is an ideal compound for this kind of analysis, featuring the fluorescence active napthalene group, a result of the $\pi \rightarrow \pi^*$ transitions. The typical response of fluorescence quenching upon anion complexation allows the detection of anions and the ability to monitor the extent of host-guest interactions via fluorescence titration experiments (Fc^+ being much more effective at fluorescence quenching than Fc).

The 1,2-*bis*-functional ferroceneboronic ester compound (**6a**), which was prepared in Chapter three, shows the potential to bind fluoride in a chelating fashion, due to the favourable spacial arrangement of boryl functions. The chelation of fluoride allows for much stronger binding and a more stable host-guest complex, which in turn may make crystallisation of the host-guest complex possible. Previous attempts to isolate crystals of a host-guest complex have been unsuccessful, despite the very crystalline nature of the hosts. However, if compound **6a** does chelate fluoride, the iron centre may then not be electron rich enough to undergo a visual colorimetric response to fluoride, as previously observed with mono-fluoride bound receptors (**1c**). A useful modification to this system, towards a colorimetric sensor for fluoride, would be the preparation of the 1,2,1',2'-tetrafunctionalised compound, with now two binding sites potentially capable of chelating fluoride.

4.5 References

1. See, for example H. Yamamoto, A. Ori, K. Ueda C. Dusemund, S. Shinkai, *Chem. Commun.*,1996, 407. H. E. Katz, *J. Am. Chem. Soc.,* 1986, **108**, 7640. S. Solé, F. P. Gabbaï, *Chem. Commun.,* 2004, 1284.
2. C. Dusemund, K. R. A. Samankumara Sandanayake, S. Shinkai, *J. Chem. Soc, Chem. Commun.*, 1995, 333.
3. A. P. de Silva, H. Q. N. Gunaratne, T. Gunnlaugsson, A. J. M. Huxley, C. P. McCoy, J. T. Rademacher, T. E. Rice, *Chem. Rev.*, 1993, **115**, 11216.
4. C. R. Cooper, N. Spencer, T. D. James, *Chem. Commun.*, 1998, 1365.
5. S. Jacobsen, R. Pizer, *J. Am. Chem. Soc.*, 1993, **115**, 11216.
6. J. Yoon, A. W. Czarnik, *J. Am. Chem. Soc.*, 1992, **114**, 5874.
7. S. Yamaguchi, S. Akiyama, K. Tamao, *J. Am. Chem. Soc.*, 2001, **123**, 11372.
8. M. Melaimi, F. P. Gabbaï, *J. Am. Chem. Soc.*, 2005, **127**, 9680.
9. T. W. Hudnall, F. P. Gabbaï, *J. Am. Chem. Soc.*, 2007, **129**, 11978.
10. C. Bresner, J. K. Day, N. D. Coombs, I. A. Fallis, S. Aldridge, S. J. Coles, M. B. Hursthouse, *Dalton. Trans.*, 2006, 3660.
11. S. Aldridge, C. Bresner, I. A. Fallis, S. J. Coles, M. B. Hursthouse, *Chem. Commun.*, 2002, 740.
12. C. Bresner, S. Aldridge, I. A. Fallis, C. Jones, L. Ooi, *Angew. Chem. Int. Ed.,* 2005, **44**, 3606 and references cited therein.
13. K. N. Brown, P. T. Gulyas, P. A. Lay, N. S. McAlpine, A. F. Masters, *J. Chem. Soc. Dalton. Trans.*, 1993, 835.

14. C. Bresner, I. A. Fallis, S. Aldridge, unpublished results.

15. N. G. Connelly, W. E. Geiger, *Chem. Rev.*, 1996, **96**, 877.

16. L. Eberson, F. Radner, *Acc. Chem. Res.*, 1987, **20**, 53.

17. A. B. P. Lever, *Inorganic Electronic Spectroscopy,* Elsevier, Amsterdam, 2nd edn., 1984, pp. 659-671.

18. W. Likussar, D. F. Boltz, *Analytical. Chemistry.,* 1943, **43**, 1265.

19. D. T. Sawyer, J. S. Valentine, *Acc. Chem. Res.,* 1981, **14**, 393.

20. S. Fukuzumi, S. Mochizuki, T. Tanaka, *Inorg. Chem.*, 1989, **28**, 2459.

21. C. D. Entwistle, T. B. Marder, *Angew. Chem. Int. Ed.*, 2002, **42**, 2927.

22. (a) C. Elschenbroich, M. Wolf, O. Burghaus, K. Harms, J. Pebler, *Eur. J. Inorg. Chem.,* 1999, 2173. (b) L. Weber, I. Domke, C. Schmidt, T. Braun, H. G. Stammler, B. Neumann, *Dalton. Trans.,* 2006, 2127.

23. S. Arimori, M. G. Davidson, T. M. Fyles, T. G. Hibbert, T. D. James, G. I. Kociok-Köhn, *Chem. Commun.*, 2004, 1640.

Chapter Five

The Synthesis and Characterisation of Ferrocene Based Boron-Containing Lewis Acidic Oligomers and Polymers

5.1 Introduction

Since the initial preparation of a well characterised transition metal containing polymeric compound in the 1970's by Pittman and co-workers, the field of organometallic polymers and oligomers has found vastly increasing research attention and a number of important and interesting applications, such as multi-electron catalysis, optical and electronic devices, electron storage devices, surface modification of electrodes and sensor intensification.[1] There exist two main classes of ferrocene-containing organometallic polymers; type **I** polymers featuring ferrocenyl moieties as pendant substituents to the polymer main-chain, for example polyvinylferrocene, and type **II** polymers featuring ferrocene as the integral part of the polymer backbone, for example poly(ferrocenylene)s.

The key interests with respect to the work presented within this chapter are type **II** polymers featuring the ferrocene moiety coupled with Lewis acidic organoboron centres. Ferrocene is a particularly useful fragment in the above-mentioned applications due to its reversible redox chemistry, high thermal stability and good solubility, whilst the vacant p-orbital at the boron centre provides the potential for achieving π-conjugation along a polymer chain, the key feature which has led to extensive application in the development of molecular wires and sensor devices.

Initial preparation of a boron-bridged poly(ferrocenylene) stemmed from investigation of the ring opening chemistry of boron-bridged ferrocenophanes by Manners *et al.* and has sparked vast research interest.[2,3] The preparation of boron-bridged ferrocenophanes was preceded by research into the preparation of silicon-bridged ferrocenophanes. In an attempt to maximise the tilt angle of the ferrocenophane the authors successfully prepared an analogous compound bridged by an element of smaller covalent radius, namely boron.

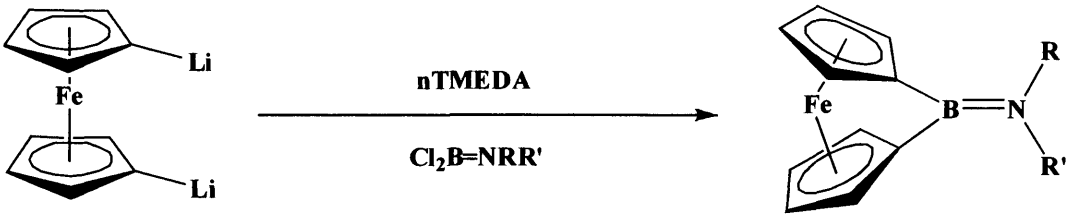

Figure 5.1 The preparative scheme for boron-bridged ferrocenophanes

Preparation of boron-bridged ferrocenophanes was achieved by reaction of dilithioferrocene with TMEDA and aminodichloroboranes. As predicted by the authors, on the basis of covalent radii, the product was found to have the largest known tilt angle of 32.4(2)° (*c.f.* 31.1(1)° as determined for the sulphur-bridged ferrocenophane). The ring-opening polymerisation chemistry of these compounds was investigated via a differential scanning calorimetry study to examine possible polymeric products formed.[4]

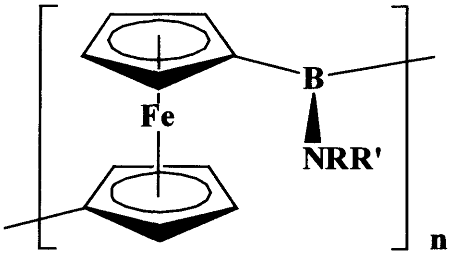

Figure 5.2 A polyferrocenylborane

Polymerisation was carried out by heating the monomer to 180°C in a sealed Pyrex tube for two hours; the resulting red glassy material was found to be very sparingly soluble in common solvents and to consist mainly of low molecular weight oligomers.

The advantageous electronic properties presented by borylene-bridged polyferrocenylenes have prompted the development of novel synthetic routes to such compounds by Wagner *et al.*[5]

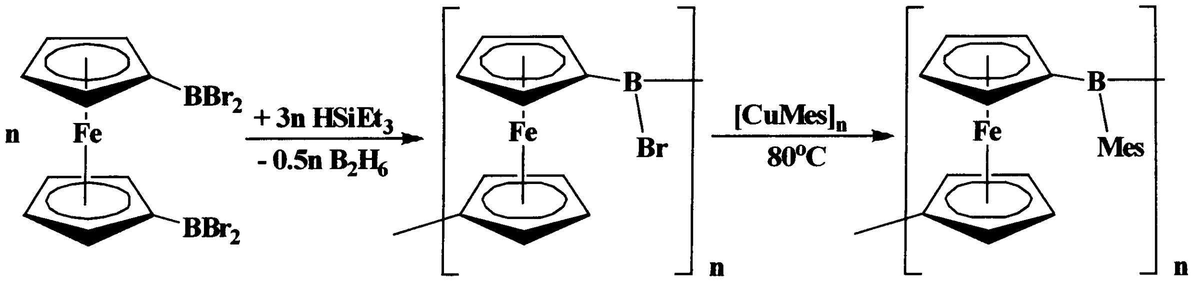

Scheme 5.1 Synthetic route to borylene-bridged polyferrocenylene

Wagner *et al.* reported a simple, quantitative coupling reaction between $FcBBr_2$ and $HSiEt_3$ to produce a diferrocenyl borane Fc_2BBr. An analogous synthetic procedure was then applied in the preparation of the corresponding polymeric species using a disubstituted $Fc[BBr_2]_2$ precursor. The polymeric product was found to be highly air and moisture sensitive and insoluble in conventional inert solvents. In order to resolve such problems the authors substituted the remaining bromide for a mesityl group by reaction of the polymer with CuMes. The mesityl moiety was chosen to provide steric protection to the Lewis acidic while also aiding solubility, and the resulting mesityl substituted polymer was found to be only slightly air-sensitive and highly stable thermally. In order to determine the molecular weight of the polymeric product MALDI TOF-TOF mass spectra were acquired and the product was found to comprise a series of three polymers each with different capping fragment combinations, Mes-Mes, Mes-Fc and Fc-Fc, characterised by a pattern of peaks in the spectrum with a constant separation corresponding to the repeat unit. Using these compounds the authors proved the existence of π-conjugation and thus electronic communication between the ferrocenyl moieties *via* the three-coordinate boron centre. Cyclic Voltammetry was performed to compare the dinuclear and polymeric products using ferrocene as a reference compound. Two reversible redox waves of equal intensity were observed for the dinuclear compound arising from the sequential one-electron oxidation of each iron centre, a large separation between the two redox waves indicating pronounced electronic communication between the two ferrocenyl fragments. Two redox waves were also observed in the cyclic voltammogram of the polymer, the first wave being irreversible and assigned to the two terminal iron centres. The second (reversible) redox wave was observed at much higher potentials than the dinuclear compound, which was assigned to the oxidation of neutral ferrocene fragments adjacent to ferrocenium centres. Again a very large splitting between the redox waves was observed, thereby providing additional evidence for electronic communication.

5.2 Aims of research

The implication of boronic esters in anion sensing and the opportunity for enhanced selectivity in the specific recognition of anions i.e. fluoride and the advantages of anion chelation have been discussed in Chapters Three and Four. Cation binding by macrocyclic Lewis basic frameworks is a widely explored area of research interest[6,7,8] a logical extension of this approach suggests that macrocyclic Lewis acidic systems might prove useful synthetic targets in the application of fluoride chelation. Hence the synthesis of Lewis acid based macrocyclic structures featuring the ferrocene fragments is a key goal. Likewise the potential applications of solid-state sensor materials have highlighted organometallic polymers as an exciting class of functional compounds. One such application, that of molecular wires, requires that electronic communication along a polymer chain, is possible. This is achieved using the vacant p-orbital of three-coordinate boron centres; incorporation of redox active fragments such as ferrocene provides a convenient means of monitoring electronic communication. Hence considerable research effort has been expended on the development of routes to ferrocene-based polymers featuring boron centres within the backbone. To date such routes have involved ring-opening polymerisation, coordination polymerisation or B-H/B-C exchange[4,5,9] and the preferential formation of short chain oligomers has proven a downfall of such methods. This chapter targets investigation into the factors controlling assembly of boronic ester units into poly-, oligomeric or macrocyclic products using a simple condensation methodology, with electrochemical investigation to observe possible inter-metallic electronic communication.

5.3 Experimental

Preparation of $FcBO_2C_8H_{12}O_2BFc$ (**7a**)

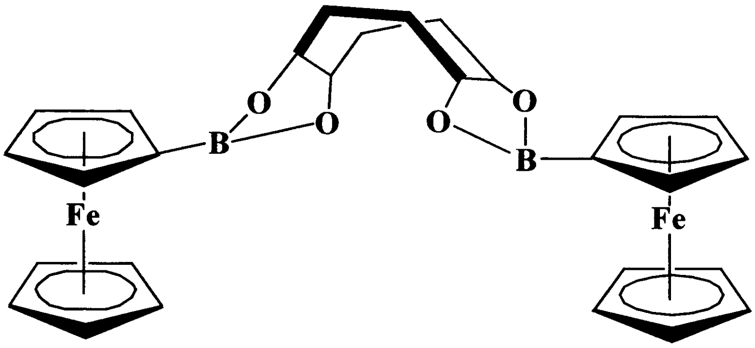

(1R,2S,5R,6S)-tetrahydroxycyclooctane (0.124 g, 7.03 mmol) was weighed into a Schlenk, dried *in vacuo* for two hours and dissolved in toluene (150 ml). Triethylamine (0.40 ml, 28.1 mmol) was added gradually to the stirred tetraol solution via syringe. 1-dibromoborylferrocene (0.5 g, 14.1 mmol) was weighed into a Schlenk and dissolved in toluene (100 ml); this solution was added to the stirring tetraol solution dropwise via cannula over a period of 1 h. After stirring for 24 h the cloudy orange reaction mixture was filtered through celite and toluene was removed in vacuo to yield an air-stable yellow powder (yield: 212 mg, 53 %). Slow diffusion of hexanes into a chloroform solution of **7a** at room temperature afforded small plate-like crystals suitable for X-ray diffraction. ^{1}H NMR (400 MHz, [D]chloroform, 20 °C): δ 1.84 [s, 4H, CH_2 of cyclooctane ring], 2.11 [s, 4H, CH_2 of cyclooctane ring], 4.08 [s, 10H, C_5H_5], 4.34 [m, 8H, C_5H_4], 4.59 [d J = 8 Hz, 4H, CH of chelate]. $^{13}C\{^1H\}$ NMR (75.5 MHz, [D]chloroform, 20 °C): δ 25.0 [CH_2 of cyclooctane ring], 68.5 [C_5H_5], 72.2 [C_5H_4], 73.7 [C_5H_4], 78.5 [CH of chelate], quaternary of C_5H_4 not observed. $^{11}B\{^1H\}$ NMR (96 MHz, [D]chloroform, 20 °C): δ 32.5. MS(EI): M^+ = 564.1 (100 %), exact mass (calc.) *m/z* 564.1024, (obs.) 564.1028. IR (KBr disc, cm^{-1}): ν 2943 w, 2677 w, 1499 md, 1480 s, 1381 s, 1324 s, 1324 s, 1301 s, 1231 md, 1189 w, 1126 s, 1104 w, 1032 w, 817 md. UV/Vis (chloroform): λ_{max} 444 nm, $\varepsilon = 431\ cm^{-1}\ mol^{-1}\ dm^3$. Crystal data: $C_{28}H_{30}B_2Fe_2O_4$, orthorhombic, Pnma, a = 29.8942(10) Å, b =10.7482(3) Å, c =7.4301(3) Å, V = 2387.36(14) Å^3, Z = 4, D_{calc} = 1.569 Mg m^{-3}, $\mu(MoK\alpha)$ = 1.251 mm^{-1}. A suitable crystal was covered in pre-dried mineral oil and mounted at 120(2) K. 2868 unique reflections were collected ($2.33 < \theta < 27.5°$). Final R-factor: $R_1 = 0.077$.

Preparation of poly/oligomeric [fcBO$_2$C$_8$H$_{12}$O$_2$B]$_n$ (**7c**)

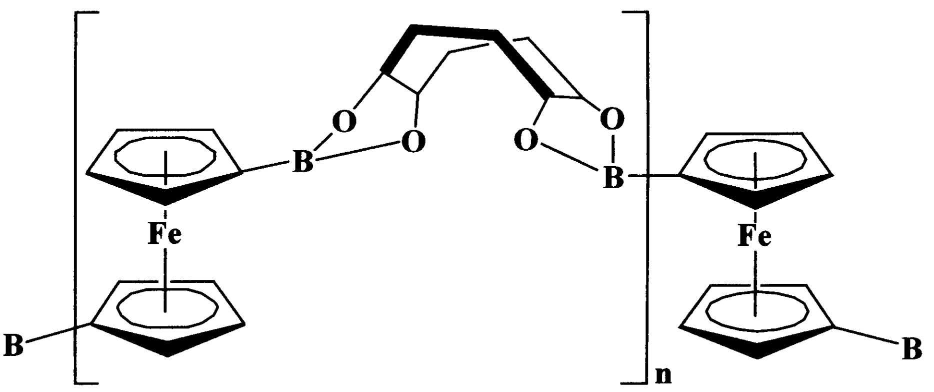

Ferrocene-*bis*-boronic acid (0.254 g, 9.25 mmol) and (1R,2S,5R,6S)-tetrahydroxycyclooctane (0.162 g, 9.25 mmol) were weighed into a thick-walled pressure tube. Acetone (40 ml) was added, the pressure tube was sealed and the reaction mixture heated with stirring to 80 °C for 24 h. A yellow solid formed during the course of the reaction, which was isolated by filtration and dried under vacuum. The solid product was washed with chloroform until washings became colourless; the chloroform solution was reduced to dryness in vacuo to yield a powdery yellow solid (16.8 mg, 4.8 %). Crystals suitable for X-ray diffraction were grown by slow diffusion of ether into a chloroform solution of macrocyclic side-product **7b**, which is discussed in greater detail in section 5.4.2. The remaining portion of the yellow solid was found to be insoluble in a wide range of solvents and hence was shown to be an oligo/polymeric product by MALDI mass spectrometry. Yield of polymeric product **7c** (241 mg, 69 %). Spectroscopic data for **7b**: MS(EI): M^+ = 564.2 (100 %), 756.3 (12 %). Crystal data: $C_{36}H_{40}B_4Fe_2O_8$, orthorhombic, Pbcn, a = 19.6222(11) Å, b = 7.8609(3) Å, c = 21.3982(11) Å, V = 3300.6(3) Å^3, Z = 4, D_{calc} = 1.521 Mg m^{-3}, μ(MoKα) = 0.934 mm^{-1}. A suitable crystal was covered in pre-dried mineral oil and mounted at 120(2) K. 3366 unique reflections were collected ($2.95 < \theta < 26.4°$). Final R-factor: $R_1 = 0.091$.

Preparation of $FcB(OCH_2)_2C(CH_2O)_2BFc$ (**8a**)

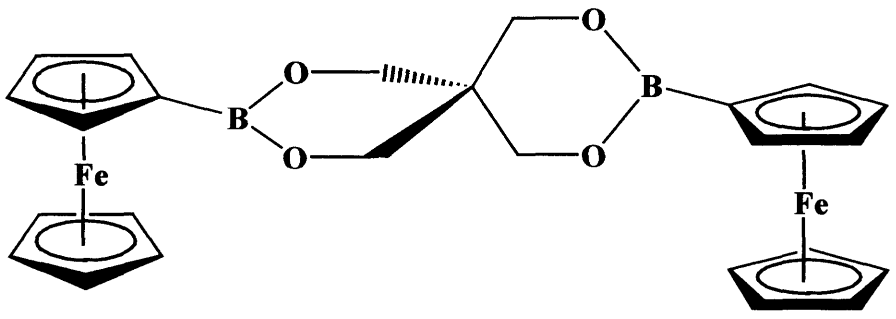

To solution of ferroceneboronic acid (0.2 g, 8.70 mmol) in acetone (40 ml) in a thick-walled pressure tube was added pentaerythritol (0.059 g, 4.35 mmol). The pressure tube was sealed and heated with stirring to 80°C for 24 hours. The resulting acetone solution was then filtered and reduced to dryness in vacuo to a yield a bright yellow powder (172 mg, 75 %). Crystals suitable for X-ray diffraction were grown by slow diffusion of ether into a chloroform solution of **8a**. ^1H NMR (400 MHz, [D]chloroform, 20 °C): δ 3.97 [s, 8H, CH_2], 4.08 [s, 10H, C_5H_5], 4.16 [m, 8H, C_5H_4]; $^{13}C\{^1H\}$ NMR (75.5 MHz, [D]chloroform, 20 °C): δ 36.2 [spiro-C], 64.5 [CH_2], 68.1 [CH of C_5H_5], 71.0, 71.9 [CH of C_5H_4], quaternary of C_5H_4 not observed. $^{11}B\{^1H\}$ NMR (96 MHz, [D]chloroform, 20 °C): δ 33.6. IR (KBr disc, cm^{-1}): ν 3313 md, 1753 w, 1495 s, 1376 s, 1299 md, 1238 md, 1168 md, 1175 md, 1014 md. UV/vis ($CHCl_3$) $\lambda_{max}(\varepsilon)$ 445 nm (123.7 mol^{-1} cm^{-1} dm^3). MS(EI): M^+ = 524.1 (100 %), exact mass (calc.) *m/z* 524.0726, (obs.) 524.0556. Crystal data: $C_{26}H_{27}B_2Cl_3Fe_2O_4$, monoclinic, P2(1)/n, a = 22.5093(3) Å, b = 5.8951(3) Å, c = 22.9770(5) Å, β= 119.110(1)°, V = 2663.80(15) Å^3, Z = 4, D_{calc} = 1.604 Mg m^{-3}, μ(MoKα) = 1.422 mm^{-1}. A suitable crystal was covered in pre-dried mineral oil and mounted at 150(2) K. 6331 unique reflections were collected (3.12 < θ < 27.8°). Final R-factor: R_1 = 0.059.

Preparation of [fcB(OCH$_2$)$_2$C(CH$_2$O)$_2$B]$_2$ (**8b**)

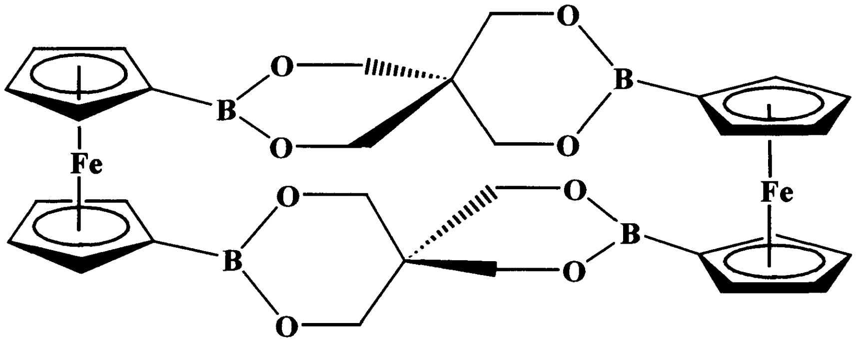

To solution of ferrocene*bis*-boronic acid (400 mg, 7.3 mmol) in acetone (40 ml) in a thick walled pressure tube was added pentaerythritol (200 mg, 7.3 mmol). The pressure tube was sealed and the reaction mixture heated with stirring to 80°C for 24 h. During the course of the reaction a yellow solid formed which was isolated by filtration and extracted with chloroform to a yield a bright yellow powder (393 mg, 80 %). Crystals suitable for X-ray diffraction were grown by slow diffusion of ether into a chloroform solution of **8b**. ^{1}H NMR (400 MHz, [D]chloroform, 20 °C): δ 4.03 [br s, 16H, CH$_2$], 4.30 [m, 8H, C$_5$H$_4$], 4.30 [m, 8H, C$_5$H$_4$]; ^{13}C{^{1}H} NMR (75.5 MHz, [D]chloroform, 20 °C): δ 36.5 [spiro-C], 64.9 [CH$_2$], 71.6, 73.7 [CH of C$_5$H$_4$], quaternary of C$_5$H$_4$ not observed. ^{11}B{^{1}H} NMR (96 MHz, [D]chloroform, 20 °C): δ 27.6. IR (KBr disc, cm^{-1}): ν 3102 md, 3082 md, 1486 s, 1333 s, 1296 s, 1261 s, 1188 s, 1175 md, 1045 md, 973 md. UV/vis (CHCl$_3$) $\lambda_{max}(\varepsilon)$ 454 nm (410.9 mol^{-1} cm^{-1} dm^3). EI-MS m/z (%) 676.1 (100), correct isotope distribution for 4B, 2Fe atoms. Exact mass (M$^+$): calc. 672.1308 (^{10}B$_4$ isotopomer); meas. 672.1307. Elemental analysis: calc. for 2·¼CHCl$_3$ C 51.51, H 4.61; meas. C 51.54, H 4.70. Crystal data: C$_{60}$H$_{64}$B$_8$Fe$_4$O$_{16}$, monoclinic, P12$_1$1, a = 11.9633(6) Å, b = 9.9176(5) Å, c = 13.4452(6) Å, β= 114.889(3)°, V = 1446.96(13) Å^3, Z = 1, D$_{calc}$ = 1.553 Mg m^{-3}, μ(MoKα) = 1.251 mm^{-1}. A suitable crystal was covered in pre-dried mineral oil and mounted at 150(2) K. 4291 unique reflections were collected (2.34 < θ < 27.7°). Final

R-factor: $R_1 = 0.046$.

Preparation of Fc$BO_2(C_6H_2)O_2BFc$ (**9a**)

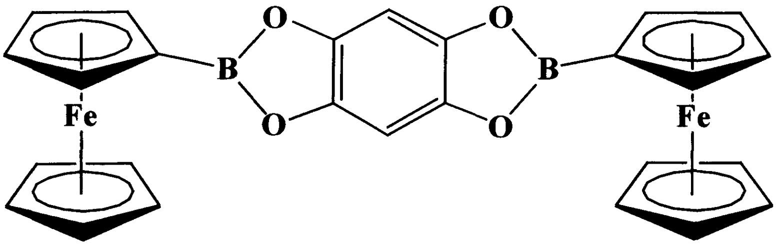

To a solution of dibromoborylferrocene (165 mg, 4.63 mmol) in toluene (40 ml) was added a solution of 1,2,4,5-tetrakis(trimethylsilyl)benzene (100 mg, 2.33 mmol) in toluene (30 ml) dropwise. The reaction vessel was sealed and heated to 80°C for 48 h. After hot filtration, toluene was removed in vacuo to yield a yellow powder, which was washed with hexanes and recrystallised from hexanes at –30°C. The resulting yellow solid was isolated and dried in vacuo (101 mg, 41 %). ^1H NMR (400 MHz, [D]chloroform, 20 °C): δ 3.95 [s, 10H, C_5H_5], 4.30 [m, 4H, CH of C_5H_4], 4.72 [m, 4H, CH of C_5H_4], 6.97 [s, 2H, aromatic CH]. $^{13}C\{^1H\}$ NMR (75.5 MHz, [D]chloroform, 20 °C): δ 68.1[C_5H_5], 73.7 [CH of C_5H_4], 74.0 [CH of C_5H_4], 98.9 [aromatic CH], quaternary of C_5H_4 not observed. $^{11}B\{^1H\}$ NMR (96 MHz, $CDCl_3$) δ 33.9. MS(EI): M^+ = 530.0 (100 %), exact mass (calc.) *m/z* 530.0257, (obs.) 530.0233. IR (KBr disc, cm^{-1}): ν 2965 s, 1493 md, 1458 s, 1383 md, 1337 w, 1262 md, 1142 s, 1026 w, 1231 md, 1189 w, 1126 s. UV/Vis (chloroform): $\lambda_{max}(\varepsilon)$ 439 nm (104.7 mol^{-1} cm^{-1} dm^3).

5.3.1 *Electrochemical (CV) analysis of* **7a**, **8a**, **9a** and **8b**.

Electrochemical analyses was carried out under the following conditions: electrolyte, 0.1 M [$^nBu_4N$][PF_6] in dry dichloromethane; reference electrode standard, 0.1 M [$^nBu_4N$][PF_6], 0.01 M silver nitrate in acetonitrile. Initially the electrolyte solution was degassed with argon to remove any dissolved oxygen before background cyclic voltammetry (CV) scans were recorded to guarantee the purity of the electrolyte solution prior to addition of the compound. Once a clean flat background CV had been measured a small sample of the compound (*ca* 2-5 mg) was added and the solution was further degassed to purge the solution of any additional dissolved oxygen and to dissolve the compound by agitation before spectral acquisition.

5.4 Results and discussion

5.4.1 Synthesis of oligomeric ferrocene based Lewis acids

Preliminary synthesis of dinuclear Lewis acids was carried out, prior to the attempted preparation of polymeric and oligomeric species, in order to obtain reliable characterising data on soluble compounds. Initial preparation of the cyclooctane-bridged di-ferrocenyl species (**7a**) was achieved via reaction of two equivalents of the dibromoboryl ferrocene precursor with one equivalent of (1R,2S,5R,6S)-tetrahydroxycyclooctane and four equivalents of triethylamine (Scheme 5.2). This synthetic route is identical to that applied in the preparation of *mono*-, *tris*- and *tetrakis*-functional boron-containing Lewis acids described in chapter three.

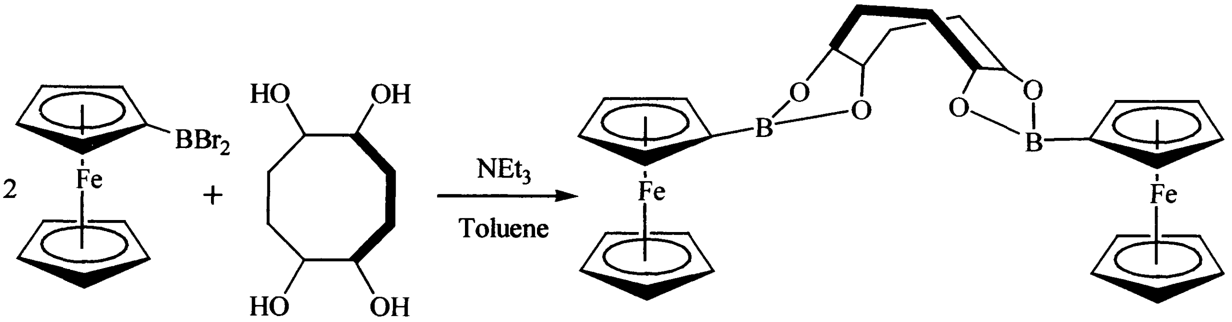

Scheme 5.2 Synthetic route to **7a** via a dibromoboryl ferrocene precursor

This synthetic procedure provided a route to the air-stable dinuclear product **7a**, obtained as a yellow powder in 53 % yield. The product was found to be freely soluble in chloroform and preliminary characterisation was made via ^{1}H, ^{11}B and ^{13}C NMR spectroscopy, each of which substantiate the proposed structure. The ^{11}B NMR spectrum of **7a** displays a characteristic signal at δ_B 32.5; the ^{1}H NMR spectrum exhibits a singlet resonance for the unsubstituted Cp ligand, and a multiplet for the C_5H_4 groups, while the CH groups of the chelate ring are observed as a doublet, and the four CH_2 groups of the cyclooctane ring give rise to two broad singlets between 1.8 and 2.1 ppm. The ^{13}C NMR spectrum is very simple displaying the expected number of peaks in the Cp region (*ca.* 70 ppm), a CH chelate resonance at a higher chemical shift (78 ppm) and two signals attributed to the CH_2 groups of the cyclooctane ring at lower shifts (*ca.* 25 ppm). Mass spectrometry data confirms the expected molecular ion peak along with the correct isotope pattern. Slow diffusion of hexanes into a chloroform solution of **7a** at room temperature afforded small plate-like crystals suitable for X-ray diffraction. The solid-state structure of this compound displays each atom of the $O_2C_8H_{12}O_2$ bridge disordered over two sites, for clarity the two disordered components are separately illustrated pictorially in Figure 5.3, showing the two positions of the bridging ligand; selected bond lengths and angles are listed in Table 5.1.

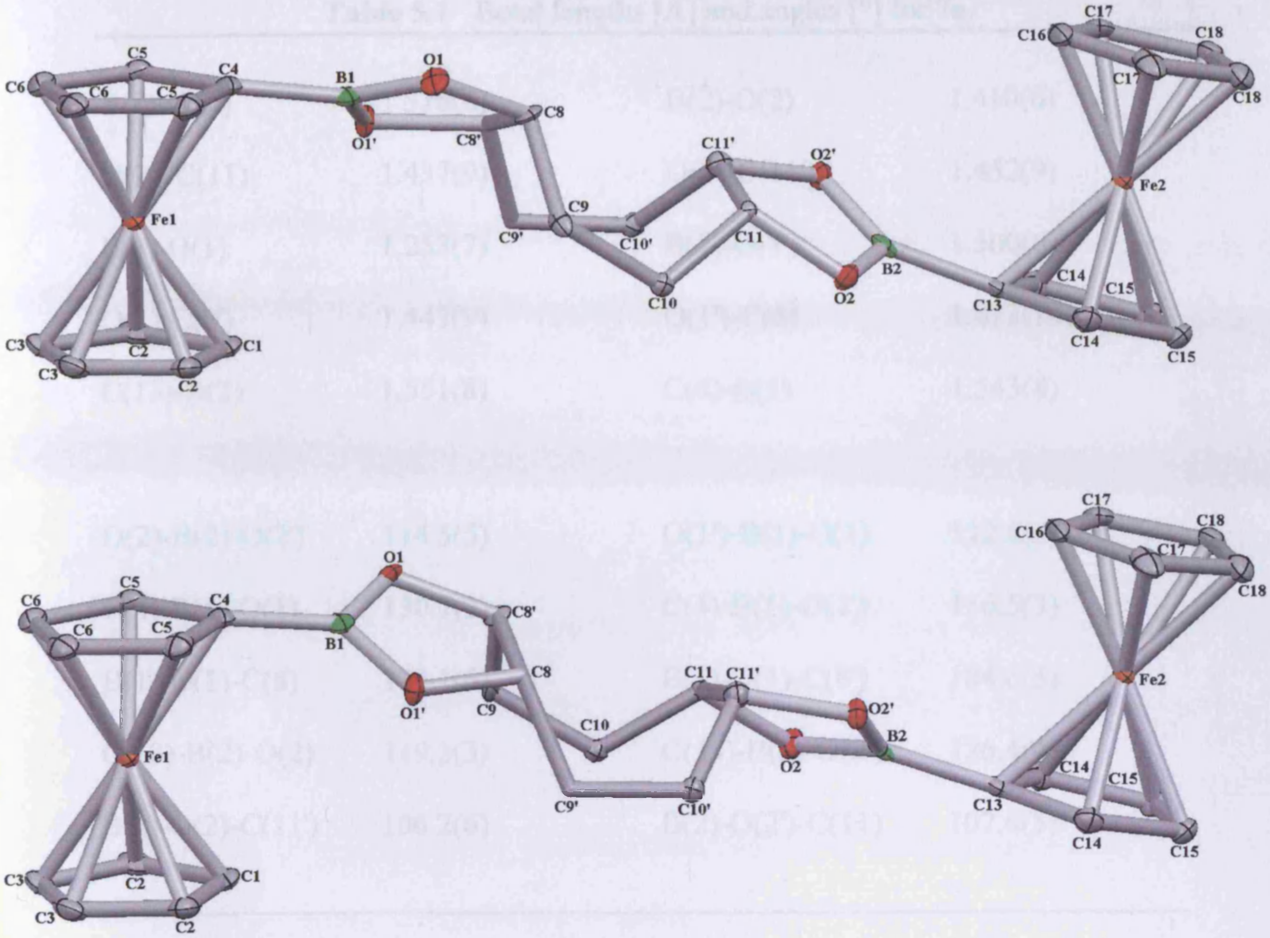

Figure 5.3 - Molecular structure of $FcBO_2C_8H_{12}O_2BFc$ (**7a**). ORTEP ellipsoids set at the 30 % probability level. Hydrogen atoms omitted for clarity.

Table 5.1 Bond lengths [Å] and angles [°] for **7a**.

B(2)-O(2')	1.326(6)	B(2)-O(2)	1.410(6)
O(2')-C(11)	1.437(9)	O(2)-C(11')	1.452(9)
B(1)-O(1)	1.253(7)	B(1)-O(1')	1.500(6)
O(1)-C(8')	1.443(9)	O(1')-C(8)	1.473(10)
C(13)-B(2)	1.551(8)	C(4)-B(1)	1.543(8)

O(2)-B(2)-O(2')	114.5(5)	O(1')-B(1)-O(1)	112.6(5)
C(4)-B(1)-O(1)	130.7(3)	C(4)-B(1)-O(1')	116.5(3)
B(1)-O(1)-C(8)	111.1(5)	B(1)-O(1)-C(8')	104.6(5)
C(13)-B(2)-O(2)	119.3(3)	C(13)-B(2)-O(2')	126.4(4)
B(2)-O(2)-C(11')	106.2(6)	B(2)-O(2')-C(11)	107.6(5)

The molecular structure of **7a** displays typical bond lengths and angles in general. The average B-O bond length was calculated at 1.377 Å, which are similar to those observed for analogous ferroceneboronic ester compounds discussed in chapter three (*ca.* 1.37 Å). The O-B-O bond angles of 114.5(5) and 112.6(5)° are typical for five-membered boronic ester rings and are consistent with those previously observed for analogous boronic esters of ferrocene (see chapter three).

In exploring a general route to organometallic ferrocene-containing polymers, oligomers and macrocycles, the simple condensation reaction between ferroceneboronic acid and various tetraols has been exploited. Subsequent preparations of compound **7a** have followed this methodology, in which the reactants (ferroceneboronic acid and (1R,2S,5R,6S)-tetrahydroxycyclooctane in this case) are simply dissolved in acetone and heated to reflux in a sealed thick-walled pressure tube, eliminating water as a by-product (Scheme 5.3).

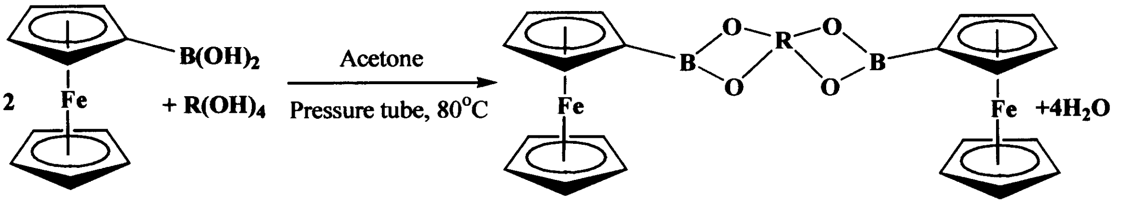

Scheme 5.3 Outline of the condensation methodology

Products are either soluble in acetone or precipitate out of solution, giving a simple work-up in either situation. This methodology inhibits possible side-reactions that may occur when very sensitive starting materials are used; hence products are obtained in very high purity and high yield (*ca.* 75 %).

Analogous 1:1 reaction of ferroceneboronic acid with pentaerythritol was carried out to prepare compound **8a**, in which the two ferrocenyl ligands are bridged by a pentaerythritol moiety (Figure 5.4).

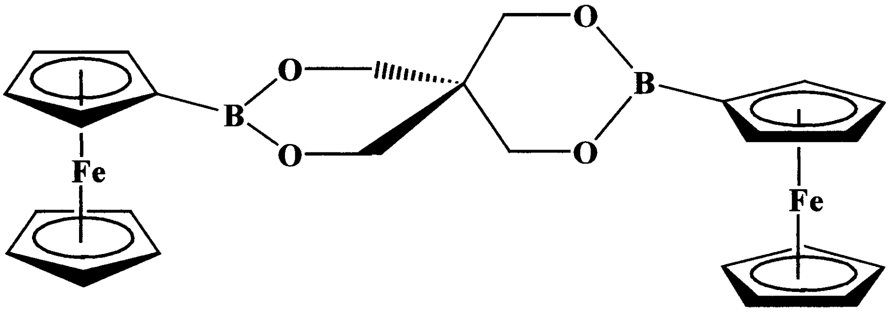

Figure 5.4 *$FcB(OCH_2)_2C(CH_2O)_2BFc$* (**8a**)

The yellow powder was isolated in 75 % yield and in very high purity after removal of the acetone reaction solvent and water by-product in vacuo. Characterising data in the form of multinuclear NMR, IR and UV spectroscopies and mass spectrometry are consistent with formation of compound **8a**. ^{11}B NMR revealed the product peak as a broad signal at δ_B 33.6 ppm, consistent with the characteristic signal for a boronic ester fragment (δ_B *ca.* 30 ppm), and with previously reported boronic ester shifts (see Chapter Three). ^{1}H NMR shows a broad signal for all the eight CH_2 protons; the ferrocenyl protons are observed as a singlet for the C_5H_5 protons and a multiplet for the C_5H_4 protons. ^{13}C NMR data also substantiates formation of the desired product; the spiro-C has a very distinctive chemical shift of 36 ppm, and the CH_2 groups are measured at 65 ppm. The ferrocenyl carbons show three signals in the Cp region of the spectrum, as the signal due to the quaternary carbon centre was not observed. Mass spectrometry confirmed the expected molecular ion peak, verified by accurate mass measurement and isotopic profiling. Crystals suitable for X-ray diffraction were grown by slow diffusion of ether into a chloroform solution of **8a**. The molecular structure is shown in Figure 5.5, relevant bond lengths and angles are listed in Table 5.2.

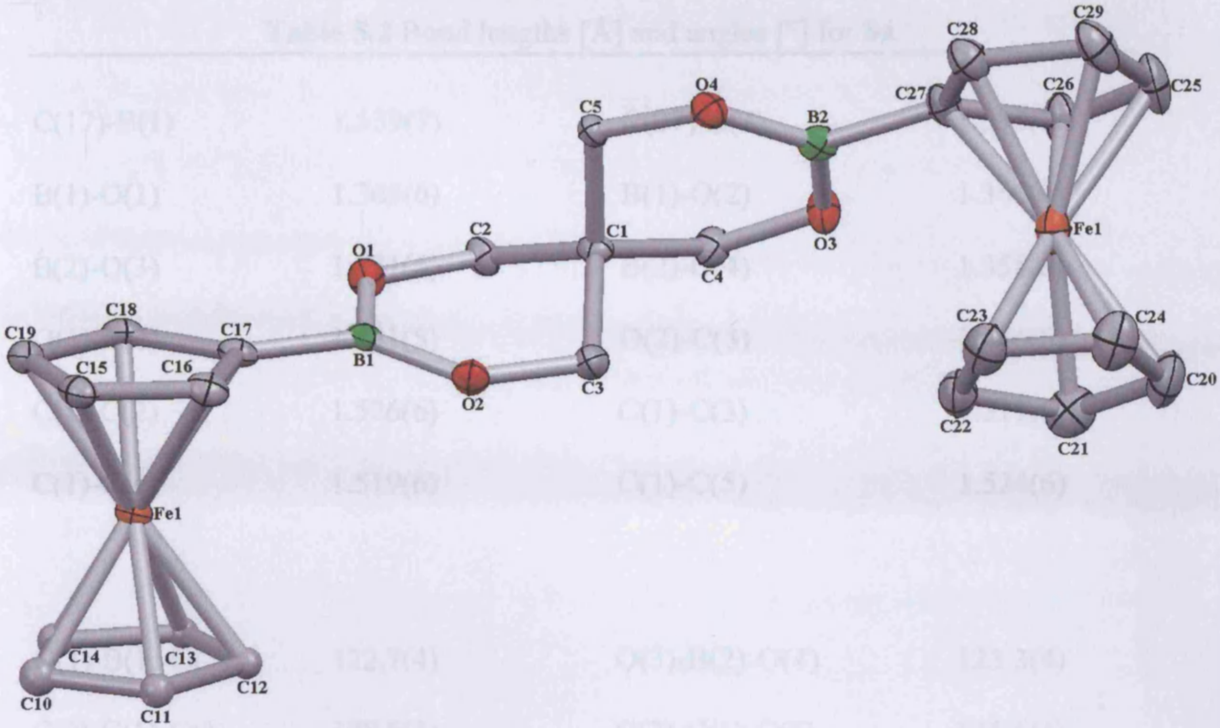

Figure 5.5 Molecular structure of *$FcB(OCH_2)_2C(CH_2O)_2BFc$* (**8a**). Hydrogen atoms omitted for clarity; ORTEP ellipsoids set at the 50 % probability level. Atoms C10-C14 remain isotropic due to a high degree of disorder and difficulty in modelling these atoms anisotropically.

Table 5.2 Bond lengths [Å] and angles [°] for **8a**.

C(17)-B(1)	1.539(7)	C(27)-B(2)	1.553(7)
B(1)-O(1)	1.363(6)	B(1)-O(2)	1.366(6)
B(2)-O(3)	1.371(6)	B(2)-O(4)	1.358(6)
O(1)-C(2)	1.441(5)	O(2)-C(3)	1.446(5)
C(1)-C(2)	1.526(6)	C(1)-C(3)	1.519(6)
C(1)-C(4)	1.519(6)	C(1)-C(5)	1.524(6)
O(1)-B(1)-O(2)	122.7(4)	O(3)-B(2)-O(4)	123.3(4)
C(2)-C(1)-C(3)	108.5(3)	C(2)-C(1)-C(5)	111.6(4)
C(5)-C(1)-C(4)	109.7(4)	C(3)-C(1)-C(5)	109.7(4)
C(17)-B(1)-O(1)	116.0(4)	C(17)-B(1)-O(2)	120.5(4)
C(27)-B(2)-O(3)	115.9(5)	C(27)-B(2)-O(4)	120.5(4)
B(1)-O(1)-C(2)	120.5(4)	B(1)-O(2)-C(3)	119.8(4)
B(2)-O(3)-C(4)	120.5(4)	B(2)-O(4)-C(5)	118.8(4)

The molecular structure of **8a** displays some characteristic features; the sum of angles about the boron centre is found to be 359.9(12)°, indicative of boron in a trigonal planar environment, however the breakdown of angles is unusual. The O-B-O angles (ca. 123°) in this compound are substantially larger than previously observed for similar boronic esters of ferrocene (ca. 114°). This feature is probably an effect of geometry constraints forced in forming the six-membered heterocyclic ring, where in previous structures the boron center has been constrained within a five-membered heterocycle. This opening of the O-B-O angle in a six-membered heterocyclic ring has been previously observed in the ferrocene-boronic ester compound featuring a propane backbone, in which the O-B-O angle was found to be 123.3(4)°.[10] The pentaerythritol bridging unit has an almost perfect tetrahedral core geometry, as such the ferrocenyl fragments are almost perpendicular to each other, and in each case the boryl moiety is twisted out of the plane of the Cp ligand by *ca.* 13.0°. B-O bond lengths [1.363(6), 1.371(6), 1.366(6) and 1.358(6)] which are similar to B-O bond lengths previously observed for analogous compounds prepared in chapter three (*ca.* 1.37 Å).

Compound **9a** was prepared with a view to investigating whether or not the benzene bridge is capable of supporting electronic communication between the two iron centres. Electronic communication can be detected by electrochemical methods and this molecule was specifically designed for this purpose, featuring the redox active ferrocene fragment. Compound **9a** (Figure 5.6) was synthesised via an alternative method, involving reaction of the *tetrakis*(trimethylsilyloxy) derivative of benzene with dibromoborylferrocene. The use of a trimethylsilyl precursor as the source of "RO⁻" eliminates the need for butyllithium, and means that this reaction can be applied to diols that are difficult to obtain as dry precursors.

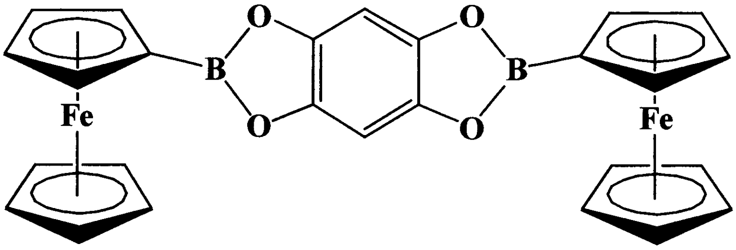

Figure 5.6 Fc$BO_2(C_6H_2)O_2BFc$ (**9a**)

The product was characterised via multi-nuclear NMR, UV and IR spectroscopy and mass spectrometry. ^{11}B NMR provides rapid confirmation of formation of a boronic ester, the product displaying a broad peak at δ_B 34 ppm, a characteristic shift for boronic esters. The ^1H NMR spectrum is very simple; the two aromatic protons give rise to a very distinctive peak at 6.9 ppm; the ferrocenyl fragment displays a singlet for C_5H_5 and two multiplets for the C_5H_4 protons. The aromatic CH fragment is also very distinctive in the ^{13}C NMR spectrum, observed at 99 ppm, along with the C_5H_5 carbons at 68 ppm and two further signals at 73 and 74 ppm for the C_5H_4 carbons. Mass spectrometry, including accurate mass measurement, confirmed the expected molecular ion peak. Numerous crystallisation attempts were made, using various methods and various solvent systems, however all were unsuccessful.

5.4.2 Synthesis of macrocyclic and polymeric ferrocene based Lewis acids

Minor modification to the previously discussed condensation methodology was made, involving the corresponding 1:1 condensation reaction of ferrocene*bis*-boronic acid with tetraols. This reaction was thought to provide a convenient route to polymeric products, as such this reaction was carried out with tetraols (1R,2S,5R,6S)-tetrahydroxycyclooctane and pentaerythritol. The 1:1 reaction of ferrocene-bis-boronic acid with (1R,2S,5R,6S)-tetrahydroxycyclooctane led to the formation of a mixture of products; both macrocyclic and polymeric. The macrocyclic product $[fcBO_2C_8H_{12}O_2B]_2$ (**7b**) was isolated in very low yield (5 %) as a yellow powder (Figure 5.7).

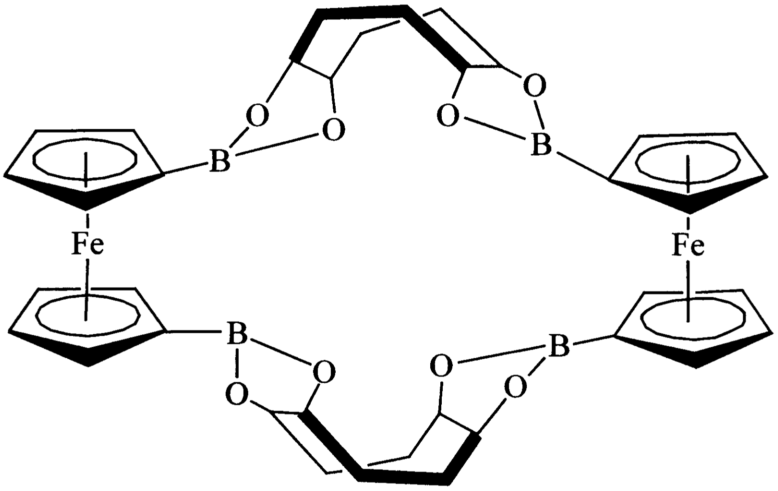

Figure 5.7 *[fcBO$_2$C$_8$H$_{12}$O$_2$B]$_2$* **(7b)**

Crystals suitable for X-ray diffraction were grown by diffusion of ether into a chloroform solution of the product. X-ray crystallography and mass spectrometry were the only pieces of characterising data gained due to the very low yield of product, however mass spectrometry confirmed the dinuclear nature of the product. This reaction was repeated under identical conditions and a similar distribution of products was observed. The solid-state structure of compound **7b** is illustrated pictorially in Figure 5.8; selected bond lengths and angles are listed in Table 5.3.

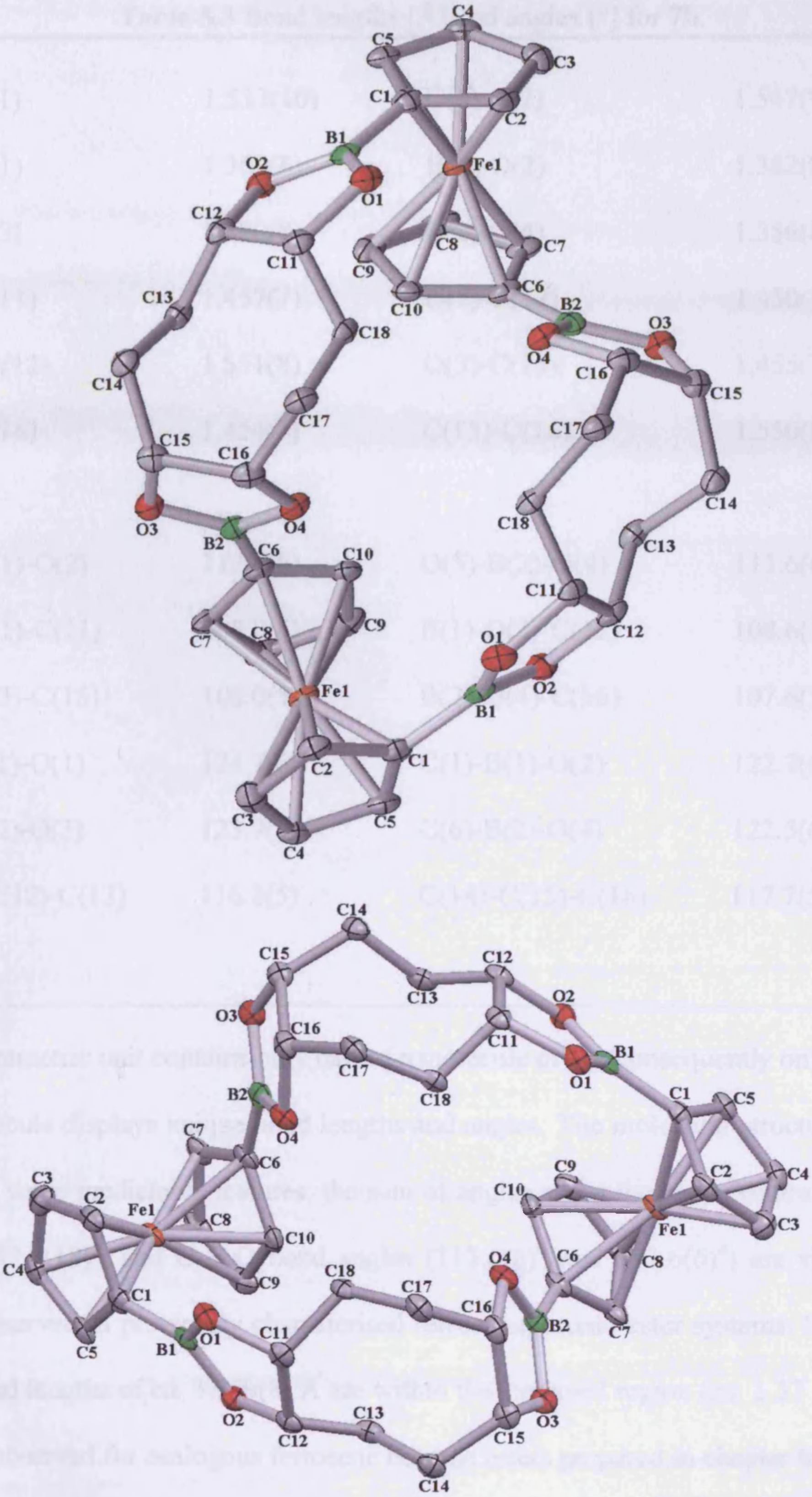

Figure 5.8 Molecular structure of *$[fcBO_2C_8H_{12}O_2B]_2$* (**7b**)

ORTEP ellipsoids set at the 50 % probability level.

Table 5.3 Bond lengths [Å] and angles [°] for **7b**.

C(1)-B(1)	1.533(10)	C(6)-B(2)	1.547(9)
B(1)-O(1)	1.369(8)	B(1)-O(2)	1.382(9)
B(2)-O(3)	1.380(8)	B(2)-O(4)	1.356(8)
O(1)-C(11)	1.457(7)	O(2)-C(12)	1.450(7)
C(11)-C(12)	1.551(8)	O(3)-C(15)	1.455(7)
O(4)-C(16)	1.454(7)	C(15)-C(16)	1.550(8)
O(1)-B(1)-O(2)	112.6(6)	O(3)-B(2)-O(4)	113.6(6)
B(1)-O(1)-C(11)	108.0(5)	B(1)-O(2)-C(12)	108.6(5)
B(2)-O(3)-C(15)	108.0(5)	B(2)-O(4)-C(16)	107.6(5)
C(1)-B(1)-O(1)	124.7(6)	C(1)-B(1)-O(2)	122.7(6)
C(6)-B(2)-O(3)	123.9(6)	C(6)-B(2)-O(4)	122.5(6)
C(11)-C(12)-C(13)	116.2(5)	C(14)-C(15)-C(16)	117.7(5)

The asymmetric unit contains only half of a molecule of **7b**, consequently only half of the molecule displays unique bond lengths and angles. The molecular structure of **7b** presents some predictable features: the sum of angles about the boron centre is found to be 359.9(18)°, and O-B-O bond angles (112.6(6)° and 113.6(6)°) are similar to those observed in previously characterised ferroceneboronic ester systems. Observed B-O bond lengths of *ca.* 1.369(8) Å are within the expected region (*ca.* 1.37 Å, based on that observed for analogous ferrocene boronic esters prepared in chapter three) and are similar to those observed in the open-chain species **7a**. The boryl fragments are observed to display a substantial twist out of the plane of the Cp ligand (*ca.* 23°); additionally the cyclopentadienyl rings are almost perfectly eclipsed; these features are probably due to the geometric constraints necessitated by forming the macrocycle. The torsion angle [B(1)-Cp(centroid)- Cp(centroid)-B(2)] was calculated to be 78.12°.

The polymeric product (**7c**) was isolated as the major product of the reaction (69 %), the yellow powdery product was found to be insoluble in all common solvents examined (hexanes, toluene, dichloromethane, chloroform, acetone, methanol, dimethylformamide, dimethylsulfoxide, and water), and hence was presumed to oligo/polymeric prior to analysis. The insolubility of the product precluded characterisation by conventional methods, such as NMR and mass spectrometry. However MALDI mass spectrometry has allowed assessment of the composition of the poly/oligomer (Figure 5.9).

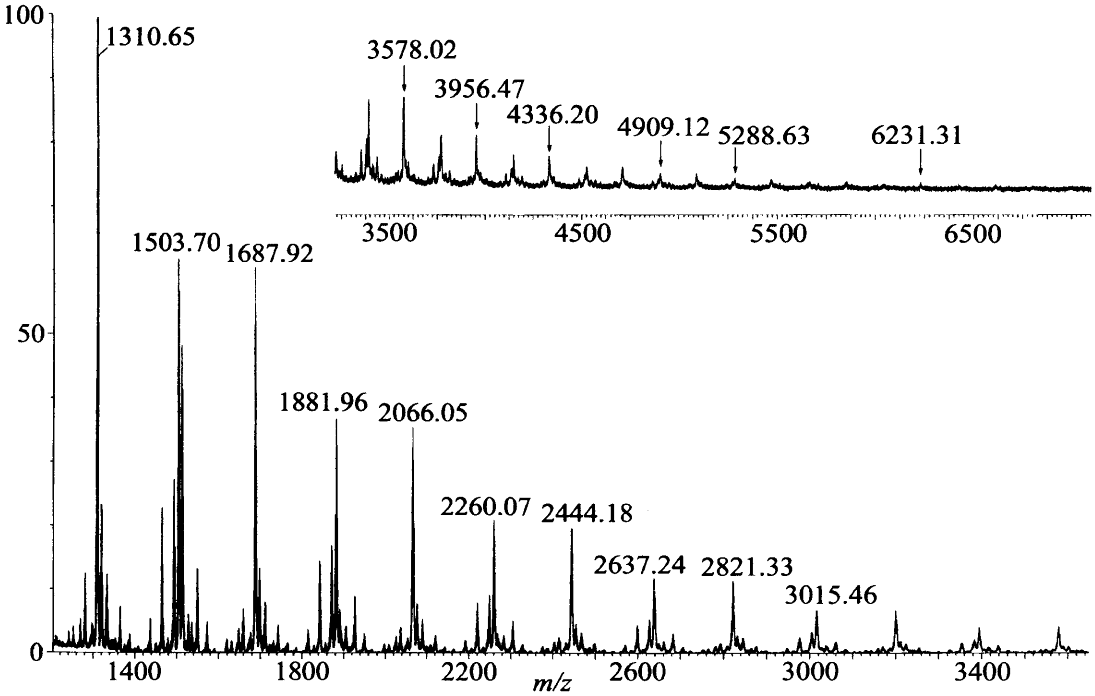

Figure 5.9 MALDI mass spectrum of **7c**.

The MALDI mass spectrum reveals a mixture of chain terminating groups, as displayed by the two series of peaks. One series corresponds to chains containing one ferrocenyl [Fc, $(\eta^5\text{-}C_5H_5)Fe(\eta^5\text{-}C_5H_4)$] and one diol [$BO_2C_8H_{12}(OH)_2$] terminus [*m/z*

= 378*n* + 370 (where *n* = 2 – 17)], the other series corresponds to polymer chains featuring two ferrocenyl termini [*m*/*z* = 378*n* + 186 (where *n* = 2 – 17)], both are shown below in Figure 5.10.

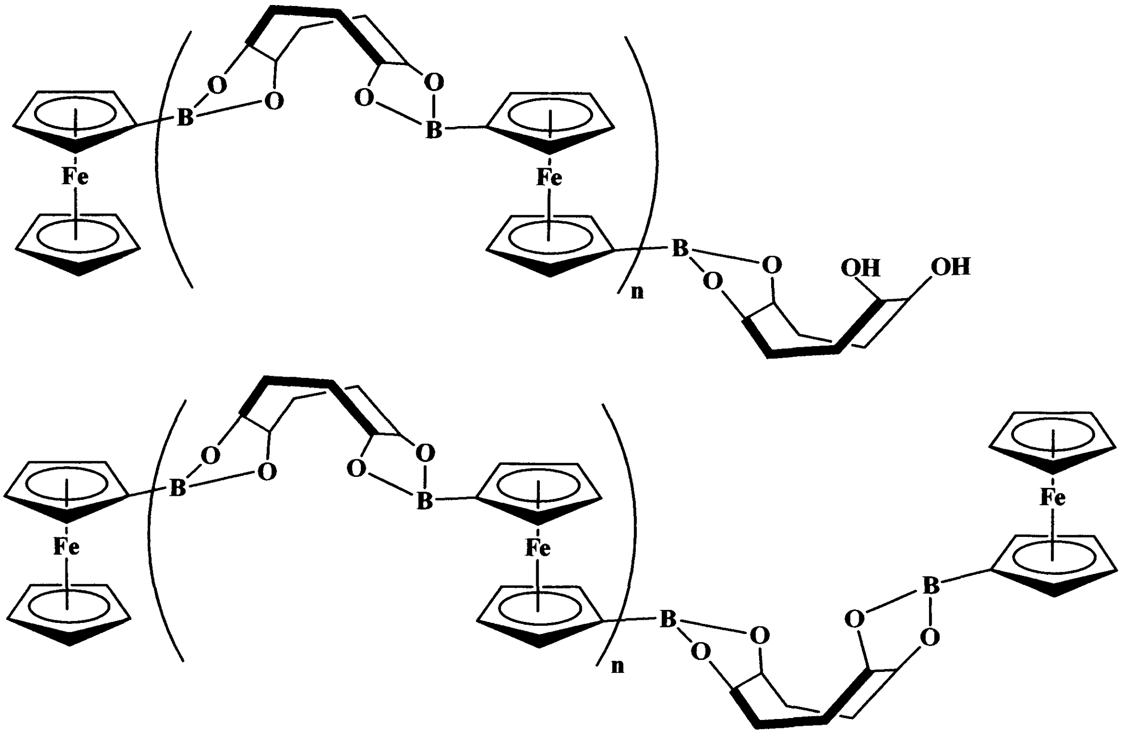

Figure 5.10 Polymeric products featuring different combinations of chain-terminating groups.

Similar spectra, featuring a mixture of chain terminating groups, have been recently observed by Wagner *et al.* in the preparation of borylene-bridged poly(ferrocenylenes).[5]

In the analogous 1:1 condensation reaction of ferrocene-bis-boronic acid with pentaerythritol a very different product distribution is obtained. The product was found to be freely soluble in chloroform, which immediately indicated that the product in this case was unlikely to be polymeric. The solid product was washed with chloroform until washings became colourless; the resulting orange powder was isolated after removal of volatiles in vacuo in 80 % yield (Figure 5.11).

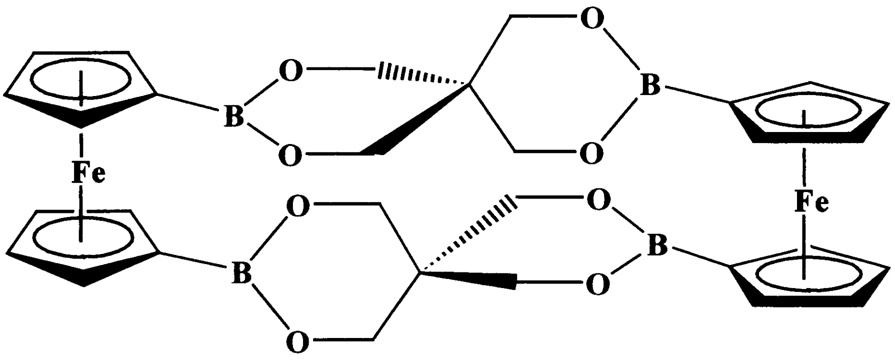

Figure 5.11 *[fcB(OCH$_2$)$_2$C(CH$_2$O)$_2$B]$_2$* (**8b**)

A combination of multinuclear NMR (^{1}H, ^{13}C, ^{11}B), IR and UV spectroscopies, mass spectrometry and elemental microanalysis are consistent with the formation of the macrocycle **8b**. ^{11}B NMR revealed the product peak at δ_B 28 ppm, consistent with the observed shift for the mono-bridged analogue **8a** (δ_B 33 ppm). The ^{1}H NMR spectrum of **8b** shows a single broad resonance for all eight CH$_2$ protons at *ca.* 4 ppm, and just two ferrocenediyl signals in the Cp region. The spiro-C centre displays a characteristic signal in the ^{13}C NMR spectrum (37 ppm), the CH$_2$ carbons are observed at a higher shift (65 ppm) and a further two signals between 71 and 73 ppm were observed for the Cp carbons. Mass spectrometry (including accurate mass measurement) is consistent with the expected molecular ion peak. Crystals suitable for X-ray diffraction were grown by slow diffusion of ether into a chloroform solution of **8b**, and single crystal X-ray diffraction was consistent with the product being formulated as the macrocyclic dimer *[fcB(OCH$_2$)$_2$C(CH$_2$O)$_2$B]$_2$* shown below in Figure 5.12; selected bond lengths and angles are listed in Table 5.4.

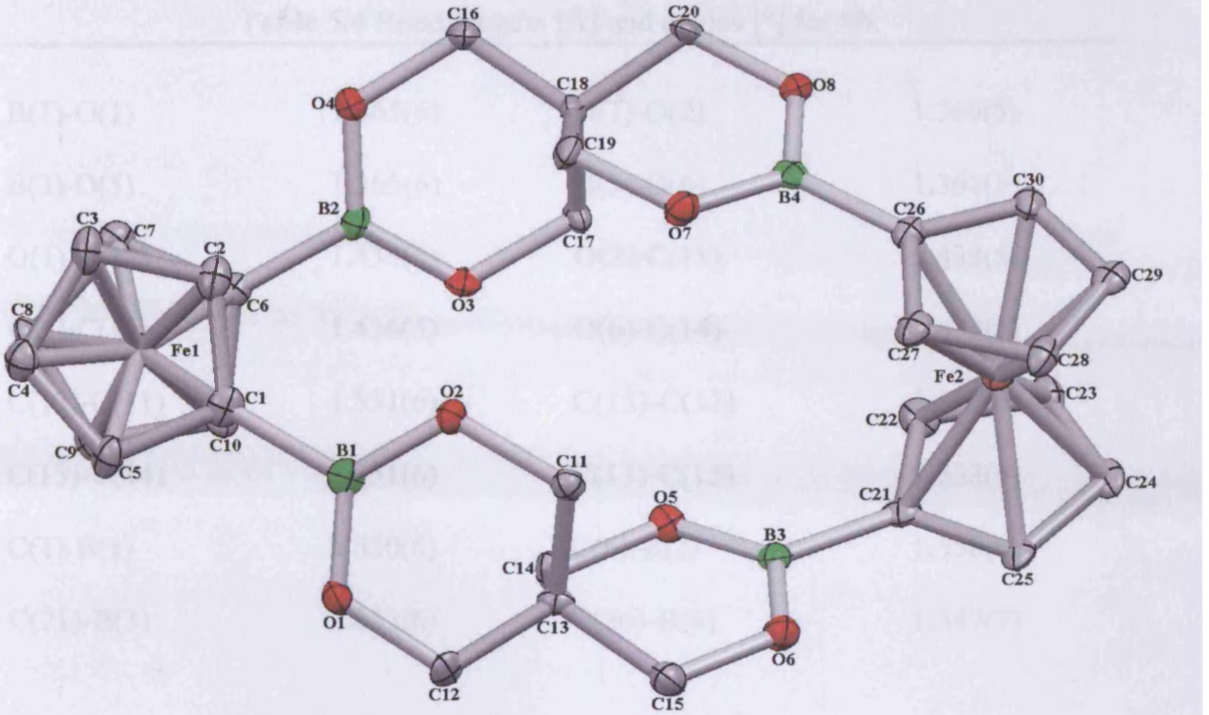

Figure 5.12 Molecular structure of *[fcB(OCH$_2$)$_2$C(CH$_2$O)$_2$B]$_2$* (**8b**) ORTEP ellipsoids set at the 50 % probability level. Hydrogen atoms omitted for clarity.

Table 5.4 Bond lengths [Å] and angles [°] for **8b**.

B(1)-O(1)	1.365(6)	B(1)-O(2)	1.360(5)
B(3)-O(5)	1.365(6)	B(3)-O(6)	1.361(5)
O(1)-C(12)	1.434(5)	O(2)-C(11)	1.438(5)
O(5)-C(15)	1.436(5)	O(6)-C(14)	1.434(5)
C(13)-C(11)	1.531(6)	C(13)-C(12)	1.527(5)
C(13)-C(14)	1.531(6)	C(13)-C(15)	1.532(5)
C(1)-B(1)	1.550(6)	C(6)-B(2)	1.556(6)
C(21)-B(3)	1.553(6)	C(26)-B(4)	1.547(7)
O(1)-B(1)-O(2)	123.3(4)	O(3)-B(2)-O(4)	123.2(4)
O(5)-B(3)-O(6)	123.2(4)	O(7)-B(4)-O(8)	122.6(4)
C(1)-B(1)-O(1)	118.9(4)	C(1)-B(1)-O(2)	117.8(4)
C(21)-B(3)-O(5)	119.1(4)	C(21)-B(3)-O(6)	117.6(4)
C(11)-C(13)-C(12)	108.3(3)	C(11)-C(13)-C(14)	110.8(3)
C(11)-C(13)-C(15)	110.6(3)	C(5)-C(1)-C(2)	106.4(4)
B(1)-O(1)-C(12)	119.9(3)	B(1)-O(2)-C(11)	119.9(3)

The molecular structure of **8b** displays similar bond angles at boron to **8a**, the sum of angles about the boron centre is 359.9(12)°, again the O-B-O bond angles (123.3(4)°) are larger than those previously observed (*ca.* 114°), a result of formation of the six-membered heterocycle, which widens the O-B-O, closing one of the Cp(C)-B-O angles slightly. B-O bond lengths of *ca.* 1.365(6) Å are consistent with B-O bond lengths of previously discussed analogous compounds (see chapter three). Whereas with the analogous macrocyclic compound **7b** the boryl fragment was twisted out of the plane of the Cp ligand by a substantial amount (*ca.* 23°), this is reduced in compound **8b** where the corresponding torsion is *ca.* 10°. The torsion angle [(B(1)-Cp(centroid)-Cp(centroid)-B(2)] of 62.0° is slightly smaller than that observed for the analogous cyclooctanetetraol based macrocycle (**7b**) [B(1)-Cp(centroid)-Cp(centroid)-B(2) of 78.1°]. The molecular structure of **8b** conforms to approximate chiral D_2-symmetry; NMR measurements made at -50°C show four distinct signals for the ferrocenediyl C_5H_4 protons, implying that this dissymmetric structure is maintained in solution within the lower temperature ranges (Figure 5.13). Just two C_5H_4 signals are observed at room temperature along with a single broad signal observed for all eight CH_2 protons at 25°C which sharpens on warming to 50°C. Such changes are consistent with a fluxional racemisation process involving concerted rotation about the two centroid-Fe-centroid axes (Figure 5.14).

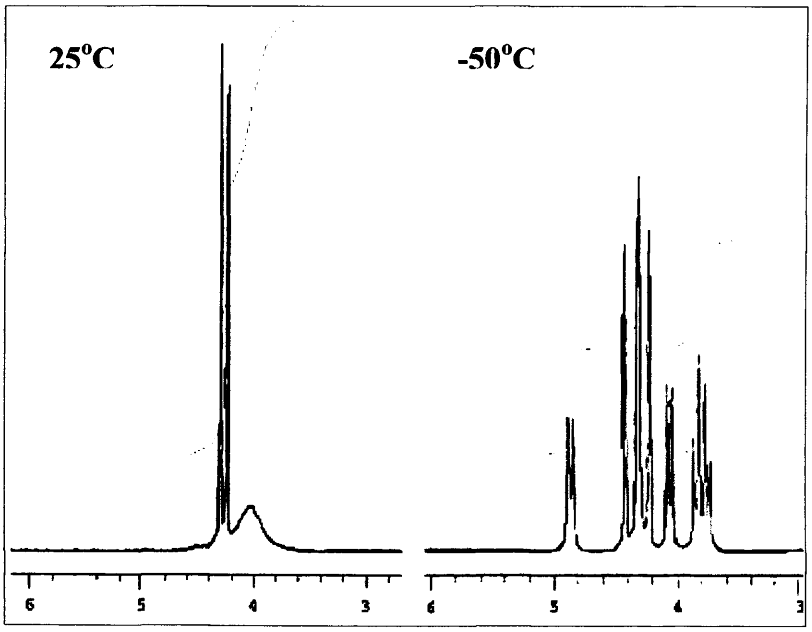

Figure 5.13 ^1H NMR spectra of compound **8b** in $CDCl_3$ at room temperature and –50°C.

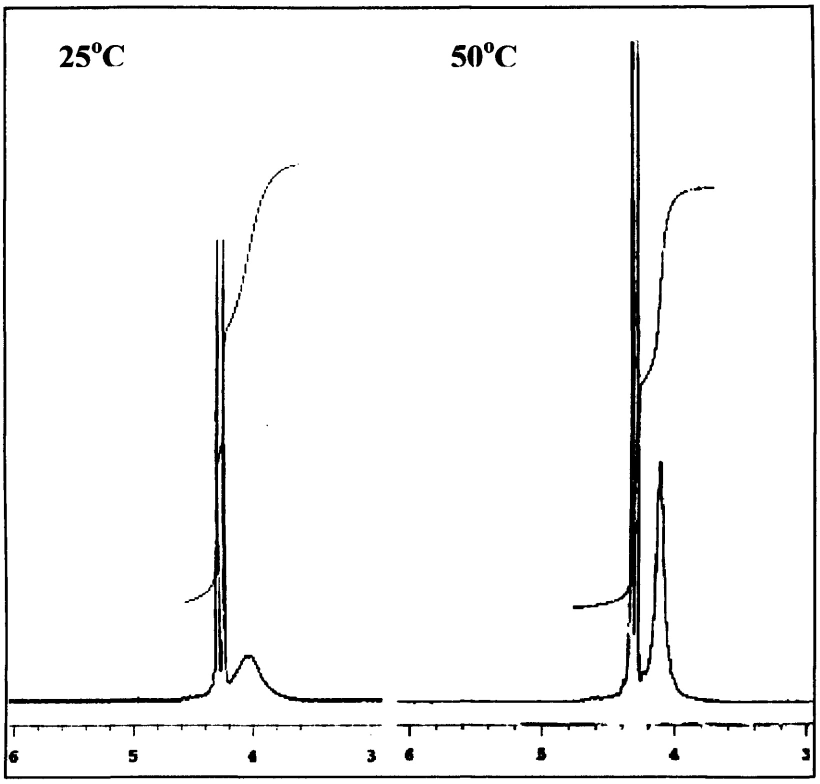

Figure 5.14 ^{1}H NMR spectra of compound **8b** at room temperature and 50°C.

The reactions of ferrocene*bis*-boronic acid with cyclooctanetetraol and pentaerythritol display remarkably high selectivity for the formation of either polymer or macrocycle. The reaction of cyclooctantetraol with ferrocene*bis*-boronic acid favours formation of polymeric over macrocyclic products, in this reaction the macrocycle **7b** was only ever isolated in minor yield (< 5 %). The reaction conditions were varied; temperature and concentration were systematically altered with little or no effect on the product distribution. The reaction mixture was spiked with an alcohol (ethane-1,2-diol), in an attempt to inhibit polymer formation by blocking polymerisation sites with chain terminating groups, but the reaction was found still to favour formation of polymeric products. By contrast the reaction of pentaerythritol with ferrocene*bis*-boronic acid was found to favour formation of macrocyclic products with no trace of polymeric products observed.

It has previously been demonstrated in studies of Lewis basic polymeric/macrocyclic systems that backbone conformational geometry and flexibility are key features in determining the selectivity for either product.[8] It also seems logical that the geometry and flexibility of the linker may be a factor in determining the product distribution in the case of compounds **7b**, **7c** and **8b**, since such high selectivity has been observed. The pentaerythritol and cyclooctanetetraol ligands exhibit very different geometrical features, in the case of **8b** exclusive formation of macrocyclic product implies that the reaction intermediate $(HO)_2BfcB(OCH_2)2C(CH_2O)_2BfcB(OCH_2)_2C(CH_2OH)_2$ (Figure 5.15) is highly preorganised such that macrocyclisation is preferred, and that the rate of macrocyclisation must be very high. In closer examination of the molecular structure of **8b** it is apparent that the BO_2 planes are significantly twisted with respect to each other (mean torsion angle 61.4°) and exhibit a 'bite-angle', [mean B-C(spiro)-B] angle of 137.6°, i.e. in a chain of $(HO)_2BfcB(OCH_2)2C(CH_2O)_2BfcB(OCH_2)_2C(CH_2OH)_2$ the $fcB(OH)_2$ and $C(CH_2OH)_2$ fragments are forced close to each other because of the B-C(spiro)-B angle of the bridging ligand, promoting subsequent condensation reaction at this site to form the macrocycle. Furthermore for a macrocyclic system featuring rigid bridging groups (such as pentaerythritol) the loss of conformational entropy is likely to be small compared with one comprised of more flexible bridging units (such as cyclooctanetetraol).

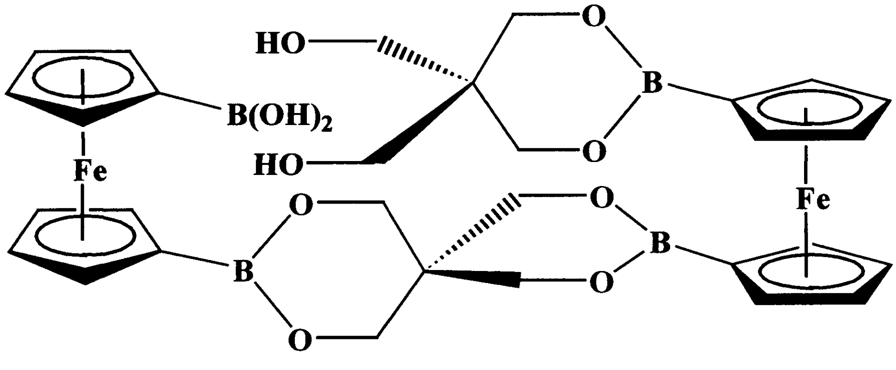

Figure 5.15 Likely reaction intermediate in preparation of **8b**.

In contrast, the geometry of the bridging $BO_2C_8H_{12}O_2B$ unit reveals that the cyclooctanetetraol framework adopts a more linear geometry in compound **7a**, the B-C(ipso) angles being in a more linear arrangement than those in **8b**, thus is preorganised so as to favour the formation of a linear chain. Hence by careful choice of tetraol linking agent, the simple condensation synthesis of multinuclear Lewis acids can be driven with high selectivity towards either macrocyclic or polymeric products. Further studies targeting exploitation of this synthetic control towards size specific anion chelation and soluble Lewis acid polymers were subsequently undertaken, along with electrochemical analyses.

5.4.3 Electrochemical and NMR analysis of anion binding by oligomeric and macrocyclic Lewis acids

The ability of an organometallic polymer to propagate an electronic signal along its chain is a useful property and one that is being exploited for the purpose of developing molecular wires and for the enhancement of sensor signals. The successful detection of very toxic substances such as Sarin and Soman (see chapter four) and other chemical warfare agents requires very highly sensitive materials, capable of responding very rapidly to a very low dose of toxic material. Investigations towards compounds that meet these requirements have recently focussed on organometallic polymers that can provide amplification of a sensor signal. A critical feature of these systems is the inter-metallic electronic communication. Such compounds, capable of electronic communication, have certain chemical features that allow the conjugation of electrons to run along a whole chain, for example a delocalised electron rich group linked to a fragment featuring a vacant orbital as means of accepting electron density. Main chain organoboron polymers are valuable candidates for optical sensor materials as a result of the extended π-conjugation between delocalised electron rich spacers and the vacant p-orbital of boron. These substances have the potential for sensor signal amplification upon binding of a guest molecule to a suitable receptor, namely the Lewis acidic boron centre, within the conjugated polymer.[11] The electrochemical properties and reactivity of organoboron polymers towards anions have been investigated by a number of research groups.[12,13] The above-mentioned organoboron dinuclear (**7a**, **8a**, **9a**), macrocyclic (**8b**) and polymeric (**7c**) products were made with a view to investigating both their anion binding and electronic properties. Assessment of the binding properties of the dimeric and macrocyclic analogues offers insight into the suitability of the polymeric species to act as anion specific sensors offering switchable conductivity and enhancement of both signal response and sensor kinetics. Macrocyclic Lewis acid systems featuring a binding cavity also offer enhanced stability in the host-guest complex.

NMR investigations have been performed, using mainly ^{11}B and ^{19}F NMR techniques to study fluoride binding. ^{1}H NMR spectra become very complex after the addition of fluoride, which has meant that the effectiveness of NMR as an analytical technique to monitor fluoride binding is drastically reduced. In the case of **8b** for example, up to four binding sites for fluoride anions are available and it is not possible to reliably monitor the change in chemical shift of a single peak in the ^1H NMR spectrum as a function of fluoride concentration. Compound **7a** was treated with excess quantities of fluoride as [$^nBu_4N$]F in chloroform solution under anaerobic conditions, followed by spectral acquisition. The addition of a source of fluoride to **7a** was found to cause an upfield shift in the ^{11}B NMR spectra, from the fluoride-free species (δ_B 32.5 ppm) to a broad resonance at δ_B 3.8 ppm. This upfield shift of *ca.* 28 ppm is consistent with formation of a four-coordinate anionic boronate centre, and with shifts previously observed for analogous compounds (**4b**, **4c** and **2b**) when treated with fluoride (see chapter four). The ^{19}F NMR signal resulting from fluoride treatment (δ_F -134.3 ppm) supports the complexation of F^-, since the chemical shift is significantly different from the [$^nBu_4N$]F itself (δ_F -122.7 ppm). The chemical shift is also consistent with that observed for the fluoride-adduct of **2b** (δ_F -130.8 ppm).[14] The ^{19}F resonance appears broader than the source, possibly due to unresolved ^{19}F / ^{11}B coupling. The orange solution of **7a** was not observed to change colour on addition of fluoride, after exposure of the NMR sample to air for 24 h. This finding is consistent with the behaviour of analogous mono-boronic esters of ferrocene (see chapter four), in which it is found that the binding of one equivalent of fluoride is not sufficient that subsequent electron donation to the iron centre allows aerobic oxidation, which would be accompanied by an orange to green colour change.

Compound **8b** was treated with different sources of fluoride and with various anions. Treatment of **8b** with excess quantities of [$^nBu_4N$]F or KF with 18-crown-6 in chloroform solution under anaerobic conditions, leads to upfield shifts in the ^{11}B NMR spectrum of *ca.* 22 ppm, from the parent compound (δ_B 27.6 ppm) to a broad resonance at δ_B 4.3 ppm. These shifts are consistent with the binding of an anionic donor to three-coordinate boron. The ^{19}F NMR signal resulting from fluoride treatment with [^{n}Bu$_4$N]F supports the complexation of F$^-$ (δ_F -136.8 ppm), this chemical shift being markedly different from the source (δ_F -122.7 ppm), the observed chemical shift is also consistent with that observed for the fluoride-adduct of **2b** (δ_F -130.8 ppm).[14] Again the ^{19}F resonance appears broader than the source, perhaps due to coupling of ^{19}F to ^{11}B nuclei. A solution of **8b** treated with fluoride was not observed to change colour after exposure to air for 24 h. While the lack of colorimetric response was expected for mono-functional compound (**7a**), compound **8b** features two binding sites per iron centre, and hence the possibility of forming a 2:1 adduct. Thus this observation provides some information on the binding stoichiometry. If one equivalent of fluoride were bound at *each* Lewis acidic boron centre, a colour change from orange to green would be expected to result, since the electrochemical shift (based on that previously measured for **2a**) would be expected to be sufficient that it would be oxidised by atmospheric oxygen. The NMR data is however strongly suggestive of some form of Lewis acid-fluoride interaction taking place, however determination of the mode of binding requires further investigation.

The use of ferrocene has been particularly extensive in the development of organometallic polymers capable of inter-metallic electronic communication, acting as the backbone of the polymer in many cases. The reversible redox chemistry of ferrocene provides a convenient method of analysis. Electrochemical methods, particularly cyclic voltammetry, can provide a valuable insight into the mechanisms of electron transfer reactions involved in redox processes, capable of detecting electronic communication between redox active centres. For example in the simple case of compound **7a**, where just two ferrocene units are bridged by a cyclooctanetetraol linker group, electronic communication (if it were to occur) would be manifested by the presence of two oxidation waves. Thus as one iron centre becomes oxidised, the neighbouring site becomes more difficult to oxidise and therefore does so at a higher oxidation potential and two oxidation waves are observed. The peak-peak separation provides an estimate of the degree of interaction between the two iron centres, and have been observed in a range of $\Delta E_{1/2}$ = 0.16-0.29 V, depending on the spacer group.[15] In a situation where no electronic communication is occurring and both iron centres are in equivalent chemical environments, we would expect to observe just a single redox wave, as the oxidation of one iron centre cannot affect the oxidation potential of the second.

In previous anion binding studies, the mono-functional analogue **2a** was found to act as a selective receptor for fluoride, with the binding event in dichloromethane being accompanied by a cathodic shift in oxidation potential of the iron centre from +131 mV to –403 mV, a total shift of -534 mV (see chapter four). Electrochemical analyses were performed on the dinuclear compounds **7a**, **8a**, **9a**, and macrocycle **8b**, to gain some insight as to whether the polymeric analogues of these compounds might show evidence of electronic communication. The insolubility of the polymeric product **7c** has precluded electrochemical analysis of this compound. Analyses of the remaining compounds were made in dichloromethane solution, and for all measurements ferrocene was used as a reference compound. The CVs of compounds **7a**, **8a**, **9a**, and **8b** are shown below in Figures 5.16, 5.17 5.18 and 5.19, and a summary of relevant information is shown below in Table 5.5.

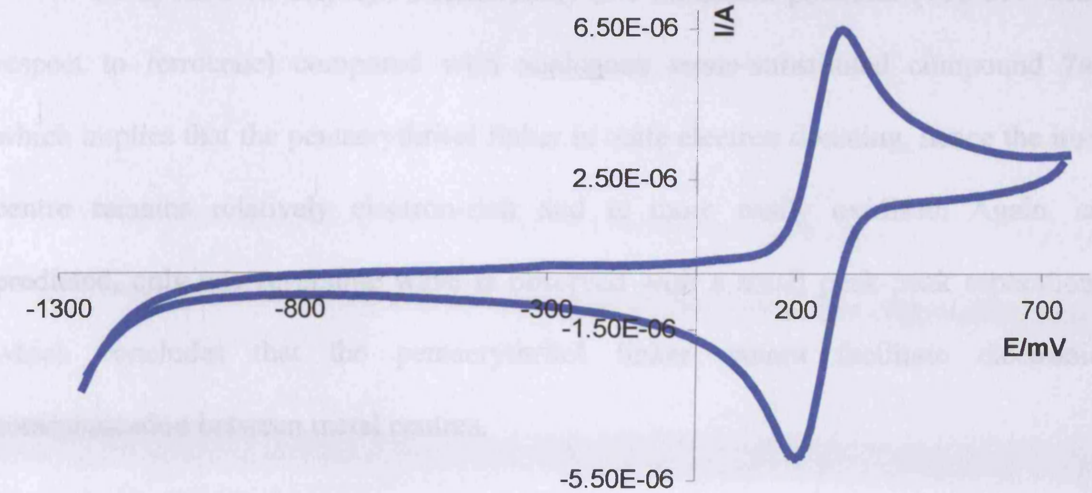

Figure 5.16 Cyclic Voltammogram of compound **7a**.

It is evident from the CV scans that the saturated cyclooctanetetraol spacer unit is not sufficient to allow extended conjugation and inter-metallic electronic communication, and as expected only a single redox wave is observed.

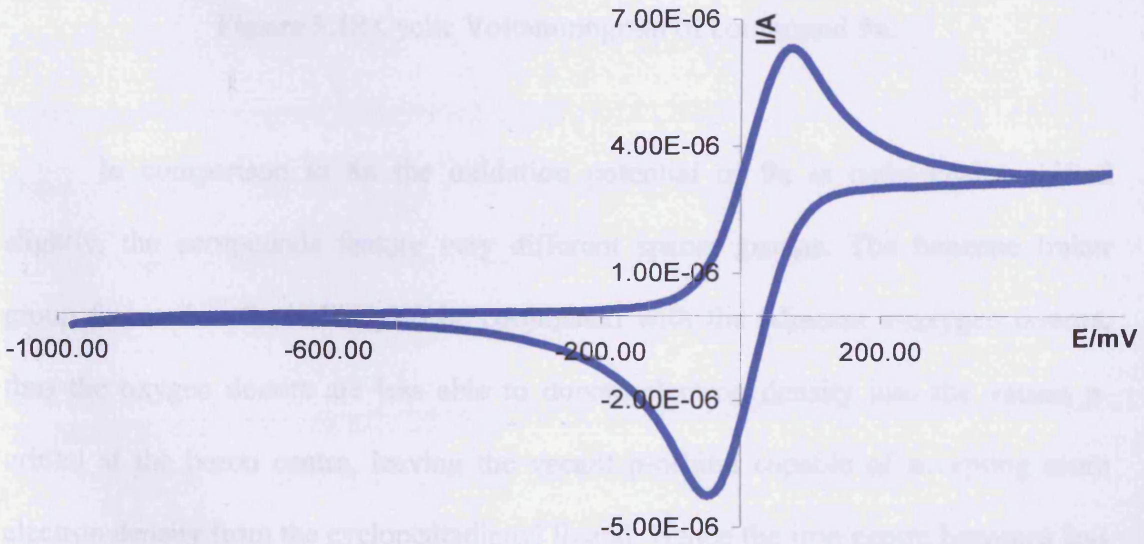

Figure 5.17 Cyclic Voltammogram of compound **8a**.

Compound **8a** displays a remarkably low oxidation potential (+15 mV with respect to ferrocene) compared with analogous *mono*-substituted compound **7a**, which implies that the pentaerythritol linker is quite electron donating, hence the iron centre remains relatively electron-rich and is more easily oxidised. Again, as predicted, only one reversible wave is observed with a small peak-peak separation, which concludes that the pentaerythritol linker cannot facilitate electronic communication between metal centres.

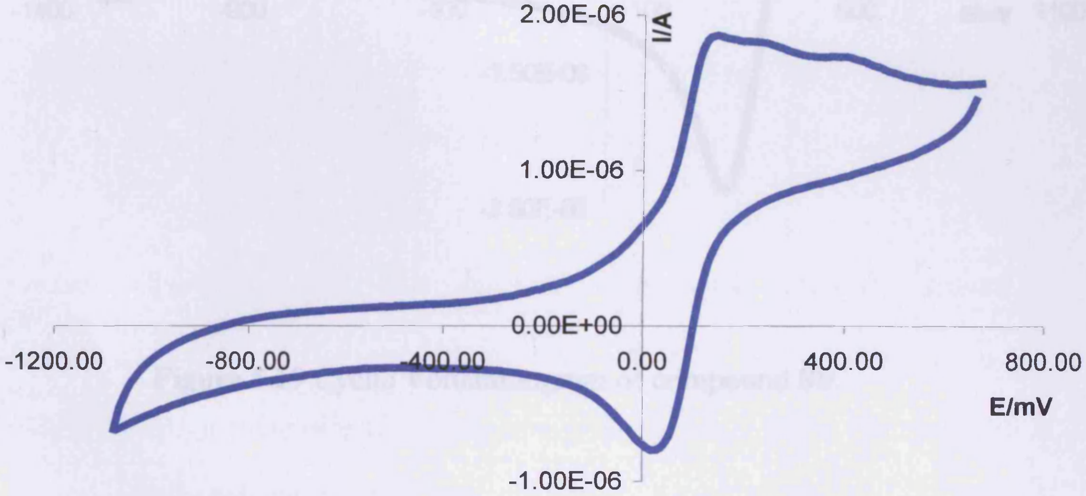

Figure 5.18 Cyclic Voltammogram of compound **9a**.

In comparison to **8a** the oxidation potential of **9a** is cathodically shifted slightly, the compounds feature very different spacer groups. The benzene linker group featured in **9a** is likely to be conjugated with the adjacent π-oxygen donors, thus the oxygen donors are less able to donate electron density into the vacant p-orbital at the boron centre, leaving the vacant p-orbital capable of accepting more electron density from the cyclopentadienyl ligand. Hence the iron centre becomes less electron-rich and more difficult to oxidise. One interesting point to note about the CV scan of **9a** is the lack of multiple redox waves; the incorporation of the delocalised benzene spacer group, which was thought to be capable of supporting electronic communication between two metal centres, has proven unsuccessful.

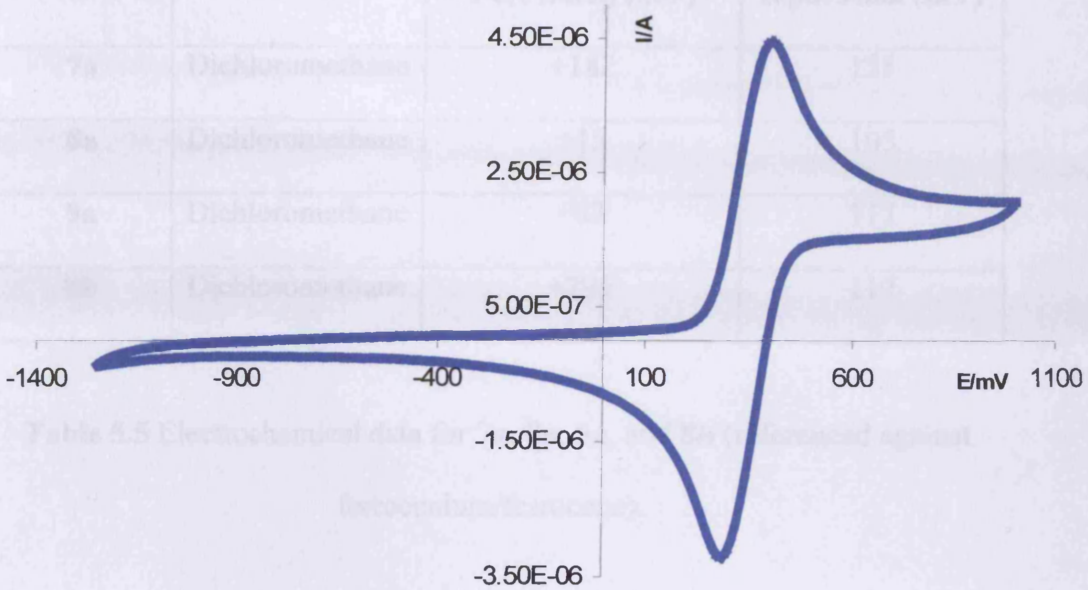

Figure 5.19 Cyclic Voltammogram of compound **8b**.

The unusual macrocyclic structure of compound **8b** is reflected in the oxidation potential of the compound (+416 mV), this value is not similar to any of the analogous boronic esters of ferrocene reported in Chapters Three and Four. Again, a small peak-peak separation (117 mV) is observed, along with a single redox wave, both of which provide significant proof that the pentaerythritol linker is not capable of supporting electronic communication through the vacant p-orbital at boron between two iron centres. Although it has already been implied from previous electrochemical studies that none of the above-mentioned compounds are capable of supporting electronic communication, from the perspective of developing colorimetric sensors for fluoride these compounds are still of interest.

Compound	**Solvent**	**Potential Relative to FcH (Ref.) (mV)**	**Peak-Peak separation (mV)**
7a	Dichloromethane	+182	121
8a	Dichloromethane	+15	105
9a	Dichloromethane	+67	117
8b	Dichloromethane	+295	117

Table 5.5 Electrochemical data for **7a**, **8a**, **9a**, and **8b** (referenced against ferrocenium/ferrocene).

Electrochemical analysis also provides a convenient analytical method for monitoring the process of fluoride binding. The effect of fluoride binding on the oxidation potential of the ferrocene moiety is very pronounced in the CV spectrum as a result of the electronic changes that take place at the boron centre. Prior to fluoride binding the boryl groups act as net electron acceptors; this effect is reversed on the binding of fluoride, the resulting four-coordinate borate moiety acts as an electron donor, the ferrocene fragment becomes more electron rich, and hence is oxidised at a lower potential. Electrochemical analysis of anion binding was performed on compounds **8a** and **9a**. The novel dimer **8a** displayed a cathodic shift of *ca.* –456 mV on addition of 2 equiv. [^{n}Bu$_4$N]F. The CV scan for **8a** treated with solid [^{n}Bu$_4$N]F in dichloromethane solution is shown in Figure 5.20, with the CV scan for the parent compound overlaid.

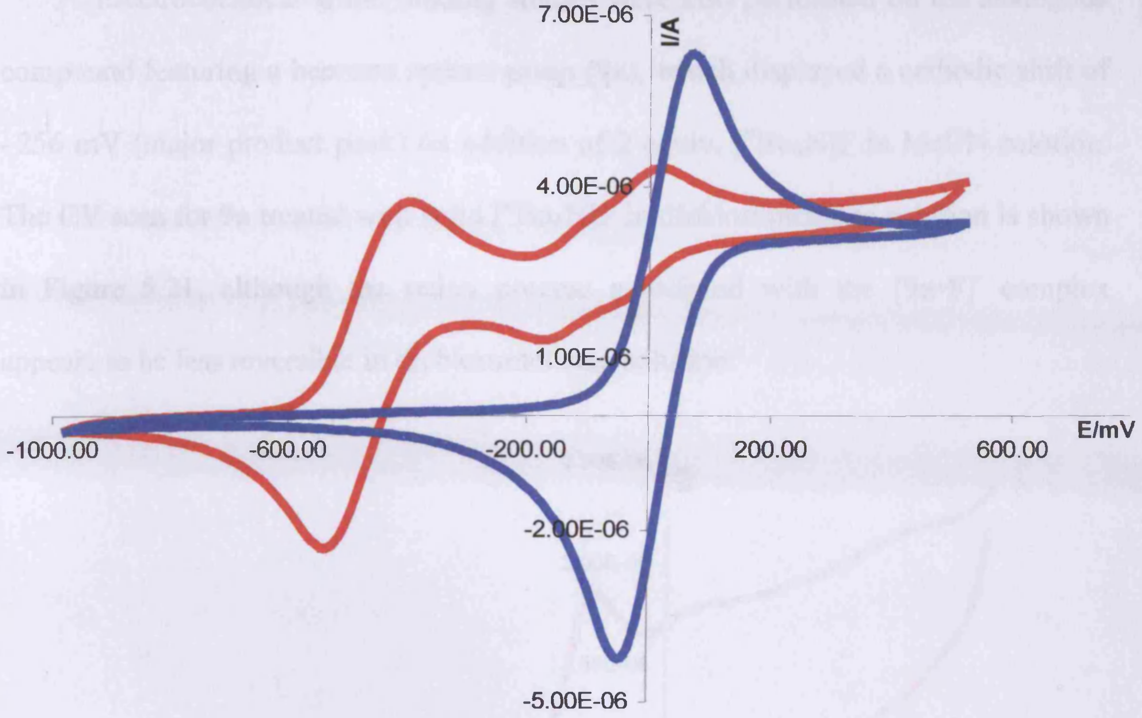

Figure 5.20 Cyclic voltammogram of **8a** (blue trace) and **8a** plus 2 equivalents of [^{n}Bu$_4$N]F (red trace) in dichloromethane.

The observed cathodic shift of –456 mV provides substantial proof of a host-guest interaction between **8a** and fluoride anions, this shift is similar to those observed for the mono-functional analogues **1a** (-482 mV), **1b** (-442 mV) and **2a** (-534 mV) described in chapter four. The magnitude of the cathodic shift suggests that one fluoride is being bound at each of the two boron centres. From previous anion binding studies on boronic esters of ferrocene, it has been determined that in order to undergo aerobic oxidation by atmospheric dioxygen, the net cathodic shift must be *ca.* 1000 mV. The potential associated with the O_2/O_2^- redox couple in non-aqueous solution is known to be strongly dependant on pH. For example, for $O_2 + e^- \rightarrow O_2^-$, $E_{1/2} = -1000$ mV versus Fc^+/Fc in DMF, while for $O_2 + H^+ + e^- \rightarrow HO_2$, $E_{1/2} = -280$ mV also referenced against Fc^+/Fc in DMF.[19] Thus it is obvious from this evidence why **8a** does not display an orange to green colour change upon aerobic exposure to fluoride.

Electrochemical anion binding studies were also performed on the analogous compound featuring a benzene spacer group (**9a**), which displayed a cathodic shift of –256 mV (major product peak) on addition of 2 equiv. [^{n}Bu$_4$N]F in MeCN solution. The CV scan for **9a** treated with solid [^{n}Bu$_4$N]F in dichloromethane solution is shown in Figure 5.21, although the redox process associated with the **[9a•F]**$^-$ complex appears to be less reversible in dichloromethane solution.

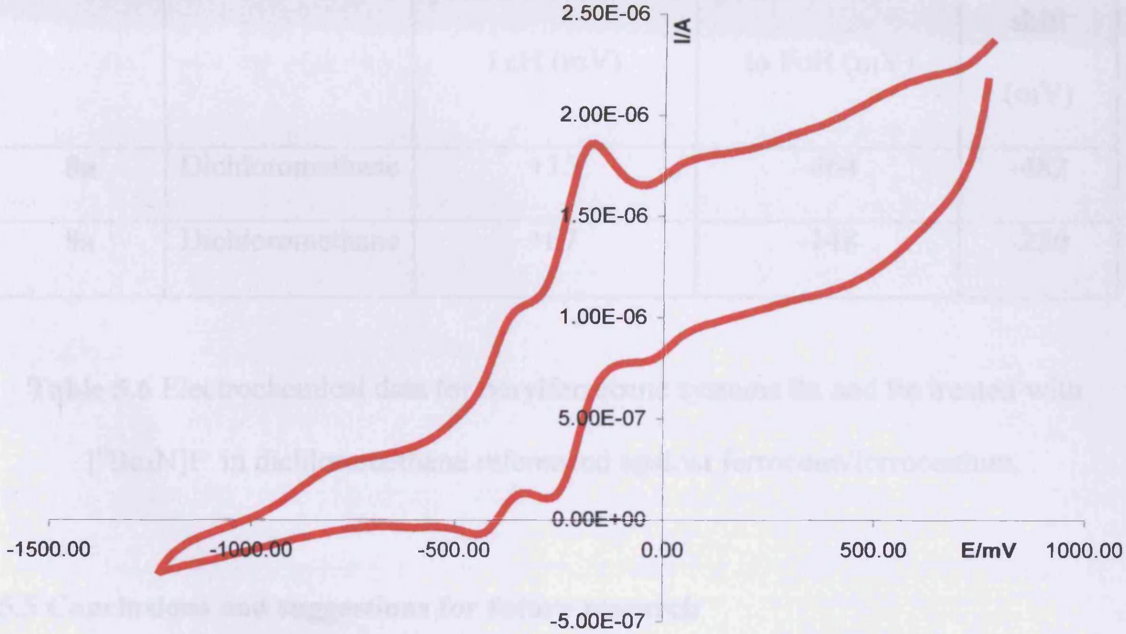

Figure 5.21 Cyclic voltammogram of **9a** plus 2 equivalents of [^{n}Bu$_4$N]F in dichloromethane.

The observed cathodic shift provides some evidence of a host-guest interaction between **9a** and fluoride anions, although the magnitude of the cathodic shift is much smaller than that observed for dimeric analogue **8a** (see table 5.6 below). The CV scan for **9a** treated with fluoride shows two peaks, which might provide evidence for electronic communication between the two iron centres in the **[9a•F]**$^-$ complex, perhaps formation of the electron-donating four coordinate boron centre facilitates electronic communication via the delocalised benzene spacer. Alternatively it is possible that the mono-fluroide adduct is formed, thus there are two different boron centres – one three coordinate (shifted a smaller amount from the free receptor) and one four coordinate (shifted a larger amount from the free receptor).

Compound	Solvent	Initial oxidation potential relative to FcH (mV)	F^- adduct potential relative to FcH (mV)	Cathodic shift (mV)
8a	Dichloromethane	+15	-464	-482
9a	Dichloromethane	+67	-148	-256

Table 5.6 Electrochemical data for borylferrocene systems **8a** and **9a** treated with $[^nBu_4N]F$ in dichloromethane referenced against ferrocene/ferrocenium.

5.5 Conclusions and suggestions for future research

Investigation into the electrochemical properties of oligomeric and macrocyclic compounds has revealed that there is no electronic communication occurring between redox centres. Compounds **7a**, **8a** and **8b** feature saturated cyclooctanetetraol or pentaerythritol linker groups; delocalised linker groups are more likely to sustain a conjugative interaction. Careful choice of an appropriate electron-rich unsaturated linker group, featuring the necessary geometry to favour polymer or macrocycle, is required to advance towards compounds suitable to access solid-state sensor systems with switchable conductivity and enhancement of both signal response and sensor kinetics. A wide range of compatible tetra-ol reagents are available, allowing the opportunity to systematically vary geometry, conformational rigidity and stereochemistry. Whilst select choice of linker group can be made to promote electronic communication, the use of for example, redox-active ortho-quinone linkers, in this way the redox properties of the polymer might perhaps be tuned to meet specific requirements.

The insolubility of the polymeric product (**7c**) has hindered characterisation of that product by conventional methods such as NMR, mass spectrometry, UV and IR spectroscopies, and has precluded anion binding and electrochemical studies. There stands vast scope for alteration of solubility properties by minor modification to the linker group, for example by variation at X in the 1,4-X_2-tetrahydroxybenzene linker used in the preparation of **9a**. Incorporation of long-chain alkanes will enhance organic solubility, whilst inclusion of alcohols, sugars or carboxylate groups will increase aqueous solubility of polymeric products.

Cross-linking for enhanced polymer strength can be promoted by spiking the tetra-ol component with hexa-ols, capable of undergoing a condensation reaction to bridge two or more parallel polymer chains, in this way the degree of cross-linking may also be tuned by adding quantitatively less or more hexa-ol to the tetra-ol component. Another method of tuning cross-linking is by spiking the ferrocene-diboronic acid with the *tris*- or *tetrakis*-boronic acid analogues. Use of *tris*- or *tetrakis*-boronic acids and hexa-ols may also provide the scope to prepare dendrimeric compounds. Addition of chain-terminating rigid diols i.e. catechol to the tetra-ol component of the reaction mixture, or by addition of ferroceneboronic acid to the ferrocene-diboronic acid component allows the possibility to control polymer chain length.

5.6 References

1 W. J. Patterson, S. P. McManus, C. U. Pittman Jr, *J. Polym. Sci.*, 1974, **12**, 4, 837.

2 H. Braunschweig, R. Dirk, M. Müller, P. Nguyen, R. Resendes, D. P. Gates, I. Manners, *Angew. Chem. Int. Ed. Engl.,* 1997, **36**, 21, 2338.

3 F. Jäkle, A. Berenbaum, A. J. Lough, I. Manners, *Chem. Eur. J.*, 2000, **6**, 2762.

4 A. Berenbaum, H. Braunschweig, R. Dirk, U. Englert, J. C. Green, A. J. Lough, F. Jäkle, I. Manners, *J. Am. Chem. Soc.*, 2000, **122**, 5765.

5 J.B.Heilmann, M. Schebitz, Y. Qin, A. Sundararaman, F. Jakle, T. Kretz, M. Bolte, H.W. Lerner, M. C. Holthausen, M. Wagner. *Angew. Chem. Int. Ed.*, 2006, 45, 920.

6 K. P. Dancey, K. Hendrick, P. M. Judd, P. G. Owsten, R. Peters, P. A. Tasker, A. Deu, R. W. Turner, *J. Am. Chem. Soc.,* 1981, **103**, 4952.

7 F. H. Carre, R. J. P. Corriu, T. Deforth, W.E. Douglas, W. S. Siebert, W. Weinmann, *Angew. Chem. Int. Ed,* 1998, **37**, 652.

8 *Macrocycle Synthesis*, D. Parker ed., OUP, Oxford, 1996.

9 M. Scheibitz, J. B. Heilmann, R. F. Winter, M. Bolte, J. W. Batz, M. Wagner, *Dalton. Trans.,* 2005, 159.

10 S. Aldridge, I. Fallis, N. D. Coombs, unpublished results.

11 D. T. McQuade, A. E. Pullen, T. M. Swager, *Chem. Rev.,* 2000, **100**, 2537.

12 W. Kaim, A. Schulz, *Angew. Chem. Int. Ed.*, 1984, **23**, 615.

13 M. Miyata, Y. Chujo, *Polym. J.,* 2002, **34**, 967.

14 S. Aldridge, C. Bresner, I. A. Fallis, S. J. Coles, M. B. Hursthouse, *Chem. Commun.,* 2002, 740.

15 P. Nguyen, P. Gómez-Elipe, I. Manners, *Chem. Rev.,* 1999, **99**, 1515.

Appendix One

Kinetics Equations

Part **I** – Calculation of rate constant for **2b**, **3b** and **4b** with excess fluoride.

$$\begin{tikzcd}
[\text{Receptor}] + 2\text{F}^- \arrow[r, shift left, "k_1"] & {[\text{Receptor.2F}]^{2-}} \arrow[l, shift left, "k_2"] \arrow[d, "k_3"', "\text{oxidant}"] \\
 & {[\text{Receptor.2F}]^-}
\end{tikzcd}$$

Rate = k_3 [Ox] $[(\text{Receptor.2F})^{2-}]$ **(1)**

Using steady state approximation for the concentration of $[(\text{Receptor.2F})^{2-}]$:

0 = Rate of change of concentration of $[(\text{Receptor.2F})^{2-}]$

= $k_1[\text{Receptor}][\text{F}^-]^2 - k_2[(\text{Receptor.2F})^{2-}] - k_3[\text{Ox}][(\text{Receptor.2F})^{2-}]$

So, by rearranging:

$[(\text{Receptor.2F})^{2-}] = k_1[\text{Receptor}][\text{F}^-]^2 / (k_2 + k_3[\text{Ox}])$ **(2)**

Substituting this in to equation **1** gives:

Rate = $k_3[\text{Ox}][(\text{Receptor.2F})^{2-}] = k_1k_3[\text{Ox}][\text{Receptor}][\text{F}^-]^2 / (k_2 + k_3[\text{Ox}])$ **(3)**

If we make the assumption that $k_2 \gg k_3[\text{Ox}]$ (i.e. we ignore the $k_3[\text{Ox}]$ term on the bottom), then equation **3** simplifies to

Rate = $k_3[\text{Ox}][(\text{Receptor.2F})^{2-}] = k_1k_3[\text{Ox}][\text{Receptor}][\text{F}^-]^2 / k_2$ **(4)**

And since $K = k_1 / k_2$ equation **4** becomes

Rate = $k_3K[\text{Ox}][\text{Receptor}][\text{F}^-]^2$ **(5)**

We then assume pseudo first order kinetics by assuming that (using experimental conditions such that) [Ox] and $[F^-]$ do not change.

Part **II** – Calculation of binding stoichiometry.

(i) Kinetics as a function of fluoride concentration investigated.
Rate = v = $k[F^-]^n$ (**6**)

(ii) In our case:
$v = k[F^-]^n[\text{Receptor}]$ (**7**)
$\ln(v) = \ln k + n\ln[F^-] + \ln[\text{receptor}]$ (**8**)
For initial period in which [receptor] is effectively constant, therefore:
$\ln(v_i) = n\ln[F^-] + \text{constant}$ (**9**)
Initial rates (v) estimated by fitting a linear function to the absorbance vs time data for kinetic runs of varying fluoride concentrations.

(iii) Plot of $\ln(v_i)$ vs. $\ln[F^-]$ has a gradient of n to determine binding stoichiometry.

References:

K. J. Laidler, *Chemical Kinetics,* Harper and Row: New York, 1987; Chapter 2.

Appendix Two

List of Publications

Colorimetric fluoride ion sensing by polyborylated ferrocenes: structural influences on thermodynamics and kinetics. Joanna. K. Day, Christopher. Bresner, Natalie. D. Coombs, Ian. A. Fallis, Li-ling. Ooi, Simon. Aldridge, *Inorg. Chem.,* 2008, **47**, 793.

Synthesis of polymeric and macrocyclic Lewis acids: Influence of backbone on degree of aggregation. J. K. Day, C. Bresner, I. A. Fallis, L. Ooi, D. J. Watkin, S. J. Coles, L. Male, M. B. Hursthouse, S. Aldridge, *Dalton. Trans.,* 2007, **32**, 3486.

Fluoride anion binding by cyclic boronate esters: Influence of backbone chelate on receptor integrity. C. Bresner, J. K. Day, N. D. Coombs, I. A. Fallis, S. Aldridge, S. J. Coles, M. B. Hursthouse, *Dalton. Trans.,* 2006, **30**, 3660.

Influence of ligand backbone flexibility in group IV metal complexes of tetradentate mixed tertiary amine/alkoxide ligands. J. K. Day, R. E. Baghurst, R. R. Strevens, M. E. Light, M. B. Hursthouse, B. F. Stengel, I. A. Fallis, S. Aldridge, *New. J. Chem.,* 2007, **31**, 135.

Insertion reactions of dicyclohexylcarbodiimide with aminoboranes, -boryls and –borylenes. G. A. Pierce, N. D. Coombs, D. J. Willock, J. K. Day, A. Stasch, S. Aldridge, *Dalton. Trans.,* 2007, **39**, 4405.

Halide abstraction by $Na[B(C_6H_3(CF_3)_2\text{-}3,5)_4]$: Synthesis and structural characterisation of the Rhodium (I) cations $[(\eta^6\text{-arene})Rh(PPh_3)_2]^+$ (arene = benzene, toluene). O. Buttler, A. Al-Fawaz, D. L. Kays, J. K. Day, L. Ooi, S. Aldridge, *Z. Anorg. Allg. Chem.,* 2006, **632**, 2187.

Substitution, abstraction and addition chemistry of low-coordinate gallium and indium ligand systems. N. D. Coombs, N. R. Bunn, D. L. Kays, J. K. Day, L. Ooi, S. Aldridge, *Inorg. Chim. Acta.,* 2006, **359**, 3693.

Cationic terminal borylene complexes: Interconversion of amino and alkoxy borylenes by an unprecedented Meerwein-Ponndorf Hydride transfer. D. L. Kays, J. K. Day, S. Aldridge, R. W. Harrington, W. Clegg, *Angew. Chem. Int. Ed.,* 2006, **45**, 3513.

Cationic terminal borylene complexes: A synthetic and mechanistic investigation of M:B metathesis chemistry. D. L. Kays, J. K. Day, L. Ooi, S. Aldridge, *Angew. Chem. Int. Ed.,* 2005, **44**, 7457.

Halide abstraction as a route to cationic transition-metal complexes containing two-coordinate gallium and indium ligand systems. N. R. Bunn, S. Aldridge, D. L. Kays, N. D. Coombs, J. K. Day, L. Ooi, S. J. Coles, M. B. Hursthouse, *Organometallics.,* 2005, **24**, 5891.

Toward cationic gallane- and indanediyl complexes: Synthetic approaches to three-coordinate halogallyl and –indyl precursors. N. R. Bunn, S. Aldridge, D. L. Kays, N. D. Coombs, J. K. Day, L. Ooi, S. J. Coles, M. B. Hursthouse, *Organometallics.,* 2005, **24**, 5879.

Appendix Three - Table Of Compounds

1a	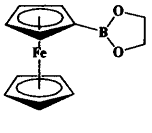	**3c**	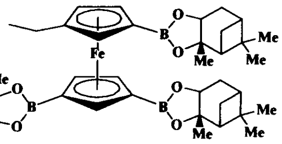	**6a**	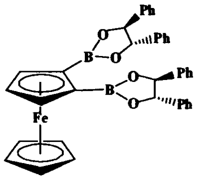
1b	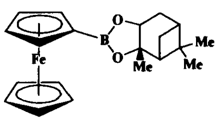	**4a**	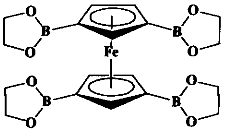	**7a**	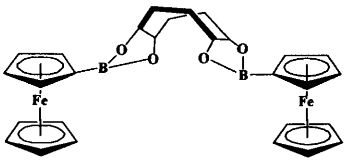
1c	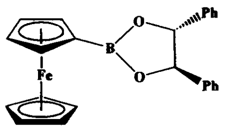	**4b**	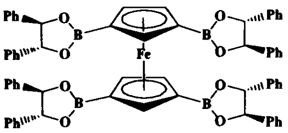	**7b**	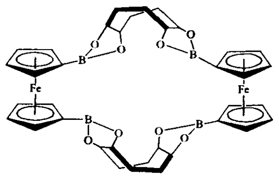
2a	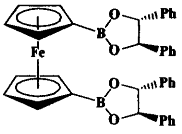	**4c**	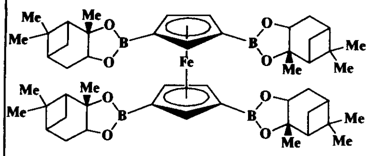	**7c**	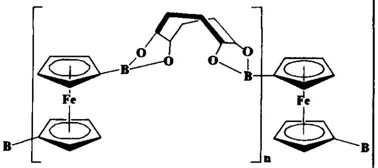
2b	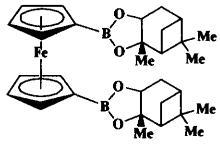	**4d**	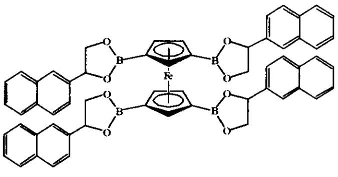	**8a**	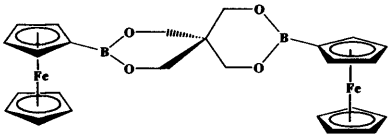
3a	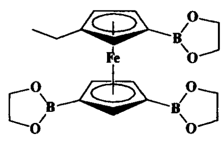	**5a**	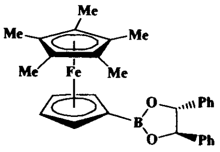	**8b**	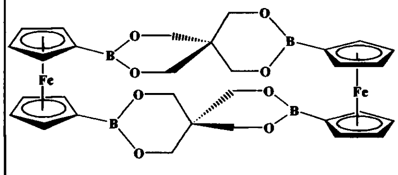
3b	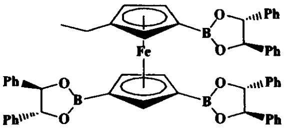	**5b**	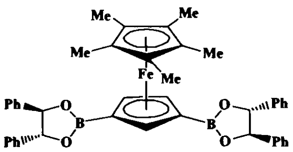	**9a**